
Shape and Chemical Anisotropic Particles in Low Dielectric Constant Media

A thesis submitted to The University of Manchester
for the degree of a Doctor of Philosophy in the
Faculty of Engineering and Physical Sciences

Sean Butterworth
School of Chemistry



2013

Table of Contents

Table of Contents	2
Final Word Count	8
Table of Figures	9
Copyright Statement	22
Abstract	23
Declaration	24
Acknowledgements	25
1 Introduction	26
1.1 Opening Statement	27
1.2 Bistable Display Technology	27
1.2.1 Cell Designs	28
1.2.2 Material Requirements for Electrophoretic Displays	31
1.3 Colloidal Materials	34
1.3.1 Colloidal Stability	34
1.4 Electrophoresis of Colloidal Material	42
1.5 Charges in Non Polar Systems	44
1.5.1 Comparison to Aqueous Media	45
1.5.2 Ion Stability in Low Dielectric Media and the Role of Surfactant	46
1.5.3 Charging of Particles in Non-Polar Solvents	49
1.5.4 Electrodynamics of Non-Aqueous Colloid Systems	50
1.6 Non Aqueous Dispersion Polymerisation	52
1.6.1 Flory-Huggins Theory and Solvent Choice	53
1.6.2 Role of Stabiliser during the Reaction	55
1.7 Formation and Uses of Shape Anisotropic Particles	56
1.7.1 Formation of Shape Anisotropic Particles	56
1.7.2 Uses of Shape Anisotropic Particles	63
1.8 Aims and Objectives of the Project	65

1.9 References	66
2 Spherical Seed Particle Synthesis	71
2.1 Introduction	72
2.2 Optimisation of Dispersion Polymerisation to Give Uncrosslinked Poly(Methyl Methacrylate) Particles	72
2.2.1 Components of Dispersion Polymerisation	73
2.2.2 Effect of Solvent Choice	75
2.2.3 Varying the Monomer Concentration	81
2.3 Crosslinked Particle Formation	84
2.3.1 Addition of Crosslinker and Mechanistic Implications	85
2.3.2 Batch Method of Formation	86
2.3.3 Implications of Crosslinker Addition at the Critical Time to Particle Nucleation, t_c	87
2.3.4 Finding the Critical Time to Particle Nucleation	88
2.3.5 Effect of Crosslinker Addition Rate	91
2.4 Chemical Attachment of P(HAS- <i>g</i> -MMA) Stabiliser to the Particle Surface	100
2.5 Conclusions	102
2.6 References	103
3 Monomer Choice and Modelling Monomer-Particle Interactions	104
3.1 Introduction	105
3.1.1 Dynamic Swelling Method for Anisotropic Particle Formation	105
3.2 Prediction of Particle Morphology by Interfacial Energy Minimisation	106
3.2.1 Contact Angle Measurements	108
3.3 Monomer Selection and Solubility Parameters	109
3.3.1 Hansen Solubility Parameters	110
3.4 Characterisation of Polymer Substrates	115

3.5 Calculating the Surface Energy of Polymer Films, $\gamma_{S,A}$	118
3.6 Measuring the Monomer - Dodecane Interfacial Tension, $\gamma_{M,D}$	123
3.6.1 Measuring the Interfacial Tension of Liquids by the Pendant Drop Technique	123
3.6.2 The Monomer - Dodecane Interfacial Tension, $\gamma_{M,D}$	124
3.7 Calculating the Dodecane - Substrate Interfacial Tension, $\gamma_{D,S}$	127
3.8 Measuring the Contact Angle between Polymer Substrates and Monomers Submerged in Dodecane, $\theta_{M,S}$	130
3.9 Calculating the Polymer Substrate - Monomer Interfacial Tension, $\gamma_{S,M}$	132
3.10 Summing the Total Interfacial Tension for the System	134
3.10.1 Expected Particle Morphology	135
3.11 Limitations to Predicting Particle Morphology by Summing the Total Interfacial Tension for the System	136
3.12 Conclusions	137
3.13 References	137

4 Second Stage Polymerisation Reactions of Methyl Methacrylate with Poly(methyl methacrylate) Seed Particles	139
4.1 Introduction	140
4.2 Initial Seed Dispersions	140
4.3 Second Stage Polymerisation Reactions under Batch Conditions	140
4.3.1 Standard Conditions	141
4.3.2 Monomer Conversion and Particle Growth	141
4.3.3 Second stage Polymerisation Reactions	143
4.3.4 Second Stage Polymerisation Reactions with Methyl Methacrylate and Crosslinker	146
4.4 Monitoring Particle Swelling	148
4.5 Reaction Mechanism during Second Stage Polymerisation Reaction	151
4.6 Implications of Varying the Crosslinking Polarity and Reactivity	154
4.6.1 Hansen Solubility Parameters	155

4.6.2 Implications of Monomer Reactivity	157
4.7 Second Stage Polymerisation Reactions – Effect of Crosslinking Monomer Polarity and Reactivity	160
4.8 Effect of Changing Other Reaction Conditions	163
4.8.1 Varying Chain Transfer Agent Concentration	164
4.8.2 Varying Initial Seed Particle Total Solids Content	166
4.8.3 Effect of Replacing Polar Crosslinking Monomer for Polar Monofunctional Monomer	168
4.9 Rationalisation of Findings with Polar Monomer Inclusion	170
4.9.1 Varying Crosslinking Monomer	170
4.9.2 Changing Chain Transfer Agent Concentration	171
4.9.3 Implications of Precipitation to Seed Particle Surface	172
4.10 Sequential Second Stage Polymerisation Reactions	172
4.10.1 Effect of EGDMA on Sequential Second Stage Polymerisation Reactions	173
4.10.2 Effect of GDMA on Sequential Second Stage Polymerisation Reactions	174
4.10.3 Effect of EGDMA followed by GDMA Sequential Second Stage Polymerisation Reactions	176
4.10 Conclusions	178
4.11 References	179

5 Second Stage Polymerisation Reactions of 2-Hydroxyethyl methacrylate and *N*-Hydroxyethyl acrylamide with Poly(methyl methacrylate) Seed Particles

5.1 Introduction	182
5.2 Standard Reaction Conditions	182
5.3 Second Stage Polymerisation Containing HEMA-MMA	183
5.3.1 Use of EGDMA Crosslinked Seed Particles	184
5.3.2 Use of GDMA Crosslinked Seed Particles	187
5.4 Second Stage Polymerisation Containing HEAm-MMA	192
5.5 Rationalisation of Results	196

5.5.1 Reaction Mechanism	198
5.5.2 Reactions Failing at High Polar Monomer Concentration	200
5.6 Focusing on Dumbbell-like Particles	201
5.6.1 Monomer Conversion Profile	202
5.6.2 Implications on Particle Size	202
5.7 Anisotropy of Samples	206
5.7.1 Proof of Janus Character – Fluorescence Spectroscopy	207
5.7.2 Proof of Janus Character – Selective Surface Functionalisation	209
5.8 Conclusions	212
5.9 References	213
6 Surface Charging and Zeta Potential	215
6.1 Introduction	216
6.2 Zeta Potential and Particle Size Measurement Theory by Light Scattering	216
6.2.1 Particle Size Measurements	216
6.2.2 Zeta Potential Measurements	218
6.3 Zeta Potential of Spherical Seed Particles	220
6.3.1 Switching Videos for Spherical Seed Particles	221
6.4 Zeta Potential of Particles with Increasing HEMA Content	222
6.4.1 Switching Videos for Dumbbell-like Particles	223
6.5 Zeta Potential of Particles with Increasing HEAm Content	224
6.6 Conclusions	225
6.7 References	226
7 Summary and Further Work	228
7.1 Introduction	228
7.2 Summary of Work	228
7.3 Further Work	232
7.4 References	234

8 Experimental	235
8.1 List of Materials	236
8.2 Characterisation Techniques	236
8.2.1 Nuclear Magnetic Resonance (NMR)	236
8.2.2 Total Solids Content (TSC) and Monomer Conversion	236
8.2.3 Gel Permeation Chromatography (GPC)	237
8.2.4 Particle Size and Zeta Potential Measurements	238
8.2.5 In-plane Switching Videos	238
8.2.6 SEM Imaging of Samples	239
8.2.7 Thermal Gravimetric Analysis (TGA)	239
8.2.8 Differential Scanning Calorimetry (DSC)	239
8.3 Synthetic Procedures	240
8.3.1 Formation of Uncrosslinked Spherical Particles	240
8.3.2 Formation of Crosslinked Spherical Particles	241
8.3.3 Seeded Non Aqueous Dispersion Polymerisation: Toward Different Particle Morphologies	242
8.3.4 “Locking on” of Physisorbed Polymeris Stabilier	245
8.3.5 Synthesis of Polymers for Modelling Studies by Solution Polymerisation	246
8.4 Characterisation of P(HSA-g-MMA) Polymeric Stabiliser	248
8.4.1 Molecular Weight of Stabiliser	249
8.4.2 ¹ H NMR Spectra	250
8.4.3 Thermal Characteristics	250
8.5 References	251
9 Appendices	252
9.1 GPC Traces for Modelling Polymer Substrates	253
9.2 ¹ H Spectra of Statistical Copolymers of P(MMA _x -co-HEMA _y)	256
9.3 Contact Angle vs. Time for Surface Energy Calculations	258
9.4 Contact Angle vs. Time for Monomer on Substrates under Dodecane	262
9.5 Seed Dispersions	265

9.6 DLS Traces for Monomer Swelling	267
9.7 Effect of Increasing Hydrophilic Crosslinker Concentration	269

Final word count: 48644

Table of Figures

Figure 1-1, a, an electrophoresis cell, b, display pixels in an electrophoretic display and c, an example of a final commercial device.	28
Figure 1-2, schematic view of a Gyicon device.	29
Figure 1-3, SiPix microcup design for an electrophoretic display.	30
Figure 1-4, E Ink dual particle system with microcapsules.	30
Table 1-1, list of the dielectric constants of common chemicals.	32
Figure 1-5, schematic diagram of the Helmholtz model showing the drop in electrical potential with distance.	35
Figure 1-6, schematic diagram of the Gouy-Chapman double layer and the electrical potential drop off with distance.	36
Figure 1-7, schematic representation of the Stern layer.	37
Figure 1-8, DLVO curve of interaction potential between two spheres.	38
Figure 1-9, schematic representing the excluded volumes associated with particle overlap present in steric stabilisation.	39
Figure 1-10, examples of graft (top) and block (bottom) copolymer stabilisers.	41
Figure 1-11, chemical structure of the P(HSA- <i>g</i> -PMMA).	41
Figure 1-12, schematic representation of a PMMA–latex particle, stabilized by a polymer with poly(12-hydroxystearic acid) hairs.	42
Figure 1-13, schematic view of the forces acting on a particle during electrophoresis.	43
Figure 1-14, optical images of; a, PMMA particles and b, PMMA particles with the additon of a AOT dispersed in dodecane.	46
Figure 1-15, the chemical structure of di-(2-ethylhexyl) sodium sulfosuccinate (AOT).	47
Figure 1-16, schematic view of a colloid particle being charged by reverse micelles, by adsorption to the particle surface.	50
Figure 1-17, schematic view of primary particle formation and growth in dispersion polymerisation.	53

Figure 1-18, role of dispersant in aiding nucleation growth; a, self-nucleation, b, aggregative nucleation, c, micellar nucleation and d, agglomeration.	56
Figure 1-19, SEM images of ellipsoids produced by ion beam bombardment, the dashed circle in a, represents the original spherical silica spheres and the arrow represents the direction of the ion beam.	57
Figure 1-20, schematic diagram of a device for stretching polymer films.	58
Figure 1-21, example of particles produced by Champion <i>et al.</i> where a, is the initial particles before stretching.	59
Figure 1-22, schematic diagram showing the wetting of the new monomer domain on the crosslinked particles surface.	60
Figure 1-23, schematic view of the forces affecting the swelling of a crosslinked polymer particle by monomer in water.	62
Figure 1-24, schematic view of work by Kim <i>et al.</i> , showing linear and perpendicular growth depending on the crosslinking densities of the material.	63
Figure 1-25, examples of how colloidal molecules can be used to represent molecules.	64
Table 2-1, approximate values for dispersion polymerisation reaction components.	72
Figure 2-1, schematic view of the P(HSA-g-MMA) steric stabiliser.	73
Table 2-2, half-life of Vazo-67 at various temperatures.	74
Figure 2-2, SEM images of supernatant liquid after sequential centrifugation steps (20 min at 2500 rpm) where; a, is 1 st , b, the 2 nd , c, the 3 rd and d, the final cleaned dispersion for comparison.	75
Figure 2-3, DLS traces for particles produced in different ratios of hexane and dodecane.	76
Table 2-3, average particle size by DLS.	76
Figure 2-4, reaction temperature profile and vazo-67 half-life during the polymerisation reaction for; a, SRB-088-0%xl in pure dodecane and b, SRB-077-0%xl in 2:1 hexane: dodecane solvent mixture.	78

Figure 2-5, resultant particles from changing the solvent system, a, SRB-088-0% xl with pure dodecane solvent and b, SRB-077-0% xl with a hexane/ dodecane solvent mixture.	79
Table 2-4, showing particle size and polydispersity data for dispersion SRB-088-0%xl and SRB-077-0%xl.	79
Figure 2-6, monomer conversion vs. time over the polymerisation reaction for; a, SRB-088-0%xl in pure dodecane and b, SRB-077-0%xl in 2:1 hexane: dodecane solvent mixture.	80
Figure 2-7, instability window proposed by Antl <i>et al.</i> for non-aqueous dispersion polymerisation reactions with respect to monomer concentration, the dashed lines show the boundary of the unstable region.	81
Figure 2-8, resultant particles with changing the monomer concentration where; a, is 10 wt. % monomer, b, 20 wt. %, c, 30 wt. %, d, 35 wt. %, e, 40 wt. % and f, 50 wt. % monomers.	82
Figure 2-9, size distributions for resultant particles with changing the monomer concentration where; a, is 10 wt. % monomer, b, 20 wt. %, c, 30 wt. %, d, 35 wt. %, e, 40 wt. % and f, 50 wt. % monomers.	83
Table 2-5, particle size and coefficient of variation measurements for the dispersions of increasing monomer concentration.	83
Figure 2-10, resultant particles when dispersion polymerisation is run at 60 wt. % monomer and size distribution plot.	84
Figure 2-11, schematic view of the dispersion polymerisation mechanism.	85
Figure 2-12, resultant particles with increasing EGDMA concentration by the batch method with; a, 0 wt. %, b, 0.5 wt. %, c, 1.0 wt. %, d, 1.5 wt. %, e, 2 wt. %.	86
Figure 2-13, SEM micrographs of resultant particles with crosslinking monomer added before t_c left, at t_c , centre and after t_c , right which correspond to SRB-254-1% EGDMA, SRB-325-1% EGDMA and SRB-043-1% EGDMA.	87
Figure 2-14, monomer conversion and particle size vs time for SRB-091-1% EGDMA with lines of best fit to exemplify the inflection point.	88

Figure 2-15, SEM micrographs of the reaction mixture for SRB-091-1% EGMDA at selected times, a $t = 5$, b $t = 8$, c $t = 9$, d $t = 10$, e $t = 13$.	89
Figure 2-16, transmitted light of wavelength 550 nm vs. time for the reaction, for SRB-145-0%xl.	90
Figure 2-17, transmitted light at t_c at a wavelength of 550 nm, for different polymerisation reactions.	91
Figure 2-18, resultant particles for SRB-101-1% EGMDA after 1 wt. % EGDMA was injected into the reaction vessel at t_c .	92
Figure 2-19, resultant particles for SRB-113-1% EGMDA after 1 wt. % EGDMA was injected into the reaction vessel at t_c .	93
Figure 2-20, showing DLS results for SRB-113-1% EGMDA and the sample diluted by a factor of four in THF.	94
Table 2-6, showing the z-average diameter of SRB-113-1% EGDMA before and after THF dilution.	94
Figure 2-21, DSC traces for samples of increasing crosslinker concentration, where; a, is SRB-118-0% xl, b, is SRB-202-1% EGDMA, c, is SRB-133-2% EGDMA and d, is SRB-135-3% EGDMA.	95
Table 2-7, showing the glass transition temperatures of samples of increasing EGDMA content.	95
Figure 2-22, effect of increase the EGDMA concentration on particle size and morphology, with; a, SRB-131-1% EGDMA, b, SRB-133-2% EGDMA, c, SRB-135-3% EGDMA and SRB-5% EGDMA.	97
Table 2-8, particle size measurements and coefficient of variation on dispersions with increasing EGDMA content.	98
Table 2-9, Alternative crosslinking monomers used to produce spherical particles.	98
Table 2-10, particle size measurements and coefficient of variation for particles produced with different crosslinkers.	99
Figure 2-23, 1 wt. % crosslinked particle dispersions with different crosslinkers; a, BDDMA, b, HDDMA, c, GDMA and d, GDGDA.	100

Figure 2-24, showing SEM images and size distribution plots of dispersions before and after chemical attachment of the P(HSA-g-MAA) stabiliser to the particle surface, where; a, is SRB-326-1% GDMA before attachment and b, after attachment.	101
Table 2-11, showing particle size data for SRB-326-1% GDMA before and after chemical attachment of the stabiliser.	101
Figure 3-1, schematic view of how the dynamic swelling method proceeds, from seed particles to doublet particles.	105
Figure 3-2, showing the extreme particle architectures	107
Figure 3-3, schematic representations of solutions to equations 3-2, 3-3 and 3-4 predicting particle morphologies by summing the total interfacial energy of the system.	108
Figure 3-4, schematic view of sessile drop interactions at the three phase point as described by the Young equation.	109
Figure 3-5, example Teas plot for the solubility window of a given polymer.	111
Figure 3-6, ternary plot of different solvents based on their Hansen solubility parameters.	113
Figure 3-7, chemical structure of MMA, HEMA and HEAm.	113
Table 3-1, Hansen solubility parameters for the second stage monomers, with radii of interaction calculated against PMMA and dodecane.	114
Figure 3-8, contact angle vs. time for MMA, HEMA and HEAm on a PMMA substrate.	115
Table 3-2, molecular weight data for the different polymers used to model particle-monomer interactions.	116
Figure 3-9, ¹ H NMR spectra of P(MMA _{60-co} -HEMA ₄₀), inset shows comparison of other polymers for compositional analysis based upon the ratio between the peaks.	117
Table 3-3, copolymer compositional analysis for the statistical copolymers synthesised.	117

Figure 3-10, schematic view of measuring the surface energy of a substrate, the solid-air interfacial tension, with the experimentally measured contact angle in grey, the calculated interfacial tension in bold and the known liquid surface tension shown.	119
Table 3-4, surface tension components for given solvents.	119
Figure 3-11, sessile drops of water (left) and diiodomethane (right) after 1 s contact on a PMMA-35 <i>KDa</i> substrate.	120
Figure 3-12, contact angle vs. time plot and drop volume vs. time plot, for water and diiodomethane on a PMMA-35 <i>KDa</i> substrate.	120
Table 3-5, average advancing contact angles formed by the probe liquids on polymer substrates.	121
Table 3-6, calculated surface energies, γ_s , of polymer substrates.	122
Figure 3-13, characteristics of measuring surface tension by the pendant drop method.	124
Figure 3-14, schematic view of measuring the monomer-dodecane interfacial tension, shown in bold.	124
Figure 3-15, pendant drops formed between the liquid and air for a, water, b, HEMA and c, HEAm and the liquid and dodecane for; d, water, e, HEMA and f, HEAm.	125
Table 3-7, the monomer-dodecane interfacial tension, $\gamma_{L,D}$, measured by pendant drop method.	125
Table 3-8, monomer-dodecane interfacial tension measured by Du Noüy ring method.	126
Figure 3-16, schematic view of how the monomers may acts surfactant-like molecules in dodecane where; a, shows HEMA-dodecane, b, HEAm-dodecane and c, water-dodecane with polar units shown in blue.	126
Figure 3-17, schematic view of experimentally measuring the dodecane-substrate contact angle, in grey and calculating the dodecane-substrate interfacial tension, bold, and known values shown.	127
Figure 3-18, images showing the dodecane contact angle after 1 s on substrates of; a, PMMA-28 <i>KDa</i> , b, PMMA-35 <i>KDa</i> , c, P(MMA ₉₈ -MAA ₂) and d, P(MMA ₉₈ -MAA ₂)-stabiliser.	128

Table 3-9, dodecane-substrate contact angles and calculated dodecane-substrate interfacial tension.	129
Figure 3-19, schematic view of measuring the contact angle formed between monomer and substrate under dodecane, in grey and known values shown.	130
Figure 3-20, contact angle vs. time, a, and drop volume vs. time, b, for HEMA, HEAm and water on a PMMA-35 <i>KDa</i> substrate.	130
Table 3-10, equilibrium advancing contact angles for monomers and water on different polymer substrates	132
Figure 3-21, schematic view of calculating the monomer-substrate interfacial tension submerged in dodecane, in bold and known values shown.	132
Table 3-11, calculated interfacial tension between substrate and monomer droplet, $\gamma_{S.L}$.	133
Table 3-12, results from calculating the expected particle morphology.	134
Figure 3-22, expected particle morphologies after polymerisation for HEMA, HEAm and MMA.	136
Figure 4-1, seed dispersion, SRB-325-1% EGMDA and size data, based on counting 100 particles.	140
Figure 4-2, monomer conversion vs. time plot for seed particle formation (1 st stage), SRB-077-0%xl and second stage reaction, SRB-409-1% EGDMA.	142
Figure 4-3, SEM images and size distributions for resultant dispersions when the monomer feed was added at; a, 30 min., b, 1 hr., and c, 4 hr.	144
Table 4-1, particle size data for dispersions produced for varying the monomer / particle mixing time.	144
Figure 4-4, SEM images and size distribution plots for reactions with varied monomer / particle ratios, where; a, 1:1, b, 2:1, c, 4:1 and d, 5:1.	145
Table 4-2, particle size data for dispersions which the monomer/ particle ratio was changed.	146
Figure 4-5, SEM images and size distributions for resultant dispersions when the monomer / particle mixing time.	147
Table 4-3, particle size data for dispersions shown in Figure 4-5.	147

Table 4-4, DLS data for MMA swelling of seed particle dispersion SRB-131-1% EGDMA.	149
Figure 4-6, DLS traces for monomer swelling experiments, 2:1 monomer / particle ratio.	150
Figure 4-7, schematic representation of the equilibrium between the MMA monomer penetrating the particle and staying in solution.	151
Table 4-5, Hansen solubility parameters for MMA, ethyl acetate and butyl acetate against PMMA and dodecane.	151
Figure 4-8, proposed reaction mechanism based upon precipitation of growing polymer chains to a particle surface.	152
Figure 4-9, mechanism for the formation of colloidal clusters, based upon a heterogeneous nucleation route. Showing (i) coalescence, (ii) nuclei expulsion and (iii) nuclei mutual repulsion.	153
Table 4-6, list of the crosslinking monomers of increasing hydrophilicity.	154
Figure 4-10, Teas plot for the crosslinking monomers along with PMMA, MMA and Dodecane for comparison. The dashed circle is a representation of the solubility sphere for PMMA.	155
Table 4-7, calculated solubility parameters for the monomers used and the relative energy difference against dodecane, in order of decreasing interaction.	156
Figure 4-11, schematic representation of different polymer architectures which could be formed in a copolymerisation reaction.	157
Table 4-8, reactivity ratios for MMA – equivalent monomer.	159
Figure 4-12, SEM images for reactions containing 1 wt. % polar monomer in the second stage reaction with; a, a no crosslinker comparison, b, EGDMA, c, GDMA, d, AHPMA and e, GDGDA.	161
Figure 4-13, Size distribution graphs for dispersions containing 1 wt. % polar monomer in the second stage reaction with; a, no crosslinker for comparison, b, EGDMA, c, GDMA, d, AHPMA and e, GDGDA.	162
Table 4-9, particle size data for dispersions shown in Figure 4-12, with the seed dispersion shown in italics.	163

Figure 4-14, SEM images and size distribution plots for dispersions with varying chain transfer agent concentration; a, 0 wt. %, b, 1 wt. %, c, 2 wt. % and d, 4 wt. % of monomers.	165
Table 4-10, particle size data for dispersions shown in Figure 4-14.	166
Figure 4-15, SEM images and size distribution plots for dispersions with varying total solids content in the seed dispersion where; a, is 1 % solid (SRB-348-1% GDMA), b, is 5 % solid (SRB-346-1% GDMA), c, is 10 % solid (SRB-350-1% GDMA) and d, is 20 % solid (SRB-347-1% GDMA).	167
Table 4-11, particle size data for dispersions shown in Figure 4-15.	168
Figure 4-16, SEM images and size distribution plots for dispersions with; a, 1 wt. % GDMA b, 2 wt. % GDMA and c and d, with equivalent moles of HEMA in the second stage polymerisation.	169
Table 4-12, particle size data for dispersions shown in Figure 4-16.	170
Figure 4-17, showing the effects of varying the chain transfer and initiator concentration from Elsesser <i>et al.</i>	171
Figure 4-18, SEM images of resultant particles from sequential shell-growth steps with the inclusion of 1 wt. % EGDMA and size distribution plots.	173
Table 4-13, particle size data for dispersions shown in Figure 4-18.	174
Figure 4-19, SEM images and size distribution plots for resultant dispersions after sequential second stage polymerisation reactions with 1 wt. % GDMA in the feed, where; a, is the first, b, the second and c, the third consecutive polymerisation reaction.	175
Table 4-14, particle size data for dispersions shown in Figure 4-19.	176
Figure 4-20, SEM images and size distribution plots for resultant dispersions after sequential second stage polymerisation reactions with 1 wt. % EGDMA in the first polymerisation and then 1 wt % GDMA in the others.	177
Table 4-15, particle size data for dispersions shown in Figure 4-20.	178
Table 5-1, Hansen solubility parameters for PMMA, MMA, HEMA and HEAm.	182

Figure 5-1, SEM images of reactions with increasing HEMA concentration in the monomer feed with an EGDMA crosslinked seed particle.	184
Figure 5-2, size distribution plots for reactions with increasing HEMA concentration in the monomer feed with EGDMA crosslinked seed particles.	185
Table 5-2, particle size data and aspect ratio for particles with increasing HEMA concentration in the monomer feed and EGDMA crosslinked seed particles.	186
Figure 5-3, SEM images of reactions with increasing HEMA concentration in the monomer feed with an GDMA crosslinked seed particles.	188
Figure 5-4, size distribution plots for reactions with increasing HEMA concentration in the monomer feed with GDMA crosslinked seed particles.	189
Table 5-3, particle size data and aspect ratio for particles with increasing HEMA concentration in the monomer feed and GDMA crosslinked seed particles.	190
Figure 5-5, SEM images and particle size data for SRB-293-HEMA.	191
Figure 5-6, SEM images of reactions with increasing HEAm concentration in the monomer feed with an GDMA crosslinked seed particles	193
Figure 5-7, size distribution plots for reactions with increasing HEMA concentration in the monomer feed with GDMA crosslinked seed particles.	194
Table 5-4, particle size data for particles with increasing HEAm concentration in the monomer feed and GDMA crosslinked seed particles.	195
Table 5-5, Hansen solubility parameters of statistical copolymers of P(MMA _x -co-HEMA _{100-x}) and P(MMA _x -co-HEAm _{100-x}) with radius of interaction and relative energy difference calculations against PMMA.	197
Figure 5-8, ternary plot shown the Hasen parameters for MMA, PMMA and HEAm, with prediction for MMA –HEAm mixtures	198

Figure 5-9, mechanism for the formation of colloidal clusters, based upon a heterogeneous nucleation route.	199
Figure 5-10, droplets formed when; a, HEMA and b, HEAm, is mixed in dodecane in the presence of particle and the P(HSA-g-MMA) stabiliser, under reaction concentrations.	200
Figure 5-11, SEM image of pseudo-suspension polymerisation of HEAm occurring in SRB-411-60% HEAm.	201
Figure 5-12, monomer conversion profile for SRB-413-40% HEMA.	202
Figure 5-13, schematic view of treating dumbbell-like particles as two touching spheres.	202
Figure 5-14, showing the measurement of the lobe ratio which can be done by, a, measuring across the whole particle width and b, along the length of the whole particle.	203
Table 5-6, showing measured and expected lobe ratio, r_{seed}/r_{lobe} .	204
Table 5-7, showing the difference between experimentally measured lobes in dumbbell-like particles compared to the seed particles.	204
Table 5-8, glass transition temperatures of homopolymers and polymer blends estimated from the Fox equation.	205
Figure 5-15, SEM images of a, SRB-364-40% HEMA and b, SRB-395-40% HEAm.	206
Figure 5-16, schematic view of particles resulting from a second stage polymerisation where; a, is an ideal core-shell particle, b and c, show deviations from ideal.	208
Figure 5-17, chemical structure of a, vinyl anthracene and b, vinyl naphthalene.	208
Figure 5-18, SEM images and particle size data for, a, seed dispersion containing 1 wt. % vinyl anthracene and b, second stage polymerisation containing 40 wt. % HEMA and 1 wt. % vinyl naphthalene.	209
Table 5-9, particle size data for fluorescent particles produced.	209
Figure 5-19, reaction of chlorosilane to a surface with free hydroxyl groups.	210
Figure 5-20, chemical structure of 1H,1H,2H,2H-perfluorodecyl trichlorosilane.	210

Figure 5-21, SEM images and particle size data for, a, seed dispersion containing 40 wt. % HEMA and b, surface treatment with perfluoro silane.	211
Table 5-10, particle size data for particles before and after surface treatment with perfluoro silane.	211
Figure 6-1, chemical structures of charging surfactants where; a, the positive charging agent sorbitan trioleate, Span 85 and b, the negative charging agent dioctyl sodium sulfosuccinate, AOT .	216
Figure 6-2, intensity of scattered light as function of time for, a, small particles and b, large particles, c shows the autocorrelation function for larger particles, 1 and small particles, 2.	217
Figure 6-3, schematic view of principal features of a LDE experiment.	218
Figure 6-4, phase plot for; a negatively charge aqueous polystyrene latex, top, and a non-aqueous PMMA sample with (green) and without (red) charging surfactant (3 wt. % AOT), bottom.	219
Figure 6-5, SEM images of dispersions, a, SRB-131-1% EGDMA and b, SRB-288-1% GDMA.	220
Table 6-1, zeta potential data for crosslinked spherical seed particles, run at 20 V.	220
Figure 6-6, still images of particle switching taken at 1 s intervals for SRB-131-1% EGDMA where; a, is at t = 0 s, b, is at t = 1 s, c, is at t = 2 s... Formulation is 3 wt. % particles 3 wt. % AOT charging surfactant and is driven at a 120 V.	221
Figure 6-7, still images of particle switching taken at 2 s intervals for SRB-288-1% GDMA where; a, is at t = 0 s, b, is at t = 2 s, c, is at t = 4 s... Formulation is 3 wt. % particles 3 wt. % Span 85 charging surfactant and is driven at a 120 V.	222
Figure 6-8, SEM images of, a, SRB-344-1 % HEMA, b, SRB-364-40 % HEMA and c, SRB-293-HEMA particles.	223
Table 6-2, zeta potential data for particles of increasing HEMA content, run at 20 V.	223

Figure 6-9, still images of particle switching taken at 2 s intervals for SRB-293-HEMA where; a, is at t = 0 s, b, is at t = 2 s, c, is at t = 4 s... Formulation is 3 wt. % particles 3 wt. % Span 85 charging surfactant and is driven at a 120 V.	224
Figure 6-10, SEM images of resultant particles after second stage polymerisation with; a, 1 w.t % HEAm in the monomer feed and b, 40 w.t % HEAm in the monomer feed.	225
Table 6-3, zeta potential data for particles of increasing HEAm content, run at 20 V.	225
Figure 6-11, schematic view of non-uniform charging.	226

Copyright Statement

- i. The author of this thesis (including any appendices and/or schedules to this thesis) owns certain copyright or related rights in it (the “Copyright”) and s/he has given The University of Manchester (the “University”) certain rights to use such Copyright, including for administrative purposes.
- ii. Copies of this thesis, either in full or in extracts and whether in hard or electronic copy, may be made only in accordance with the Copyright, Designs and Patents Act 1988 (as amended) and regulations issued under it or, where appropriate, in accordance with licensing agreements which the University has from time to time. This page must form part of any such copies made.
- iii. The ownership of certain Copyright, patents, designs, trademarks and other intellectual property (the “Intellectual Property”) and any reproductions of copyright works in the thesis, for example graphs and tables (“Reproductions”), which may be described in this thesis, may not be owned by the author and may be owned by third parties. Such Intellectual Property and Reproductions cannot and must not be made available for use without the prior written permission of the owner(s) of the relevant Intellectual Property and/or Reproductions.
- iv. Further information on the conditions under which disclosure, publication and commercialisation of this thesis, the Copyright and any Intellectual Property and/or Reproductions described in it may take place is available in the University IP Policy (see <http://www.campus.manchester.ac.uk/medialibrary/policies/intellectualproperty.pdf>), in any relevant Thesis restriction declarations deposited in the University Library, The University Library’s regulations (see <http://manchester.ac.uk/library/aboutus/regulations>) and in the University’s policy on presentation of Theses

Abstract

The University of Manchester, Faculty of Engineering and Physical Sciences

Sean Butterworth

A thesis submitted for the degree of Doctor of Philosophy

Shape and Chemical Anisotropic Particles in Low Dielectric Constant Media

Date: 2nd April 2013

Electrophoretic displays (EDPs) are an attractive low power technology for small to large area displays. Such display technology has seen a surge of research interest with the launch of successful e-readers in the market place, owing to their lower power consumption and paper-like quality. This work aims to look at the influence of shape on the electrophoretic mobility of particles for such devices.

Crosslinked poly(methyl methacrylate) (PMMA) precursor particles with a narrow size distribution were produced by non aqueous dispersion polymerisation utilising a pump-feed method. To produce shape anisotropic particles an adapted version of the dynamic swelling method for polar media was chosen. Suitable monomers were screened by the use of Hansen solubility theory to find monomers which interact with PMMA but not the solvent. It was found that 2-hydroxyethyl methacrylate (HEMA) and *N*-hydroxyethyl acrylamide (HEAm) were two such suitable monomers, methyl methacrylate (MMA) was also used as a control series.

It was found that cluster-like particle morphologies could be produced by the MMA system by the inclusion of small quantities of crosslinking monomer. This was due to precipitation of higher molecular weight polymer segments to the seed particle surface. The cluster-like morphology could be enhanced by use of a polar crosslinking monomer and by sequential reactions. For the polar system, it was found that the reactions with pure monomer were unclear, due to the solubility mismatch of the monomer and the solvent system. This was overcome by a copolymerisation with MMA. The system showed different particle morphologies could be produced by varying the polar monomer content. In one case a sample of pure dumbbell-like particles could be produced. These dumbbell-like particles are thought to be chemical as well as shape anisotropic owing to monomer composition.

EPD evaluation for the particles was undertaken and showed that all particles can become highly charged in low dielectric constant media, but that the shape anisotropic particles are prone to adsorption to the cell walls and electrodes.

The work outlined in this thesis shows the first reporting of shape anisotropic polymeric particles produced in low dielectric constant solvents system.

Declaration

No Portion of this work referred to in this thesis has been submitted in support of an application for another degree or qualification of The University of Manchester or any other university or any other institute of learning.

Sean Butterworth, 2nd April 2013

Acknowledgements

I would first like to thank my supervisors Prof. Steve Yeates and Prof. Brian Saunders for all the help over the years, not only for academic help, but for all the proof reading, of my thesis, and the many presentations I've had to give over the years and for putting up with me on the train for hours to Chilworth.

I would also like to thank, Dr. J. Henry Wilson, Dr. Lousie Farrand, Dr. Roger Kemp and Dr. Mark Goulding at Merck for the opportunities to work at Chilworth and all the useful discussions, particularly on the particle charging front. My thanks also go to everyone at Merck Chilworth and all attendees at the Merck CASE conferences for making them an enjoyable time.

I cannot write my acknowledgements without thanking the people at OMIC and Manchester in no particular order; Dave Crouch for telling us all the same five stories "that reminds of a time when...", Pete Wills for working at the same pace as me throughout constantly comparing who's done more and the many laughs over the years, Seb Sprick for being the OMIC work horse and the keeper of the quotes list, Pete Deakin for many nights on the beers in Manchester or on conferences, Chris Muryn and Scott Lewis for helping me out in my time of need when all were SEM's were broken or busy, Helen Wright for laughs in the lab and Jon Behrendt for useful discussions and being a good house mate for two years, finally to all the support staff in the chemistry department and especially Emma for having the chemistry café open in the morning and learning all our orders.

I would also like to thank my family in particular my mum and dad for unwavering support of everything I've done and not just in my academic life, the same goes to Simon, although he may show it in his own way!

Finally Laura for having to put up with me at home when driven crazy by the lack of human contact, proof reading, keeping me sane and just being there.

1 Introduction

1.1 Opening Statement

In life displays are everywhere, from billboards to computer screens to digital watches and mobile phones. The technology behind such displays is ever advancing, in particular improving picture quality, producing light weight and more energy efficient screens for TV's and computers. However it is becoming increasingly important to produce mobile products, i.e. tablet computers and smart phones. This then requires a mobile power source capable of running the product; this is problematic when using new technology in which the battery can only last a few days without charging.

Bistable displays, a display in which power is only applied to change the image, have an edge over competition as they can be charged infrequently due to their bistable nature. These displays may not be able to play video media, and tend to be monochrome, but are perfect for still images. This opens up the application for many areas, and recent years have seen the rise of the Amazon Kindle and other e-readers. However this is only one application, bistable displays have been used in many products, from low end mobile phones, to watches and USB flash drives to indicate the amount of storage space left. In the future when bright vibrant full colour displays can be produced large area signage could be replaced with interactive low power billboards which are sent data wirelessly.

This is a EPSRC CASE sponsored Ph.D. project with Merck's advanced technologies wing, in Chilworth, Southampton and the Organic Materials Innovation Centre (OMIC) at the University of Manchester. Merck are working towards new fluids to be used for electrophoretic displays, in particular full colour systems, which can be sold direct to the manufacturer to be built into their devices. This project will be concerned primarily with the effect of shape and structure of nanoparticles rather than colour.

1.2 Bistable Display Technology

Bistable display technology has attracted a great deal of attention in recent years with the success of electronic books and e-readers in the market place, such as the Amazon Kindle. However the use of such technology is not only limited to electronic books, and can be applied to any situation where the display of information is required, such as signage. A

bistable display is able to display an image with or without power being applied to the device. A classic example of such a device is an electrophoretic display which works on the principle of moving charged particles in an applied electric field from one side of the display to the other. Figure 1-1 below shows the idea behind electrophoretic display, from electrophoresis to final marketable device.

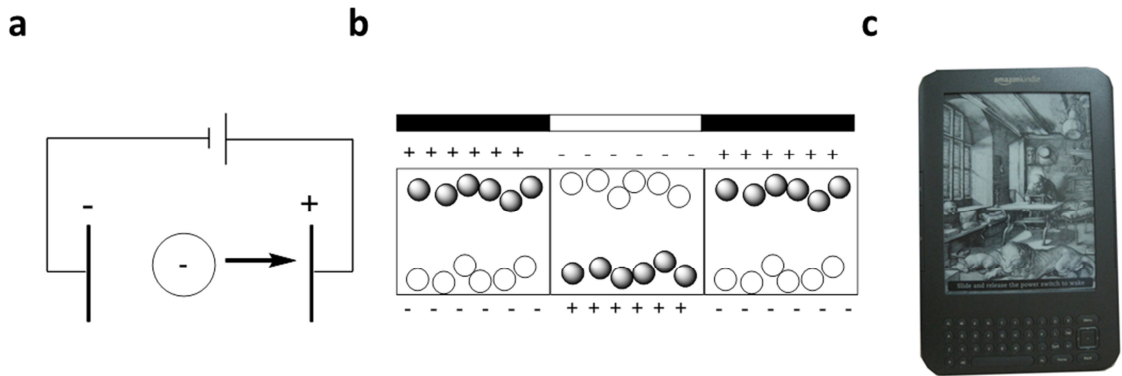


Figure 1-1, showing a, an electrophoresis cell in which a negative particle moves to the positive electrode, b, display pixels in an electrophoretic display which utilise the movement of particles to build an image, and c, an example of a final commercial device, the Amazon Kindle.

The technology has only been available in monochrome until recently with the launch of the E Ink Triton Imaging Film.¹ Monochrome images are built up by using white reflective particles and black absorbing particles in different pixels to produce an image, the new E Ink Triton Imaging Film works by having a colour filter on top of the display pixels to allow the reflection of coloured light and not just white light; this is mounted above the display pixel screen.¹ The problem with using a colour filter however is that it will obviously cut back on the reflected light intensity as a large proportion of the incident light will be absorbed as it passes through the filters. This means a bright full colour display by this method is not easy to achieve without back lighting.

1.2.1 Cell Designs

An image is produced by an electrophoretic display, by the movement of particles from one side of the pixel / cell to the other. These particles then interact with any incoming light through the front of the display passing through a transparent electrode. The light is

then scattered back out of the display to give a white reflective pixel or absorbed to give a black pixel. The particles can be held at the front, back or at points in the middle of the display pixel, by the use of extra electrodes, allowing for degrees of grey scale into any image produced.

1.2.1.1 Gyricon Design

A Gyricon device was the first example of e-paper and was developed by Xerox in the 1970's.² The device contains particles which are encapsulated and filled with an oil to allow movement. The particles have two different contrasting hemispheres, one black and one white, which are also charged oppositely.³ The different charge allows the particles to rotate to face the opposite electrode to build a monochrome image. A schematic view of a Gyricon device is shown below.

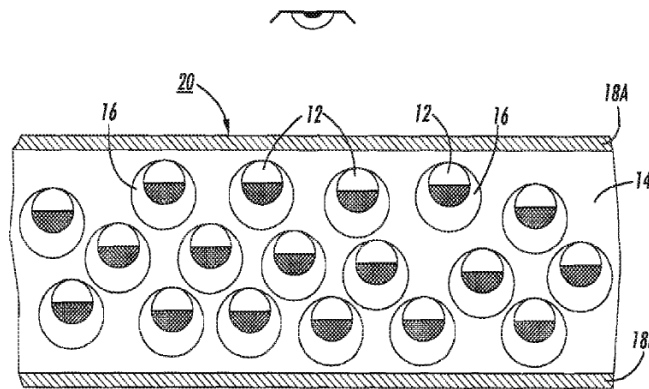


Figure 1-2, schematic view of a Gyricon device, with the Gyricon particles suspended in liquid capsules allowing free rotation.⁴

Gyricon Particles are examples of Janus particles, Janus particles deriving their name from the two faced Roman god Janus, and refers to particles which have two differing sides. In this case chemically different, and charge different from one hemisphere to the other.

1.2.1.2 SiPix Microcup Design

The SiPix cell only uses white reflective particles which are dispersed into a fluid containing a dissolved black dye. Each display pixel is sandwiched between two electrodes, this is then mounted onto a ridged backplane. One of the electrodes must be transparent i.e. indiumtin oxide (ITO) to allow light to enter the system. The SiPix system incorporates a 'microcup' design shown in Figure 1-3, this allows for easy roll-to-roll production.

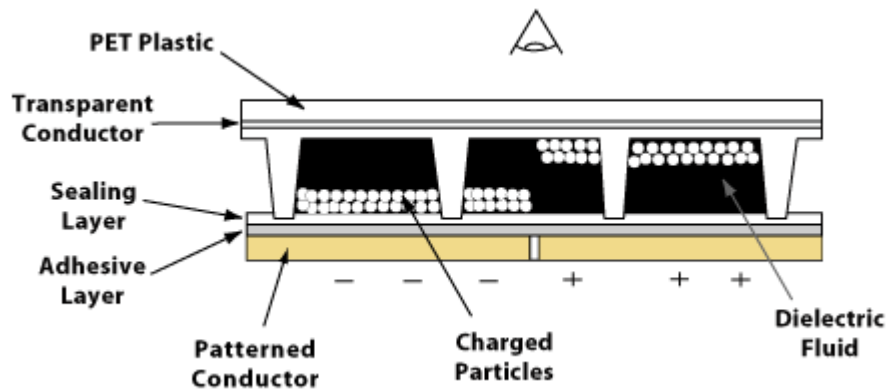


Figure 1-3, SiPix microcup design for an electrophoretic display.⁵

1.2.1.3 E Ink Dual Particle System

The E ink system consists of two types of particles dispersed into a fluid, one positively charged the other negatively charged; this suspension is then added into microcapsules along with other stabilising and charging additives. This dual particle system allows for ease of grey scale incorporation and the microcapsule design can enable the displays to be completely flexible.⁶ Figure 1-4 below shows a schematic view of the E Ink microcapsule technology, which as with the SiPix design the particles are sandwiched between electrodes with the top being a transparent ITO electrode.

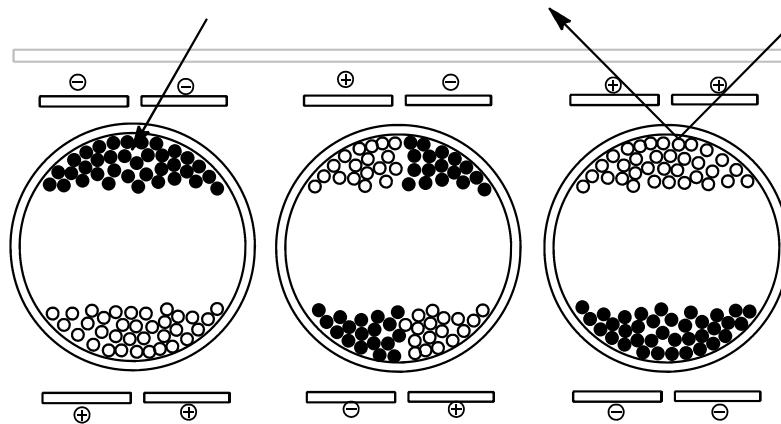


Figure 1-4, E Ink dual particle system with microcapsules.⁷

The microcapsules are produced by taking the desired particle formulation in a hydrocarbon solvent and a reactive oil soluble species, such as dodecane epoxide. This mixture is then emulsified and the now viscous fluid is spread over a substrate. This

substrate can be one of the electrodes; a polymerisation reaction is then initiated forming the microcapsules. This mixture is then sandwiched with another electrode, which squashes the layer of microcapsules removing excess of the electrophoretic 'ink' and any air.⁸

The microcapsules produced for the E Ink system are designed to have a refractive index that matches the oil within the particles. This enables the system to appear more optically transparent again aiding higher contrast ratios. The contrast ratio is the contrast difference between a white and black pixel, the higher this ratio the greater the paper-like feel the device will have. Having a high contrast ratio also gives a wider viewing angle.

1.2.2 Material Requirements for Electrophoretic Displays

All electrophoretic display devices work on the same idea of moving charged particles through a fluid to scatter or absorb light at a specific interface. However the materials used are required to have certain characteristic features. First each display pixel must have a number of electrodes, one at the top, which is optically transparent and another at the bottom. Each pixel must be filled with a fluid with a low dielectric constant, such as a long chain hydrocarbon, which must also be non-volatile and inert so it will not become oxidised by the electrodes. The need for a low dielectric medium in the pixel is to allow a constant electric field to develop between the electrodes. If a polar medium i.e. water, with dielectric constant, $\epsilon = 78.3$,⁹ is used then the electric field strength will drop significantly as a function of distance due to the ability for the water molecules to screen the charge. However if an oil is used i.e. dodecane $\epsilon = 2.0$,⁹ there is no screening of the charge so the full electric field strength can be felt across the length of the cell. A list of dielectric constants of common solvents is shown below.

Table 1-1, list of the dielectric constants of common chemicals.¹⁰

Solvent	Dielectric Constant, ϵ (at 298K)
Water	78.3
Ethanol	24.3
<i>i</i> -Butanol	18.3
Cyclohexanol	17.0
Chloroform	4.8
Tetralin	2.8
Dodecane	2.0
Cyclohexane	2.0
Hexane	1.9

1.2.2.1 Particle Requirements

Particles used in an electrophoretic display must have certain characteristic features in order to function effectively in the display.

Size: First these particles must be sub-micron in diameter so that when they pack together at an electrode allowing them to efficiently scatter light. The size is also important as it is directly linked to the density of the particles. In order to be bistable particle must not appreciably settle, which is a problem for particles of high density.

Poly(methyl methacrylate) (PMMA) has a density¹¹ 1.19 g/cm³, whereas dodecane has a density¹² of 0.746 g/cm³. This difference allows for the potential settling of particles over short time scales. The rate at which particles sediment out of suspension can be approximated by the Stokes-Einstein relationship, this equation takes into account the densities of each component, along with factors such as particle size and the viscosity of the fluid. The Stokes-Einstein equation of particles settling is given in equation 1-1.

$$v = \frac{(\rho_p - \rho_f)gr^2}{9\eta} \quad 1-1$$

Where, v , is settling rate, ρ_p and ρ_f , being the density of the particle and fluid respectively, g is acceleration under gravity, r , the particle radius and η , is the viscosity of the fluid.

Refractive index: This is a very important attribute as if the scattering is not high enough then the contrast of the overall image will not have a paper like quality. Pigment particles have been used such as titanium dioxide for its high refractive index ($n = 2.5$)¹³ and its natural white reflective colour. However such inorganic pigment particles have been known to have problems with adsorption to the electrode walls of the display cell, due to the high electrode and particle interactions for metal oxide pigments. Polymeric materials such as poly(methyl methacrylate) (PMMA) are also widely used but have lower refractive indices ($n = 1.5$)¹⁴ however they do not suffer from the problem with adsorption to the electrode walls to the same extent.

Core shell systems have also been researched for example polymer encapsulated pigment such as TiO₂-polystyrene core shell particles.¹⁵ These particles will not suffer from adsorbing to the electrode walls and will also have a high refractive index. This high refractive index is crucial to the working of the device. Although the colour of the particles is important the ability of the particles to scatter light effectively is just as important. Using particles of titanium dioxide with a refractive index of $n = 2.5$ gives a difference in optical refractive index with the surrounding dielectric liquid of $\Delta n = 1.3$, giving a very short scattering length of a few microns¹⁶ in comparison with a liquid crystal display $\Delta n < 1$ allowing for very high contrast ratios and viewing angles which gives the paper like quality to the device.

Charge: The particles must also be charged in order for them to move electrophoretically across the display. In order to achieve this charging additives such as polybutene-succinimide (PBS) are added to the dielectric solution to give the particles a net charge. PBS has been found to give a negative charge to TiO₂ in cyclohexane with a zeta-potential of over -50 mV.¹⁴

Size distribution: One final attribute which is required for the colloidal particles in these devices is that they must be roughly monodisperse with respect to size, this will allow for uniform packing of the particles at the electrode interface.

1.3 Colloidal Materials

Colloidal materials are a two phase system with one phase dispersed in another. The dispersed phase can be droplets of liquid, solid particles or air bubbles, and the continuous phase can be a liquid solvent or solids and gases. 'Colloidal materials' is a very general terms which encompasses a very large range of products such as; paints, cosmetic items such as toothpaste and shampoo and liquid detergents. Colloidal particles are small typically in the 10's of nm to 100 μm in size; as such they have a high surface area to volume ratio.

1.3.1 Colloidal Stability

As a consequence of the particle size of colloidal material colloids are not inherently stable. As the particles are subject to multiple collisions due to Brownian motion or when under shear, such as mixing, they interact frequently. Due to this it is important to understand what happens during collisions, taking into account the large surface area to volume ratio of colloidal particles. Particles which collide together will interact and can form aggregates. Such aggregates can be split into coagulation and flocculation. Coagulation generally forms an irreversible densely packed 'coagulum', whereas flocculation forms loosely held 'flocs' which in most cases can be broken up by mixing or shaking of the sample. In order to prevent this colloidal material must be stabilised against aggregation by the use of charged groups, or large steric layers.

1.3.1.1 *Electrostatic Stabilisation*

When charged particles are suspended in an liquid such as water charged species can be stabilised against recombination due to the fact that they will be solvated leading to the charge on the particle being shielded by a diffuse double layer of charges. This ability to shield the charge on the particles by the electric double layer is paramount in order to stabilise any charged dispersion toward aggregation and coagulation.

1.3.1.1.1 The Helmholtz Model

This simple picture was proposed in 1879 by Helmholtz¹⁷ and consists of simple monolayers of charged counterions. The Helmholtz model says that a monolayer of counter ions will line up on the surface of the particle which can be treated as a solid to counter act the charge on the particle. The separation distance between the counterions, δ ,

and the surface will be the hydration sphere of each ion. This then has the implication that all the electrical potential, ψ , of the particle surface will drop to zero across this distance δ , shown in Figure 1-5.

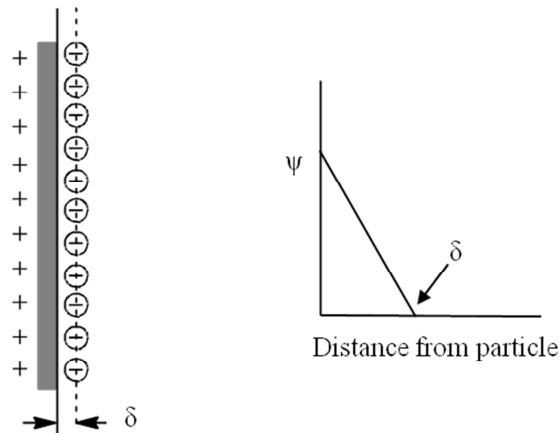


Figure 1-5, schematic diagram of the Helmholtz model showing the drop in electrical potential with distance.

1.3.1.1.2 The Gouy-Chapman Model

The Gouy-Chapman model builds on the Helmholtz model by introducing the idea of a diffuse electrical double layer and not a fixed layer of counterions on the surface.^{18,19} The model states that the double layer is not fixed as it should be removed by diffusion of particles under thermal motion, as it would want to make a uniform concentration of ions in solution and not have a high concentration at the surface of the particle. So an equilibrium will exist between the electrical potential of the particle surface and the counterions induced by random Brownian motion. This will give rise to a potential gradient from the surface of the particle until its electrical potential is completely neutralised by associated counterions. This diffuse double layer and the potential gradient is shown schematically in Figure 1-6.

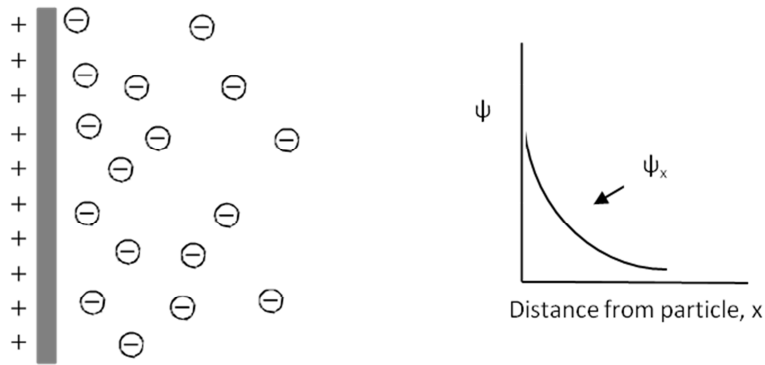


Figure 1-6, schematic diagram of the Gouy-Chapman double layer and the electrical potential drop off with distance.

The Gouy-Chapman model has four major assumptions:

- The ions are treated as point charges.
- The ions do not adsorb onto the surface.
- The dielectric constant of the medium is constant within the double layer.
- The charge on the surface of the particle is uniform over the surface.

The third assumption, that the dielectric constant of the medium is the same in the double layer as the bulk of the solution, does not hold, as close to the particle surface in the inner portion of the double layer the electric fields can be large enough to induce dielectric breakdown. The value of the dielectric constant in this region can be orders of magnitude different to that of the bulk of the solution.

The fourth assumption states that the particle surface is uniform, this may not be an issue depending on the system under investigation but in general the surface charge is not uniform across the particle. This is especially problematic for non aqueous systems where it is known that charges of different sign can interact with the particle surface.²⁰ Thus leading to particles which are not uniformly charged.

1.3.1.1.3 The Stern Model

The Stern model of the electric double layer splits the double layer into inner and outer regions, resembling both the Helmholtz model and the Gouy-Chapman model respectively. The Stern model overcomes the assumptions of point charges and allows for ion adsorption to the surface of the particles.²¹

In the Stern model there exists the Stern plane, which is a monolayer of particles at a distance, δ , from the surface which is equivalent to the size of the hydrated ions radii. This number of counterions is not like the Helmholtz double layer as it does not completely shield the charge on its own leading to neutrality. The population of the Stern layer is assumed to be given by the Langmuir adsorption isotherm, shown in Figure 1-7.

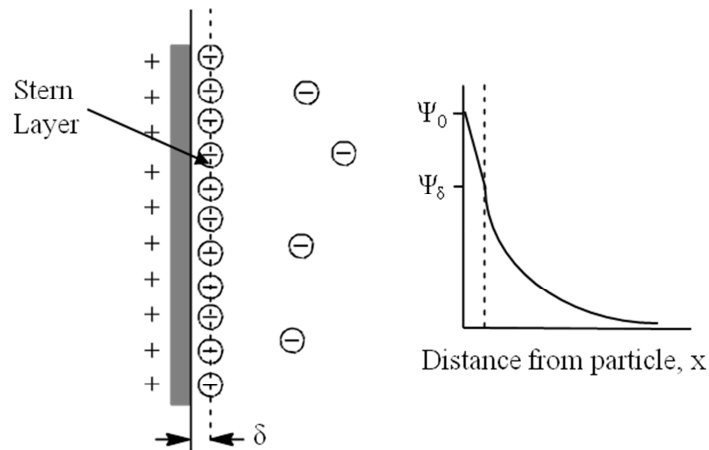


Figure 1-7, schematic representation of the Stern layer.

As the Stern layer does not completely shield the charge it is assumed that the electrical potential tends to zero in the Gouy-Chapman region but drops linearly in the Stern layer. The electrical potential will drop linearly in the Stern layer due to the fact that the surface is surrounded by counterions which will counter act the charge on the surface of the particle. However as the surface is not completely covered with a monolayer of ions it will not tend to zero in the Stern layer, the potential decays to zero over the Gouy-Chapman diffuse layer.

1.3.1.1.4 DLVO Theory

Named after its founders in the 1930's and 1940's, Derjauin and Landau²² from the Soviet Union and Verwey and Overbeek²³ from the Netherlands, DLVO theory states that the stability of a colloidal material toward aggregation is determined by the overall interaction potential between two spherical particles. Plotting curves for the attractive, Φ_A , and repulsive, Φ_R , components between two spherical particles and then adding these together gives the DLVO curve. The DLVO curve has a maximum potential, Φ_M , which can be thought of as an 'potential energy barrier' to aggregation, once overcome aggregates will form residing in the primary energy minimum, the DLVO curve is shown in Figure 1-8.

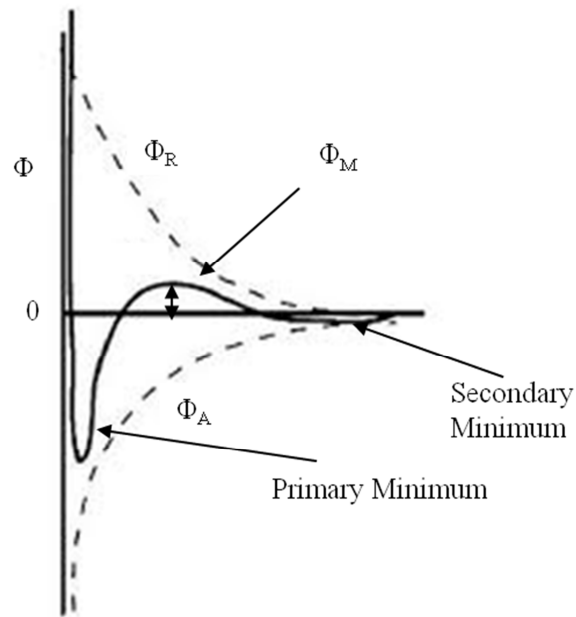


Figure 1-8, DLVO curve of interaction potential between two spheres.²⁴

To overcome this barrier to aggregation, particles must have a certain energy, this energy will be from Brownian motion of the particles under thermal motion, of which the average approximates to, kT . Therefore the barrier height, Φ_M , can give an insight into colloidal stability. The presence of a secondary minimum in Figure 1-8 is responsible for the formation of loose flocks which can be easily disrupted upon agitation of the system. From DLVO theory the concentration at which coagulation rapidly occurs can be estimated. From Figure 1-8 if $\Phi_M = 0$, then there is no barrier preventing coagulation. This means that when particles collide with energy of any value of kT it is highly probable that they will aggregate irreversibly. DLVO theory does have limitations for example it does not allow for the modelling of colloidal crystal formation, at low salt concentrations.

1.3.1.2 Steric Stabilisation

Charged particle systems although generally very stable, can only produce dispersions of low solids content. This is due to the fact that as more charged particles are added to the system they will reach a point in which the particles are forced to approach the double layers of other particles and end up aggregating.

In a non aqueous system charge stabilisation does not occur due to the low dielectric constant of the media. This effectively removes any of the repulsive interactions between the particles allowing for contact and aggregation to occur. So if a system is required to

have high total solids content (TSC) and remain stable in a solvent of low dielectric constant the dispersed particles have to be stabilised against aggregation by steric stabilisation.

Steric stabilisation can be used in both aqueous and non aqueous systems and a range of stabilisers can be used depending upon solvent choice and particle composition. In most cases a steric stabiliser will be polymeric in nature, as the stabiliser has to be large enough to overcome Van der Waals attractive interactions. In order to do this the polymer chains will penetrate into the solvent to give an inaccessible shell around the particle. So as two particles come closer together the stabiliser will become compressed, this also gives an increased local concentration giving an unfavourable entropy decrease. This is shown schematically below in Figure 1-9, as two particles approach at a distance, h , their respective polymeric stabiliser layers of thickness, δ , interact. This forces the concentration of polymer chains in the overlapped region to double causing repulsion between the two particles.

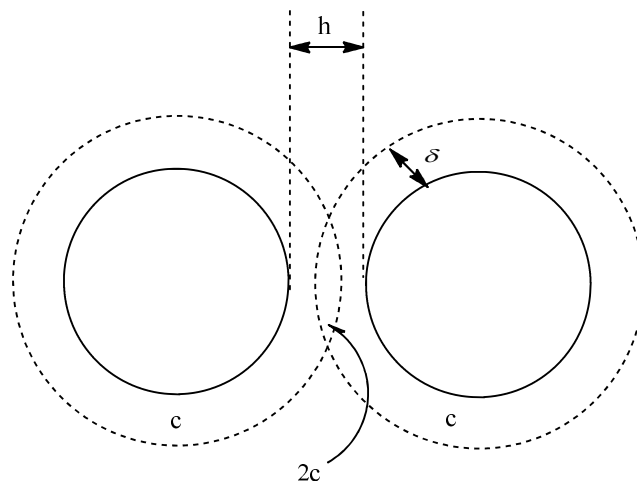


Figure 1-9, schematic representing the excluded volumes associated with particle overlap present in steric stabilisation.²⁵

As two colloidal particles approach, the steric stabilising layers on each particle will become compressed, this lack of freedom in the stabilising polymer gives a strong entropic driving force to move the particles apart. This can be enhanced if the polymer segment-solvent interactions are more favourable than the polymer segment-polymer segment interactions.

A shortcoming of steric stabilisation is the lack of a strong long range force available to repel each polymer particle unlike electrostatic stabilisation, but this is compensated for by a very strong short ranged repulsion force. This allows for higher loading of samples in a steric stabilised system over an electrostatic stabilised system. This means that particles will be constantly attracted towards each other due to Van der Waals interactions, so if the stabiliser does not completely cover the surface of the dispersed particle it will result in aggregation. Also if the polymeric stabiliser chains are not solvated by the continuous phase the system will aggregate as the effective barrier breaks down as the stabiliser layer thickness drops and becomes too small to be effective.

1.3.1.2.1 Types of Stabiliser

In order for a stabiliser to work it must be closely associated with the polymer particle which is growing in solution. This is so the stabiliser will adsorb to the surface of the growing particle. However if there is an addition of strong solvent to the system the stabiliser might become completely solvated by the continuous phase and desorb from the surface of the particle. This will lead to coagulation and aggregation of the polymer particles. To get round this problem the stabiliser can be covalently linked to the surface of the particle and thus will be anchored in place. Figure 1-10 below shows different types of stabiliser which can be used, these can be simple linear polymers, block copolymers or graft copolymers. These polymers will work as polymeric steric stabilisers if one moiety in the copolymer is strongly associated with the particle i.e. if A is polystyrene based it will strongly adsorb to a polystyrene particle suspended in solution. However if B in the example is a simple alkyl chain it will be solvated by the continuous phase (a hydrocarbon), forming hairs or loops into the continuous phase stabilising the particle. For aqueous and polar systems poly(vinyl pyrrolidone)²⁶ or poly(vinyl alcohol)²⁷ can be used as steric stabilisers, as these polymers will be solvated by the aqueous or alcoholic continuous phase. These stabilisers will be attached to the particle surface by physisorption and can potentially be removed by washing with a good solvent.

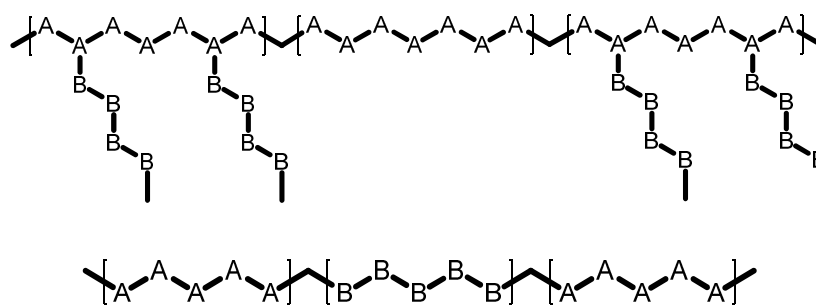


Figure 1-10, examples of graft (top) and block (bottom) copolymer stabiliser structures.

Some stabilisers allow for the chemisorption of the backbone via chemical reaction between the particle and the physisorbed stabiliser. Chemical anchoring can be achieved by different methods dependent upon the functionality at the dispersed particle surface and that of the stabiliser. An example is epoxide ring opening reactions between the groups in the colloid particle and the stabiliser this is shown diagrammatically. A classic example of a steric stabiliser for hydrocarbon media is shown below, and is based on a poly(methyl methacrylate) back bone with poly(12-hydroxystearic acid) hairs grafted to it, P(HSA-*g*-PMMA), and the structure is shown in Figure 1-11.

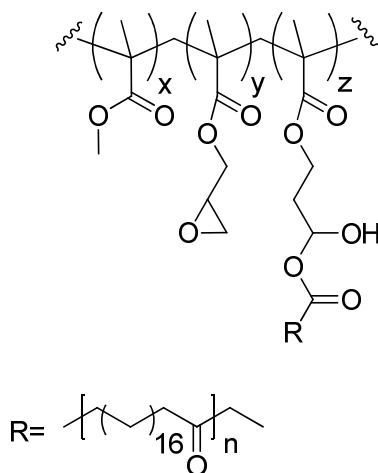


Figure 1-11, chemical structure of P(HSA-*g*-PMMA).

An idealised attachment of the stabiliser to the particle is shown in Figure 1-12, where the stabiliser has been chemically attached to the particle surface.

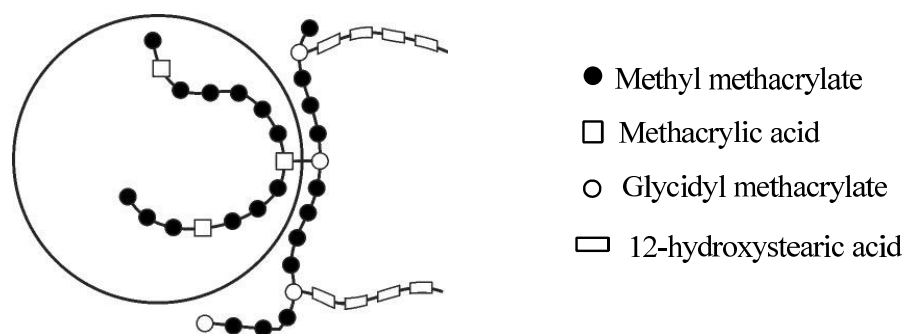


Figure 1-12, schematic representation of a PMMA–latex particle, stabilized by a polymer with poly(12-hydroxystearic acid) hairs.²⁸

Other examples of stabilisers for PMMA particles in hydrocarbon solvents are, block copolymers by controlled radical polymerisation, such as poly(methyl methacrylate-*b*-octadecyl acrylate) (PMMA-ODA)²⁹ and silicone based stabilisers such as poly(methyl methacrylate-*b*-dimethyl siloxane) (PMMA-*b*-PDMS).³⁰

1.4 Electrophoresis of Colloidal Material

Electrophoresis is the movement of suspended particles in solution under an applied electric field. This movement is due to the fact that the surface of the particles is charged and is drawn toward an electrode of opposite charge. The phenomenon of electrophoresis is well understood and is used in many areas, from biological applications like protein separation and analysis³¹ to separation of colloidal material.³²

Figure 1-13 shows a schematic representation of the forces acting upon a particle during electrophoresis. The electrostatic attraction is due to the fact that the particle is charged and moves to the electrode of opposite charge. Drag however is due in part to the viscosity of the medium the particles are suspended in; this retardation force is also due to ions moving past each other. Additionally according to Stern theory of charged colloidal material a fixed layer of counterions will move with the particle however the free ions in the Gouy-Chapman layer will not move with the particle and will therefore add to the strength of the drag force felt on the particle.

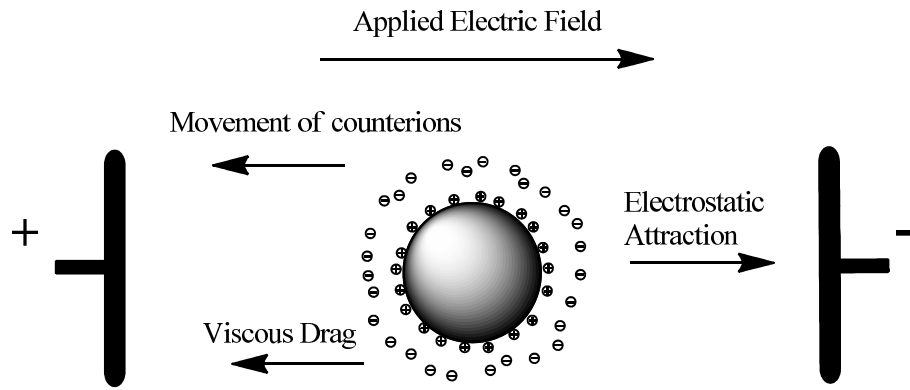


Figure 1-13, schematic view of the forces acting on a particle during electrophoresis.

The particles velocity moving in a applied electric field depends upon, the applied electric field strength, E , the charge on the particle, q and the sum of all retardation forces acting on the particle. For a particle moving at constant velocity, v , the force of attraction must equal the retardation force; given by the following equation:

$$v = \frac{qE}{f} \quad 1-2$$

Where, f , is the friction coefficient which is based on size and shape of the particle. The equation assumes there is no charge gradient within the medium and as such is a constant value. From equation 1-2 the electrophoretic mobility, m , is given by:

$$m = q/f \quad 1-3$$

Equations 1-2 and 1-3 assume that the particles are spherical and have evenly charged surfaces. This is a major problem as treating non-spherical particles as pure spherical objects may not hold. This is especially true if different areas within the particle structure have a different chemical make-up and may therefore have a different charge density associated with them.

1.5 Charges in Non-Polar Solvents Systems

When thinking of ion dissociation the immediate thought is of a system similar to dissolving a salt into water, ions become solvated by the highly polar water molecules creating a solvation sphere, however this does not happen in non aqueous systems. The low dielectric constant of hydrocarbons ($\epsilon_{Oil} = 2$ opposed to $\epsilon_{Water} = 72$) prevents the ions from dissociating because it is not thermodynamically viable due to the lack of any charge screening effects. If this idea held true, then it would be assumed that charges cannot exist in low dielectric media. This is not the case, as the fundamental driving force for such dissociation to occur is still present; the differences in electronic properties of the materials. The build-up of charge has caused major problems in certain industries. One example is of the petrochemical industry, when processing hydrocarbon media charges can build to the point where they dissipate through sparking, with explosive consequences. In 1958 Klinkenberg and Minne³³ published a book on the electrostatics in such systems and found the species responsible for such charge build up.

How charged species are created and how they are maintained is still a subject for debate with academic groups working to answer this question.

1.5.1 Comparison to Aqueous Media

Surface charging in non aqueous media is problematic, as it is well known that in polar media where ions readily dissociate and are protected from recombination by the fact that they are hydrated (solvated) by the polar solvent, this is not possible in an oil or solvent with low dielectric constant. Each of the ions will have an energy $\approx kT$, which is available to break apart the ion pairs. The Coulombic attraction (Φ_{att}) between the ion pair is given by the following equation:

$$\Phi_{att} = \frac{1}{4\pi\epsilon\epsilon_0} \frac{e^2}{r} \quad 1-4$$

Where; e , is the elementary charge, ϵ , the dielectric constant for the medium, ϵ_0 , permittivity of a vacuum and r , the ion separation distance. If the attractive energy is comparable to kT , then the ion pair should remain dissociated. When $\Phi_{att} \approx kT$ then separation distance defines the Bjerrum length, λ_B .

$$\lambda_B = \frac{1}{4\pi\epsilon\epsilon_0} \frac{e^2}{kT} \quad 1-5$$

The Bjerrum length is the minimum distance between ions required to form a stable dissociative state. For water at room temperature the Bjerrum length is 0.7 nm which is roughly twice the size of a typical hydration sphere. However the Bjerrum length for two ions in a solvent of low dielectric constant i.e. dodecane ($\epsilon = 2$) becomes 28 nm. So for a stable dissociative state to occur in dodecane for monovalent ions, each ion must be 28 nm apart to stop them from recombining.³⁴ In order to maintain a stable dissociative state the ions must be ‘hidden’ in large structures or be large molecular ions. The consequence of such a large Bjerrum length has two major implications.

First the concentration of molecular ions will be extremely small because the solvation energy of an ion scales as $\lambda_B/2a$ where, a , is the ionic radius.³⁵ Due to the lack of charge carriers in oil the screening of electrical charge is negligible giving rise to extremely long ranged charge interactions. This can be explained by considering the following dissociation equilibrium of monovalent electrolyte;



If the law of mass action is applied to the equilibrium above an equation is given for the total number of free ions per unit volume, as described in equation 1-7. The law of mass action predicts and models solution behaviour in dynamic equilibrium. It is described with two effects, a kinetic effect which is concerned with elementary reactions and associated rate constants and the other part is concerned with the reaction mixture composition at equilibrium.

$$\rho_{ion} = \sqrt{\frac{3\rho}{\pi a^3} \exp\left(\frac{-\lambda_B}{2a}\right)} \quad 1-7$$

Where, ρ , is the number density of the electrolyte and a , is the radius of a molecular ion, and the degree of dissociation is assumed to be small. If $a = 0.25$ nm at the solute concentration of 10 mM then the above equation gives an ionic concentration of $\approx 10^{-13}$ mol dm⁻³.³⁶ From this the Debye length can be calculated which describes the length at which mobile charge carriers can screen an electrical charge. As such the Debye

length can be thought of as the thickness of the electric double layer and is given by the following equation:

$$k^{-1} = \frac{1}{\sqrt{4\pi\lambda_B\rho_{ion}}} \quad 1-8$$

Solving for the Debye length in a system of low dielectric constant gives a length of $\approx 100 \mu\text{m}$, whereas in typical aqueous electrolyte solutions the Debye length is in the order of 10's of nm.

The second implication of a colloidal system with a large Bjerrum length is the small value for double layer capacitance. As such the capacitance is nearly 40 times smaller in oil than a comparable aqueous environment.³⁷ The result of this is that only a minute charge on a colloid is sufficient to give a large surface potential, in non aqueous systems. Hsu *et al.*³⁸ measured particles with charges as low as 200-900 electrons on 800 nm colloids in oil. But the corresponding surface potentials work out to be -140 mV comparable to highly charged aqueous colloidal systems. This high charge generates high electrostatic repulsions. This is shown in Figure 1-14 below in which PMMA particles have been dispersed in dodecane where they can be seen to reversibly flocculate, but upon the addition of the inverse micelles (12 mM AOT) the particles do not come within three particle distances of each other.

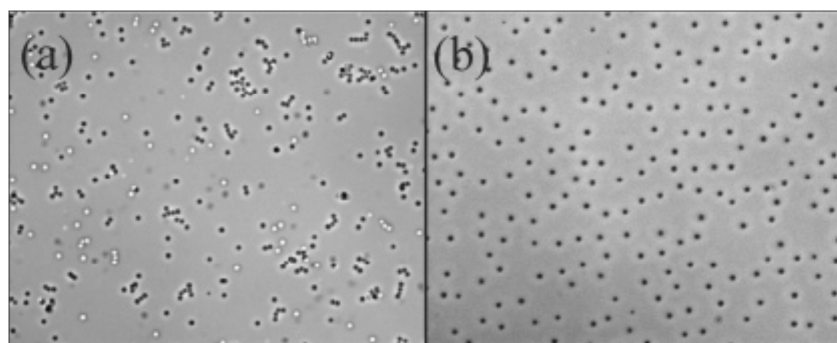


Figure 1-14, optical images of; a, PMMA particles and b, PMMA particles with the addition of a AOT dispersed in dodecane.³⁸

1.5.2 Ion Stability in Low Dielectric Media and the Role of Surfactant

As previously discussed the size of the Bjerrum length, λ_B , for non aqueous systems has many implications, the major one is that simple ions cannot exist in solution as they would

combine rapidly and form a salt. The ions must be trapped or captured in a large structure such as polymers or surfactants in which the charged species can exist in the core. However as the Bjerrum length is so large in low dielectric media ($\lambda_B = 28.3$ nm) unless the structure is of this size then an equilibrium will be set up between bound and free ions. This is the case in most surfactant systems, as a surfactant micelle may only be 5 nm in size but still will aid charge formation.

1.5.2.1 *Micelle Formation in non Aqueous Systems*

Micelles form in aqueous systems by the balance of intermolecular forces and the changes in entropy associated with the hydrophobic tails shedding their hydration layer and becoming solvated by other hydrophobic tails, which leads to a large increase in entropy.³⁹ The principles of micelle formation in non aqueous media have been published in 1976 by Fowkes,⁴⁰ and depend upon intermolecular forces and entropy changes. Solvents of low dielectric media do not self-associate like water so the introduction of a solute will generally increase the entropy of the system so there is no entropic driving force. The driving force is the strong intermolecular interactions between the head groups. If such interactions are greater than that of the interactions with the solvent then reverse micelles will form. These interactions tend to be dominated by donor-acceptor interactions between the surfactant and the solvent and the surfactant with itself. From this it is clear that water holds a key part in micelle formation as the donor-acceptor reactions of reverse micelles can be greatly enhanced by the addition of an amphipathic molecule such as water as it can act as either an acid or base. Also the addition of water into the micelle core allows for an increased ability for the micelle to stabilise charged species.

1.5.2.2 *di-(2-ethylhexyl) Sodium Sulfosuccinate (AOT)*

Di-(2-ethylhexyl) sodium sulfosuccinate or Aerosol OT is one of the most studied surfactant molecules in this field as it can form micelles in water and in hydrocarbon media. The structure of AOT is shown below.

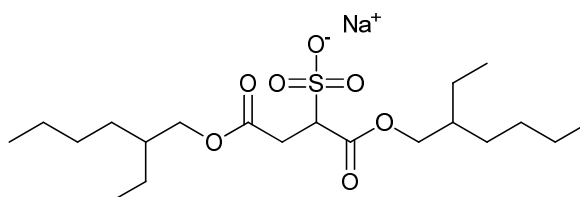


Figure 1-15, the chemical structure of di-(2-ethylhexyl) sodium sulfosuccinate (AOT).

It has been found that the solvent has a large effect upon micelle size, and can vary from a molecular weight of 10,000 with a aggregation number of 23 in water, to 1,800 with a aggregation number of 4 in ethanol to 25,000 with a aggregation number of 56 in cyclohexane.⁴¹ AOT was used to study the conductivity of low dielectric solvents and the effect of water doping into the system by Mathews and Hirschorn.⁴² It was found that increasing the water content increased the conductivity of the solution. The increase in conductivity at low water levels gave an increase of orders magnitude, but at higher concentrations viscosity effects made data interpretation difficult. The authors concluded that the small increases in water content aid the hydration of the surfactant head groups within the core of the micelle, hence giving increased conductivity.

This idea of trace amounts of water in the system increasing the conductivity of a micelle solution was also studied by Randriamalala *et al.*⁴³ by studying the field induced dissociation of ions in different AOT solutions. They found that the conductance increased with the field up to $5.5 \times 10^6 \text{ Vm}^{-1}$. This was true for solutions above and below the critical micelle concentration (CMC) for AOT. With the low field conductivity data for the anhydrous solutions the results were consistent with the following model which they proposed.

- Only small charge carriers exists at concentrations below 10^{-3} M .
- There is a steady increase in size observed upto 10^{-3} M .
- There is no change in the size of charge carriers above 10^{-3} M .

Randriamalala *et al.* also found that the conductivity of the solutions increased as the water concentration was increased along with the micelle size. This means that as water was added to the system the number of charge carriers must be increased. This apparent conductivity below the CMC of AOT was investigated by Denat *et al.*⁴⁴ They measured the conductivity of solutions from 10^{-5} to 10^{-1} M and did not see an increase in conductivity around the apparent CMC point of 10^{-3} M . They explain this result by saying that associated structures of AOT will always occur at low concentrations. They suggest that a trimer will form at low concentrations which will allow for equilibrium to be set up for bound and unbound ion pairs allowing conduction.

1.5.3 Charging of Particles in Non-Polar Solvents

When a particle is dispersed in an aqueous system it can become electrically charged due to adsorption and desorption of surface groups such as hydroxyl and carboxylic acid groups, or acid-base interactions between the surfactant and particle.⁴⁵ However in a non aqueous system this situation is very unlikely as any desorbed protons or hydroxyl groups cannot be complexed by the solvent.

However if a non aqueous electrolyte such as AOT is added to the system then the particles will become charged. If a solution of a non aqueous electrolyte is considered then the charge-exchange reactions will be equal, so there will be an equal amount of both positive and negative charges in the solution. However when particles are considered in this system then they will carry the opposite charge to that of the association structures in solution. But as the particle surface is large it is possible for multiple electrolytes to interact with the surface producing signs of both charge on the surface. The sign of the charge is dependent upon the relative acidity of the micelle core with respect to the particle surface. If the micelle core is more acidic it will be negatively charged therefore when they interact with a particle surface they will leave the opposite charge on the surface, leaving it positive. This is the opposite situation to what happens in aqueous dispersions.

A potential mechanism for this was proposed by Fowkes *et al.*⁴⁶ They suggest that particles become charged by the adsorption of uncharged electrolyte onto the surface followed by ion-exchange with surface groups, which is then followed by the desorption of charged electrolyte. As the most common ion that is exchanged is a proton they suggest an acid-base mechanism for the interactions. This idea of acid-base interactions also allows for the opposite charging observed in non aqueous systems compared to that of aqueous systems. This mechanism will also be highly sensitive to any water in the system, and any water adsorbed to the particle surface will help the process as any electrolyte which has undergone ion-exchange can leave the surface with added water content to give added stability to the ion. A schematic view of a colloid particle acquiring charge through adsorption of inverse micelles is shown below.

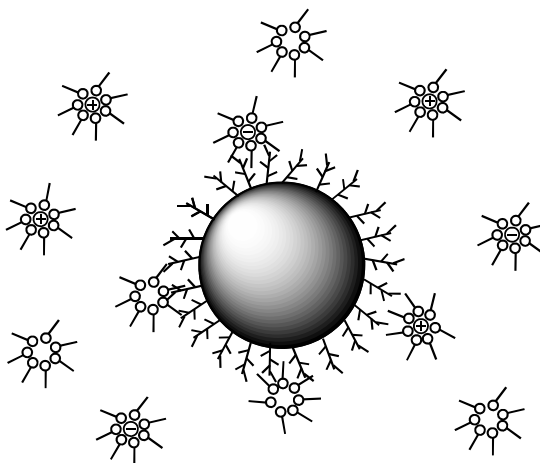


Figure 1-16, schematic view of a colloid particle being charged by reverse micelles, by adsorption to the particle surface.³⁶

This mechanism was verified by Fowkes *et al.*⁴⁶ experimentally using carbon particles suspended in a white oil stabilised with ^{14}C labelled copolymers of long chain methacrylates and vinylpyridine. These particles were electrodeposited and the electrodes examined for the ^{14}C . They found that the carbon particles were plated on the anode and the ^{14}C labelled copolymer was on the cathode. This means that the particles were negatively charged and the copolymer charged positive. The result from this electrostatic stability infers that the charge is not due to the adsorption of the basic copolymer, but rather the extraction of a proton by micelles from the basic polymer to generate negatively charged particles.

1.5.4 Electrodynamics of non Aqueous Colloid Systems

The movement of particles due to an external field obeys the same laws as a system which is aqueous based, however due the number of charged species is far lower giving a lower conductivity, and as a result the electric fields used to study them tend to be larger. This leads to four effects which are common place in non aqueous colloid systems but rarely encountered in aqueous dispersions:⁴⁷

- A long time is required for the relaxation of the electric field created upon charge separation.
- The build-up of space-charge layers at electrodes.
- The formation of non uniform electric fields.

- Electrohydrodynamic instability.

1.5.4.1 Space-Charge Effects

When an electric field is applied to a dispersion of charged particles, the particles and ions move to the electrode of opposite charge. This motion will carry on until the particles / ions reach the electrodes. If these particles reach the electrode and are not neutralised by the electrode they will form a space-charge layer. This layer of charged species reduces the effective electric field strength between the electrodes. If the electric field strength is lowered then the motion of the remaining particles / ions will be reduced. To the observer it can appear as if the remaining particles have lower charge. If this effect is rapid the dispersion will act like that of an uncharged dispersion and no directional motion will be apparent. This effect can be misleading and could lead to misinterpretation of data.

This effect is prevalent in non aqueous systems and not really observed for aqueous dispersions for two reasons. First the bulk of the current is carried by ions; these ions are far more likely to exchange charge at the electrodes rather than particles at the electrode walls. Even if the electric field builds up at the electrode, it can only do so until some component of the dispersion, usually water, begins to be oxidized or reduced.

The build-up of particles at the electrode walls due to space charge effects will have a substantial effect on the performance of any display device. If the particles become adsorbed to the electrode walls over time, effectively building space-charge layers, the electrophoretic mobility of the particles will be decreased. This will decrease the refresh rate of the display and ultimately lead to failure.

1.5.4.2 Electrohydrodynamic Instabilities

Almost all fluids are populated by a variety of charge carriers which in an applied electric field will move. If the motion of the charge carriers is small then the motion can be simply treated as the motion of particles and the counter motion can be ignored. However this is an approximation whose limits must be estimated. This general analysis has been presented as an analogy to Bernard instability.⁴⁸ Bernard instability can be described as the movement of a fluid like that in convection currents, i.e. cooler fluid will be drawn down as it is denser than the hot fluid at the bottom giving rise to a convection cell.

For uniform conduction, the threshold voltage, V_c , from laminar into the turbulent regime is approximated by:

$$V_c = \frac{30\eta}{(\rho D \epsilon_0)^{1/2}} \quad 1-9$$

Where; ρ , is the density of the fluid, D , is the dielectric constant for the medium and η is the viscosity, so mixing occurs within the fluid.

Laminar flow is where the fluid flows in parallel layers with little or no disruption between the layers. Turbulent flow is a different regime where the fluid is churned up in vortex like mixing. Note the limit is a voltage, not an electric field. Since electrophoresis is a field-dependant measurement, the smaller the gap between electrodes the higher the field can be before electrohydrodynamic instabilities set in, stopping particles from moving in a laminar fashion.

1.6 Non Aqueous Dispersion Polymerisation

There are many applications in which polymeric nano- and micro-particles are required to be produced in the absence of water such as; pharmaceuticals,⁴⁹ biocompatible particles, surface coatings,^{50,51} conjugated polymer particles⁵² and for fundamental studies of soft matter⁵³ and particle charging mechanisms in non aqueous solvents. The production of particles by non aqueous dispersion (NAD) polymerisation has been around for many years and was developed as a consequence of the surface coatings industry which is why a lot of the original literature is confined to patents^{54,55} rather than academic publications. It has seen a recent revival due to new emerging technologies such as electrophoretic displays,⁵⁶ and modelling the particle movement with confocal microscopy.^{57,58}

In a NAD system the monomer is miscible with the continuous phase along with the initiator and stabiliser. So prior to initiation the reaction mixture is completely homogeneous. However when the monomer starts to react the polymer formed is not soluble in the continuous phase, leading to precipitation of the polymer. In the presence of a stabiliser, the growing polymer chains stay suspended in solution, these initial primary

particles or particle nuclei then aggregate to give larger stabilised particles. A schematic diagram for the particle formation in dispersion polymerisation is shown in Figure 1-17.

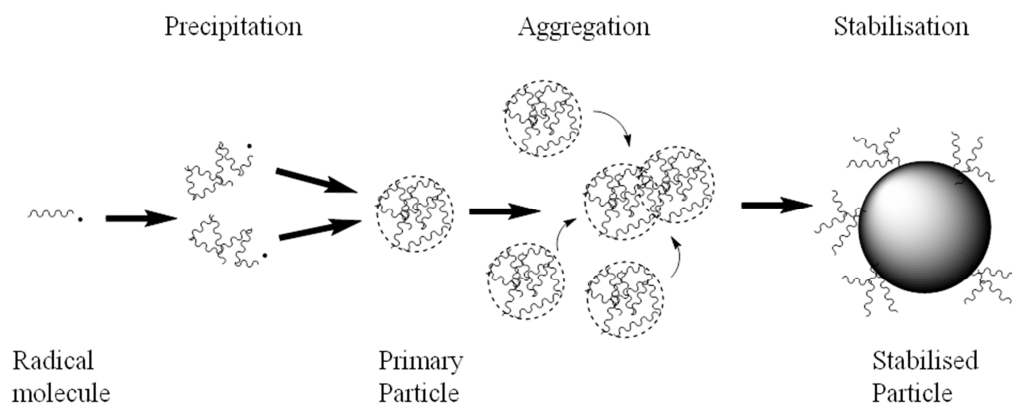


Figure 1-17, schematic view of primary particle formation and growth in dispersion polymerisation.⁵⁹

As dispersion polymerisations are very sensitive toward monomer, solvent, stabiliser and the resultant polymer choices, there is little window for changing reaction conditions once an optimum has been found for one system. This can be a problem when wanting to produce polymer particles with added functionality by the addition of co-monomers. This is due to the fact that any co-monomer added will change the solubility of the precipitating polymer chain and monomer partitioning within the system and will lead to problems, such as secondary nucleation or particle aggregation if the stabiliser cannot adsorb to the surface. Problems will also occur if a difunctional monomer is used as it can change the kinetics of primary particle growth, leading again to aggregation of particles. Also the increase in molecular weight can give rise to non-uniform particles.⁶⁰

1.6.1 Flory-Huggins Theory and Solvent Choice

Flory-Huggins theory can be used to understand the mixing of polymer and solvent by considering entropic and enthalpic energy changes. These are based on the characteristics of the polymer chain and the solvent strength.⁶¹

The entropic change can be calculated by the equation:

$$\Delta S = -k(N_1 \ln \phi_1 + N_2 \phi_2) \quad 1-10$$

Where, k is the Boltzmann constant, N_1 and N_2 are the number of solvent and polymer molecules respectively and ϕ_1 and ϕ_2 are the volume fractions for the solvent and polymer respectively.

The enthalpic change can be calculated from the following equation:

$$\Delta H = kT\chi_1 N_1 \phi_2 \quad 1-11$$

Where, T is the absolute temperature and χ_1 is the interaction parameter per solvent molecule. The enthalpic term comes from the summing of the internal energy change when dealing with the difference in solvent-solvent and polymer-polymer interactions when they mix, giving rise to polymer-solvent interactions, calculating for constant volume then converts to enthalpy.⁶²

These can then be equated by the Gibbs free energy equation:

$$\Delta G = \Delta H - T\Delta S \quad 1-12$$

Giving the equation:

$$\Delta G = kT[N_1 \ln \phi_1 + N_2 \ln \phi_2 + N_1 \phi_2 \chi_1] \quad 1-13$$

As the value of ΔS is lowered by longer chained polymer molecules reducing ΔG , solvent choice determines χ_1 hence the solubility of the polymer. The interaction parameter χ_1 is closely linked to reaction temperature for any given solvent-polymer pair, and an important constant is that the theta temperature⁶³ for the system occurs when $\chi_1 = 1/2$. Under these conditions the system behaves as if its molecules and their configurations are random, simplifying any theoretical treatment.

Polymers will dissolve in the solvent if $\Delta G < 0$, so for the choice of the solvent systems for NAD a solvent must be chosen which ΔG will be negative for the monomer, but will become positive for the polymer. From this thermodynamic treatment effective monomer and solvent choices can be made which will lead to potentially successful dispersion polymerisation reactions.

1.6.2 Role of the Stabiliser during the Reaction

The nature and quantity of dispersant used has a major effect on the number of particles formed and therefore the size of particles being formed, on the occurrence of nucleation. The rate of nucleation is linked to the tendency for the growing polymer to associate with the dispersant, along with the solubility of the growing polymer in the continuous phase.

There are three scenarios for nucleation growth in which the stabiliser can help the polymer grow:

- **Self-Nucleation**
The stabiliser stabilises growing chains against capture by particles at lower molecular weights. So this will reduce the probability of capture, therefore produce nuclei which will allow more particles to form in the reaction system.
- **Aggregative Nucleation**
The stabiliser participates in the formation of new nuclei and reduces the interfacial tension. This will lower the activation energy and threshold of molecular weight, and will also reduce the capture of new nuclei producing more nuclei and therefore more particles.
- **Micellar Nucleation (may only occur in aqueous systems)**
The stabiliser forms micelles from which nuclei are formed by initiation of monomer solubilised inside them. The stabiliser will also migrate to cover the particle surface. So the total particle surface area is governed by the amount of stabiliser used, therefore the number of particles is controlled by amount of dispersant used.

The role of the stabiliser is also to stabilise the growing and formed particles from coagulation, this process will also help produce a higher number of particles as there is no agglomeration in the system. So again the total surface area is governed by the amount of

dispersant used and therefore is linked to number of particles and particles size, Figure 1-18.

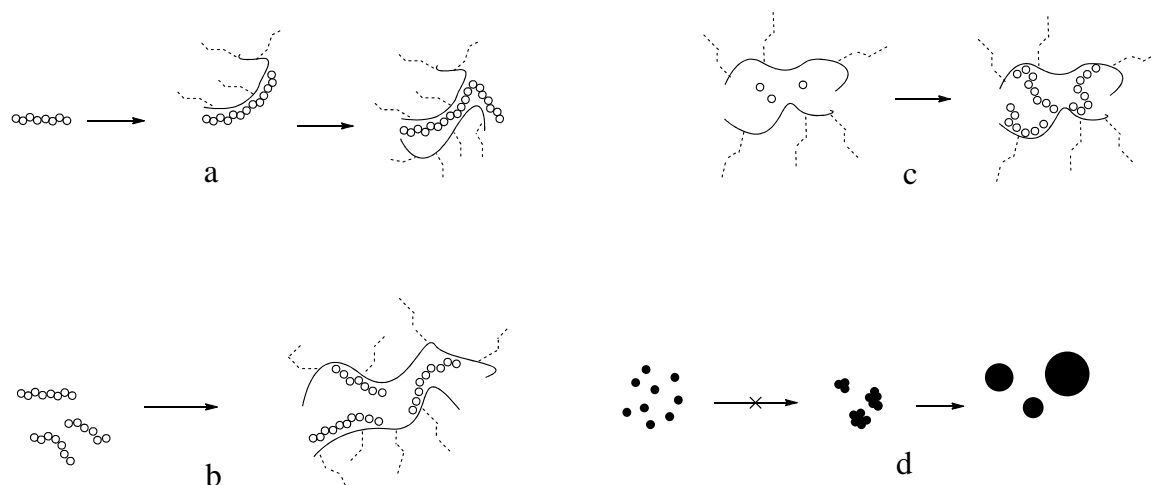


Figure 1-18, role of dispersant in aiding nucleation growth; a, self-nucleation, b, aggregative nucleation, c, micellar nucleation and d, agglomeration.²⁵

1.7 The Formation and Uses of Shape Anisotropic Particles

The formation of shape anisotropic or non-spherical particles is a recent field with much interest in studying the properties of such particles, such as photonics and colloidal crystals.⁶⁴ The production of anisotropic particles with multiple chemistries will also be interesting, such as dumbbell-like particles containing two different fluorescent dyes, one in each lobe, for cell imaging. This could be further extended to MRI contrasting agents. Much work in this area has been done by using aqueous emulsion polymerisation or by dispersion polymerisation in water / ethanol mixtures where the high interfacial tension between the continuous phase and the monomer and polymer can play a favourable role in the production of anisotropic particles.

1.7.1 Formation of Shape Anisotropic Particles

There are multiple ways of producing shape anisotropic particles such as stretching particles in a film above their glass transition temperature, T_g ,⁶⁵ particle deformation by ion beam bombardment,⁶⁶ formation of new polymer domains on an existing polymer surface (the dynamic swelling method),⁶⁷ lock and key methods⁶⁸ and by controlled cluster

formation.⁶⁹ The formation of shape anisotropic particles has been reviewed by S-M Yang *et al.*⁷⁰ in 2008 and the formation of colloidal clusters by E. Duguet *et al.*⁷¹ in 2011. In both of these review articles there is no mention of the formation of shape anisotropic particles in low dielectric constant media. Although a number of ways to produce shape anisotropic particles have been reported the methods of most interest for this project are the one which can be industrially scaled.

1.7.1.1 Anisotropic Particles by Ion Bombardment

This method is used to produce ellipsoidal particles which are generally inorganic in nature such as silica. Spherical particles are produced by whichever method suits the production of the particles required. These particles are then deposited as a monolayer to form colloidal crystals and subjected to an ion beam of xenon at an angle to the substrate.⁷² This then deforms the particles into an oblate or prolate ellipsoid shape. The angle which the ion beam hits the particles can be changed resulting in different aspect ratios of the resultant particles.⁷³ The aspect ratio of the particles can also be altered by changing the strength of the ion beam as demonstrated by van Dillen *et al.*⁶⁶ where they deformed particles with differing strengths of the xenon ion beam. These results are shown below in Figure 1-19.

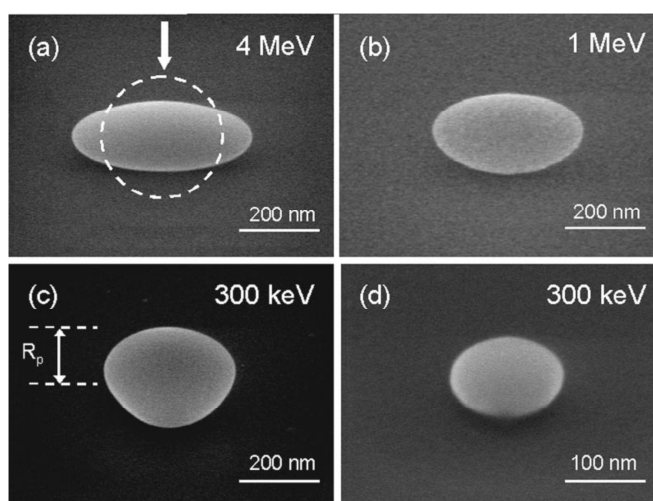


Figure 1-19, SEM images of ellipsoids produced by ion beam bombardment, the dashed circle in a, represents the original spherical silica spheres and the arrow represents the direction of the ion beam.⁷⁴

1.7.1.2 Particle Stretching

The principle of the stretching method is to create spherical particles by emulsion or dispersion polymerisation, which is subsequently dispersed into a poly vinyl alcohol (PVA) solution of which a film is cast. This film can then be stretched causing voids to

form next to the polymer particles. If this is then heated to the T_g of the dispersed particles they will melt and flow to fill the voids if possible. This process can be done the other way round so the particles are heated and melted before stretching which gives different results. After the stretch has been performed and the particles cool back to a glassy state the PVA film can be easily dissolved by washings with a water / alcohol mixture and centrifugation. This method was first reported by Nagy and Keller in 1989⁶⁵ but the method was first properly described by Ottewill *et al.* in 1993.⁷⁵ In which they reported the production of ellipsoidal shaped particles of polystyrene up to 5 μm , all of which were monodisperse.

However to stretch the particles a mechanical device will be required, such as a small rack to stretch a film. A schematic of a device is shown in Figure 1-20 below. This must then be immersed in an oil bath to heat the particles to the necessary temperature.

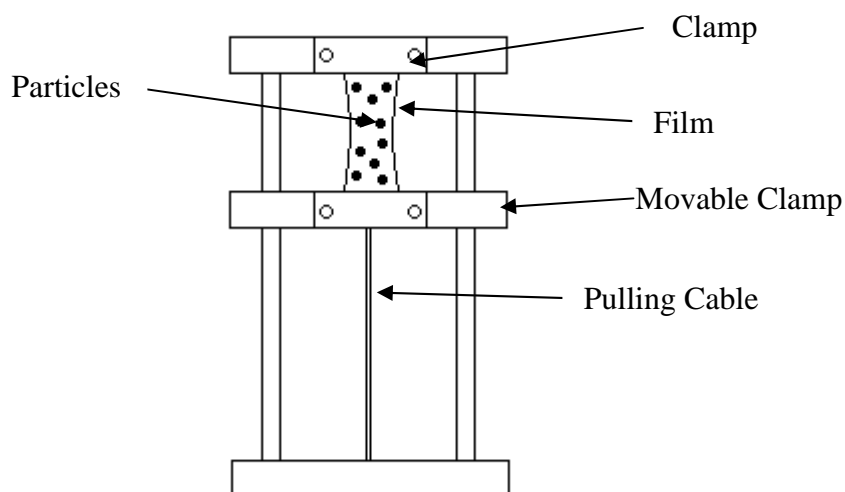


Figure 1-20, schematic diagram of a device for stretching polymer films.

Champion *et al.*⁷⁶ demonstrated this method producing a large array of different shaped particles dependent upon whether the dispersed spheres were heated before or after stretching. Stretching can be done in multiple directions which will affect the resultant particles shape. As stretching in one direction will only elongate one side of the particle, by stretching in two directions worm-like particles can be made, stretching done in all four directions opens up a lot of variety such as UFO-like and disk-like particles, dependent upon the T_g of the suspended particles and the stretching ratio used. Examples of such particles produced by Champion *et al.* are shown below.

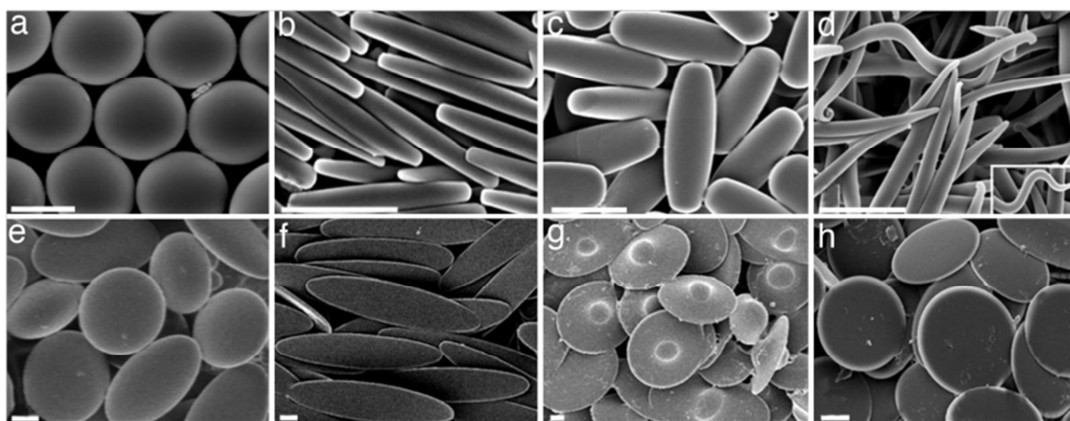


Figure 1-21, example of particles produced by Champion *et al.*⁷⁶ where a, is the initial particles before stretching.

This method has also been used to study the crystal packing of non-spherical colloids by Lu *et al.*^{77,78} in which they state that the void volume is less than that of spherical particles. Lele and Furst⁷⁹ also came to the same conclusions when studying colloids crystals produced by stretching of particles. This method of producing shape anisotropic particles has also been shown to work for zinc sulfide particles and well as silica and core-shell particles of these two materials. This gives rise to the idea that any form of inorganic particles which undergo this plastic deformation could be used to produce ellipsoidal particles.⁸⁰

1.7.1.3 Dynamic Swelling Method

This method was first reported by Sheu *et al.*⁶⁷ in 1990 in which they reported the formation of ellipsoidal and egg-like singlets, symmetric and asymmetric doublets, ice cone like and popcorn-like multiplets. Their study was based on phase separation in polymer interpenetrating networks and studied the effects of varying the crosslinking density. It was Okubo who first coined the phrase dynamic swelling method⁸¹ when they reported the production of snowman-like particles. It has also been shown that the size of any protrusions formed during this process can be tuned as it is due to an increase in elastic stress on the crosslinked seed particle upon heating and polymerisation expelling the monomer inside the crosslinked network.

Although this method cannot produce such a wide variety of different shapes like the stretching method, it does not require the stretching of a film and the physical mechanism required for such a process. The dynamic swelling method represents an industrially

scalable process. It also allows for the incorporation of different monomers in different parts of the particles formed, thus leading to interesting particle properties concerning colloidal crystal packing and electrophoresis.

This particle swelling and phase separation has also been thought of in terms of the new domain (protrusion of monomer) as wetting the surface of the crosslinked seed particle. This can be described by Youngs' equation:

$$\gamma_{P,A} = \gamma_{P,M} + \gamma_{M,A} \cos\theta \quad 1-14$$

Where, $\gamma_{P,A}$ is the interfacial tension between the particle and the continuous phase and $\gamma_{P,M}$ and $\gamma_{M,A}$ are the interfacial tension difference between particle and monomer, and the interfacial tension difference between the monomer and the continuous phase respectively and θ is the contact angle. This theory assumes the particle surface is flat, which does not hold for colloidal systems but can give an easy qualitative view of the system. According to equation 1-14, as θ increases so does the size of the new domain. This is shown schematically in Figure 1-22.

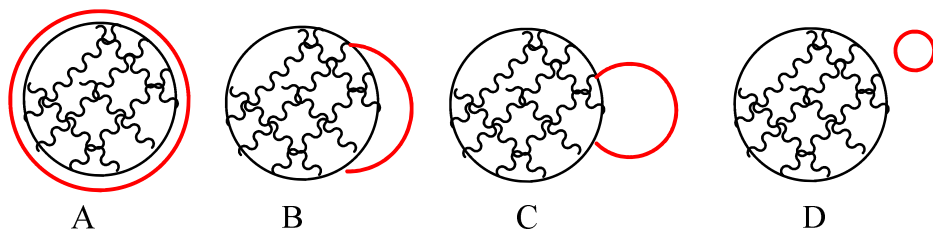


Figure 1-22, schematic diagram showing the wetting of the new monomer domain on the crosslinked particles surface.⁸²

Figure 1-22, a, represents a highly favourable interaction between the monomer and the crosslinked seed particle, $\theta = \infty$, b, represents a favourable interaction with a low value of θ , c, shows an unfavourable interaction with a high value of θ and d, a highly unfavoured interaction where $\theta = 0$. Ottewill *et al.*⁸³ also used this idea to produce composite particles in aqueous media by engulfment looking for a regime where $\theta = \infty$, producing particles of multiple different internal domains.

Thermodynamic treatment of the dynamic swelling method has been done by Sheu *et al.*⁸⁴ in which they considered the free energy changes upon expansion and contraction of

crosslinked polystyrene particles while undergoing swelling by monomer giving the equation:

$$\Delta G_{m,p} = \Delta G_m + \Delta G_{el} + \Delta G_t \quad 1-15$$

Equation 1-15 says that the chemical potential of the monomer in a particle, $\Delta G_{m,p}$, is the sum of the mixing force, ΔG_m , the elastic-retractile force, ΔG_{el} and the particle water interfacial tension, ΔG_t . At the point of swelling equation 1-15 will be equal to zero.

Substituting in the Flory-Huggins expression^{85,86} for $\Delta G_{m,p}$:

$$\Delta G_{m,p} = \ln(1 - v_p) + v_p + \chi_{mp}v_p^2 \quad 1-16$$

Where, v_p , is the volume fraction of polymer in the swollen particle and χ_{mp} , is the monomer-polymer interaction parameter.

The Flory-Rehner equation⁸⁷ for ΔG_{el} :

$$\Delta G_{el} = RTNV_m(v_p^{1/3} - v_p/2) \quad 1-17$$

Where, R is the gas constant, T , is the absolute temperature for the system, N being the effective number of chains per unit volume and V_m , is the molar volume of monomer.

The Morton equation⁸⁸ for ΔG_t :

$$\Delta G_t = 2V_m \gamma / r \quad 1-18$$

Where, γ is the interfacial tension for the water-particle interface, and thus giving the equation:

$$\ln(1 - v_p) + v_p + \chi_{mp}v_p^2 + RTNV_m \left(v_p^{1/3} - v_p/2 \right) + 2V_m \gamma / r = 0 \quad 1-19$$

From the calculations it can be shown that ΔG_m makes a negative contribution to $\Delta G_{m,p}$ promoting particle swelling, whereas ΔG_{el} and ΔG_t make positive contributions to $\Delta G_{m,p}$

promoting the contraction of the crosslinked particle, these forces are summed up schematically below.

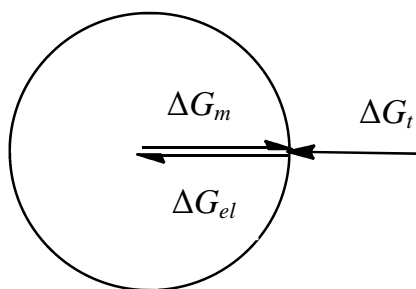


Figure 1-23, schematic view of the forces affecting the swelling of a crosslinked polymer particle by monomer in water.⁸⁴

Particle swelling will occur when $\Delta G_{m,p} < 0$ and reaches an equilibrium when $\Delta G_{m,p} = 0$. To trigger phase separation (the expulsion of monomer) $\Delta G_{m,p} > 0$. The phase separation can be controlled by varying the interfacial tension and the temperature under which the particles are swollen.

All the research done in this area has been in aqueous systems or water / alcohol mixtures. Where there is a high interfacial tension between monomer droplets and the continuous phase which will aid in the swelling of polymer particles by any added monomer. As any monomer added to the suspension will be forced into the particle due to the high interfacial tension between particles and the highly polar medium.

Kim *et. al.*⁸⁹ have studied the effect of the crosslinking density on producing non-spherical polymer particles, and can predict if a particle will grow linearly to produce rods or perpendicularly to produce triangles, when producing a secondary protrusion. This is achieved by controlling the crosslinking density in the seed particles and crosslinking the new protrusion to a different extent to the original seed particle; this can be seen in Figure 1-24. If the crosslinking density of lobe a is greater than lobe b then linear growth is seen from b. However if the crosslinking densities are similar then perpendicular growth will occur. To prove this mechanism they produced large particles to image with an optical microscope and watched the phase separation take place over time.

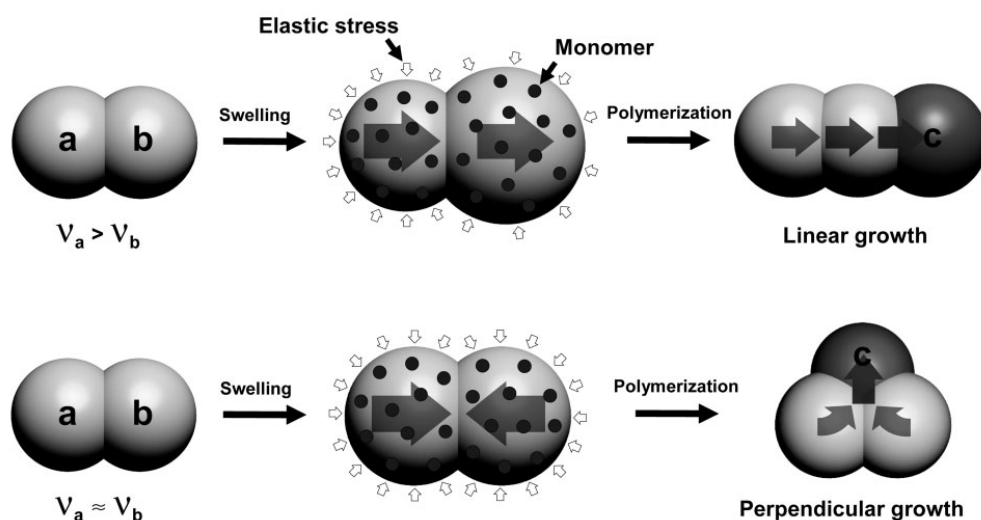


Figure 1-24, schematic view of work by Kim *et. al.*, showing linear and perpendicular growth depending on the crosslinking densities of the material.⁸⁹

1.7.2 Uses of Anisotropic Particles

1.7.2.1 Colloidal Molecules

Colloidal particles such as silica and polymer uniform particles have attracted a lot of attention recently as a scale model for atoms. This idea of studying colloidal hard spheres as atomic equivalents has been used to enrich scientific understanding of many physical phenomena ranging from phase transition to particle-particle interactions.⁹⁰ However a purely spherical system is limited to a number of arrangements and now groups studying such fundamentals are moving toward anisotropic particles and colloidal clusters, and to study the effect on macroscopic properties such as optical properties. This field ultimately lead to van Blaaderen introducing the term “colloidal molecules” based on the idea that colloids can be treated as micro-scale atoms and allow the assembly of far more complex molecules.^{91,92} Figure 1-25 below shows how colloidal clusters can be used as molecular counterparts to study interactions.

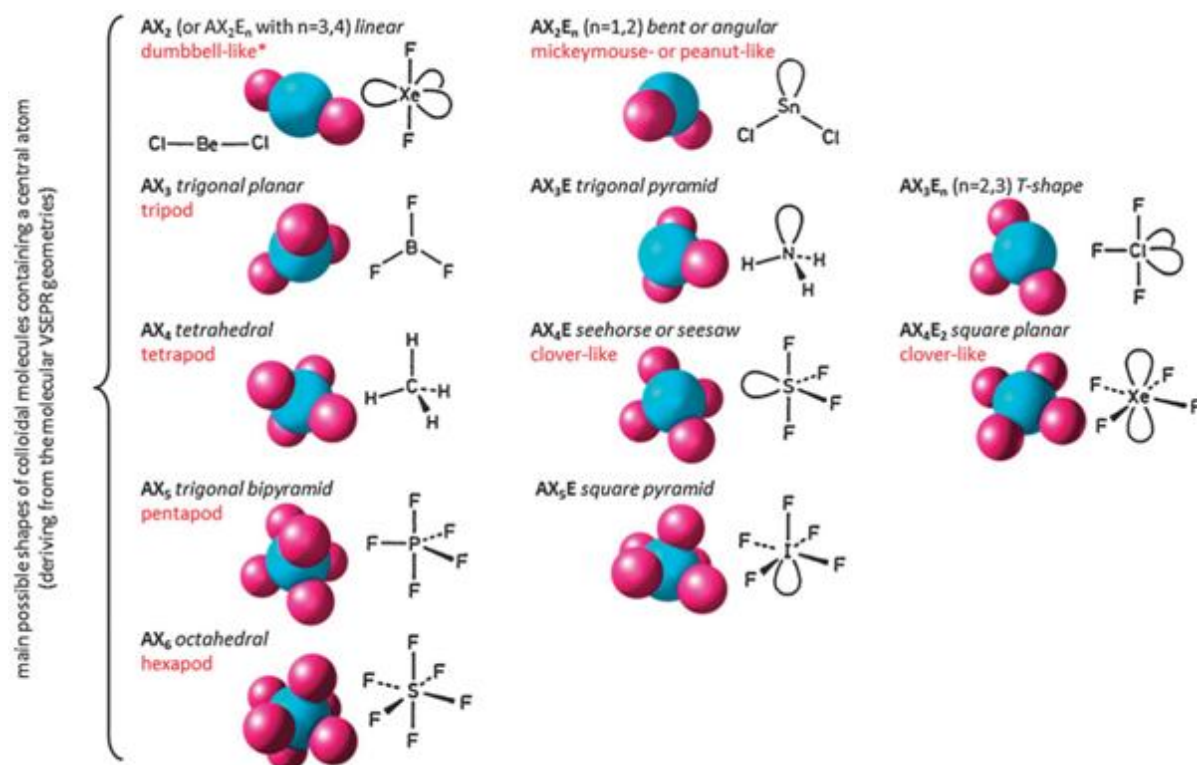


Figure 1-25, examples of how colloidal molecules can be used to represent molecules.⁷¹

The production of such an array of particle shapes is not only limited to colloidal clusters, but can be produced by methods motioned earlier. These particles possess many peculiar properties owing to their unusual shape for example electronic and optical properties⁹³ and also their cluster-cluster interactions due to their shape can give interesting properties. A short review article by Glotzer and Solomon⁹⁴ published in 2007 discusses the possible uses and routes to colloidal molecules of complex shape. They conclude by saying that design rules are needed to totally understand such systems and that current focus of bottom up 'forward' approaches of making nanoparticles and creating clusters from them is only so good. They rationalise this by saying that thermal fluctuations will inhibit the formation of certain structures and geometries at small nano and micro scale to large scales such a millimetre scale.⁹⁵ However a 'reverse engineering' approach may provide some other answers such as, how do we create a crystal structure of colloids by self-assembly with a diamond lattice ordering for optical properties? One example is to produce colloidal carbon mimics i.e. a colloidal tetrahedral system to allow for the lattice to be created by colloidal clusterisation as proposed by Zhang *et al.*⁹⁶ by computer simulation. Such clusters have

been reported by different methods such as; particle fusion to give tetrahedra⁹⁷ and the use of gold nano patches particles to give ‘sticky patches’⁹⁸ as examples.

1.7.2.2 Biological Applications

The use of anisotropic particles, such as dumbbell-like particles, could have major implications in biological fields, such as imaging and drug delivery. With dumbbell-like particles both lobes could be loaded with different drugs, with receptor sites on each side complementary to the drug in question.

Another example of dumbbell-particles being potentially interesting is if each lobe was loaded with different fluorescent dyes and used for cell imaging. This will allow for imaging with different wavelengths of incident light. Particles of multiple compartments have been produced by co-jetting of polymers into a non-solvent which then forms particles.⁹⁹

1.8 Aims and Objectives of the Project

The overall aim of this project was to produce shape anisotropic particles in a controlled scalable manor, using solvents of low dielectric constant for evaluation in electrophoretic display devices. Understanding the resultant particle formation will be important so aspects can be modelled and build understanding which can be passed to Merck. Particle evaluation for electrophoretic displays will primarily be done at Merck owing to special equipment, i.e. production of test cells.

The particles must be produced in non-polar media to avoid lengthy solvent exchange processes which will reduce the yield of any particles produced. If produced in low dielectric solvent then the particles can simply be dispersed into the correct solvent for use.

The goals of the project are therefore:

- Consider industrially saleable processes to produce polymer nanoparticles, which are considered in the introduction.
- To produce spherical polymeric particles and optimise the system to give uniform particles. This must then be extended to the production of crosslinked particles to allow for greater chemical stability toward solvent exchange.

- Monomers must be screened to assess their potential to produce shape anisotropic particles in a seeded non aqueous dispersion polymerisation reaction, analogous to the dynamic swelling method. Once short listed the monomer-particle interactions were probed further to gain understanding into potential morphology changes upon a seeded dispersion polymerisation reaction (second stage polymerisation). This will also allow for predictability to be built into the procedure to allow easy processing of new monomers for shape anisotropic particles if desired.
- Assess the effect of methyl methacrylate as second stage monomer with the addition of crosslinking monomers, again to give greater chemical stability to the particles.
- Assess the ability of the chosen monomers to produce shape anisotropic particles in a second stage reaction, and optimise the process.
- Evaluate seed dispersions and any interesting samples for electrophoretic display applications. This included zeta potential measurement on the dispersions along with specialist tests at Merck, such as production of test switching cells.

1.9 References

¹ http://www.eink.com/display_products_triton.html

² Xerox Corporation, *United States Patent*, 1979, 4143103

³ Xerox Corporation, *United States Patent*, 1978, 4126854

⁴ Xerox Corporation, *United States Patent Publication*, 2008, US 2008/0024466 A1

⁵ <http://www.sipix.com/technology/epaper.html>

⁶ E Ink Corp., *United States Patent*, 2004, US 6,727,881 B1

⁷ Xerox Corporation, *United States Patent*, 2006, 20060222976

⁸ E Ink Corporation, *World Intellectual Property Organisation*, 1999, WO 00/60410

⁹ G. W. Gokel, *Dean's Handbook of Organic Chemistry*, McGraw-Hill, New York, 1976, p 4.98

¹⁰ I. M. Smallwood, *Handbook of Organic Solvent Properties*, Elsevier, 1996

¹¹ J. Brandup, E. H. Immergut, E. A. Grulke, A. Abe and D. R. Bloch, *Polymer Handbook*, John Wiley & Sons, 4th edn. 1998

- ¹² D. R. Caudwell, J. P. M. Trusler, V. Vesovic and W. A. Wakeham, *Int. J. Thermophys.*, 2004, **25**, 1339
- ¹³ Design Institute for Physical Properties, *DIPPR Project 801 – Full Version*, Design Institute for Physical Properties, 2009
- ¹⁴ J. H. Kim, N. H. Lee, H. J. OH, C. R. Yoon, W. W. Kim, J. S. Song, C. J. Jeon and S. J. Kim, *Advances in Science and Technology*, 2006, **45**, 368
- ¹⁵ M. P. L. Werts, M. Badila, C. Brochon, A. Hebraud and G. Hadziioannou, *Chem. Mater.*, 2008, **20**, 1292
- ¹⁶ B. Comiskey, J. D. Albert, H. Yoshizawa and J. Jacobson, *Nature*, 1998, **394**, 253
- ¹⁷ T. Cosgrove, ‘*Colloid Science - Principles, Methods and Applications*’, John Wiley & Sons, 2010
- ¹⁸ G. Gouy, *J. Phys.*, 1910, **9 (4)**, 457
- ¹⁹ D. L. Chapman, *Phil. Mag.*, 1913, **25 (6)**, 475
- ²⁰ R. Kemp, R. Sanchez, K. Mutch and P. Bartlett, *Langmuir*, 2010, **26**, 6967
- ²¹ O. Stern, *Z Elektrochem.*, 1924, **30**, 508
- ²² B. V. Derjaguin and L. Landau, *Acta Physico-chim., USSR*, 1941, **14**, 633
- ²³ E. J. Verwey, and J. T. G. Overbeek, ‘*Theory of the Stability of Lyophobic Colloids*’, Elsevier, 1948
- ²⁴ J. C. Berg, *An Introduction to Interfaces & Colloids The Bridge to Nanoscience*, World Scientific Publishing, Singapore, 2009, Chap. 7
- ²⁵ K. Barrett, *Dispersion Polymerization In Organic Media*, Wiley-Interscience, 1975
- ²⁶ W. Yang, D. Yang, J. Hu, C. Wang and S. Fu, *J. Polym. Sci. A.*, 2001, **39**, 555
- ²⁷ M. Okubo and E. I. T. Yamashita, *J. Polym. Sci. A.*, 1998, **96**, 2513
- ²⁸ G. Bosma, C. Pathmamanoharan, E. H. A. de Hoog, W. K. Kegel, A. van Blaaderen and H.N. W. Lekkerkerker; *J. Colloid and Interface Sci.*, 2002, **245**, 292
- ²⁹ H. V. Harris and S. J. Holder, *Polymer*, 2006, **47**, 5701
- ³⁰ R. H. Pelton, A. Osterroth and M. A. Brook, *J. Colloid Interface Sci.*, 1990, **137**, 120
- ³¹ Y. Peng, A. Pallandre, N. T. Tran and M. Taverna, *Electrophoresis*, 2008, **29**, 157
- ³² Y. Okamoto, F. Kitagawa and K. Otsuka, *Electrophoresis*, 2006, **27**, 1031
- ³³ A. Klinkenberg and J. L. van der Minne, *Electrostatics in the Petroleum Industry*, Elsevier, New York, 1958
- ³⁴ J. C. Berg, *An Introduction to Interfaces & Colloids The Bridge to Nanoscience*, World Scientific Publishing, Singapore, 2009, Chap. 5
- ³⁵ A. Parsegian, *Nature*, 1969, **221**, 844

- ³⁶ G. S. Roberts, R. Sanchez, R. Kemp, T. Wood and P. Bartlett, *Langmuir*, 2008, **24**, 6530
- ³⁷ J. Lyklema, *Fundamentals of Interface and Colloid Science. Vol. II: Solid-Liquid Interfaces*, Academic Press, London, 1995
- ³⁸ M. F. Hsu, E. R. Dufresne and A. D. Weitz, *Langmuir*, 2005, **21**, 4881
- ³⁹ M. J. Rosen, '*Surfactants and Interfacial Phenomena*', John Wiley & Sons, 1978
- ⁴⁰ F. M. Fowkes, '*The Interactions of Polar Molecules, Micelles and Polymers in Non Aqueous Media*', in K. Shinoda, '*Solvent Properties of Surfactant Solutions*', Dekker, New York, 1967 p 65
- ⁴¹ A. Kitahara, T. Kobayashi and T. Tachibana, *J. Phys Chem.*, 1962, **96**, 1794
- ⁴² M. B. Mathews and E. Hirschorn, *J. Colloid Sci.*, 1953, **8**, 86
- ⁴³ Z. Randriamalala, A. Denat, J. P. Gosse and B. Gosse, *IEEE Trans. Elect. Insul.*, 1985, **EI-20**, 167
- ⁴⁴ A. Denat, B. Gosse and J. P. Gosse, *J. Electrostatics*, 1982, **12**, 197
- ⁴⁵ C.E. Espinosa, Q. Guo, V. Singh and S. H. Behrens, *Langmuir*, 2010, **26**, 16941
- ⁴⁶ F. M. Fowkes, H. Jinnai, M. A. Mostafa, F. W. Anderson and R. J. Moore, *ACS Symp. Ser. 240, American Chemical Society*, Washington, DC, 1984, p 331
- ⁴⁷ I. D. Morrison, *Colloid Surface A*, 1993, **71**, 1
- ⁴⁸ N. J. Felici, *J. Electrostatics*, 1977, **4**, 119
- ⁴⁹ K. Müller, M. Klapper and K. Müllen, *J. Polym. Sci.A: Polym. Chem.*, 2007, **45**, 1101
- ⁵⁰ Rhom and Haas Company, *European Patent*, 1987, 0272021
- ⁵¹ R. Biermans, *United States Patent*, 2007, 20070295655
- ⁵² K. Müller, M. Klapper and K. Müllen, *Macromol. Rapid Commun.*, 2006, **27**, 586
- ⁵³ A. I. Campbell and P. Bartlett, *J. Colloids Interface Sci*, 2002, **256**, 325
- ⁵⁴ Imperial Chemical Industries, *British Patent*, 1962, 893,429
- ⁵⁵ Rohm and Hass, *British Patent*, 1963, 934,038
- ⁵⁶ D-G. Yu and J. H. An, *J. Polym. Sci. A: Polym. Chem.*, 2004, **42**, 5608
- ⁵⁷ T. Vissers, A. Wysocki, M. Rex, H. Löwen, C. P. Royall, A. Imhof and A. Van Blaaderen, *Soft Matter*, 2011,**7**, 2352
- ⁵⁸ G. Bosma, C. Pathmamanoharan, E. H. A. De Hoog, W. K. Kegel, A. Van Blaaderen, H. N. W. Lekkerkerker
- ⁵⁹ M. Yasuda, H. Seki, Hideki. Yokoyama, H. Ogino, K. Ishimi and H. Ishikawa, *Macromolecules*, 2001, **34**, 3261
- ⁶⁰ M. T. Elsesser, A. D. Hollingsworth, K. V. Edmond and D. J. Pine, *Langmuir*, 2011, **27**, 917

- ⁶¹ M. Karimi, M. Heuchel, W. Albrecht and D. Hofmann, *Membrane Science*, 2007, **292**, 80.
- ⁶² J. M. G Cowie, *Polymers: Chemistry & Physics of Modern Materials*, 2nd ed., Blackie Academic & Professional, 1991
- ⁶³ P. J. Flory, *Principles of Polymer Chemistry*, Cornell University Press, 1953
- ⁶⁴ A. J. C. Kuehne, M. C. Gather and J. Sprakel, *Nature Commun.*, 2012, **3**, 1088
- ⁶⁵ M. Nagy and A. Keller, *Polym. Commun.*, 1989, **30**, 133
- ⁶⁶ T. van Dillen, A. Polman, C. M. van Kats and A. van Blaaderen, *Appl. Phys. Lett.*, 2003, **83**, 4315
- ⁶⁷ H. R. Sheu, M. S. El-Aasser and J. W. Vanderhoff, *J. Polym. Sci. A: Polym. Chem.*, 1990, **28**, 629
- ⁶⁸ S. Sacanna, W. T. M. Irvine, P. M. Chaikin and D. J. Pine, *Nature*, 2010, **464**, 575
- ⁶⁹ Y. Xia, B. Gates, Y. Yin and Y. Lu, *Adv. Mater.*, 2000, **12**, 693
- ⁷⁰ S-M. Yang, S-H. Kim, J-M. Lim and G-R. Yi, *J. Mater. Chem.*, 2008, **18**, 2177
- ⁷¹ E. Duguent, A. Désert, A. Perro adn S. Ravaine, *Chem. Soc. Rev.*, 2011, **40**, 941
- ⁷² T. van Dillen, A. Polman, W. Fukarak, A. van Blaaderen, *Appl. Phys. Lett.*, 2001, **78**, 910
- ⁷³ E. Snoeks, A. van Blaaderen, T. van Dillen, C. M. van Kats, L. Brongersma and A. Polman, *Adv. Mater.*, 2000, **12**, 1511
- ⁷⁴ T. van Dillen, A. Polman, C. M. van Kats and A. van Blaaderen, *Appl. Phys. Lett.*, 2003, **21**, 4315
- ⁷⁵ C. C. Ho, A. Keller, J. A. Odell and R. H. Ottewill, *Colloid and Polym. Sci.*, 1993, **271**, 469
- ⁷⁶ J. A. Champion, Y. K. Katare and S. Mitragotri, *PNAS*, 2007, **104**, 11904
- ⁷⁷ Y. Lu, Y. Yin, Z-Y. Li and Y. Xia, *Langmuir*, 2002, **18**, 7722
- ⁷⁸ Y. Lu, Y. Yin, Z-Y. Li and Y. Xia, *Adv. Mater*, 2001, **13**, 271
- ⁷⁹ P. P. Lele and E. M. Furst, *Langmuir*, 2009, **25**, 8875
- ⁸⁰ K. P. Velikov, T. van Dillen, A. Polman and A. van Blaaderen, 2002, *Appl. Phys. Lett.*, 2002, **81**, 838
- ⁸¹ M. Okubo, T. Yamashita and M. Shiozaki, *J. Appl. Polym. Sci.*, 1996, **60**, 1025
- ⁸² E. B. Mock, H. De Bruyn, B. S. Hawkett, R. G. Gilbert and C. f. Zukoski, *Langmuir*, 2006, **22**, 4037
- ⁸³ R. H. Ottewill, A. B. Schofield and J. A. Waters, *Colloid Polym. Sci.*, 1996, **274**, 763

- ⁸⁴ H. R. Sheu, M. S. El- Aasser and J. W. Vanderhoff, *J. Polym. Sci. A: Polym. Chem.*, 1990, **28**, 653
- ⁸⁵ P. J Flory, *J. Chem. Phys.*, 1942, **10**, 51
- ⁸⁶ M. L. Huggins, *J. Chem. Phys.*, 1942, **46**, 151
- ⁸⁷ P. J. Flory and J. Rehner, *J. Chem. Phys.*, 1943, **10**, 51
- ⁸⁸ M. Morton, S. Kaizerman and M. W. Altier, *J. Colloid Sci.*, 1954, **11**, 521
- ⁸⁹ J-W. Kim, R. J. Larsen and D. A. Weitz, *Adv. Mater.*, 2007, **19**, 2005
- ⁹⁰ D. G. Grier, *MRS Bull.*, 1998, **23**, 21
- ⁹¹ A. Van Blaaderen, *Science*, 2003, **301**, 470
- ⁹² A. Van Blaaderen, *Nature*, 2006, **439**, 545
- ⁹³ Y. Xia and N. J. Hales, *Mater. Res. Soc. Bull.*, 2005, **30**, 338
- ⁹⁴ S. C. Glotzer and M. J. Solomon, *Nature Materials*, 2007, **6**, 557
- ⁹⁵ D. H. Gracias, J. Tein, T. L. Breen, C. Hsu and G. M. Whitesides, *Science*, 2000. **289**, 1170
- ⁹⁶ Z. L. Zhang, A. S. Keys, T. Chen and S. C. Glotzer, *Langmuir*, 2005, **21**, 11547
- ⁹⁷ D. Zerrouki, B. Rotenberg, S. Abramson, J. Baudry, C. Goubault, F. Leal-Calderon, D. J. Pine and J. Bibette, *Langmuir*, 2006, **22**, 57
- ⁹⁸ G. Zhang, D. Y. Wang and H. Möhwald, *Angew. Chem. Int. Ed.*, 2005, **44**, 7767
- ⁹⁹ K. Maeda , H. Onoe , M. Takinoue , and S. Takeuchi, *Adv. Mater.*, 2012, **24**, 1340

2 Spherical Seed Particle Synthesis

2.1 Introduction

In this chapter the formation of uncrosslinked and crosslinked particles by non-aqueous dispersion polymerisation will be discussed. Understanding of the reaction mechanism allowed for the production of uniform crosslinked particles.

All dispersions produced throughout will have a unique code in the form of, SRB-X-Y. This equates to a sample number, X and aspects of the particle surface composition, Y, this allows for easy reference between multiple batches of the particle dispersions discussed.

2.2 Optimisation of Dispersion Polymerisation to Give Uncrosslinked Poly(Methyl Methacrylate) Particles

Initial process development was undertaken to optimise the dispersion polymerisation reaction toward uncrosslinked particle formation. This included, varying solvent choice and monomer concentration. This was based upon the work by Antl *et al.*¹ and as such the stabiliser, chain transfer agent and initiator concentrations were set in line with their work.

The following batch process was used throughout unless otherwise stated; see the *Experimental* (chapter 8) for specific detail.

Table 2-1, approximate values for dispersion polymerisation reaction components.

Chemical	% of Reaction Mixture
Monomer	40
Chain transfer agent	0.85
Solvent	52
Stabiliser	7
Radical Initiator	0.85

The batch method is where a dispersion is produced in a single batch with all chemicals charged into the reaction vessel prior to the start of the reaction.

2.2.1 Components of Dispersion Polymerisation

In this work methyl methacrylate (MMA) was used as the primary monomer and 2 wt. % methacrylic acid (MAA) as comonomer to enable subsequent chemical attachment of the graft stabiliser if required.

The steric stabiliser used is poly(hydroxyesteric acid)-*g*-(methyl methacrylate-*co*-glycidyl methacrylate) or P(HSA-*g*-MMA), a complex graft polymer. The polymer stabiliser has three main parts, a statistical copolymer of MMA and glycidyl methacrylate (GMA) which will physisorb to the growing PMMA particles. The GMA is incorporated to have complementary functional groups to the MAA in the particles. These two groups can be reacted together to chemically bond the stabiliser to the particle surface. The final component, the poly(hydroxyesteric acid) (PHSA), gives the stability to the PMMA colloidal particles due to the large alkyl chains which will be solvated by the hydrocarbon solvent. The characterisation of the stabiliser can be found in the *Experimental* (chapter 8).

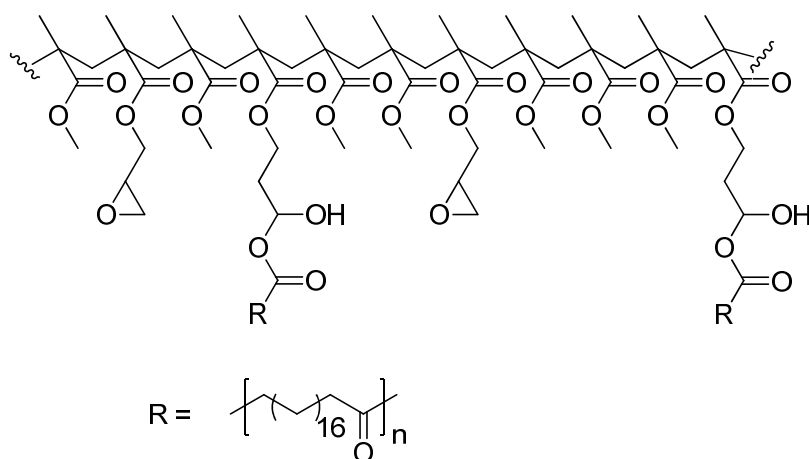


Figure 2-1, schematic view of the P(HSA-*g*-MMA) steric stabiliser.

The free radical initiator used was 2,2'-azobis(2-methylpropanitrile) or Vazo-67. The half-life, $t_{1/2}$, of Vazo-67 can be calculated by the following equation²:

$$\log t_{\frac{1}{2}} = 7492\left(\frac{1}{T}\right) - 19.215 \quad 2-1$$

Where, T , is the absolute temperature in Kelvin and $t_{1/2}$, is the half-life of the initiator in minutes.

Table 2-2, half-life of Vazo-67 at various temperatures.

Temperature (°C)	Half-life
20	1526 days
40	36 day
60	31 hr
80	1.6 hr
100	7.3 min
120	41.6 s

Cleaning the particle dispersions after a reaction is very important to remove any small particles formed by secondary nucleation as well as any excess stabiliser and unreacted monomer. This can be achieved by centrifugation of the samples and dispersal into fresh solvent. In order to ensure that only the large particles formed sediment, leaving the smaller particles from secondary nucleation in suspension, a slow speed was used.

It is known that smaller particles will sediment slower and larger particles faster by the Stokes equation shown below.

$$v = \frac{(\rho_p - \rho_f)gr^2}{9\eta} \quad 2-2$$

Where, v , is settling rate, ρ_p and ρ_f , being the density of the particle and fluid respectively, g , is acceleration under gravity, r , the particle radius and η , is the viscosity of the fluid.

Centrifugation at a slow speed however may not always sediment all the particles Figure 2-2 shows images of the supernatants of three consecutive washing steps, this will not only clean but will also serve to narrow the polydispersity of the sample.

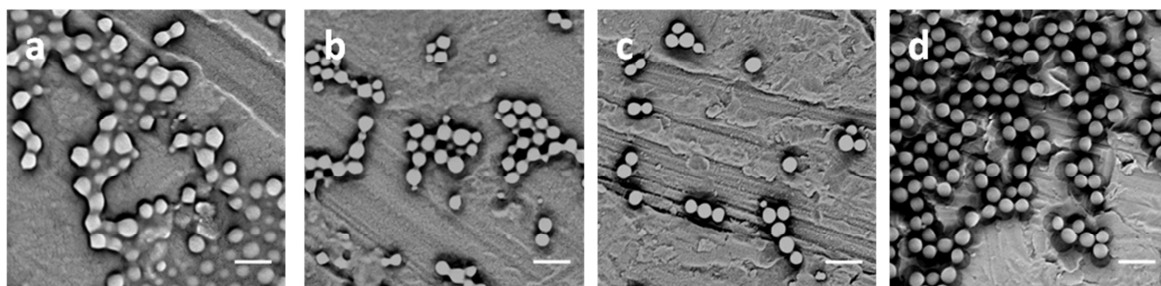


Figure 2-2, SEM images of supernatant liquid after sequential centrifugation steps and the final cleaned dispersion (20 min at 2500 rpm) where; a, is supernatant from the 1st wash step, b, is supernatant from the 2nd wash step, c, is supernatant from the 3rd wash step and d, the final cleaned redispersed pellet for comparison. Scale bars are 1 μm .

It is clear from the SEM micrographs across the series in Figure 2-2 that small particles are being removed from the sample leading to the final cleaned sample with a lower polydispersity. The image in Figure 2-2 a, shows particles which have fused together on the SEM stub, this could be due to the gold coating process.

2.2.2 Effect of Solvent Choice

The choice of solvent will have an effect upon the polymerisation reaction in terms of rate of reaction as the solvent will dictate the ceiling temperature of the reaction. This can be tailored with solvent mixtures. In this case mixtures of hexane and dodecane are considered.

Reactions at different solvent ratios were undertaken to monitor the resultant particle size to see if there was any correlation. Figure 2-3 below shows the dynamic light scattering (DLS) traces for reactions where the solvent system was; pure dodecane, 1:1 and 2:1 hexane / dodecane and pure hexane. The z-average particle size data is shown in Table 2-3.

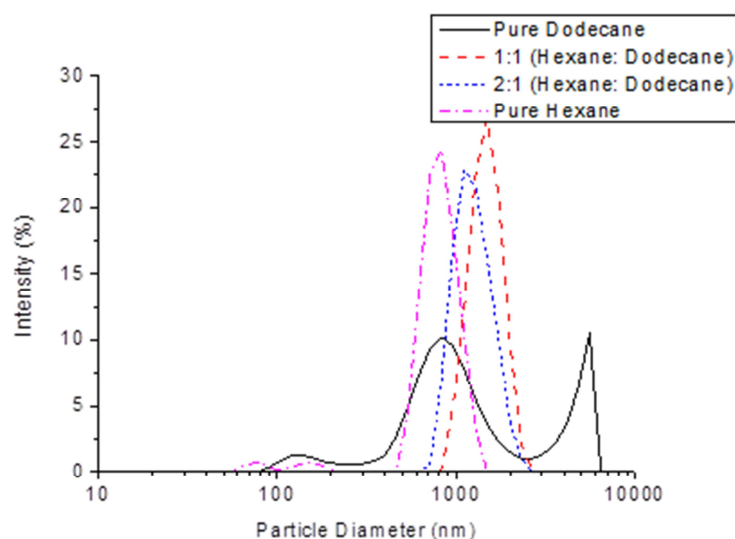


Figure 2-3, Average DLS traces for particles produced in different ratios of hexane and dodecane.

The data for the mixed solvent systems gives a single peak and shows a slight size increase between the 1:1 and 2:1 samples. However the pure solvent samples show multiple peaks seen far clearer in the pure dodecane sample, this could be attributed to sample aggregation or flocculation. It could be that during the reaction some hexane is removed due to evaporation leading to some aggregation. Whereas in the pure dodecane sample the temperature exotherm (see 2.2.2.1) and rapid release of radicals could have led to aggregation of particles, by heating the growing polymer above their glass transition temperature, T_g and allowing particle fusion.

Table 2-3, average particle diameter by DLS.

Sample	z-Average Particle Diameter (nm)
Pure dodecane	714
1:1 hexane: dodecane	725
2:1 hexane: dodecane	604
Pure hexane	928

The T_g of a polymer is the temperature boundary at which the sample goes from a glassy, brittle state into a fluid, rubbery state.³ The T_g of a polymer sample can be measured by differential scanning calorimetry, (DSC), which measures the energy required to heat an

empty reference pan and a sample pan by 1 °C. When the sample goes through a phase transition, such as the glass transition the heat flow is different between the two pans, and measures the difference. This technique allows for the experimental measurement of other phase transitions, such as the melting temperature, T_m , and in the case of crystalline samples the crystallisation temperature, T_c . The T_g of amorphous PMMA is 105 °C, depending upon the molecular weight of the sample and the heating rate used.⁴

2.2.2.1 Effect of Solvent - Temperature Profile

The polymerisation reactions were conducted at 85 °C as this was found to give a reasonable half-life for the initiator of approximately 50 min. in accordance with previous studies.⁵ However it was found that if the reactions were conducted in pure dodecane the reaction would show a reaction exotherm. The reaction temperature has been observed to increase by approximately 30 °C above the 85 °C set point. This has implications upon the radical flux during the course of the reaction. If the temperature of the reaction raises significantly then the Vazo-67 initiator will rapidly decompose. This is shown in the temperature profile (Figure 2-4 a) and also plotted is the Vazo-67 half-life at the reaction temperature. It is clear that as the reaction temperature increases it has a large effect on the half-life of the initiator.

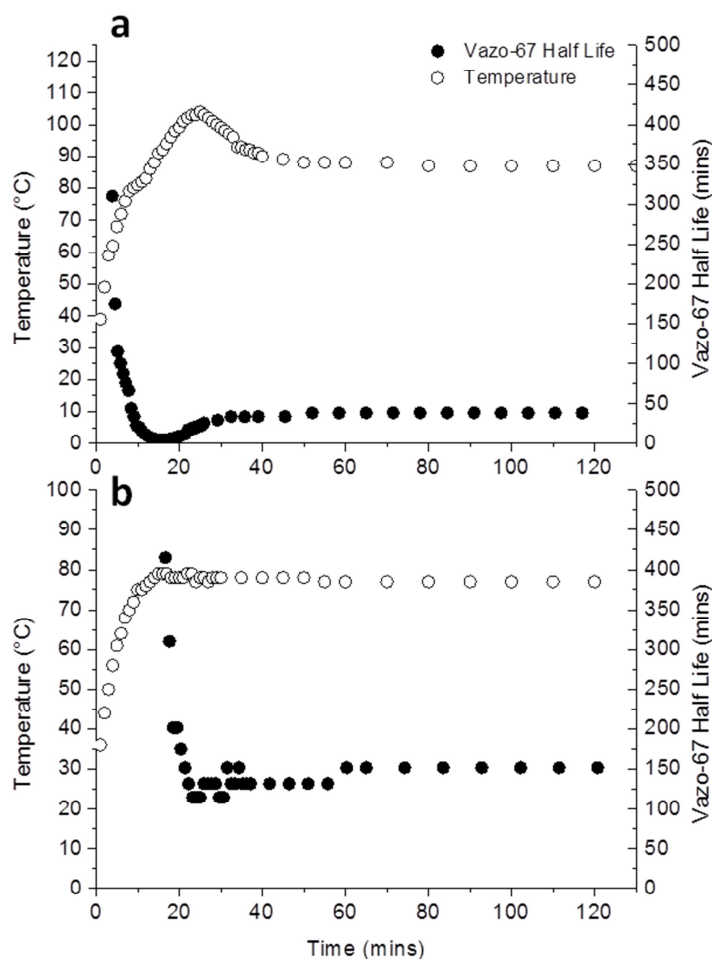


Figure 2-4, reaction temperature profile and vazo-67 half-life during the polymerisation reaction for; a, SRB-088-0%xl in pure dodecane and b, SRB-077-0%xl in 2:1 hexane / dodecane solvent mixture.

To compensate for this and to give a constant radical flux a mixed solvent system can be used. Figure 2-4 b shows the temperature profile and Vazo-67 half-life for the same uncrosslinked particles reaction but with a 2:1 solvent mixture of hexane / dodecane. As the solvent system is now in excess of hexane over dodecane the reaction temperature is held around hexane's boiling point limiting the reaction temperature approximately 80 °C.

According to equation 2-1 this will now give an initiator half-life of approximately 150 min. This will have implications with the conversion rate of monomer to polymer, due to the slow release of radicals and ultimately the resultant particles formed. Resultant particles from these reactions can be seen in Figure 2-5 along with their size distributions.

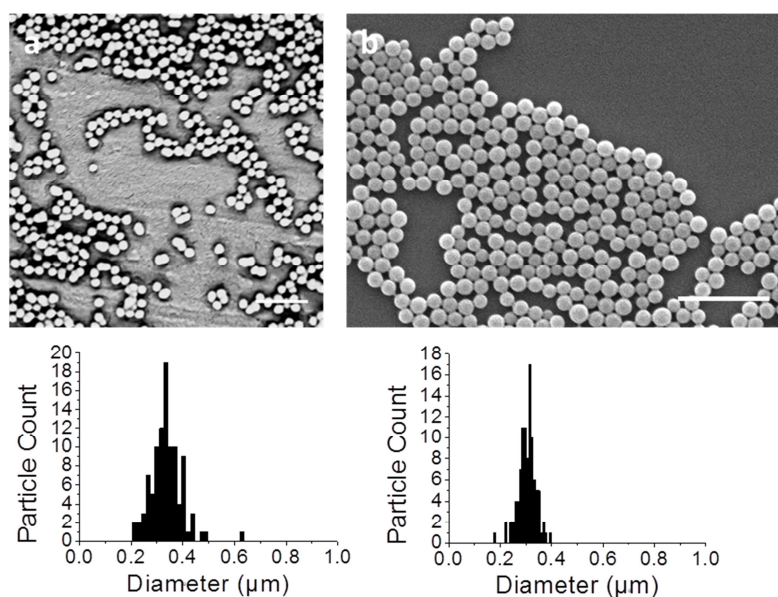


Figure 2-5, resultant particles from changing the solvent system, a, SRB-088-0% xl with pure dodecane solvent and b, SRB-077-0% xl with a hexane / dodecane solvent mixture. Scale bars are 2 μm , sizing data based on counting 100 particles.

It is clear that a mixed solvent system gives a cleaner reaction i.e. less visible aggregation, and no secondary nucleation is evident. The reaction for the mixed solvent system (SRB-077-0% xl) also shows narrower size distribution, reflected in the size distribution plots and the data in Table 2-4.

The coefficient of variation is determined by the standard deviation of the particle size measurement divided by the mean particle size. This is then turned into a percentage by multiplying by 100. Note that by convention a coefficient of variation of 10 % for a sample is deemed 'monodisperse'.

Table 2-4, showing particle size and polydispersity data for dispersion SRB-088-0%xl and SRB-077-0%xl.

Sample	Particle Diameter (nm)	Coefficient of Variation
SRB-088-0% xl	350	18 %
SRB-077-0% xl	310	11 %

2.2.2.2 Effect of Solvent - Monomer Conversion

As there is a significant exotherm in the dispersion polymerisation reaction if a single high boiling solvent is used, i.e. dodecane, which can be suppressed by using a mixed solvent system, this may have an effect on the monomer conversion.

Figure 2-6 below shows the monomer conversion profile for the two reactions in, pure dodecane and in a 2:1 hexane / dodecane mixture. The conversion profile was measured by taking aliquots from the reaction over the course of the reaction and measuring the total solids content by mass loss, which is related to the theoretical total solids content at 100 % conversion.

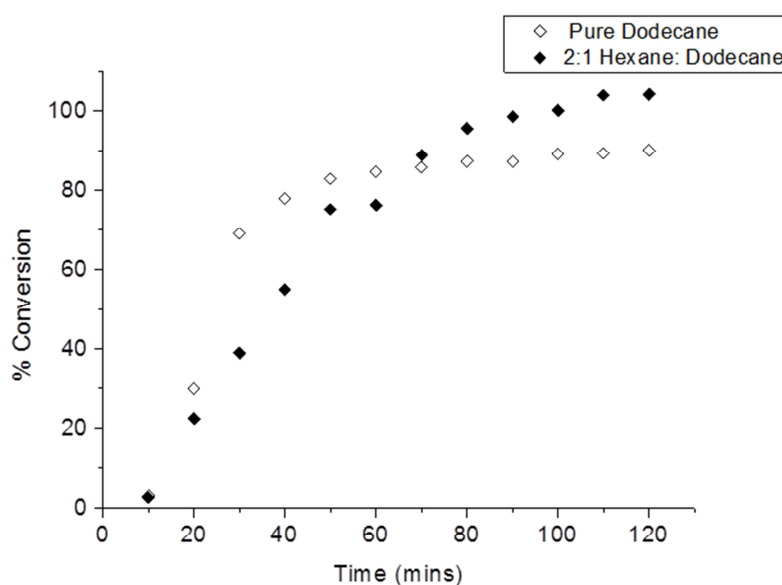


Figure 2-6, monomer conversion vs. time over the polymerisation reaction for; a, SRB-088-0%xl in pure dodecane and b, SRB-077-0%xl in 2:1 hexane: dodecane solvent mixture.

The graph shows that the dodecane reaction goes to 90 % monomer conversion but the 2:1 hexane / dodecane reaction goes above 100 % conversion. This must be due to solvent loss from the reaction mixture due to boiling hexane which does not condense. However it does show that despite the lower reaction temperature the reaction can proceed to high monomer conversion.

2.2.3 Varying the Monomer Concentration

All subsequent reactions are conducted with a mixed solvent system of hexane / dodecane in a 2:1 ratio to remove the reaction exotherm, and give a smoother radical flux, giving a constant reaction rate.

Published work by Antl *et al.*¹ states that the dispersion polymerisation reaction in hydrocarbon media has a large unstable region (Figure 2-7) with regard to monomer concentration. This instability region was mapped out. They say that below 8 wt. % monomer and above 35 wt. % monomers in the reaction should produce colloiddally stable particles using the P(HSA-g-PMMA) stabiliser.

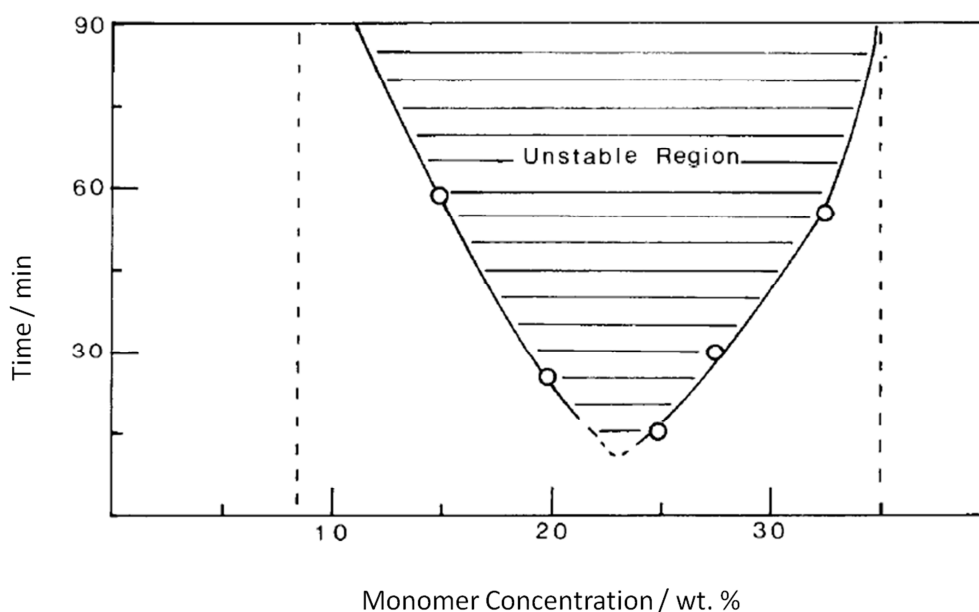


Figure 2-7, instability window proposed by Antl *et al.*¹ for non-aqueous dispersion polymerisation reactions with respect to monomer concentration, the dashed lines show the boundary of the unstable region.

This instability window was mapped out and SEM micrographs of the resultant dispersions are shown in Figure 2-8, with reactions varying from 10 wt. % to 50 wt. %. From the SEM micrographs of the samples in the instability window the dispersions are not stable individual particles and that aggregation has occurred in the reaction. The polydispersity of the samples is also very high which is reflected in the size distribution graphs in Figure 2-9. This polydispersity can be due to the fact that there is not enough monomer in the reaction mixture to grow and fuse the aggregating primary particles formed early on in the

reaction into larger stable particles. Hence why the dispersions appear as aggregated small particles of irregular shape with some grown to full size.

Samples outside the instability window at low monomer content could not be visualised by SEM as the particles formed were very small and the sample very dilute. However at high monomer concentration the resultant dispersions increase in size with monomer content and appear to become more monodisperse as reflected in the size distribution plots in Figure 2-9. Particle size data and the coefficient of variation are shown in Table 2-5.

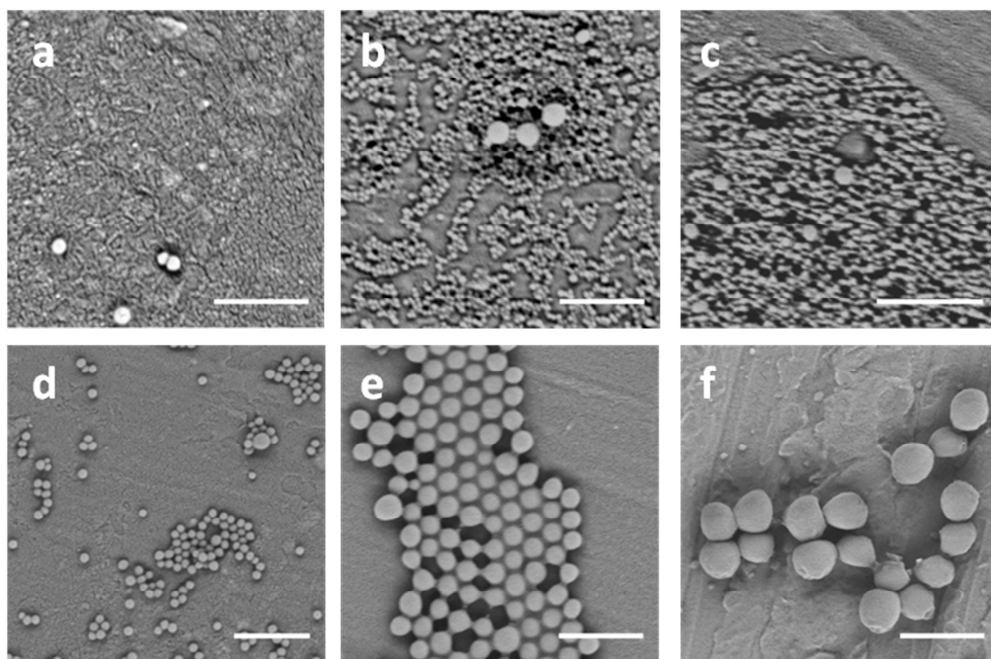


Figure 2-8, resultant particles with changing the monomer concentration where; a, is 10 wt. % monomer, b, 20 wt. %, c, 30 wt. %, d, 35 wt. %, e, 40 wt. % and f, 50 wt. % monomers. Scale bars are 2 μm .

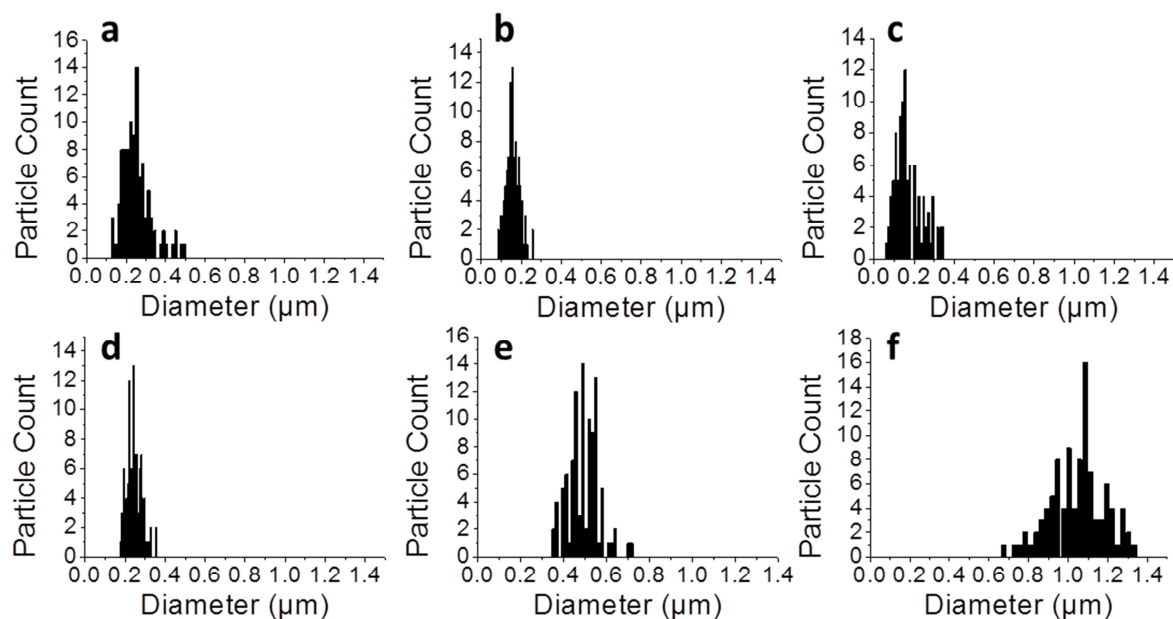


Figure 2-9, size distributions for resultant particles with changing the monomer concentration where; a, is 10 wt. % monomer, b, 20 wt. %, c, 30 wt. %, d, 35 wt. %, e, 40 wt. % and f, 50 wt. % monomers, sizing data based on counting 100 particles.

Table 2-5, particle size and coefficient of variation measurements for the dispersions of increasing monomer concentration.

Monomer Concentration (wt. %)	Particle Diameter (nm)	Coefficient of Variation
10	260	28 %
20	160	21 %
30	180	39 %
35	250	15 %
40	500	14 %
50	1060	13 %
60	2650	13 %

The trend of increasing size and decreasing polydispersity with increasing monomer concentration is evident by the data in Table 2-5. This increase in size can be pushed further with reactions at 60 wt. % monomer that still give clean dispersions as shown by Figure 2-10.

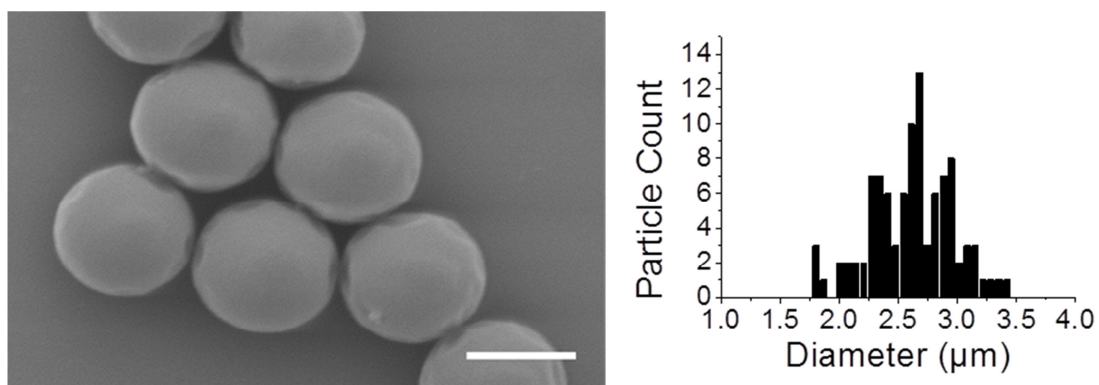


Figure 2-10, resultant particles when dispersion polymerisation is run at 60 wt. % monomer and size distribution plot. Scale bars are 2 μm , sizing data based on counting 100 particles.

By varying the monomer concentration there can be a great deal of control over the particle size and the degree of polydispersity in the sample. Note that the samples at 50 wt. % and 60 wt. % monomer no longer have a spherical morphology, this is due to beam damage by the electron microscope or from the gold coating process.

However for the application these particles are intended for, electrophoretic displays, the particle size is required to be approximately 500 nm.

Having optimised the process of uncrosslinked particle formation by a batch process optimised to give spherical particles, the appropriate conditions were used to produce spherical crosslinked particles.

2.3 Crosslinked Particle Formation

Crosslinked particles were required to produce non-spherical particles based on the dynamic swelling method, which uses highly crosslinked particles swollen with monomer to produce a protrusion of monomer from the particle surface which was then polymerised.⁶ The production of crosslinked particles was based upon the reaction conditions found earlier i.e. a mixed solvent system of hexane and dodecane, a monomer concentration approximately 35 wt. % and polymerised at 85 °C. The production of particles which are crosslinked is advantageous as they will have a greater chemical

stability with regard to solvent choice. The tuning of the reaction conditions to keep relatively monodisperse dispersions of a uniform spherical shape is vital as they will be used as precursors for non-spherical particle architectures.

2.3.1 Addition of Crosslinker and Mechanistic Implications

The key attribute of a dispersion polymerisation is that the monomer is soluble in the continuous phase solvent but the polymer is insoluble. This leads to precipitation of the growing polymers which are then stabilised by a steric stabiliser in solution. This is shown in Figure 2-11.

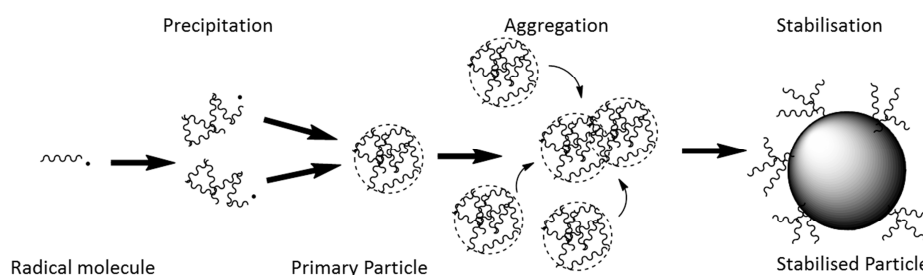


Figure 2-11, schematic view of the dispersion polymerisation mechanism.⁷

Another key attribute to dispersion polymerisation is that the number of particles is set very early on in the reaction. When growing polymer chains precipitate to form small primary particles, this is the largest number of particles available as these then aggregate together to give the final larger stabilised particles, discounting occurrences of secondary nucleation.⁸

The addition of a crosslinking monomer to the NAD reaction will affect the mechanism of particle formation. The formation of primary particles is governed by the solubility of the growing polymer in solution and if this is changed by crosslinking, effectively rapidly increasing the molecular weight of the polymer, then the kinetics of the reaction will change. This could lead to precipitating polymer segments while other small segments which have not crosslinked are still in solution giving rise to a dual population with respect to particle size. However this can be overcome to a certain extent if the reaction runs fast enough to compensate for this difference in reaction kinetics, i.e. a more reactive initiator and / or a higher reaction temperature.

Due to the fact that the reaction is so sensitive to changes in solubility before particle nucleation⁹ the first crosslinker to be assessed was ethylene glycol dimethacrylate (EGDMA). As EGDMA has a similar structure to MMA and so should have a similar solubility in hydrocarbon solvents, so will therefore not promote the precipitation of polymer chains when it becomes incorporated into the growing polymer, due to solubility mismatch with the solvent.

2.3.2 Batch Method of Formation

The batch method is where a dispersion is produced in a single batch with all chemicals charged into the reaction vessel prior to the start of the study.

2.3.2.1 Varying Crosslinker Concentration

In order to assess the ability of the batch method to produce monodisperse crosslinked particles reactions were undertaken varying the crosslinker concentration from 0 - 2 wt. % EGDMA of the total monomer concentration. SEM images of the resultant dispersions are shown in Figure 2-12.

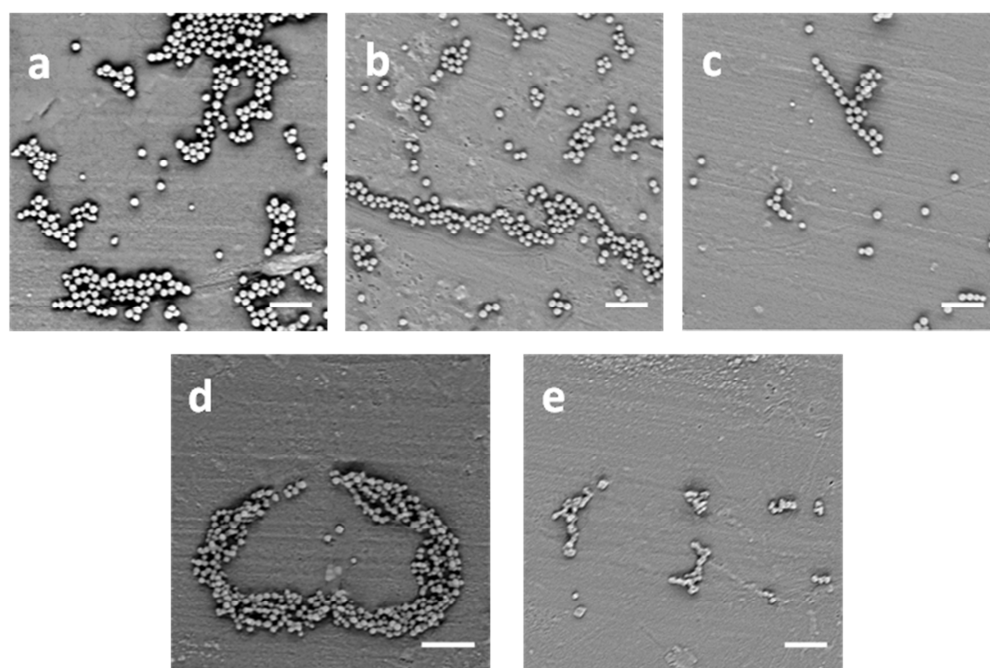


Figure 2-12, resultant particles with increasing EGDMA concentration by the batch method with; a, 0 wt. %, b, 0.5 wt. %, c, 1.0 wt. %, d, 1.5 wt. %, e, 2 wt. %. Scale bars are 2 μm .

Increasing the EGDMA concentration clearly affected the particle stability and growth during the reaction as increasing the EGDMA concentration gave higher levels of aggregates. Figure 2-12 shows that separate spherical particles were maintained up to 1 wt. % addition of EGDMA but above this the particles aggregate into larger structures.

From this set of experiments it was clear that producing crosslinked particles by a batch method does not give suitable particles for further study.

2.3.3 Implications of Crosslinker Addition at the Critical Time to Particle

Nucleation, t_c

As a dispersion polymerisation reaction is very sensitive to changes in solubility of growing chains before the onset of particle nucleation, if the crosslinking monomer is added at this critical time then the crosslinker should not affect the reaction mechanism. This critical time to particle nucleation, t_c , is the onset at which the primary particles form from precipitating polymer chains which have grown to the point at which they are no longer soluble.¹⁰

However if the addition of the crosslinking monomer is not at t_c , then different situations can arise, as shown by Figure 2-13, where 1 wt. % EGDMA was added to the reaction before particle nucleation, at the onset of particle nucleation and after particle nucleation.

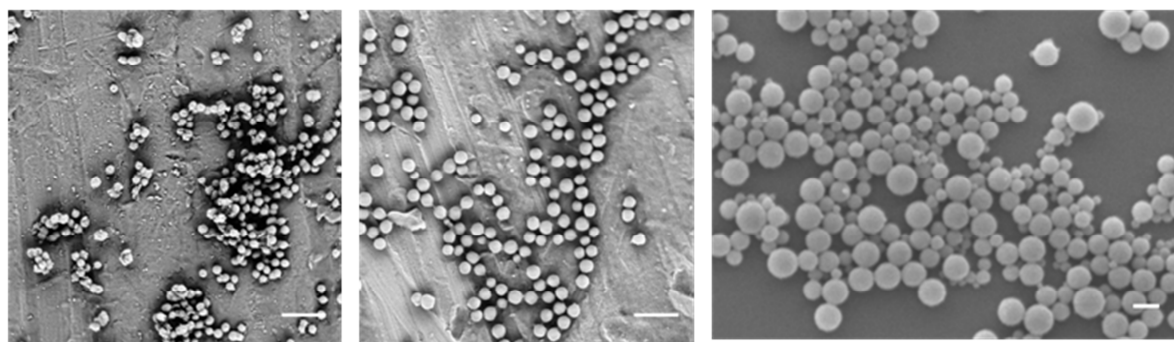


Figure 2-13, SEM micrographs of resultant particles with crosslinking monomer added before t_c left, at t_c , centre and after t_c , right which correspond to SRB-254-1% EGDMA, SRB-325-1% EGDMA and SRB-043-1% EGDMA.

It is clear from the SEM images that addition of a crosslinking monomer at the wrong time had consequences for the resultant dispersion with regards to particle morphology and

polydispersity. If the crosslinking monomer was added too soon then the reaction behaved as that of the batch method and led to particle aggregation. If the crosslinking monomer was added after t_c then a secondary population is likely to be formed of rapidly precipitated crosslinked particles, or a core-shell morphology might be produced in which the particles have a crosslinked shell but maintain an uncrosslinked PMMA core. However if the crosslinking monomer was added at t_c then the primary particles aggregate to form fully grown particles they will be crosslinked together giving uniform spherical particles.

2.3.4 Finding the Critical Time to Particle Nucleation

As the critical time to particle nucleation is the onset of the growing polymer precipitating we know that this happens approximately 10 min. into the reaction from the turbidity measurements in Figure 2-16. However to find the onset of particle nucleation the initial 20 min of a reaction was monitored for particle size and monomer conversion. The results plotted against time are shown in Figure 2-14 below.

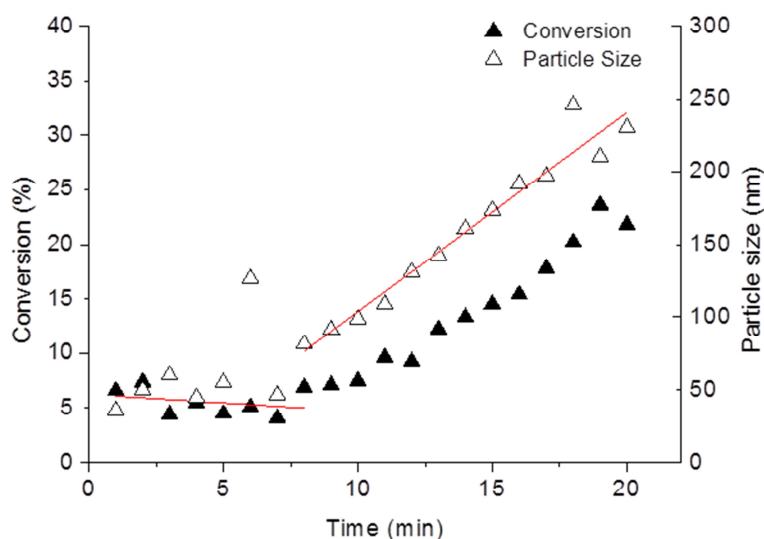


Figure 2-14, monomer conversion and particle size vs time for SRB-091-1% EGDMA with lines of best fit to exemplify the inflection point.

The results for both particle size and monomer conversion versus time show an inflection point at 8 min. It is thought that before this time the polymers are still in solution but at

8 min., they reach a critical molecular weight, precipitate and start to aggregate together. This would explain the increase in both particle size and monomer conversion.

To further confirm that the t_c is at 8 min. selected samples were taken for SEM imaging shown in Figure 2-15. Note that the polydispersity of all the samples was very high due to the fact that the reaction was cut short before aggregation of primary particles could occur in all cases, which is the major growth mechanism for the particles at this early stage in the reaction.

At $t = 5$ min. there were some particles present however these were very soft as they appear to wet the SEM stub. This is indicative of a sample which has soft gel-like particles, so fully formed particles have not yet formed. The sample being very soft could have been due to the fact that not many particles that have formed are heavily swollen with monomer so appear gel-like.

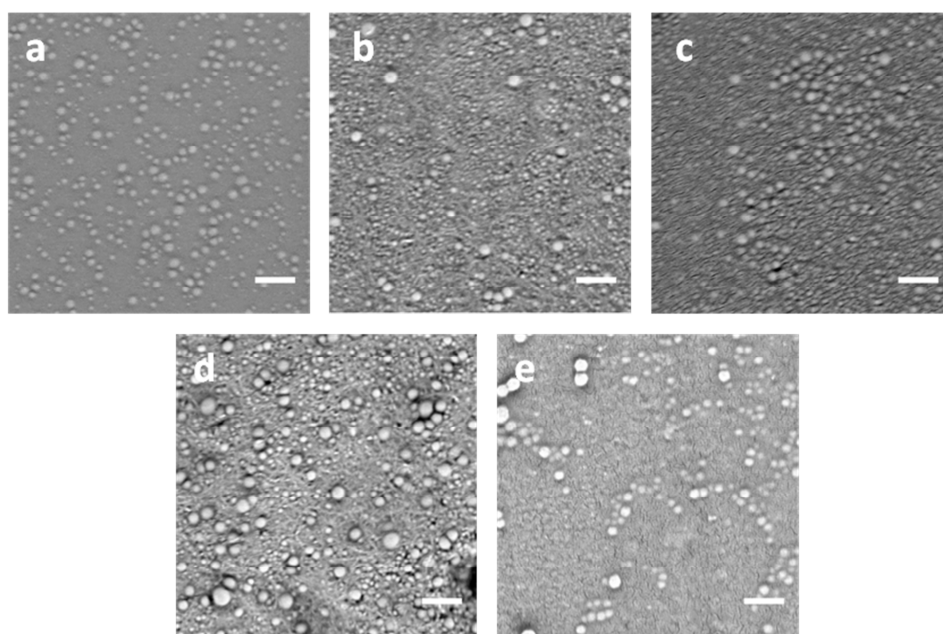


Figure 2-15, SEM micrographs of the reaction mixture for SRB-091-1% EGMDA at selected times, a $t = 5$, b $t = 8$, c $t = 9$, d $t = 10$, e $t = 13$. Scale bars are $2 \mu\text{m}$.

At $t = 8$ and $t = 9$ min. the particles on the SEM stub appear more solid in that they did not melt due to gold coating or the electron beam, meaning that the particles formed were of a higher molecular weight.

At $t = 10$ and $t = 13$ min. it is clear that full size particles started to form and that particle nucleation had occurred. This is not only from the size and the ability of the particles to maintain their shape under the electron beam but from the number of particles present on the stub.

It is clear from the inflection point in the particle size and monomer conversion versus time plot Figure 2-14 and the selected SEM images in Figure 2-15 that particle nucleation occurred at 8 min., or 10 – 12 % monomer conversion. However this is for this specific reaction (SRB-091-1% EGDMA), slight changes in reaction temperature, monomer concentration and scale will affect the critical time to particle nucleation.

2.3.4.1 Turbidity at t_c

As the polymerisation reaction proceeds and particles form, the reaction mixture became turbid and milky-white this was due to the particles scattering light. This was measured during the course of the reaction to give an indication of how the reaction is proceeding, as the amount of scattered light will be linked to the number of particles and the size of the particles. Aliquots of the reaction mixture were taken and plunged into an ice bath to rapidly cool them effectively stopping the polymerisation reaction. These were then transferred to a quartz glass cuvette and the transmitted light measured using a UV-Vis spectrometer.

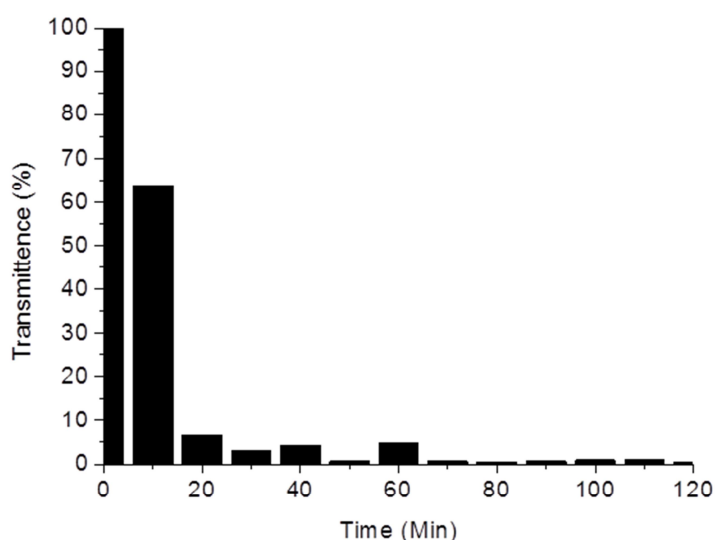


Figure 2-16, transmitted light of wavelength 550 nm vs. time for the reaction, for SRB-145-0%xl.

It is clear that upon the onset of particle nucleation the transmitted light decreased rapidly down to levels where very little light could pass through the sample and after a hour the sample effectively scattered all incident light allowing none to pass through the sample.

Measurements of the transmitted light at t_c for various reactions were undertaken to assess an average turbidity at which the onset of particle nucleation could be said to occur. Measurements were done at 550 nm and the data can be seen in Figure 2-17. It is clear that the onset of particle nucleation occurs between 7 min. 30 s. and 12 min.

All experiments measured were run under the same conditions with respect to the concentration of reactants, solvent and stabiliser in the reaction mixture. This window of time would be due to slight experimental fluctuations in reaction temperature. Also we can say that when 85 – 65 % of transmitted light can still pass through the sample primary particles have formed.

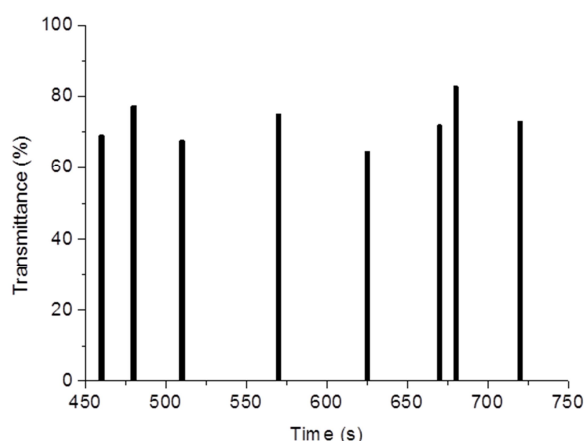


Figure 2-17, transmitted light at t_c at a wavelength of 550 nm, for different polymerisation reactions.

2.3.5 Effect of Crosslinker Addition Rate

When the crosslinking monomer solution is added to the reaction vessel at the critical time clean crosslinked particles can be formed. However the rate of addition of the crosslinking monomer solution will have a great effect on the resultant dispersion.

2.3.5.1 Injection of Crosslinking Monomer Solution

If the crosslinking monomer solution is added in full in one step at t_c then the resultant dispersion is not monodisperse smooth spheres. Figure 2-18 shows the resultant

crosslinked particles, SRB-101-1% EGDMA when the crosslinking monomer solution was added at t_c . Dispersion SRB-101-1% EGDMA shows a particle sample with two clear size distributions. From this we can infer that if the crosslinking monomer is added too quickly the result is a polymerisation akin to the batch method of producing crosslinked particles. That is the polydisperse non-uniform spheres are produced with clear evidence of secondary nucleation.

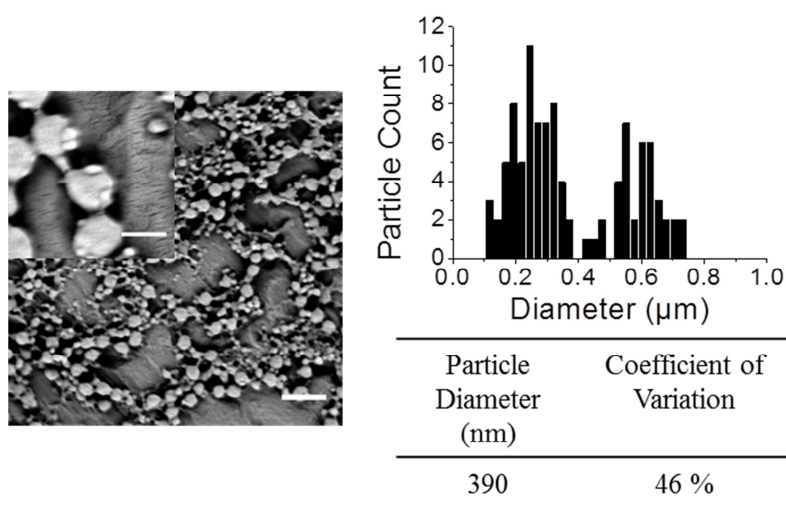


Figure 2-18, resultant particles for SRB-101-1% EGDMA after 1 wt. % EGDMA was injected into the reaction vessel at t_c . Scale bars are 2 μm and insert 500 nm, sizing data based on counting 100 particles.

2.3.5.2 Pump Feeding of Crosslinking Monomer Solution

Pump feeding the crosslinking solution into the reaction mixture over a time period should give more uniform particles as there will not be a sudden burst of crosslinking in the reaction producing secondary population highly crosslinked particles. Figure 2-19 shows SRB-119-1% EGDMA particles in which the crosslinking feed was added at a rate of 0.2 ml/min over approximately a 20 min period.

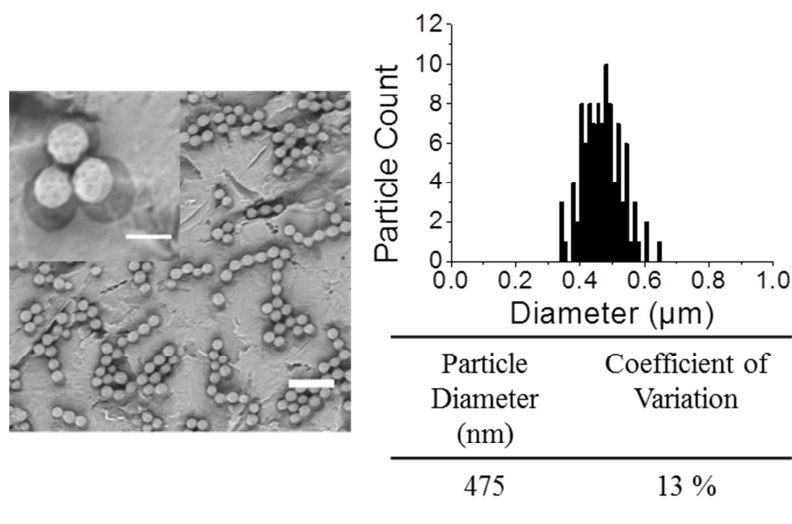


Figure 2-19, resultant particles for SRB-113-1% EGDMA after 1 wt. % EGDMA was injected into the reaction vessel at t_c . Scale bars are 2 μm and insert 500 nm, sizing data based on counting 100 particles.

SRB-112-1% EGDMA shows particles of a similar size have been produced but are far more uniform in terms of surface morphology and they are also close to being monodisperse with a coefficient of variation of 13 %. The shadowing in the image is due to gold evaporation during sample preparation opposed to gold sputtering.

As a proof of that the resultant particles are crosslinked a sample was taken and diluted by a factor of four with tetrahydrofuran (THF), a good solvent for PMMA, and the particle size measured before and after by DLS. If the particles were not crosslinked then no DLS trace would be measured as the particles would dissolve. The data is shown below in Figure 2-20 in which a clear increase in size can be seen Table 2-6 shows the measured z-average diameter and an increase of approximately 260 nm upon THF dilution.

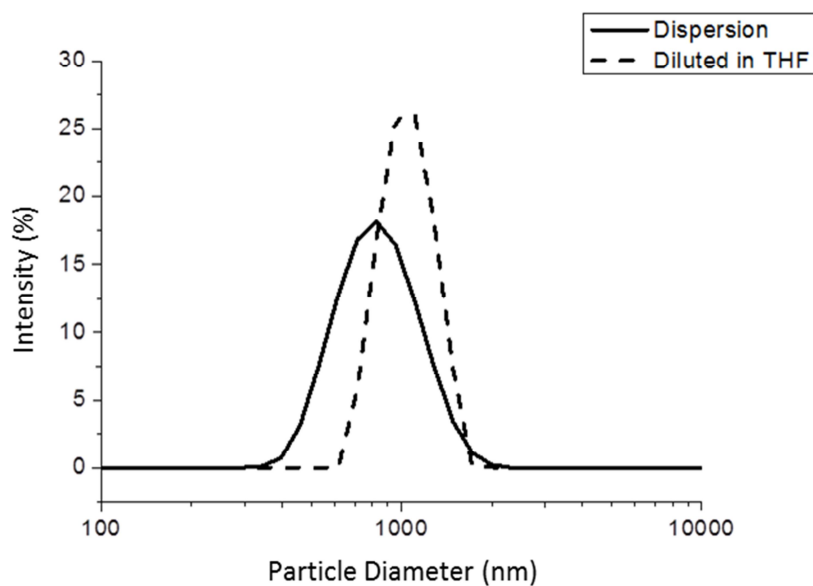


Figure 2-20, showing DLS results for SRB-113-1% EGDMA and the sample diluted by a factor of four in THF.

Table 2-6, showing the z-average diameter of SRB-113-1% EGDMA before and after THF dilution.

Sample	z-Average Diameter
Dispersion	800
Diluted in THF	1060

Differential scanning calorimetry (DSC) measurements were undertaken on samples of increasing crosslinker concentration in the monomer feed. A small quantity of the dispersion was dried in a vacuum oven in an aluminium pan until no mass loss was observed. Below in Figure 2-21 the DSC traces for samples SRB-118-0% x1, SRB-202-1% EGDMA, SRB-133-2% EGDMA and SRB-135-3% EGDMA and the T_g results obtained from the DSC experiments are shown in Table 2-7.

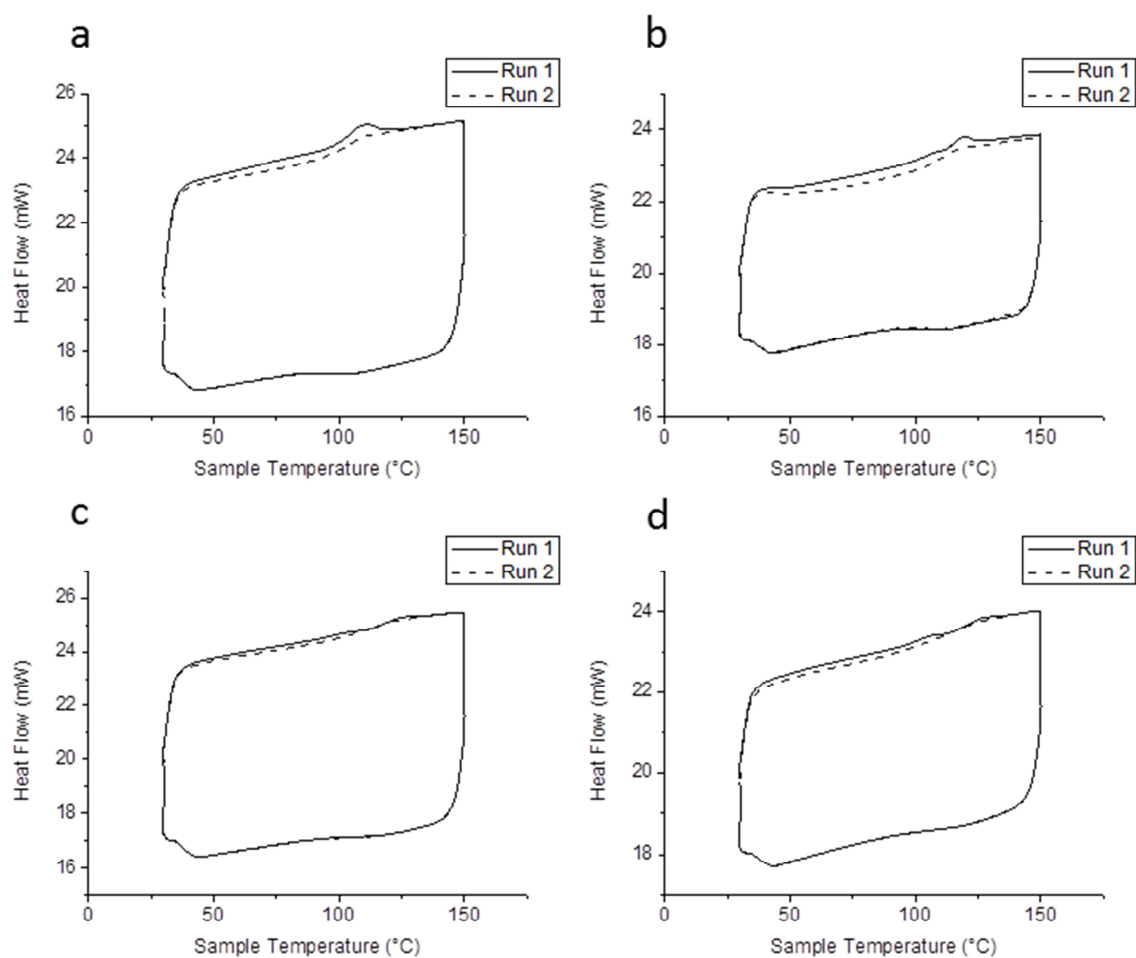


Figure 2-21, DSC traces for samples of increasing crosslinker concentration, where; a, is SRB-118-0% xl, b, is SRB-202-1% EGDMA, c, is SRB-133-2% EGDMA and d, is SRB-135-3% EGDMA.

Table 2-7, showing the glass transition temperatures of samples of increasing EGDMA content.

Sample	T_g	
	Run 1 (°C)	Run 2 (°C)
SRB-118-0% xl	101.5	103.8
SRB-202-1% EGDMA	113.6	109.9
SRB-133-2% EGDMA	118.5	113.9
SRB-133-3% EGDMA	119.5	113.0

The data shows that a glass transition temperature was measured for all samples; however the transition became increasingly unclear in the trace and the T_g increased with crosslinker content. This is an expected result as it is known that increasing the crosslinking density will increase the T_g of the sample linearly with crosslinker content.¹¹ The T_g of PMMA is approximately 105 °C, depending upon the molecular weight of the sample, heating rate, and the method used to calculate,⁴ which gives agreement with the experimental data.

Although a T_g was observed for the samples we can still conclude that the samples tested were crosslinked from the DLS trace in Figure 2-20 for a 1 wt. % crosslinked sample. The T_g is still apparent as the particles have long chains between crosslinking units which will show the glass transitional behaviour.

2.3.5.3 Effect of Increasing Crosslinker Concentration

Increasing the crosslink density of the particles could be important for future applications. In order to test the amount of crosslinker which can be added while maintaining particle uniformity particle dispersions were produced with increasing concentrations of EGDMA. Figure 2-22 shows resultant particles with 1, 2, 3 and 5 wt. % EGDMA in the crosslinker feed and their size distribution graphs.

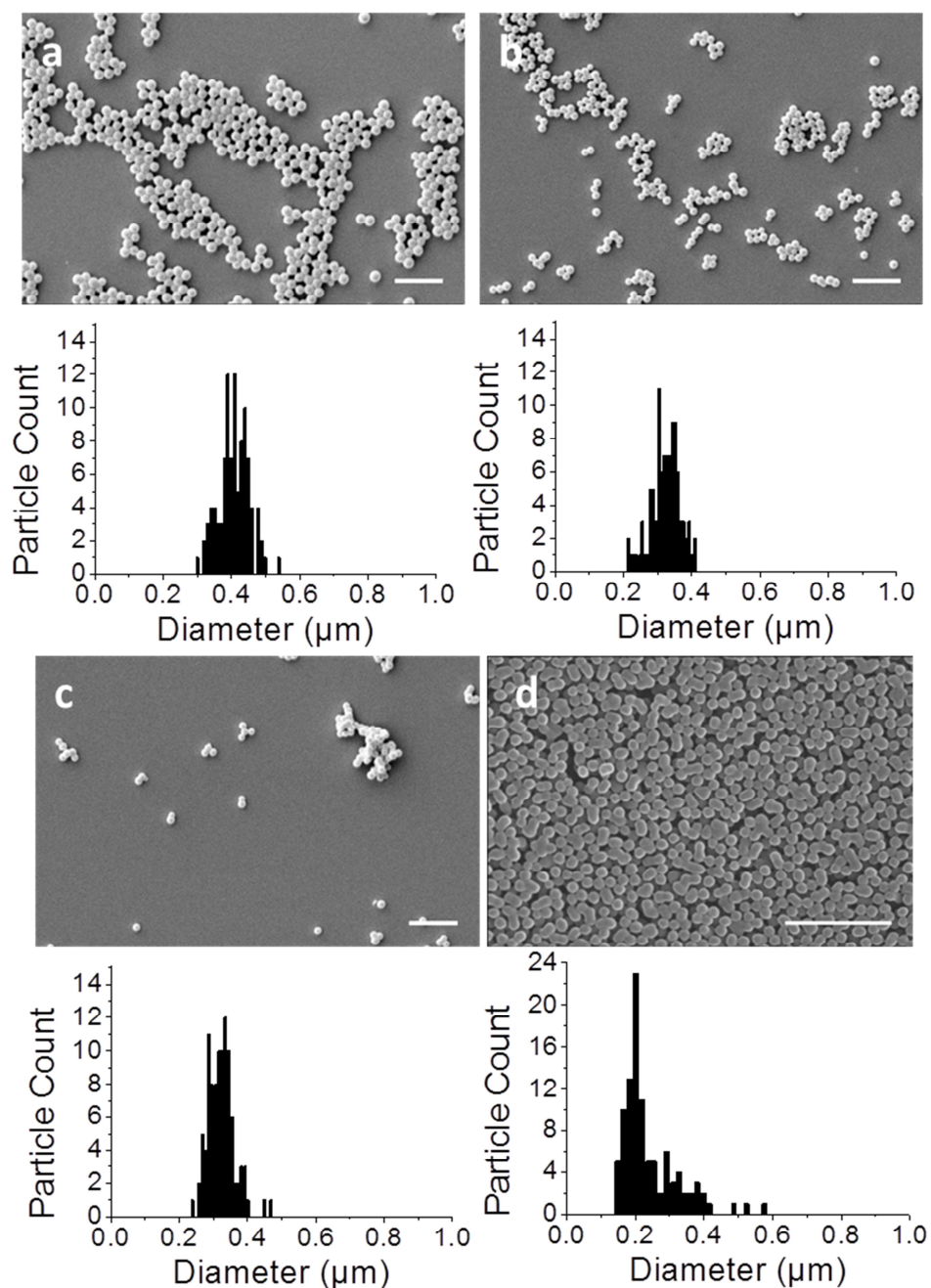


Figure 2-22, effect of increase the EGDMA concentration on particle size and morphology, with; a, SRB-131-1% EGDMA, b, SRB-133-2% EGDMA, c, SRB-135-3% EGDMA and SRB-5% EGDMA. Scale bars are 2 μm, sizing data based on counting 100 particles.

From Figure 2-22 it is clear that monodisperse particles were produced with 1, 2 and 3 wt. % EGDMA included in the monomer feed. These particles appear to be smooth spheres with narrow size distributions. However upon 5 wt. % inclusion of EGDMA in the crosslinking feed, particle fusion is occurring in the reaction leading to an increase in polydispersity. The measured particle size results are shown in Table 2-4 and show that the

samples of lower crosslinking densities have a similar size and are all close to being monodisperse. The average particle size for SRB-5% EGDMA was decreased which could be due to the crosslinks in the particles creating a tighter sphere.

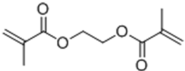
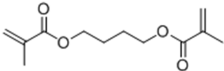
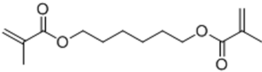
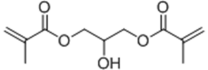
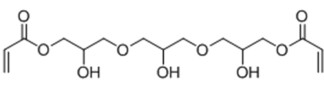
Table 2-8, particle size measurements and coefficient of variation on dispersions with increasing EGDMA content.

Sample Dispersion	Particle Diameter (nm)	Coefficient of Variation
SRB-131-1% EGDMA	410	11 %
SRB-133-2% EGDMA	330	13 %
SRB-135-3% EGDMA	330	12 %
SRB-5% EGDMA	250	33 %

2.3.5.4 Changing the Crosslinking Monomer

To prove that this method for the production of crosslinked particles is robust a number of different crosslinkers were tested. These were crosslinkers similar to EGDMA and so should have a similar solubility in the solvent. Two other crosslinking monomers which were significantly more polar than EGDMA were also tested.

Table 2-9, Alternative crosslinking monomers used to produce spherical particles.

Crosslinking Monomer	Abbreviation	Chemical Structure
Ethylene glycol dimethacrylate	EGMDA	
Butanediol dimethacrylate	BDDMA	
Hexanediol dimethacrylate	HDDMA	
Glycerol dimethacrylate	GDMA	
Glycerol 1,3-diglycerolate diacrylate	GDGDA	

From the structures of the crosslinking monomers it is clear that GDMA and GDGDA are more polar than EGDMA, this will affect the polymerisation reaction causing precipitation to occur rapidly. For this reason it is important that particle nucleation has already occurred in order to produce uniform spheres. The polarity increase of these two monomers due to

their hydroxyl groups means that they are not soluble in the hexane / dodecane solvent mixture, however they are soluble in the MMA monomer. Also the monomer GDGDA, is a diacrylate, not a dimethacrylate like the other monomers used. An acrylate group is more reactive than a methacrylate group¹² which means that the crosslinking monomer will react faster, incorporating itself into the growing polymer chains more rapidly, therefore will cause precipitation of polymer chains far faster than the other crosslinking monomers. This has implications for if the crosslinker is added at the wrong time causing aggregation and loss of colloidal stability. The resultant dispersions and size distribution plots can be found in Figure 2-23 and the sizing data in Table 2-10.

Table 2-10, particle size measurements and coefficient of variation for particles produced with different crosslinkers.

Sample Dispersion	Particle Diameter (nm)	Coefficient of Variation
SRB-113-1% BDDMA	420	10 %
SRB-133-1% HDDMA	560	11 %
SRB-288-1% GDMA	500	10 %
SRB-365-1% GDGDA	360	11 %

The data in Table 2-10 shows that all particle dispersions produced were monodisperse despite the addition of hydrophilic crosslinking monomers. The polymerisation of the hydrophilic crosslinkers GDMA and GDGDA promotes precipitation of any polymer chains faster than that of the hydrophobic crosslinkers BDDMA and HDDMA due to their immiscibility with the solvent. For this reason the addition of the crosslinker at the correct time is vital to give a monodisperse sample. The hydrophobic crosslinkers are expected to act 'EGDMA-like' and as such are expected to give smooth, spherical, crosslinked particles.

The SEM images in Figure 2-23 show particles exhibiting closed hexagonal packing; this is the ideal particle packing conformation and can only be achieved by monodisperse samples. All particles also appeared to have a smooth spherical shape.

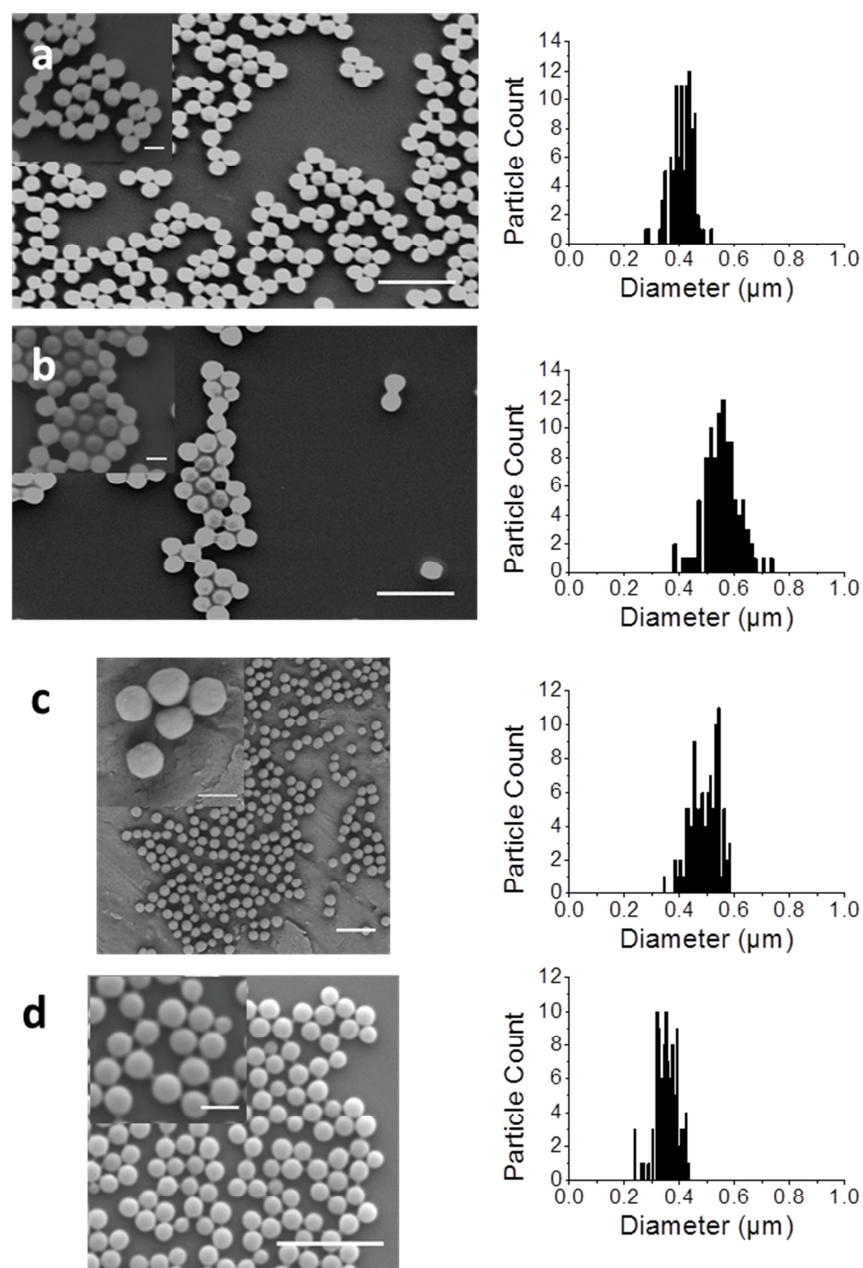


Figure 2-23, 1 wt. % crosslinked particle dispersions with different crosslinkers; a, BDDMA, b, HDDMA, c, GDMA and d, GDGDA. Scale bars are 2 μm and 500 nm on the inserts, sizing data based on counting 100 particles.

2.4 Chemical Attachment of P(HSA-*g*-MMA) Stabiliser to the Particle Surface

The P(HSA-*g*-MMA) stabiliser can be chemically attached to the surface of the polymer particles by an acid-epoxide reaction, between the glycidyl methacrylate groups in the

stabiliser backbone and the methacrylic acid within the particle. The chemical attachment of the stabiliser to the particle surface is advantageous in certain circumstances, such as when changing solvent systems. This is because the stabiliser is only physisorbed to the particle surface and can be washed off with the use of good solvents for the PMMA backbone. The procedure for chemical attachment of the stabiliser can be found in the *Experimental* (Chapter 8) and involves heating a dispersion in the presence of an amine catalyst. Below are SEM images of dispersion before and after the stabiliser attachment reaction, and particle size data.

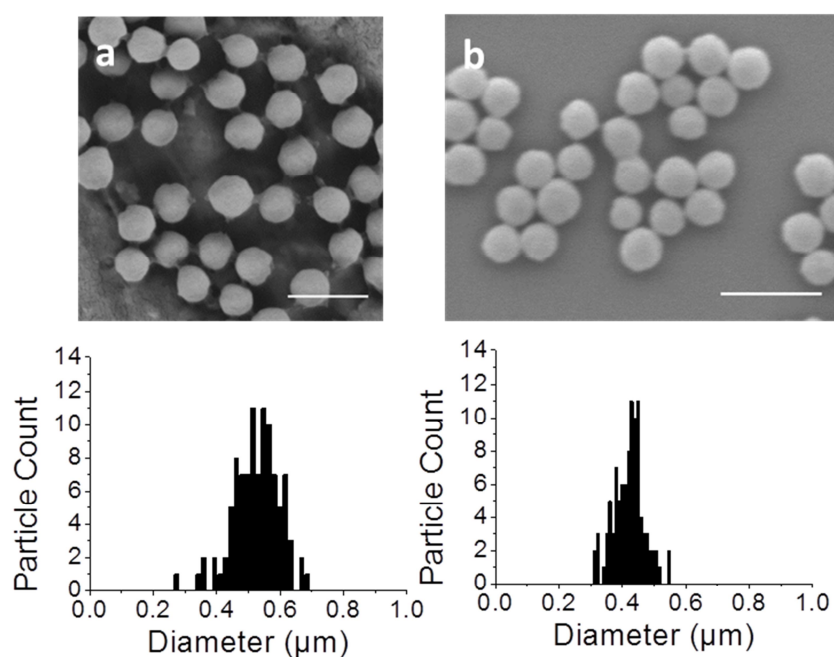


Figure 2-24, showing SEM images and size distribution plots of dispersions before and after chemical attachment of the P(HSA-g-MAA) stabiliser to the particle surface, where; a, is SRB-326-1% GDMA before attachment and b, after attachment. Scale bars are 1 μm .

Table 2-11, showing particle size data for SRB-326-1% GDMA before and after chemical attachment of the stabiliser.

Sample	Particle Diameter (nm)*	Coefficient of Variation
Before attachment	550	14 %
After attachment	430	11 %

* based on counting 100 particles

The particle size data shows that there is no statistical change in the particle size after the reaction, and the particles have retained their spherical shape. Aggregation is a potential problem during the reaction as the reaction temperature is above the T_g of the polymer particles at 120 °C.¹³ However the high temperature is necessary to allow movement of polymer chains within the particle to allow the acid-epoxide reaction to occur.

2.5 Conclusions

Monodisperse spherical particles were produced by non-aqueous dispersion (NAD) polymerisation which will be used as spherical precursor seed particles. Aspects of the NAD polymerisation reaction were probed to optimise the reaction. It was found that using a single high boiling point solvent led to particle aggregation from a large reaction exotherm. This could be avoided by using a dual solvent system of hexane and dodecane in a 2:1 ratio with no effect to the overall monomer conversion.

Monodisperse crosslinked spherical particles were obtained by the slow addition of a crosslinker solution at the critical time to particle nucleation, t_c , which was found to occur at approximately 7 - 12 min. The critical time was found by monitoring a reaction for particle size and monomer conversion with time, which show a point of inflection due to particle growth at $t = 8$ min. Different crosslinkers were used of differing polarities to produce different seed dispersions for further reactions, all with a coefficient of variation of under 15 %, despite potential problems with the reaction due to the insolubility of the crosslinker in the reaction medium. Such crosslinked particles have been proven to be crosslinked by DSC measurement and swelling of the particles in good solvent and measuring the resultant particle size by DLS. It was also shown that the P(HAS-*g*-MMA) stabiliser can be successfully attached to the particle surface without any change to the particles.

2.6 References

- ¹ L. Antl, J. W. Goodwin, R. D. Hill, R. H. Ottewill, S. M. Owens, S. Papworth and J. A. Waters, *Colloids and Surfaces*, 1986, **17**, 67
- ² http://www2.dupont.com/Vazo/en_US/products/grades/grade_selector.html
- ³ J. W. Nicholson, *The Chemistry of Polymers*, 3rd Ed. RSC Publishing, 2006
- ⁴ J. Brandup, E. H. Immergut, E. A. Grulke, A. Abe and D. R. Bloch, *Polymer Handbook*, John Wiley & Sons, 4th edn. 1998, Chapter 2, 181
- ⁵ Merck Chemicals, *Unpublished Work*
- ⁶ Jin-W. Kim, R. J. Larsen, and D. A. Weitz, *J. Am. Chem. Soc.*, 2005, **128**, 14373
- ⁷ M. Yasuda, H. Seki, H. Yokoyama, H. Ogino, K. Ishimi, and H. Ishikawa, *Macromolecules*, 2001, **34**, 3261
- ⁸ K. E. J. Barrett, *Dispersion Polymerisation in Organic Media*, Wiley, 1975
- ⁹ S. Kawaguchi and K. Ito, *Adv. Polym. Sci.*, 2005, **175**, 299
- ¹⁰ K. E. J. Barrett and H. R. Thomas, *J. Polym. Sci. A.*, 1969, **7**, 2621
- ¹¹ M. Chanda and S. K. Roy, *Plastics Technology Handbook*, 2006, CRC Press, 4th ed. Chp.1
- ¹² M. K. Mishra and Y. Yagci, *Handbook of Radical Vinyl Polymerization*, Marcel Dekker, 1998
- ¹³ R. J. R. Cairns, R. H. Ottewill, D. W. J. Osmond and I. Wagstaff, *J. Colloid Interf. Sci.*, 1976, **54**, 45

3 Monomer Selection and Modelling Monomer - Particle Interactions

3.1 Introduction

This chapter discusses work toward monomer selection for the production of nonspherical particles, and the consideration of the monomer - polymer interactions to predict resultant particle morphology based upon total interfacial energy minimisation.

3.1.1 Dynamic Swelling Method for Anisotropic Particle Formation

The dynamic swelling method, DSM, is a method of producing anisotropic particles in the form of snowman-like particles through to rods and triangular particles. The DSM method works by the swelling of a crosslinked spherical particle template with monomer, which is then heated and polymerised forming a protrusion of monomer from the particle surface. The monomer protrusion is formed due to the increase in elastic stress in the seed particle. This method has been used in emulsion and dispersion polymerisation reactions in polar solvents.

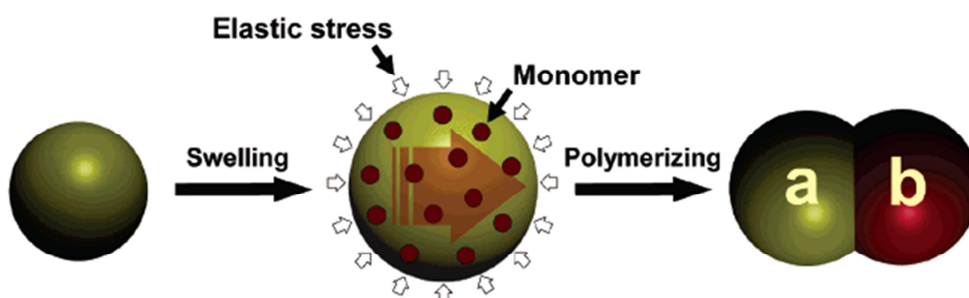


Figure 3-1, schematic view of how the dynamic swelling method proceeds, from seed particles to doublet particles.¹

It is thought that this methodology could be adapted for the production of shape anisotropic particles in non-polar media. In order to produce anisotropic particles by the dynamic swelling method there are certain prerequisites for the system, two key aspects are.

- Highly crosslinked seed particles.
- Monomer to swell the particles and phase separate upon heating.

Crosslinked uniform seed particles have been produced and outlined in *Chapter 2*.

3.2 Prediction of Particle Morphology by Interfacial Energy Minimisation

According to Waters² summing the interfacial tension of the system can lead to the prediction of particle morphologies. The model which he outlines concerns particle engulfment of one polymer with another and calculates the thermodynamically favoured state by minimisation of the interfacial energy of all the components of the system. This model works by measuring the affinity one polymer has for another which will lead to different possible morphologies. This can then be extrapolated to monomer units, of the polymer under consideration, interacting with a polymer particle and thus predict the resultant particle morphology post polymerisation. The monomer - polymer interactions can be groups together into three distinct groups:

- If the monomer is well matched for the particle then it will wet the surface and swell into the particle resulting in a growth of the particle.
- The monomer has some affinity for the particle but does not completely wet the particle, leading to some intermediate structure.
- If the monomer is mismatched to the particle then it will not wet the surface and sit on the edge of the particle with a very high contact angle or not at all with little or no swelling into the particle.

These interactions can be expressed by the Young equation,³ assuming the particle surface is a uniform flat surface. The Young equation⁴ links the contact angle formed between a liquid and a substrate, $\theta_{L,S}$, to the interfacial tension between the liquid and the substrate, $\gamma_{L,S}$, and the liquid and air, $\gamma_{L,A}$.

$$\gamma_{L,S} = \gamma_S - (\gamma_{L,A} \cos \theta_{L,S}) \quad 3-1$$

This gives rise to different conditions where different particle architectures can be obtained. In the extremes one polymer can engulf the other forming a core-shell or inverted core shell structure, or there is little or no interaction between the two and they remain separated, these architectures are shown in Figure 3-2.

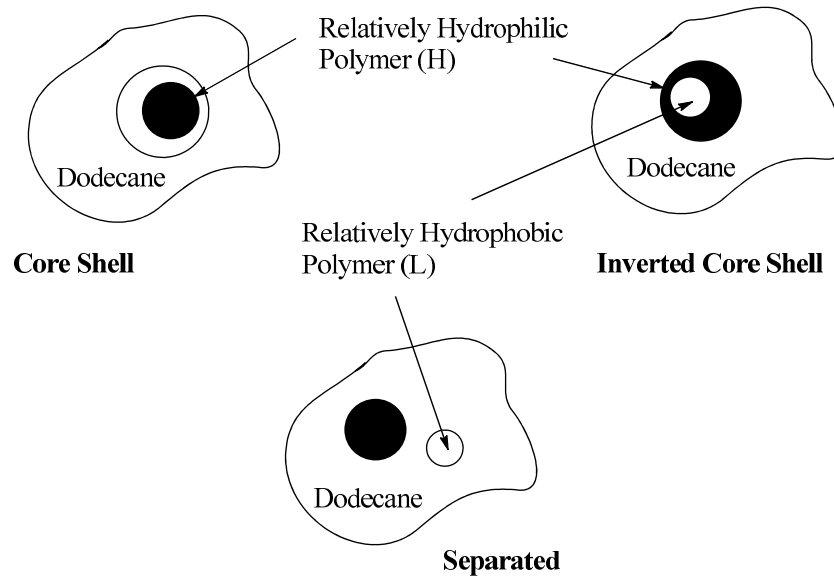


Figure 3-2, showing the extreme particle architectures.²

In the core shell architecture the hydrophilic polymer forms the core to minimise its surface in contact with the hydrophobic dodecane solvent. In an inverted core shell system this is the opposite, this system can only arise in rare cases where the hydrophilic polymer is in a far greater excess than the hydrophobic polymer. In the separated system there is no interaction between the two polymers so they remain separated in the dispersed system.

The conditions⁵ for a core shell or inverted core shell architecture are given by equation 3-2 and for a separated system given by equation 3-3.

$$\frac{\gamma_{L,D} - \gamma_{H,L}}{\gamma_{H-D}} < v_L^{2/3} - v_H^{2/3} \quad 3-2$$

$$\frac{\gamma_{L,D} - \gamma_{H,L}}{\gamma_{H-D}} > \frac{1 - v_H^{2/3}}{v_L^{2/3}} \quad 3-3$$

Where; $\gamma_{L,D}$ is the interfacial tension between the more lyophilic (hydrophobic) polymer and the dodecane solvent, $\gamma_{H,L}$ if the interfacial tension between the two polymers and γ_{H-D} the interfacial tension between the lyophilic and hydrophilic polymers.

The term on the right is the difference between the fractional volumes of each polymer, which governs if a core shell or inverted core shell particle architecture is favoured. These two situations are only the extremes, the intermediate situation between total engulfment

and separation is a region of interest, where a sphere of polymer, x , is partially engulfed by another polymer, y . This gives the conditions shown the following equation and shown diagrammatically in Figure 3-3.

$$-1 < \frac{\gamma_{X,D} - \gamma_{X,Y}}{\gamma_{Y,D}} < 1 \quad 3-4$$

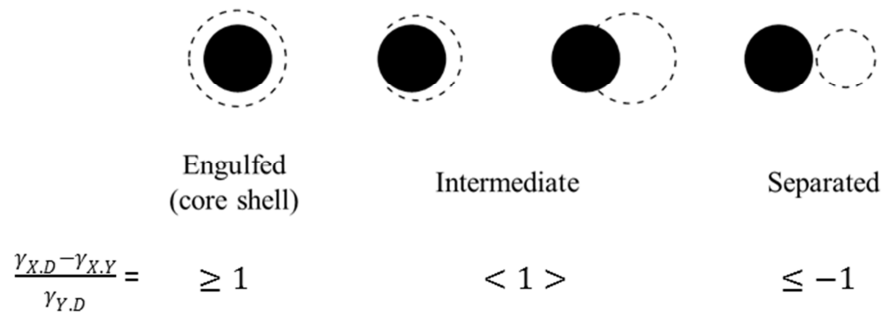


Figure 3-3, schematic representations of solutions to equations 3-2, 3-3 and 3-4 predicting particle morphologies by summing the total interfacial energy of the system.²

3.2.1 Contact Angle Measurements

The interactions between the PMMA colloid particles and the second stage monomer can be probed by means of monitoring sessile drops on polymer films; giving information into the affinity the monomer has for the substrate.

The contact angle formed by a liquid on a substrate is governed by, the interfacial tension of the liquid and the surface tension of the substrate (surface energy). The substrate can be embedded in another liquid phase. This is important for summing the total interfacial tension for the system. The wetting behaviour of a liquid on a solid substrate is given by the Young equation, shown below:

$$\gamma_S = \gamma_{SL} + \gamma_L \cdot \cos\theta \quad 3-1$$

Where; γ_S and γ_L are the surface tension components for the substrate and the liquid respectively, γ_{SL} is the interfacial tension between the two phases and θ the contact angle formed between σ_S and γ_{SL} . The components of the Young equation are shown in Figure 3-4 below.

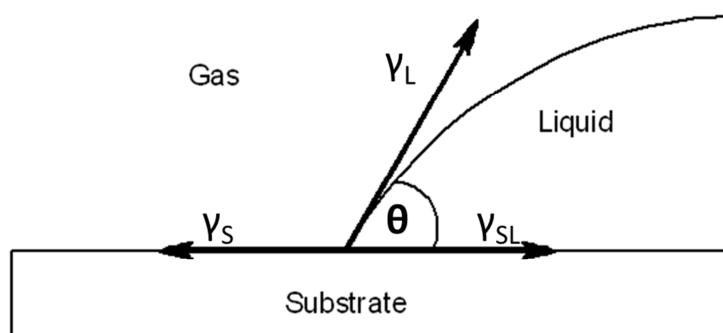


Figure 3-4, schematic view of sessile drop interactions at the three phase point as described by the Young equation.

Waters predicted particle morphology of particles dispersed in water and said that by summing the total interfacial tension differences between; seed particle, monomer and solvent the lowest energy state can be found.

In order to calculate the thermodynamically favoured morphology multiple parameters must be calculated experimentally:

- The surface free energy of each substrate used.
- The interfacial tension between the monomer and dodecane.
- The substrate - dodecane interfacial tension.
- The monomer - substrate interfacial tension embedded in dodecane.

3.3 Monomer Selection and Solubility Parameters

Solubility parameters are a measure of the miscibility of a solvent and a solute based upon the idea that 'like dissolves like'. The solubility parameter for a given molecule is therefore based upon the constituent groups within the molecule. This is then given numerical form by effectively approximating the total Van der Waals force from the cohesive energy density.^{6,7,8} This gives the most basic solubility parameter, the Hildebrand Solubility Parameter, which gives a single numerical number for each solvent which if matched to the Hildebrand number of another solvent, should yield a uniform mixture or in the case of solvent - solute should dissolve.

However the Hildebrand number is limited and does not give accurate predictions with certain systems, such as accounting for polar contributions. A much more accurate prediction can be made if the Hildebrand number is combined with a polar value, such as hydrogen bonding value, for each liquid. A more accurate picture can be obtained again if the Hildebrand value is split into three forces; hydrogen bonding, polar forces and dispersion forces. The Hansen model of solubility parameters is one such model.⁹

3.3.1 Hansen Solubility Parameters

The Hansen parameters divide the total Hildebrand value into three components, a hydrogen bonding component, a polar component and a dispersive component. The simplicity of the Hansen model is that the breakdown of the Hildebrand solubility parameter is additive,¹⁰ so:

$$\delta_t^2 = \delta_d^2 + \delta_p^2 + \delta_h^2 \quad 3-5$$

Where; δ_t is the total Hildebrand value, δ_d , dispersion component, δ_p , polar component and δ_h , hydrogen bonding component.

In order to plot out the Hansen parameters, to look at the solubility of a solute in many solvents one value must be left out to give a 2D plot, compromising accuracy. However fractional values can be obtained for each component normalising the value, which enables the production of a ternary diagram, such a diagram is known as a Teas plot. The fractional components can be found by the following equations:

$$f_d = \frac{\delta_d}{\delta_d + \delta_p + \delta_h} \quad f_p = \frac{\delta_p}{\delta_d + \delta_p + \delta_h} \quad f_h = \frac{\delta_h}{\delta_d + \delta_p + \delta_h} \quad 3-6$$

As such the total of all three components should equal 1; this now allows the drawing of a ternary diagram for any given situation. An example shown in Figure 3-5 is for the solubility of a polymer, building a solubility window.

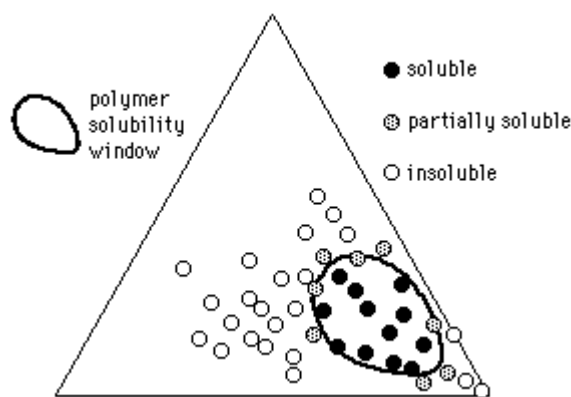


Figure 3-5, example Teas plot for the solubility window of a given polymer.¹¹

The solubility window is the envelope of good solvents of closely matched solubility parameters which will dissolve a polymer, outside that envelope are non-solvents for the polymer. To build such a diagram requires the testing of multiple solvents which is time consuming. However the ability for a given solvent to dissolve a given solute, such as a polymer, can be estimated through their respective solubility parameters. If they are far removed then they will not be miscible / dissolve, if they are close together then they will be miscible / dissolve. If a solvent partially dissolves a polymer is said to lie on the boundary of interaction.

Looking at an example of if the monomers are miscible with dodecane a radius of interaction can be calculated, with respect to dodecane and the monomers. This is related to differences in the Hansen solubility parameter components, for dodecane and the monomer in question, and is given by the following equation:

$$R_a = \sqrt{[4(\delta_{d_d} - \delta_{d_m})^2 + (\delta_{p_d} - \delta_{p_m})^2 + (\delta_{h_d} - \delta_{h_m})^2]} \quad 3-7$$

Where; δ_d , dispersive component, δ_p , polar component and δ_h , hydrogen bonding component and the subscript d and m , denote dodecane and monomer respectfully.

The radius of interaction is a theoretical boundary, in the centre sits the molecule under scrutiny and the boundary line denotes if the molecule in the middle will interact i.e. dissolve or mix, with any other molecules within it. Within the boundary molecules are predicted to interact, outside the boundary then they are predicted to not interact. So the

further removed the value for the radius of interaction the from the centre point, 0, the less interaction the pair will have.

To find the boundary line for interaction the relative energy difference (*RED*) can be calculated from the radius of interaction over the solubility radius of the molecule under scrutiny, R_a/R_0 .¹²

The *RED* value being relative to the molecule at the centre of the radius of interaction, dodecane in this case, means this can easily and quickly show if a solvent pair or solvent solute pair should interact. This can now be extended further and the three conditions, interaction, no interaction and boundary condition, can be linked to the free energy of mixing ΔG^m for the binary system. Three conditions of the *RED* value are:

- $RED < 1$, chemicals have matched solubility parameters, ΔG^m is negative, therefore interaction should occur.
- $RED > 1$, chemicals have mismatched solubility parameters, ΔG^m is positive, therefore no interaction should occur.
- $RED = 1$, boundary condition for interaction, $\Delta G^m = 0$.

Although the relative energy difference (*RED*) is effective in the ease of quantifying the interactions of a solvent – solute pair, calculating the solubility radius for a material requires extensive testing with multiple solvents. So the radius of interaction between the solute and solvent will be considered. For a well matched pair the radius of interaction would be small, therefore the smaller the R_a value the greater the interaction.

In order to produce non-spherical particles in a controlled manner by a nonaqueous dispersion polymerisation route the correct monomer choice is paramount. Drawing from parallels of the dynamic swelling method, typically used in polar solvents such as water or ethanol, the monomers used must be immiscible with the continuous phase solvent but swell the dispersed polymer particles. To this end crosslinked polymer particles were dried in a vacuum oven to remove all the solvent and then added to a range of solvents. These were then assessed to see if they interacted with the dried crosslinked PMMA and classified into three groups; no interaction, the crosslinked PMMA particles remained as a solid, the dried PMMA particles swelled in the solvent or, the polymer formed a clear gel with the solvent penetrating the network completely. This is shown in Figure 3-6 where the black diamonds represent no interaction, therefore a non-solvent, red diamonds represent

the formation of a gel, therefore a poor solvent and green diamonds represent a good solvent which swells the dried PMMA particles.

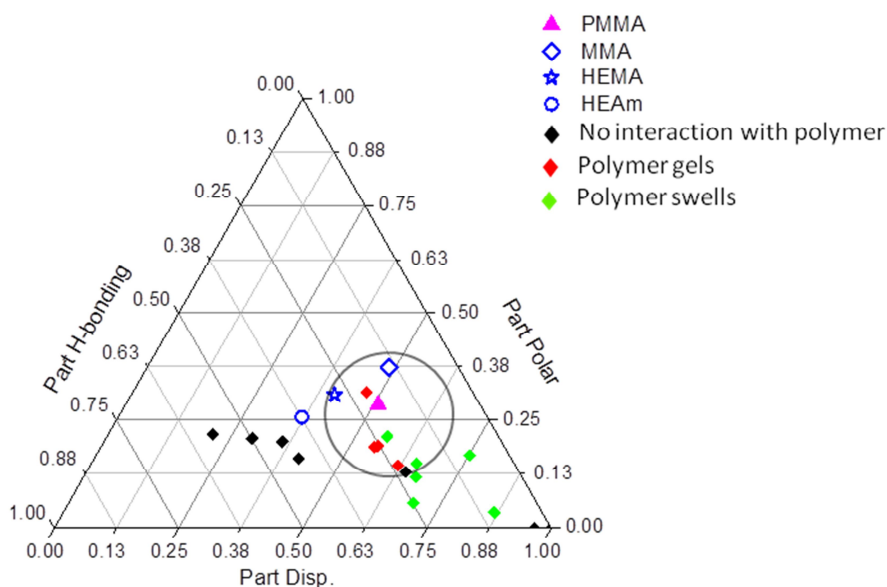


Figure 3-6, ternary plot of different solvents based on their Hansen solubility parameters.

According to the ternary plot, an estimation of the radius of interaction can be drawn for PMMA. This allows for monomers to be chosen which would act as a good, poor or non-solvent for PMMA. For a good solvent methyl methacrylate (MMA) was chosen which sits within the radius of interaction. For a poor solvent 2-hydroxyethyl methacrylate (HEMA) which sits on the boundary and a non-solvent, *N*-hydroxyethyl acrylamide (HEAm) which sits outside the radius of interaction were chosen.

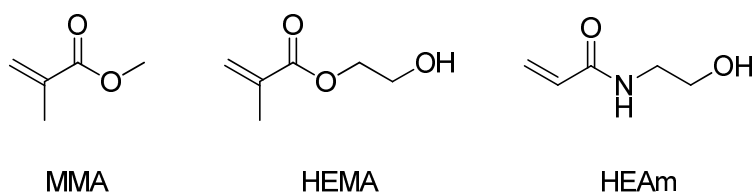


Figure 3-7, chemical structure of MMA, HEMA and HEAm.

The Hansen solubility parameters for the monomers are shown below in Table 3-1 along with the calculated radius of interaction and relative energy difference with respect to PMMA.

Table 3-1, Hansen solubility parameters for the second stage monomers, with radii of interaction calculated against PMMA and dodecane.

Chemical	Solubility Parameter (MPa ^{1/2})				Radius of Interaction
	δ_T	δ_d	δ_p	δ_h	R_a
PMMA	22.7	18.6	10.5	7.5	-
MMA	18.8	16.4	4.5	8.1	6.6
HEAm	25.7	18.0	9.4	15.8	8.5
HEMA	23.5	17.5	5.0	15.0	9.6
Dodecane	16.0	16.0	0.0	0.0	-
MMA	18.8	16.4	4.5	8.1	9.3
HEAm	25.7	18.0	9.4	15.8	18.8
HEMA	23.5	17.5	5.0	15.0	16.1

From the Hansen parameters for the monomers and the calculated R_a value we would expect all three monomers to interact with a PMMA substrate. However the degree of interaction will decrease down the table. This result is interesting as the HEAm monomer is more polar than that of HEMA so one would expect HEAm to have a lower affinity for PMMA.

They also show that MMA should be soluble in dodecane, whereas HEMA and HEAm maybe insoluble in dodecane.

The monomers interaction with a PMMA substrate was probed further by measuring the equilibrium advancing contact angles formed between PMMA and both HEMA and HEAm. The contact angle formed gives information into the wetting behaviour of the liquid on the sample substrate which is measure of the affinity one has for the other.

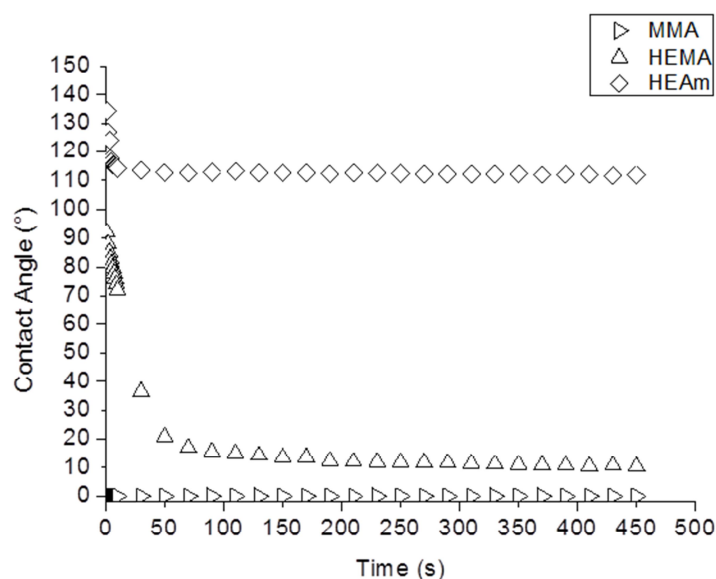


Figure 3-8, contact angle vs. time for MMA, HEMA and HEAm on a PMMA substrate.

The data clearly shows that HEAm is non-wetting with respect to PMMA and that HEMA has a good interaction with PMMA as it partially wets the surface. MMA however dissolves the substrate so contact angle measurements cannot be truly taken, but as the interaction is very favourable a contact angle of zero is shown for comparison.

3.4 Characterisation of Polymer Substrates

All the polymer substrates used for this study were produced by solution polymerisation in an appropriate solvent for the reaction, either butyl acetate or a solvent mixture of isopropyl alcohol and 2-butanone in a 30/70 ratio (v/v). These polymers were characterised by gel permeation chromatography (GPC) and by NMR spectroscopy. For the MMA-HEMA statistical copolymers the true polymer composition was calculated by ^1H proton NMR.

The GPC data for the polymers are shown in Table 3-2, all except the three most polar polymers were run in a tetrahydrofuran (THF) system, and the others were run in a dimethyl acetamide (DMA) or aqueous GPC solvent system.

Table 3-2, molecular weight data for the different polymers used to model the particle - monomer interactions.

Polymer	Mn kDa	Mw kDa	Mw/Mn
PMMA-28 <i>KDa</i>	8	28	4
PMMA-35 <i>KDa</i>	11	35	3
P(MMA ₉₈ -MAA ₂)	16	30	2
P(MMA ₉₈ -MAA ₂)-stabiliser	6	25	4
PHEMA*	62	200	3
PHEAm†	20	129	7
P(MMA _{90-co} -HEMA ₁₀)	23	90	5
P(MMA _{80-co} -HEMA ₂₀)	23	52	2
P(MMA _{60-co} -HEMA ₄₀)	22	20	2
P(MMA _{50-co} -HEMA ₅₀)*	18	45	3

*DMA † Aqueous

The GPC traces for the polymers produced can be found in the *Appendices* (Chapter 9.1).

For the statistical copolymers produced polymer compositions were calculated from the integrals in the ¹H spectra for peaks representing the differing constituents. The inset in Figure 3-9 shows two singlets from the two different monomers used, HEMA at 3.85 ppm and MMA at 3.62 ppm. Given that these represent 2 and 3 hydrogen nuclei respectively a ratio was calculated between the two giving the polymer composition. The results for the compositional analysis for the copolymers are shown in Table 3-3 and they closely match the expected values from the monomer feed ratios. This will be due to the fact that the monomer reactivity ratios will be very similar; as both have methacrylate groups open to free radical polymerisation and a large chain to hinder the propagation due to steric effects.

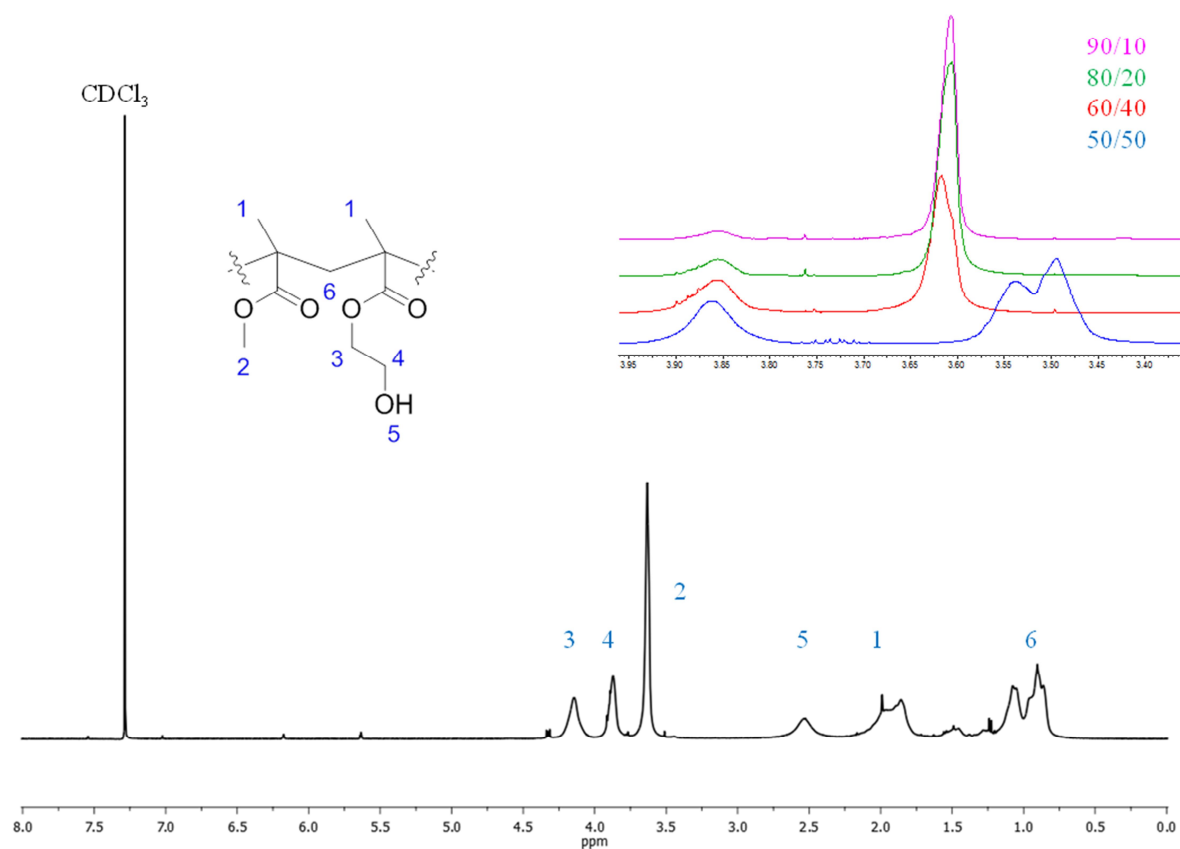


Figure 3-9, ^1H NMR spectra of $\text{P}(\text{MMA}_{60}\text{-co-HEMA}_{40})$, inset shows comparison of other polymers for compositional analysis based upon the ratio between the peaks. Note the peaks are shifted for $\text{P}(\text{MMA}_{50}\text{-co-HEMA}_{50})$ as this sample was run in DMSO-d_6 rather than CDCl_3 .

Table 3-3, copolymer compositional analysis for the statistical copolymers synthesised.

Polymer	Expected Ratio	Found by NMR
$\text{P}(\text{MMA}_{90}\text{-co-HEMA}_{10})$	9 : 1	9 : 1
$\text{P}(\text{MMA}_{80}\text{-co-HEMA}_{20})$	8 : 2	8 : 2
$\text{P}(\text{MMA}_{60}\text{-co-HEMA}_{40})$	6 : 4	6 : 4
$\text{P}(\text{MMA}_{50}\text{-co-HEMA}_{50})$	1 : 1	1 : 1

The ^1H NMR for the other statistical copolymers of $\text{P}(\text{MMA-co-HEMA})$ are given in the *Appendices* (Chapter 9.2).

3.5 Calculating the Surface Energy of Polymer Films, $\gamma_{S,A}$

To measure the surface energy of a solid substrate one of the easiest methods is to measure the wetting behaviour of a range of different liquids with different surface tensions on the substrates surface. If the surface tension (liquid - air interfacial tension) is known for the probing liquids then the surface energy of the solid substrate can be estimated.

The surface energy of any given material can be split into dispersive and polar components which combine to give the total surface energy. One method to combine their contributions is the geometric mean method by Fowkes,¹³ where the surface energy is given by equation 3-8:

$$\gamma_L(1 + \cos\theta) = 2[(\gamma_{L,P}\gamma_{S,P})^{1/2} + (\gamma_{L,D}\gamma_{S,D})^{1/2}] \quad 3-8$$

This equation was rearranged by Owens and Wendt¹⁴ to give equation 3-9.

$$\gamma_L(1 + \cos\theta)/(\gamma_{L,D})^{1/2} = (\gamma_{S,P})^{1/2}[(\gamma_{L,P})^{1/2}/(\gamma_{L,D})^{1/2}] + (\gamma_{S,D})^{1/2} \quad 3-9$$

Where; θ is the contact angle, γ_L the liquids surface tension and γ_S the substrates surface tension (surface energy). The addition of D and P denote the dispersive and polar components of the surface tension.

Given that the surface tension for a given material can be split into dispersive and polar contributions a total surface polarity, X_p , can be calculated for a given surface by the following equation:

$$X_p(\%) = \gamma_P/\gamma_T \cdot 100\% \quad 3-10$$

Given that:

$$\gamma_T = \gamma_P + \gamma_D \quad 3-11$$

Where; γ_T is the total surface energy of the substrate.

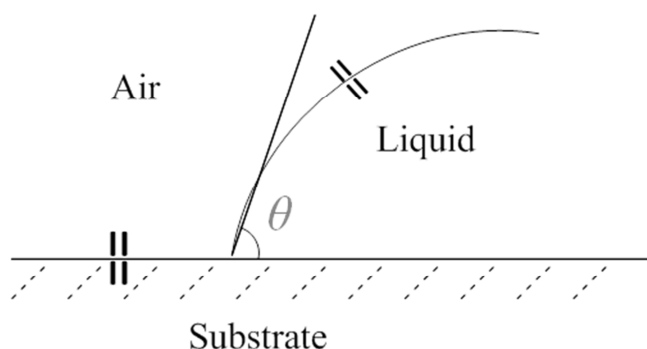


Figure 3-10, schematic view of measuring the surface energy of a substrate, the solid - air interfacial tension, with the experimentally measured contact angle in grey, the calculated interfacial tension in bold and the known liquid surface tension shown.

As the probe liquid - air interfacial tension for the standard liquids is known the air - substrate interfacial tension can be obtained by measuring the contact angle formed by the liquid and the substrate in air. This is linked to the surface energy of the substrate.

The surface energy of each of the polymer films was calculated by measuring the equilibrium advancing contact angle for water and diiodmethane which have known dispersive and polar components of their surface tension, these are shown in Table 3-4, dodecane is added for completeness.

Contact angle and surface tension measurements were obtained by use of a Kruss DSA 100 goniometer. The machine takes images of liquid drops; either sessile drops on surfaces for contact angle, or pendent drops for surface tension. Then from the drop shape profile the machine is able to calculate multiple things such as; drop width or contact angles formed with a substrate and surface tension.

Table 3-4, surface tension components for given solvents.¹⁵

Liquid	Surface Tension (mNm^{-1})		
	Total	Dispersive	Polar
Water	72.3	18.7	53.6
Diiodomethane	50.0	47.4	2.6
<i>n</i> -Dodecane	25.4	25.4	0.0

The results for the contact angles formed for these solvents on the polymer films are shown in Table 3-5, each measurement is an average of three runs. Figure 3-11 shows images captured in measuring the contact angle on a PMMA-35kDa surface. The large difference in contact angles observed is very obvious between the two probe liquids. An example of the contact angle vs. time and drop volume vs. time plots obtained is shown in Figure 3-12, for PMMA. The drop volume is also recorded in these experiments to show that the probe liquid is not absorbed by the polymer film tested which would make the experiment invalid.

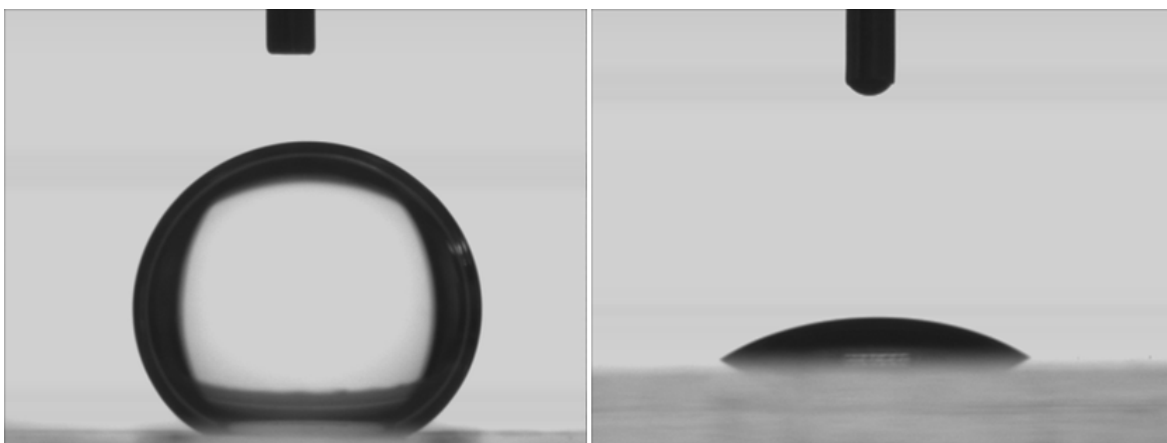


Figure 3-11, sessile drops of water (left) and diiodomethane (right) after 1 s contact on a PMMA-35 KDa substrate.

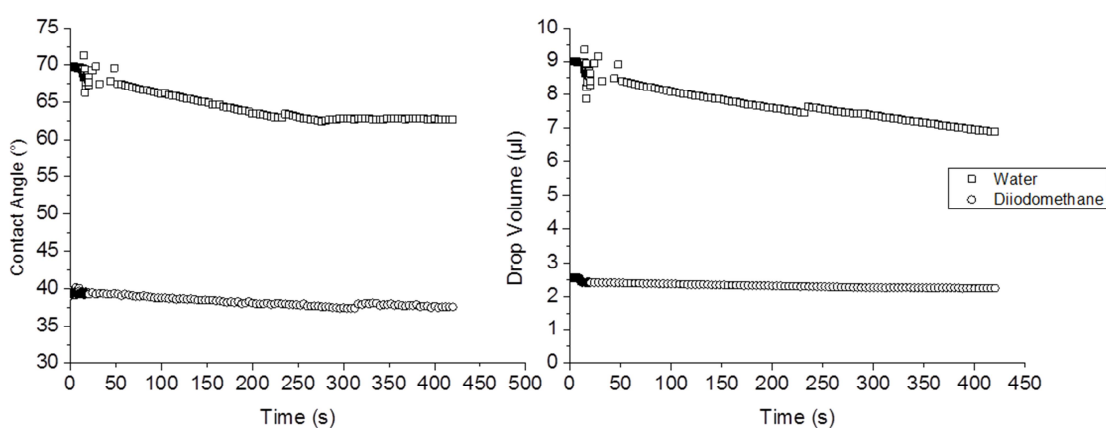


Figure 3-12, contact angle vs. time plot and drop volume vs. time plot, for water and diiodomethane on a PMMA-35 KDa substrate. Contact angle vs. Time plots for other substrates are given in the *Appendices* (Chapter 9.3).

Table 3-5, average advancing contact angles formed by the probe liquids on polymer substrates.

Substrate	Equilibrium advancing contact angle, θ , at 25 °C (°)	
	θ_{water}	$\theta_{\text{diiodomethane}}$
PMMA-28 <i>kDa</i>	62.8	30.6
PMMA-35 <i>kDa</i>	66.6	38.5
P(MMA ₉₈ -MAA ₂)	61.5	33.6
P(MMA ₉₈ -MAA ₂)-stabiliser	67.3	34.1
PHEMA	43.9	26.0
PHEAm	15.1	30.3
P(MMA _{90-co} -HEMA ₁₀)	77.4	43.4
P(MMA _{80-co} -HEMA ₂₀)	63.1	38.0
P(MMA _{60-co} -HEMA ₄₀)	58.9	36.6
P(MMA _{50-co} -HEMA ₅₀)	53.4	34.0

From the results in Table 3-5 the surface energy of each of the polymer films was calculated by the Fowkes (geometric mean) method, using the water - diiodomethane liquid pair, which are reported in Table 3-6.

It is clear that the surface polarity (X_p) of the substrate has a great influence on the contact angle formed between water and diiodomethane. This is even evident in the difference between the PMMA and P(MMA-*co*-MAA) substrates. The difference in the two PMMA substrates, PMMA-28 *kDa* and the PMMA-35 *kDa*, can be attributed to the molecular weight difference of the polymers, as the lower the molecular weight of the polymer the more chain ends will be present, which will give an artificial polarity increase. This will lead to exaggerated differences in the surface energy calculated for these films due to the high contact angles measured. The trend between the statistical copolymers of MMA and HEMA show the expected results of the water contact angle decreasing with increasing HEMA content. This is as expected as the polar monomer content is increasing, increasing the polarity of substrate.

Table 3-6, calculated surface energies, γ_s , of polymer substrates.

Substrate	γ_s at 25 °C (mNm ⁻¹)			X_p (%)
	γ_{polar}	$\gamma_{dispersive}$	γ_{total}	
PMMA-28 <i>kDa</i>	13.1	34.9	48.1	27.2
PMMA-35 <i>kDa</i>	12.1	32.0	44.1	27.4
P(MMA ₉₈ -MAA ₂)	14.6	33.2	47.8	31.1
P(MMA ₉₈ -MAA ₂)-stabiliser	10.8	43.4	45.3	20.0
PHEMA	32.6	25.6	58.2	56.1
PHEAm	43.3	27.3	70.6	61.3
P(MMA _{90-co} -HEMA ₁₀)	11.7	33.0	44.7	26.1
P(MMA _{80-co} -HEMA ₂₀)	18.2	34.8	53.1	34.4
P(MMA _{60-co} -HEMA ₄₀)	20.3	35.3	55.4	36.5
P(MMA _{50-co} -HEMA ₅₀)	22.9	36.2	59.1	38.8

The sample with the lowest surface energy was expected to be P(MMA₉₈-MAA₂)-stabiliser. This is due to the fact that this sample contains some of the PHSA-*g*-PMMA stabiliser which has long alkyl chains grafted to a PMMA backbone, making it more hydrophobic. However the high molecular weight PMMA-35 *kDa* and the P(MMA_{90-co}-HEMA₁₀) polymer are given a lower surface energy. This is a result of the molecular weight difference of the polymers. The P(MMA₉₈-MAA₂)-stabiliser sample is dissolved particles from a nonaqueous dispersion polymerisation, and this reaction utilises chain transfer agents to keep the surface smooth by cutting the molecular weight of the growing polymers. Each sample is approximately double in number average molecular weight from P(MMA₉₈-MAA₂)-stabiliser, to P(MMA_{90-co}-HEMA₁₀) to, PMMA-35 *kDa*. This will give more chain ends giving a higher polarity surface.

A small increase in the surface energy can be observed for the P(MMA₉₈-MAA₂) sample owing to the methacrylic acid incorporation and a relatively small molecular weight polymer.

A large jump in the surface energy in the statistical copolymer series can be explained by the fact that the HEMA added to the polymers would be buried under the surface as the polymers are spin coated onto clean glass. As the HEMA content is increased so is the probability of HEMA units being orientated to the surface or more able to rearrange within the sample to the surface when a water contact angle is measured. This rearrangement may

not be able to happen for the P(MMA_{90-co}-HEMA₁₀) sample as the HEMA content is too low and the time frame of the experiment too small. This is overcome by increasing the HEMA content in the polymers.

3.6 Measuring the Monomer - Dodecane Interfacial Tension, $\gamma_{M,D}$

3.6.1 Measuring Interfacial Tension of Liquids by the Pendant Drop Technique

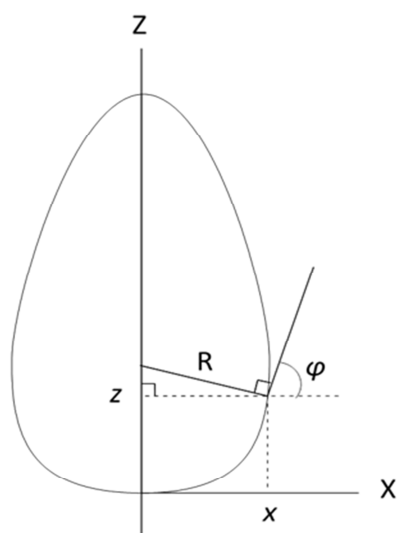
The surface tension formed between a liquid and the air or another immiscible liquid can be measured by a few different techniques such as, measuring the force it takes to pull something through the interface, as in the Du Noüy ring method, or the pendant drop method. The pendant drop method is advantageous as it is very easy and fast to perform, even with more complex experiments such as the measurement of liquid - liquid or liquid -gas interfaces.

In the pendant drop method a droplet of liquid is hung from a needle and the shape profile the drop forms is dependent upon the properties of the liquid, the embedded phase and the interfacial tension between the two. This is given by the Young-Laplace equation, equation 3-12, which describes the shape of a fluid interface by relating the interfacial tension, curvature of the interface and the change in pressure across the liquid drop.

$$\Delta p = \gamma(1/r_1 + 1/r_2) \quad 3-12$$

Where; γ is the interfacial tension, r_1 and r_2 are the principal radii of curvature and define the drop shape and Δp is the change in pressure.

The Young-Laplace equation can then be equated to coordinates (z,x) of the drop profile shown in Figure 3-13 and relate the arc length and the turning angle, ϕ , to the surface tension. This is done for multiple sites along the total drop length to give a surface tension value for the liquid.



Where; R is the radius of curvature, z and x mark the coordinates on the drop profile and φ is the turning angle on the surface of the drop

Figure 3-13, characteristics of measuring surface tension by the pendant drop method.¹⁶

3.6.2 The Monomer - Dodecane Interfacial Tension, $\gamma_{M,D}$

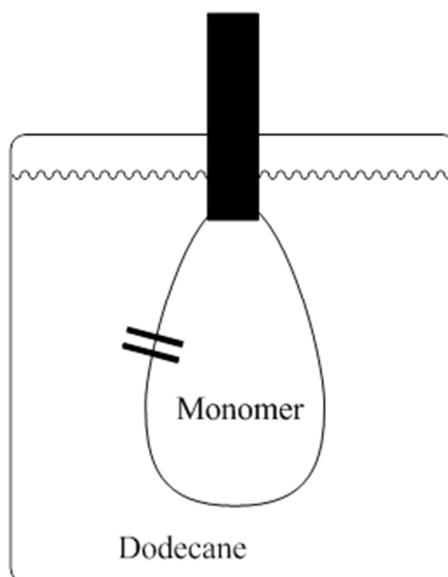


Figure 3-14, schematic view of measuring the monomer - dodecane interfacial tension, shown in bold.

The surface tension of each of the monomers used was measured by the pendant drop method in air and in an embedded phase of dodecane and the results are summarised in Table 3-7. The drop shape formed varies greatly from in air to in dodecane due to the difference in the interfacial tension. In all cases the interfacial tension decreases when the

drops are in dodecane which indicates that the liquid has a higher affinity for dodecane than air. In the case of HEMA the interfacial tension drops dramatically giving a very low interfacial tension value and as a consequence only very small drops can be produced. Figure 3-15 shows images captured of the liquid drops in air and dodecane.

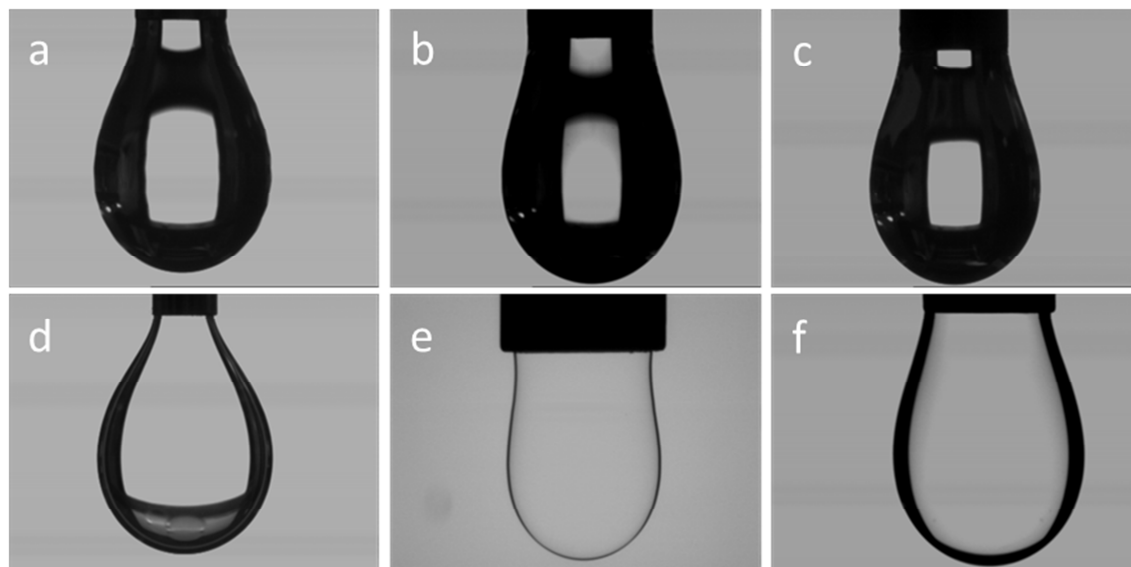


Figure 3-15, pendant drops formed between the liquid and air for a, water, b, HEMA and c, HEAm and the liquid and dodecane for; d, water, e, HEMA and f, HEAm. The needle diameter is 1.8 mm.

Table 3-7, the monomer - dodecane interfacial tension, $\gamma_{L,D}$, measured by pendant drop method.

Monomer	$\gamma_{L,D}$ (mNm ⁻¹) at 25 °C	
	In dodecane	In air
2-Hydroxyethyl methacrylate	3.5	33.8
<i>N</i> -Hydroxyethyl acrylamide	13.0	45.6
Water	43.0	71.5

The surface tension (liquid - air) value for water matches closely to the literature value, 71.9 mNm⁻¹.¹⁷ A literature value for the water - dodecane interfacial tension¹⁸ was found to be 52.34 mNm⁻¹. However finding literature values for monomers is exceedingly difficult, this is even more difficult when looking for the monomer - dodecane interfacial tension. Each experimental value for the dodecane - monomer interfacial tension was supported by

the Du Noüy ring method; see Table 3-8, in which each result was an average of three repeats.

Table 3-8, monomer - dodecane interfacial tension measured by Du Noüy ring method.

Monomer	Interfacial Tension (mNm ⁻¹)	% Difference to Pendant Drop
2-Hydroxyethyl methacrylate	2.33	33.4 %
<i>N</i> -Hydroxyethyl acrylamide	13.9	-6.5 %
Water	37.9	11.7 %

The very low values for the two monomers suggest that creating a new dodecane - monomer interface is easy and low energy. This result is counter intuitive as the two monomers are highly polar and differ greatly from dodecane. As the results have been supported by a complementary experimental technique the low interfacial tension can be believed. The very low interfacial tension values could be down to the monomers having surfactant-like behaviour. This is shown schematically in below.

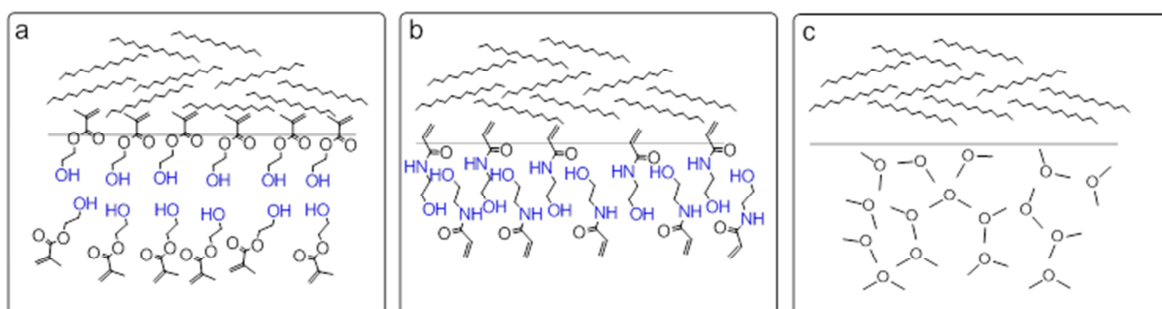


Figure 3-16, schematic view of how the monomers may act like surfactant-like molecule in dodecane, due to their hydrophilic and hydrophobic units where; a, shows HEMA - dodecane, b, HEAm - dodecane and c, water - dodecane with polar units shown in blue.

If the analogy of a surfactant is used for these monomers then HEMA would be more surfactant-like with distinct separate polar (hydroxyl group) and hydrophobic (methacrylate group) groups. The HEAm has the polar hydroxyl group but it also has a polar amide group next to the carbon - carbon double bond, which is the only part of the molecule which is hydrophobic. As the polar and hydrophobic units in HEAm are not

separated by a spacer this means that the molecule will not act surfactant-like to the same extent as HEMA. Of course water, (Figure 3-16 c), does not act as a surfactant so the two phases are separate, which is reflected in the high surface tension.

If this surfactant-like behaviour is true it would give way to some explanation as to why the interfacial tension values for the monomer are so low. It would also explain why HEMA gives a lower interfacial tension with dodecane than HEAm. This can also be linked back to the Hansen solubility parameters in Table 3-1. This shows that of the monomers MMA, HEMA and HEAm; MMA is dodecane miscible, hence no measurement can be made, HEAm is dodecane immiscible, giving rise to the higher surface tension value. Whereas HEMA sits on the boundary between miscibility and immiscibility, with a $\Delta G_m = 0$, which gives rise to the very low surface tension value calculated in both cases.

For all calculations the values obtained from the pendant drop method will be used.

3.7 Calculating the Dodecane - Substrate Interfacial Tension, $\gamma_{D,S}$

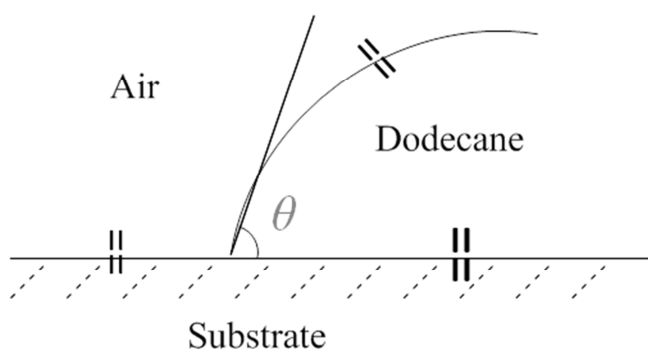


Figure 3-17, schematic view of experimentally measuring the dodecane - substrate contact angle, in grey and calculating the dodecane - substrate interfacial tension in bold and the known values are shown.

The dodecane - substrate interfacial tension was calculated from the experimental contact angle data, however due to the low surface tension of dodecane, 25.4 mN/m and low viscosity, it will wet out on most surfaces. Small contact angles are very hard to measure by this method and introduce a high amount of error in the measurement. This is from the

fact that the droplet is very hard to image and also that the droplet will not wet evenly in all directions. This problem is shown in Figure 3-18. This is an issue as the droplet must maintain a spherical shape in order for the calculations to be valid. This is why the measurement stops after a very short time frame.

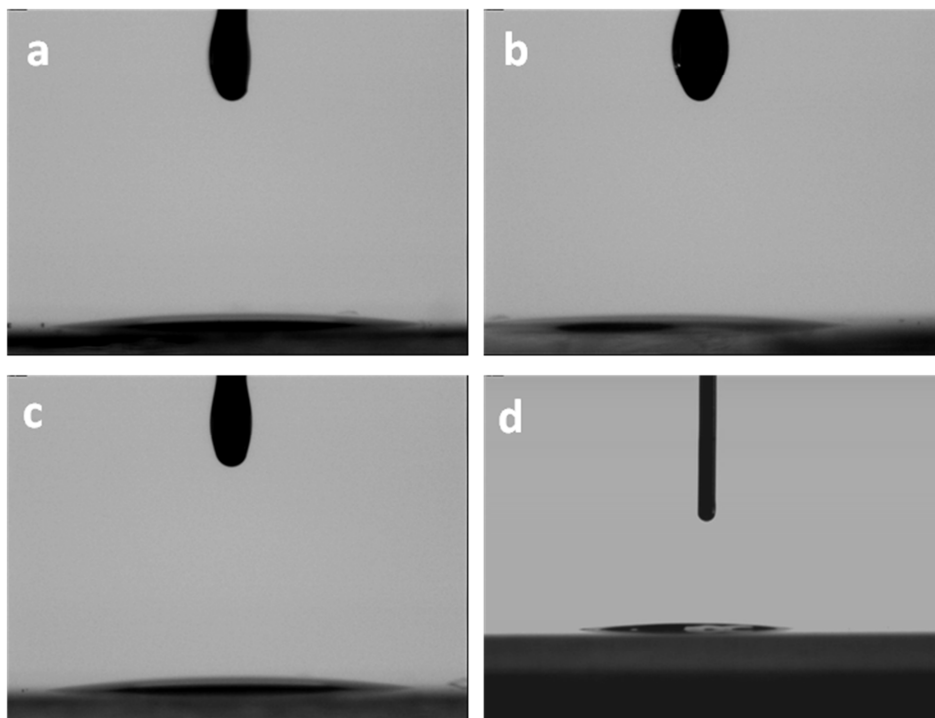


Figure 3-18, images showing the dodecane contact angle after 1 s on substrates of; a, PMMA-28 *KDa*, b, PMMA-35 *KDa*, c, P(MMA₉₈-MAA₂) and d, P(MMA₉₈-MAA₂)-stabiliser.

The resultant contact angles formed on the polymer substrates are shown in Table 3-12, however due to the low surface tension of dodecane reliable results for all substrates were not obtained, because of this the data obtained for PMMA-28 *KDa* was used for all other polymer substrates except for PHEAm where a contact angle was able to be measured.

Table 3-9, dodecane - substrate contact angles and calculated dodecane - substrate interfacial tensions.

Substrate	Equilibrium advancing contact angle, θ , at 25 °C (°)	Dodecane - substrate interfacial tension, $\gamma_{D,S}$ (mNm ⁻¹)
PMMA-28 <i>kDa</i>	2.2	19.1
PMMA-35 <i>kDa</i>	2.2*	23.1
P(MMA ₉₈ -MAA ₂)	2.2*	22.8
P(MMA ₉₈ -MAA ₂)-stabiliser	2.2*	20.3
PHEMA	2.2*	33.2
PHEAm	3.2	45.6
P(MMA _{90-co} -HEMA ₁₀)	2.2*	19.7
P(MMA _{80-co} -HEMA ₂₀)	2.2*	28.1
P(MMA _{60-co} -HEMA ₄₀)	2.2*	30.4
P(MMA _{50-co} -HEMA ₅₀)	2.2*	34.1

*unable to measure angle – taken from PMMA-28 *kDa* value

The calculated dodecane - substrate interfacial tension shows that as the hydrophilicity of the substrate increases so does the interfacial tension. This makes sense as the dodecane - substrate interfacial tension refers to the energy required to produce a new dodecane - substrate interface, and this value should be higher for a mismatched pair. This difference has solely come from the differences in the surface energies of the substrates as an accurate dodecane contact angle could not be obtained for most substrates.

3.8 Measuring the Contact Angle between Polymer Substrates and Monomers Submerged in Dodecane, $\theta_{M,S}$

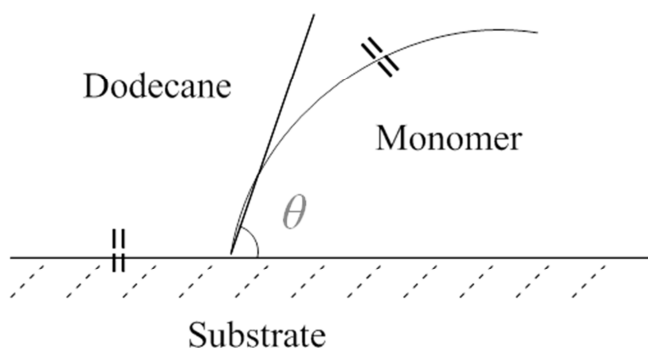


Figure 3-19, schematic view of measuring the contact angle formed between monomer and substrate under dodecane, in grey and known values shown.

Measuring the contact angle formed between monomer droplets and a polymer substrate submerged in dodecane, along with the other information calculated allows for the calculation of the interfacial tension between the monomer and polymer substrate. The results are summarised in Table 3-10 and example data for PMMA-35 *KDa* is shown in Figure 3-20

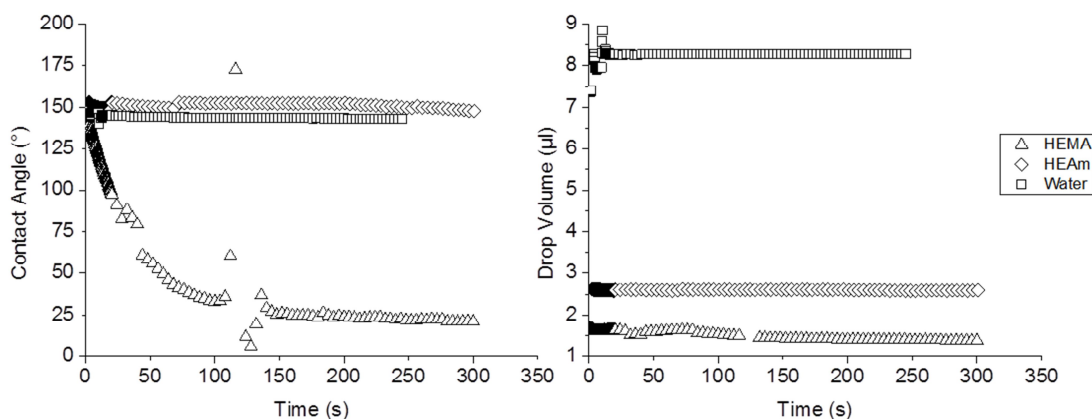


Figure 3-20, contact angle vs. time, a, and drop volume vs. time, b, for HEMA, HEAm and water on a PMMA-35 *KDa* substrate. Contact angle vs. Time plots for other substrates are given in the *Appendices* (Chapter 9.4).

For the first data set representing the particles it is clear that the inclusion of the methacrylic acid into the particle plays a large role in the affinity the hydrophilic probe liquids have on the substrate. In all cases with the different probe liquids the contact angle formed decreases with the inclusion of the methacrylic acid, and the opposite is shown with the sample substrate containing the polymeric stabiliser as this sample has a lower surface polarity yielding higher contact angles.

For the two hydrophilic polymer substrates all the angles formed are lower than all other tested substrates due to their high surface polarity. It must be noted that PHEAm is water soluble so the very low water contact angle is expected. Low contact angles are also expected when the polymers come into contact with their monomers due to the very high interaction between the two.

For the statistical copolymers P(MMA-*co*-HEMA) again the trend of a higher surface polarity, giving a lower contact angle is observed.

All the contact angles formed for HEMA in comparison to HEAm and water are very low which indicates that HEMA has a far greater affinity for all the films than the other two probe liquids. This may also be due in part to the low HEMA - dodecane interfacial tension measured. This is because as a drop wets a substrate it will also want to minimise contact with the embedded phase, in this case dodecane, and stay as a spherical droplet, despite any favourable interactions with the substrate. It is this balance of forces which changes the wetting behaviour of a given liquid on a surface. However if the interfacial tension between probe liquid and the embedded phase is very low, as in the case of HEMA - dodecane, it can wet most substrates very easily.

Table 3-10, equilibrium advancing contact angles for monomers and water on different polymer substrates.

Substrate	Equilibrium advancing contact angle, θ , at 25 °C (°) in dodecane			
	θ_{MMA}	θ_{HEMA}	θ_{HEAm}	θ_{water}
PMMA-28 <i>kDa</i>	N/A*	7.6	78.3	137.2
PMMA-35 <i>kDa</i>	N/A*	19.9	143.1	145.8
P(MMA ₉₈ -MAA ₂)	N/A*	12.9	69.07	133.4
P(MMA ₉₈ -MAA ₂)-stabiliser	N/A*	16.1	113.2	140.2
PHEMA	N/A*	3.0	2.56	76.3
PHEAm	N/A*	9.1	16.9	8.5
P(MMA _{90-co} -HEMA ₁₀)	N/A*	15.4	149.7	157.7
P(MMA _{80-co} -HEMA ₂₀)	N/A*	13.4	148.4	152.9
P(MMA _{60-co} -HEMA ₄₀)	N/A*	12.3	118.3	148.5
P(MMA _{50-co} -HEMA ₅₀)	N/A*	13.0	101.6	123.3

*soluble in dodecane

3.9 Calculating the Polymer Substrate - Monomer Interfacial Tension, $\gamma_{S,M}$

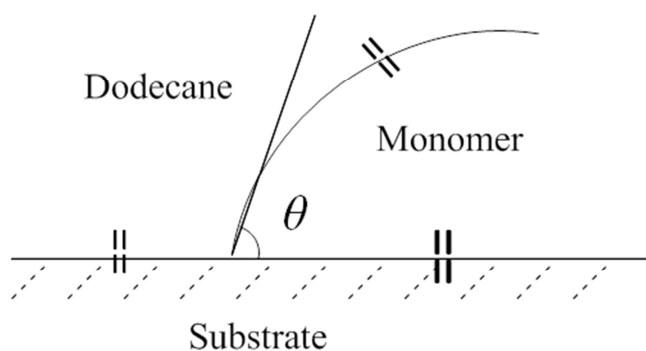


Figure 3-21, schematic view of calculating the monomer-substrate interfacial tension submerged in dodecane, in bold and known values shown.

From all the data in Tables 3-6 to 3-11 the interfacial tension between polymer substrate and monomer droplets can be calculated by the Young equation:

$$\gamma_{S,L} = \gamma_S - (\gamma_{L,D} \cos \theta_{S,L}) \quad 3-1$$

Where; $\gamma_{S,L}$ is the substrate - liquid interfacial tension, γ_S , the surface energy of the polymer substrate, $\gamma_{L,D}$, the interfacial tension between the liquid and dodecane and $\theta_{S,L}$ is the contact angle formed between the substrate and the probe liquid. The results for these calculations are summarised in Table 3-11.

Table 3-11, calculated interfacial tension between substrate and monomer droplet, $\gamma_{S,L}$.

Substrate	$\gamma_{S,L}$ (mNm ⁻¹) at 25 °C		
	HEMA	HEAm	Water
PMMA-28 <i>kDa</i>	15.9	29.5	54.7
PMMA-35 <i>kDa</i>	19.7	20.5	54.7
P(MMA ₉₈ -MAA ₂)	19.5	18.2	52.4
P(MMA ₉₈ -MAA ₂)-stabiliser	17.0	25.4	53.4
PHEMA	29.8	20.3	23.0
PHEAm	42.2	33.2	3.1
P(MMA _{90-co} -HEMA ₁₀)	16.4	30.9	59.5
P(MMA _{80-co} -HEMA ₂₀)	24.8	39.2	66.4
P(MMA _{60-co} -HEMA ₄₀)	27.0	36.6	67.1
P(MMA _{50-co} -HEMA ₅₀)	30.8	36.7	57.7

The data in Table 3-11 shows the surface energy at the interface between the polymer substrate and probe liquid which cannot be measured directly and must be calculated using the Young equation and information obtained experimentally for; the liquid - embedded phase interfacial tension, the surface energy of the solid polymer substrate and the contact angle formed between the probe liquid and the polymer substrate while all contained within the embedded phase. This surface interfacial tension is analogous to the energy required to produce more polymer - liquid interface displacing the embedded phase, in this case dodecane.

3.10 Summing the Total Interfacial Tension for the System

Equation 3-4, shown again below, shows that when the interfacial energy of the system is between -1 and 1 then some intermediate structure will be formed and if it is equal to 1 or -1 then total engulfment occurs giving a core shell or inverted core shell particle morphology respectively.

$$-1 < \frac{\gamma_{X,D} - \gamma_{X,Y}}{\gamma_{Y,D}} < 1 \quad 3-4$$

These calculations were undertaken for the system of different polymer films with the two different monomers, HEMA, HEAm and water for a comparison, the results of these calculations are shown in Table 3-12.

Table 3-12, results from calculating the expected particle morphology.

Substrate	$(\gamma_{X,D} - \gamma_{X,Y})/\gamma_{Y,D}$		
	Probe Liquid		
	HEMA	HEAm	Water
PMMA-28 <i>kDa</i>	0.940	-0.800	-0.827
PMMA-35 <i>kDa</i>	0.991	0.203	-0.734
P(MMA ₉₈ -MAA ₂)	0.975	0.357	-0.687
P(MMA ₉₈ -MAA ₂)-stabiliser	0.961	-0.394	-0.768
PHEMA	0.999	0.999	0.237
PHEAm	0.987	0.957	0.989
P(MMA _{90-co} -HEMA ₁₀)	0.964	-0.863	-0.925
P(MMA _{80-co} -HEMA ₂₀)	0.973	-0.852	-0.890
P(MMA _{60-co} -HEMA ₄₀)	0.977	-0.474	-0.853
P(MMA _{50-co} -HEMA ₅₀)	0.974	-0.201	-0.549

Although these calculations cannot be performed for MMA, we know that MMA is a good solvent for PMMA and miscible with dodecane. With this in mind a predicted morphology for MMA mixed with PMMA would be that the monomer would swell into the particles and form core-shell particles with total engulfment.

HEMA in most cases acts to give very close to a core-shell morphology, this result is to be expected as the monomer was able to wet all the surfaces to good extent. However differences were picked out with increasing hydrophilicity of the polymer substrates.

For HEMA the calculations suggest that an intermediate morphology close to that of a core shell morphology will be most favoured in the first case for modelling a particle. Again the P(MMA₉₈-MAA₂) sample shows a small increase in the affinity for HEMA over pure PMMA and says that it will prefer a more core shell morphology. The opposite is true for P(MMA₉₈-MAA₂)-stabiliser compared to PMMA which shows that a more separated morphology should be adopted.

Unsurprisingly the results from the calculations show that HEMA will adopt a core shell morphology with itself and with PHEAm. This is due to the fact that these two are a close match in terms of their surface energy. For the P(MMA-*co*-HEMA) series as the hydrophilic component is increased so the thermodynamically favoured morphology changes to a more core shell-like morphology.

For HEAm the expected morphology differs greatly from that of HEMA showing that in most cases a true intermediate structure should be obtained, the same subtle trends appear such as P(MMA₉₈-MAA₂) showing a slight increase toward a core shell-like morphology over PMMA. For the P(MMA-*co*-HEMA) copolymers the expected morphology is more extreme tending more toward a separated morphology. However the trend within the P(MMA-*co*-HEMA) data set shows that as the hydrophilic component is increased the expected thermodynamic morphology will tend toward a more core shell-like.

For the two hydrophilic polymer substrates, PHEMA and PHEAm the result is the same for that of HEMA, that a core shell morphology will be adopted.

Water, being used as a comparison to a very hydrophilic monomer, shows that an intermediate structure would be formed but would tend toward a separated structure except in the case of HEMA in which an intermediate structure would be formed.

3.10.1 Expected Particle Morphology

From the calculations summing the total interfacial tension for the system upon polymerisation of HEMA and HEAm in the presence of PMMA particles should give intermediate particles of nonspherical morphology. For HEMA the resultant morphology

should be close to that of a core shell morphology, and HEAm a more separated morphology with partial engulfment. For a MMA-PMMA particle system the expected morphology would be particle growth. This cannot be predicted by this system but would be an expected result due to the strong interactions between MMA and PMMA. These predicted structures are summed up schematically below.

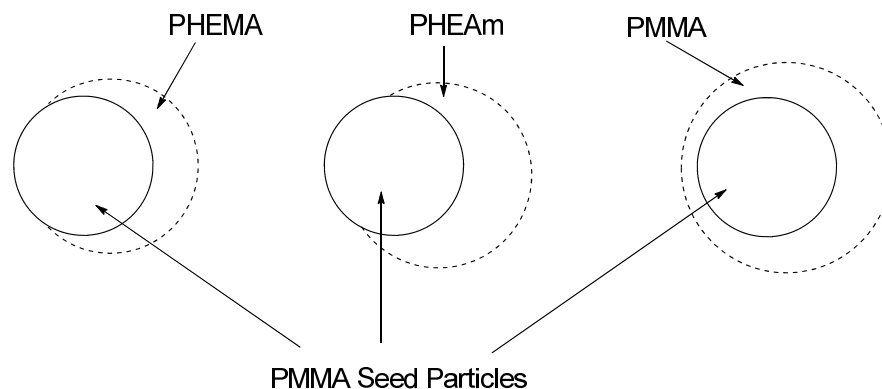


Figure 3-22, expected particle morphologies after polymerisation for HEMA, HEAm and MMA.

3.11 Limitations to Predicting Particle Morphology by Summing the Total Interfacial Tension for the System

The theory set out in the paper by Waters² was concerned with the growth of particles in a seeded emulsion polymerisation, where particles swollen with monomer grow in size but the number of particles stays constant. This situation has been shown to not occur in this nonaqueous system where the monomer does not interact so strongly with the polymer particles. However this does give an indication into what the resultant particle morphology may be post polymerisation for these monomer - polymer systems.

The system outlined was also only concerned about the thermodynamically most stable conformation between two polymers which would phase separate upon mixing to lower the interfacial energy for the system. As with growing particles by seeded emulsion polymerisation this nonaqueous system does not deal with the mixing of two preformed polymers but monomer and polymer. This will lead to some disagreement with experimental results and predicted morphology. As this only deals with the most

thermodynamically stable state it also does not take into account the kinetics of growing polymers and their increasing immiscibility in the system with time.

3.12 Conclusions

Monomers were chosen for further study based upon their Hansen solubility parameters relative to that of PMMA and their interactions with a PMMA substrate. This led to the synthesis of multiple polymers which have been produced and characterised and used to model monomer - particle interactions and to predict resultant particle morphology based on minimisation of the surface free energy of the system.

The minimisation of the surface free energy has yielded information on the resultant particle morphologies upon mixing for the two monomers 2-hydroxyethyl methacrylate (HEMA) and *N*-hydroxyethyl acrylamide (HEAm). The model predicts intermediate morphologies for the two, a more core-shell morphology for HEMA and a more separated morphology for HEAm. This morphology should be locked into place upon polymerisation.

3.13 References

- ¹ Jin-W. Kim, R. J. Larsen, and D. A. Weitz, *J. Am. Chem. Soc.*, 2005, **128**, 14373
- ² J. A. Waters, *Colloid Surface A*, 1994, **84**, 167
- ³ E. B. Mock, H. De Bruyn, B. S. Hawkett, R. G. Gilbert and C. F. Zukoski, *Langmuir*, 2006, **22**, 4037
- ⁴ T. Young, *Proceedings at the Royal Society*, London, 1804
- ⁵ R. H. Ottewill, A. B. Schofield and J. A. Waters, *Colloid Polym. Sci.*, 1996, **273**, 763
- ⁶ J. H. Hildebrand, *J. Am. Chem. Soc.*, 1918, **40**, 198
- ⁷ J. H. Hildebrand, *J. Am. Chem. Soc.*, 1916, **38**, 1452
- ⁸ J. H. Hildebrand, *J. Am. Chem. Soc.*, 1917, **39**, 2297
- ⁹ C. M. Hansen and T. S. Poulsen, '*Hansen Solubility Parameters*', CRC Press, 2nd Ed., 2007
- ¹⁰ C. M. Hanson, *J. Paint Technology*, 1967, **39**, 505

- ¹¹ J. Burke, '*Solubility Parameters: Theory and Application*', The Book and Paper Group Annual, 1984
- ¹² C. M. Hanson, '*Hansen Solubility Parameters: A User's Handbook*', CRC Press, 2000
- ¹³ F. M. Fowkes, *J. Phys. Chem.*, 1962, **66**, 382
- ¹⁴ D. K. Owens and R. C. Wendt, *J. Appl. Polym. Sci.*, 1969, **13**, 1741
- ¹⁵ Kruss Information Database, <http://www.kruss.de/en/theory/substance-properties/liquids.html>
- ¹⁶ A. W. Neumann, R. David and Y. Zuo, '*Applied Surface Thermodynamics*', CRC Press, 2nd ed. 2011
- ¹⁷ N. R. Pallas and Y. Harrison, *Colloids and Surfaces*, 1990, **43**, 169
- ¹⁸ S. Zeppieri, J. Rodriguez and A. L. Lopez de Ramos, *J. Chem. Eng. Data*, 2001, **46**, 1086

4 Second Stage Polymerisation Reactions of Methyl Methacrylate with Poly(methyl methacrylate) Seed Particles

4.1 Introduction

In this chapter the second stage seeded non-aqueous dispersion polymerisation of poly(methyl methacrylate) (PMMA) seed particles with methyl methacrylate (MMA) is considered. MMA is used as a bench mark for comparison to the polar monomer considered in *Chapter 3*.

4.2 Initial Seed Dispersions

Multiple batches of seed dispersions were used in this work all of which were of uniform size and spherical shape. The particles were crosslinked with 1 wt. % ethylene glycol dimethacrylate (EGDMA), an example is shown below in Figure 4-1. In each series of experiments the same seed particle was used where possible. Images of the other seed dispersions used can be found in the *Appendices* (Chapter 9.5).

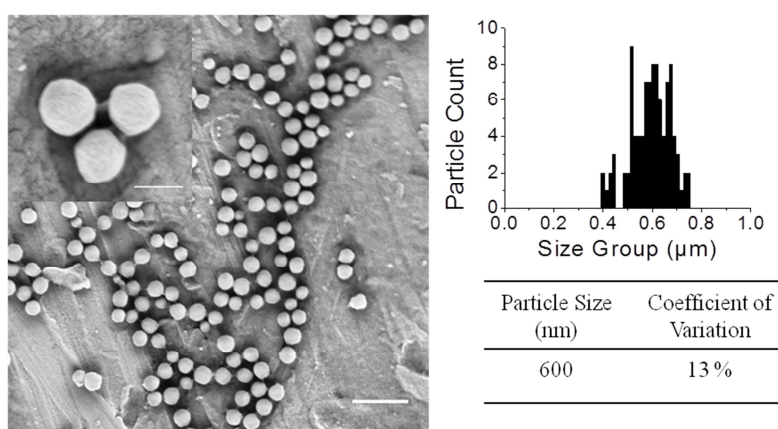


Figure 4-1, seed dispersion, SRB-325-1% EGDMA and size data, based on counting 100 particles. Scale bars are 2 μm and 500 nm for the insert.

4.3 Second Stage Polymerisation Reaction under Batch Conditions

The second stage polymerisation reactions were conducted under batch conditions. Batch conditions are where all the components of the reaction are charged into the reaction vessel and the thermally initiated polymerisation allowed to proceed.

4.3.1 Standard Conditions

Standard conditions for these reactions were as follows unless otherwise stated:

Reaction Component	Amount	Example
Initial solid content of seed dispersion	10 wt. %	10 g dispersion (1 g solid)
Monomers	4:1 monomer – solid particle	4.00 g
P(HAS- <i>g</i> -MMA) stabiliser	9.3 wt. % of total monomers	0.372 g
Radical initiator	0.5 wt. % of total monomers	0.020 g
Dodecanethiol	0.2 wt. % of monomers	0.008 g

These conditions allow for working in the stable region of 34 wt. % total solids content (TSC) outlined by Antl *et al.*¹ For specific examples of the second stage polymerisation reactions see the experimental section *Chapter 8*.

4.3.2 Monomer Conversion and Particle Growth

The second stage polymerisation reactions were carried out under different conditions which were not comparable to seed particle production. The initiator concentration was reduced from 2 wt. % to 0.5 wt. % of total monomers in order to keep the rate of polymerisation low and avoid a high radical flux. The conversion profile for the second stage polymerisation reaction is shown below in Figure 4-2.

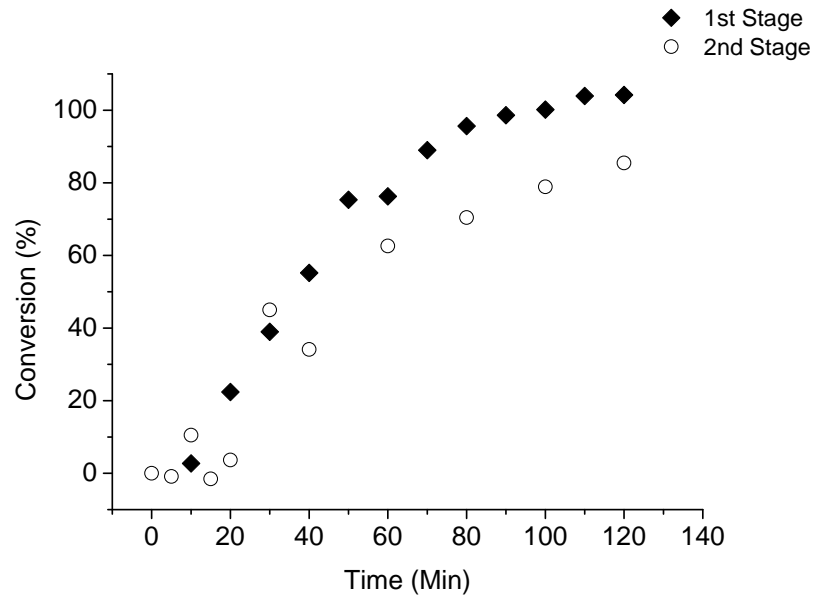


Figure 4-2, monomer conversion vs. time plot for seed particle formation (1st stage), SRB-077-0%xl and second stage reaction, SRB-409-1% EGDMA.

During the reaction the monomer feed was added over the course of the first 30 min., at which point the monomer conversion started to increase, the monomer conversion reaches a maximum of 85 % over the course of the reaction. The reactions were quenched at this point to minimise aggregation.

These reactions were undertaken with an excess of monomer in a 4:1 monomer / seed particle ratio, the particle size can be calculated by equation 4-1.

$$r_1 = r_s \left(\sqrt[3]{\left(\frac{m_1}{m_s} + 1 \right)} \right) \quad 4-1$$

Where, r_1 and r_s are the radii of the resultant particles and the seed particles respectively and, m_1 and m_s are the mass of monomer in the reaction and the mass of seed particles respectively.

This was linked to the monomer conversion for the second stage polymerisation reactions which in all cases were 85 ± 5 %.

4.3.2.1 Monomer Addition and Colloidal Stability

When the MMA is added to the particle dispersion it may swell the particle, resulting in an increase in particle size. This will lead to the formation of unprotected particle surface without adsorbed stabiliser. The MMA monomer may also wash off the stabiliser by solvating the PMMA backbone in the P(HSA-*g*-MMA) stabiliser, again resulting in unprotected surfaces. This will lead to aggregation of particles as they will not be stabilised against aggregation. To counter this, extra stabiliser was added to the monomer feed prior to reaction. This excess stabiliser allowed for the coverage of extra surface generated by particle swelling. As this extra stabiliser is dissolved in the monomer, when added to the reaction mixture the monomer will be already saturated with P(HSA-*g*-MMA) stabiliser, meaning it is less likely to wash off any stabiliser from the surface. Consideration of possible secondary nucleation is given later.

4.3.3 Second Stage Polymerisation Reactions

In this set of reactions the monomer charge did not contain any crosslinking monomer so the particles produced would result in an uncrosslinked P(MMA₉₈-*co*-MAA₂) second stage polymer, in combination with a crosslinked seed particle containing 1 wt. % EGDMA.

4.3.3.1 Varying Monomer / Particle Mixing Time

The effect of monomer mixing time was considered and the second stage polymerisation reactions were initiated after the monomer and seed dispersion were allowed to mix for differing periods of time. The resultant dispersions are shown in Figure 4-3. All the particle dispersions maintained a similar or lower level of polydispersity, despite some examples of isolated aggregation.

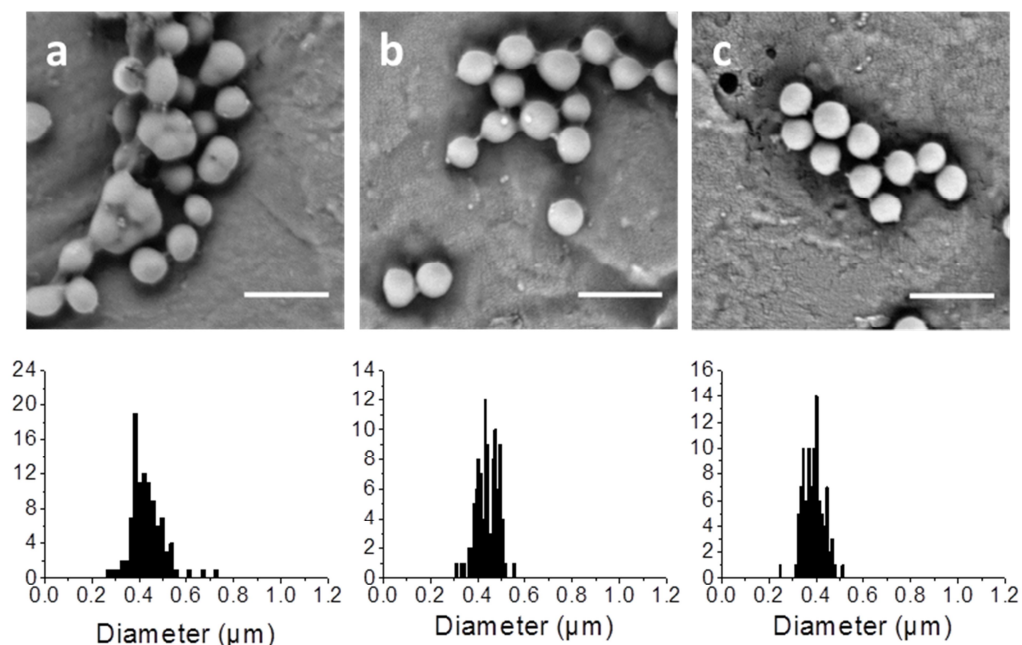


Figure 4-3, SEM images and size distributions for resultant dispersions when the monomer feed was added at; a, 30 min., b, 1 hr., and c, 4 hr. Scale bars are 1 μ m. Total solids content of the seed dispersion was 10 wt. %, monomer / particle ratio was 4:1, DDT concentration was 1 wt. % of monomers and initiator concentration was 0.5 wt. % of monomers, using SRB-243-1% EGDMA as the seed dispersion.

Table 4-1, particle size data for dispersions produced by varying the monomer / particle mixing time, shown in Figure 4-3, characteristics for the seed dispersion are given in italics.

Sample	Particle Diameter [†] (nm)	Coefficient of Variation	Expected Diameter (nm)	% Difference Expected / Experimental
<i>SRB-243-1% EGDMA</i>	<i>280</i>	<i>13 %</i>	-	-
30 min	440	16 %	406	8 %
1 hr	450	10 %	406	10 %
4 hr	390	11 %	406	-4 %

[†] based on counting 100 particles

The particle size data shows that all the particles exhibit a size increase over the initial seed dispersion and the particle growth largely reflects the predicted value by equation 4-1 at a level of 85 % monomer conversion. At longer time periods the reactions became unclear owing to aggregation and coagulum formation.

4.3.3.2 Varying Monomer / Particle Ratio

To further investigate the second stage polymerisation reaction experiments to change the monomer / particle ratio were undertaken, using a 1 hour mixing time. SEM images for this series are shown below in Figure 4-4 along with size distribution graphs.

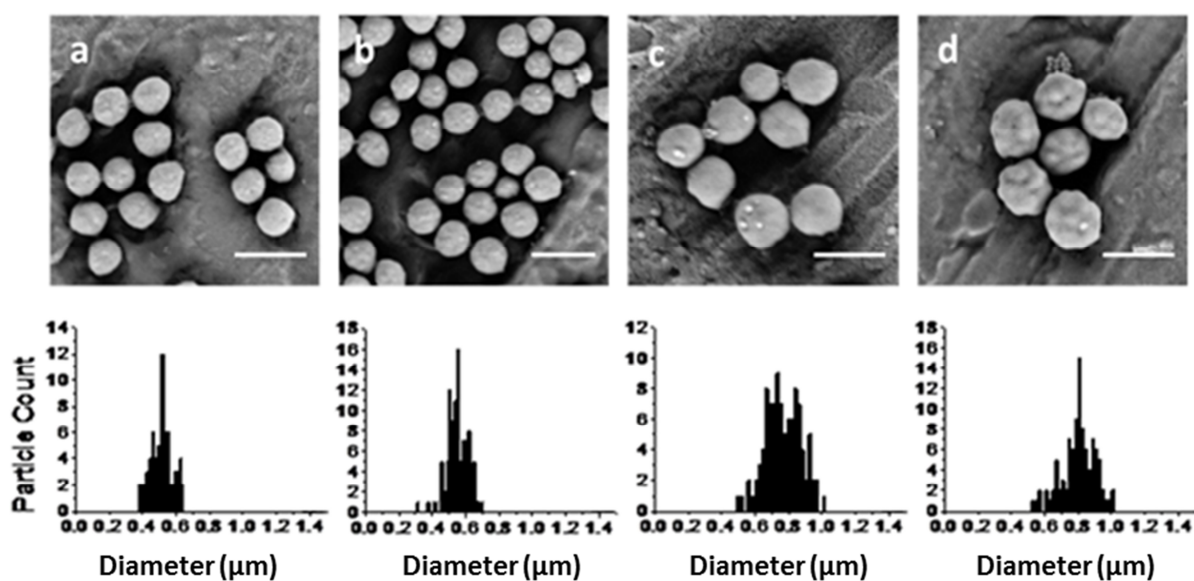


Figure 4-4 , SEM images and size distribution plots for reactions with varied monomer / particle ratios, where; a, 1:1, b, 2:1, c, 4:1 and d, 5:1. Scale bars are 1 μm . Total solids content of the seed dispersion was 10 wt. %, DDT concentration was 1 wt. % of monomers and initiator concentration was 0.5 wt. % of monomers, 1 hour mixing time prior to polymerisation, using SRB-253-1% EGDMA as the seed dispersion.

From the SEM images, Figure 4-4 an essentially smooth spherical morphology is maintained. The particle size from the SEM images in Table 4-2 shows that all the resultant dispersions were of a low polydispersity, and the trend with respect to particle size again shows growth and is in line with the expected values for swelling and growth from equation 4-1.

Table 4-2, particle size data for dispersions which the monomer / particle ratio was changed, characteristics for the seed dispersion are given in italics.

Sample	Particle Diameter [†] (nm)	Coefficient of Variation	Expected Diameter (nm)	% Difference Expected / Experimental
<i>SRB-253-1% EGDMA</i>	<i>480</i>	<i>12 %</i>	-	-
1:1	520	12 %	604	1 %
2:1	560	12 %	692	-5 %
4:1	780	14 %	821	11 %
5:1	810	12 %	872	9 %

[†] based on counting 100 particles

4.3.4 Second Stage Polymerisation Reactions with Methyl Methacrylate and Crosslinker

In this set of reactions the monomer charge contained 1 wt. % ethylene glycol dimethacrylate (EGDMA) so producing uniform particles with respect to chemistry. A crosslinked second stage polymer of P(MMA_{97-co}-MAA_{2-co}-EGDMA₁) was polymerised in the presence of crosslinked seed particles also containing 1 wt. % EGDMA. The advantages of fully crosslinked particles are that they will be more robust to changes in solvent.

Short monomer / particle mixing times were found to give clean coagulum free reactions, the monomer mixing time was set to be under 1 hour, and in one case a mixing time of 0 was used by polymerising under monomer starved conditions. Monomer starved conditions is where the monomer is fed into a reaction vessel containing the initiator at the reaction temperature over a period of time, allowing for essentially instantaneous reaction. The monomer feed was added at a constant rate over the first 20 min. of the reaction.

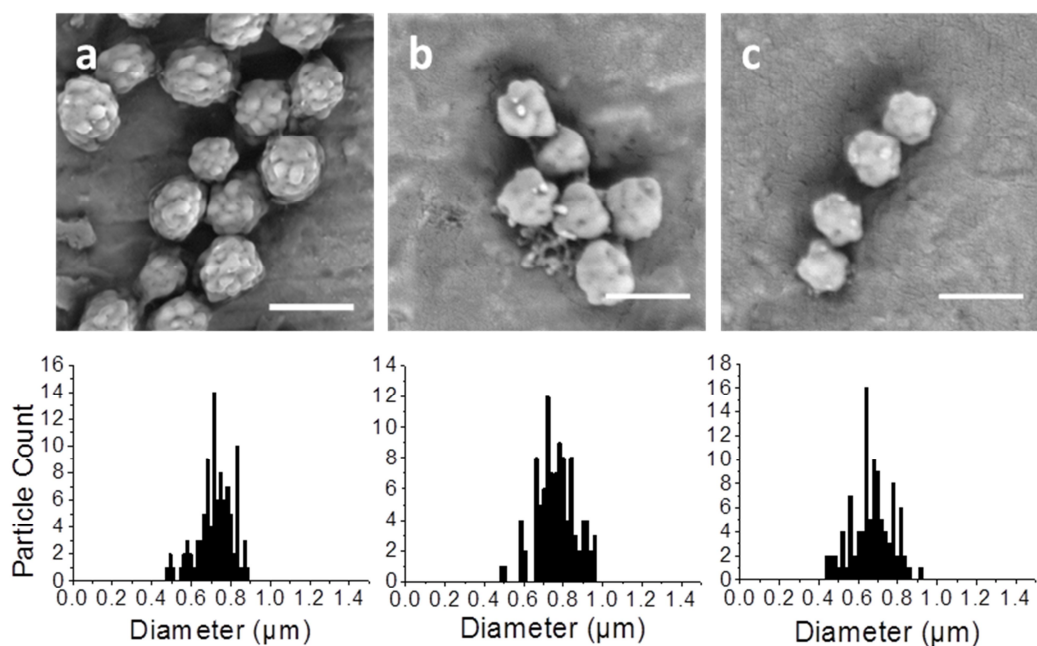


Figure 4-5 SEM images and size distributions for resultant dispersions when the monomer / particle mixing time was; a, 0 min. b, 30 min. and c, 1 hr. Scale bars are 1 μ m. Total solids content of the seed dispersion was 10 wt. %, monomer / particle ratio was 4:1, DDT concentration was 1 wt. % of monomers and initiator concentration was 0.5 wt. % of monomers. SRB-325-1% EGDMA was used as the seed dispersion for a mixing time of 0, and SRB-223-1% EGDMA used for the others.

Table 4-3, particle size data for dispersions shown in Figure 4-5, with the seed dispersions shown in italics.

Sample	Particle Diameter [†] (nm)	Coefficient of Variation	Expected Diameter (nm)	% Difference Expected / Experimental
<i>SRB-325-1% EGDMA*</i>	<i>600</i>	<i>13 %</i>	-	-
0 min.	730	12 %	872	-19 %
<i>SRB-223-1% EGDMA</i>	<i>530</i>	<i>14 %</i>	-	-
30 min.	780	13 %	770	1 %
1 hr.	680	15 %	770	-13 %

[†] based on counting 100 particles, *Seed particle for starve-fed reaction.

In all instances the particles appeared to have slight protrusions forming on the particle surface; this is exacerbated in the reaction under monomer starved conditions. Looking at the particle size data in Table 4-3 it is clear that in most cases the particles have grown to within 10 % of the calculated size, the polydispersity of the particles is largely unchanged.

It was found that again the particle size increases were in line with prediction, even with the addition of a crosslinking monomer and that the polydispersity of the sample was only slightly affected by the second stage polymerisation reaction. However reactions with monomer / particle mixing times greater than 1 hour all gave coagulum and this effect was exacerbated by the inclusion of crosslinking monomer to the charge.

4.4 Monitoring Particle Swelling

Dynamic light scattering (DLS) measurements were taken of seed dispersions with added monomer to monitor the swelling behaviour over time. The experiments were run at a monomer / particle ratio of 2:1 and 4:1 in the absence and presence of extra P(HSA-*g*-MMA) stabiliser and the addition of ethyl acetate / butyl acetate (1:1 w/w) solvent mixture which the P(HSA-*g*-MMA) was dissolved in. Note that the stabiliser was a 30 wt. % solution in ethyl acetate / butyl acetate. The results are shown in Table 4-3 below, and Figure 4-6 shows the DLS traces obtained for 2:1 monomer / particle ratio.

Table 4-4, DLS data for MMA swelling of seed particle dispersion SRB-131-1% EGDMA.

MMA / Particle Ratio 2:1		MMA / Particle Ratio 4:1		MMA / Particle Ratio 4:1 With added P(HSA-g-MMA) solution		Ethyl- and Butyl acetate (1:1, w/w)	
Time (min)	Diameter (nm)	Time (min)	Diameter (nm)	Time (min)	Diameter (nm)	Time (min)	Diameter (nm)
0	572	0	572	0	1067	0	1066
3.5	783	3.5	-	3.5	1209	3.5	1060
5	764	5	769	5	1194	5	1103
6.5	801	6.5	788	6.5	1265	6.5	1035
35*	1139	30*	772	30	1017	30	847
60	892	60	763	60*	1076	60*	1139

*Failure point

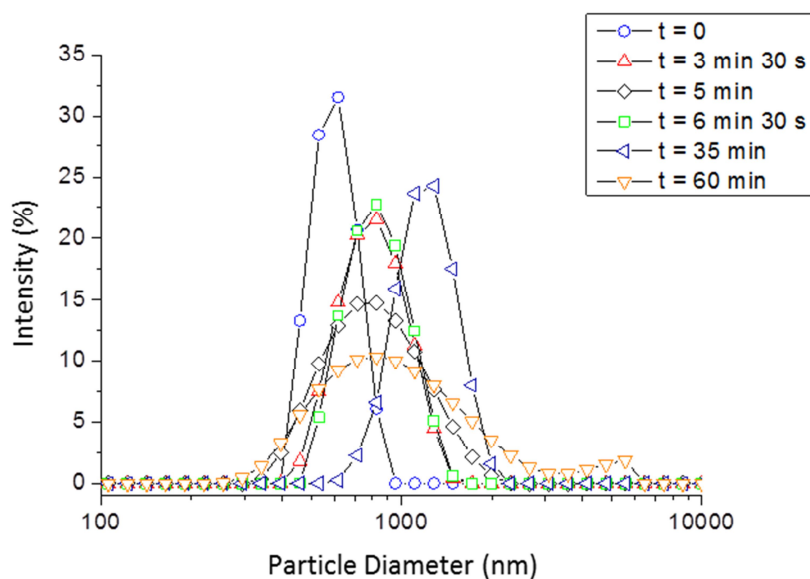


Figure 4-6, DLS traces for monomer swelling experiments, 2:1 monomer / particle ratio, the other DLS traces can be found in the *Appendices* (Chapter 9.6).

The DLS swelling experiments show that the MMA monomer swells the seed dispersion over time. This may lead to aggregation of the particles by either; swelling and fusion of the now gel-like particles, or by washing off the stabiliser. The point at which the measurement failed is shown by an increase of the peak width and appearance of secondary peaks in the DLS trace. The experiment with addition of extra P(HSA-g-PMMA) stabiliser shows pre swelling of the PMMA seed particles due to the ethyl acetate and butyl acetate in the stabiliser solution. However a small increase in particle size is observed when MMA is added and the instability point was pushed to a longer time. This is believed to be due to the extra stabiliser available in solution to adsorb to any new PMMA surface which appears.

The swelling by the ethyl acetate and butyl acetate solvent in the stabiliser solution is confirmed by the control experiment in which the mixed solvent was added to the dispersion of the same mass as the stabiliser solution.

In both cases the addition of the ethyl acetate and butyl acetate mixture swelled the particles rapidly, this pre-swelling by the solvents which will have implications for monomer swelling.

4.5 Reaction Mechanism during Second Stage Polymerisation Reaction

To understand the mechanism in the second stage reaction the monomer's solubility in the solvent and particles must first be considered. The monomer in the second stage reaction is miscible with dodecane but it also has a high affinity for the PMMA particles. This can lead to the partitioning of the monomer in the reaction mixture, leading to the formation of an equilibrium between monomer in the particles and in the solvent.

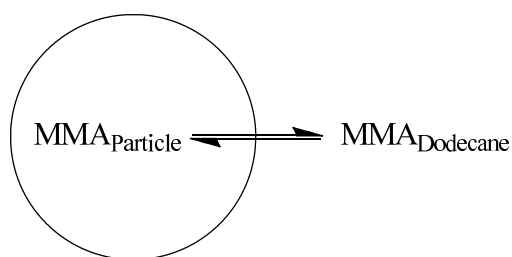


Figure 4-7, schematic representation of the equilibrium between the MMA monomer penetrating the particle and staying in solution.

From Hansen solubility parameters (Table 4-5) it was found that MMA is more miscible with PMMA than dodecane, resulting in the observed particle swelling.

Table 4-5, Hansen solubility parameters for MMA, ethyl acetate and butyl acetate against PMMA and dodecane.

Chemical	Solubility Parameter (MPa ^{1/2})				Radius of Interaction
	δ_T	δ_d	δ_p	δ_h	R_a
<i>PMMA</i>	22.7	18.6	10.5	7.5	-
Ethyl acetate	18.1	15.7	5.3	7.2	8.9
Butyl acetate	17.4	15.8	3.6	6.3	9.0
MMA	18.8	16.4	4.5	8.1	6.6
<i>Dodecane</i>	16.0	16.0	0.0	0.0	-
Ethyl acetate	18.1	15.7	5.3	7.2	9.0
Butyl acetate	17.4	15.8	3.6	6.3	7.3
MMA	18.8	16.4	4.5	8.1	9.3

Swelling of the particles with monomer will effectively lead to plasticisation of the polymer. This has the effect of lowering the glass transition temperature, T_g , of the particles causing them to turn from hard and glassy to a gel-like state. These gel-like particles can then more easily aggregate together forming coagulum. This effect explains why the experiments with longer mixing times lead to coagulum formation, this is backed up by the DLS data of MMA swelling the PMMA particles, which shows a loss of colloidal stability after 60 min.

However monomer swelling may not be the sole mechanism as reactions are performed under monomer starved conditions. Under monomer starved conditions the monomer will polymerise rapidly and will not have time to penetrate the particles. This means that precipitation of polymer from the continuous phase must be considered at the start of the reaction. Taking this into account a reaction mechanism with the pathways open to the growing polymer is shown in Figure 4-8 assuming no monomer swelling. The seed particle provides a surface for polymer precipitation.

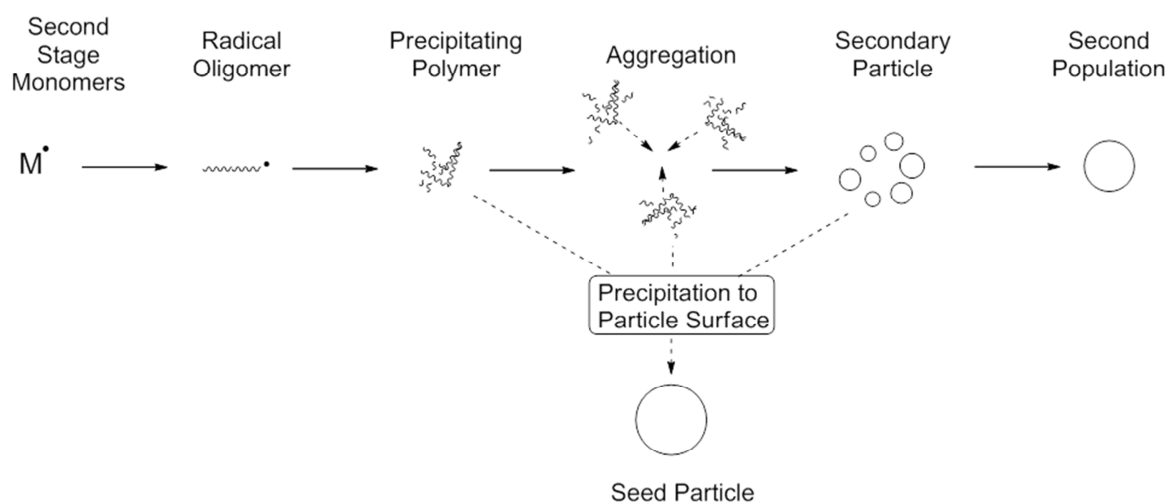


Figure 4-8, proposed reaction mechanism based upon precipitation of growing polymer chains to a particle surface.

In practice both mechanisms are likely, particle swelling by monomer and polymer precipitation. A similar mechanism was put forward by Thill *et al.*² for the formation of colloidal clusters, based upon heterogeneous nucleation.

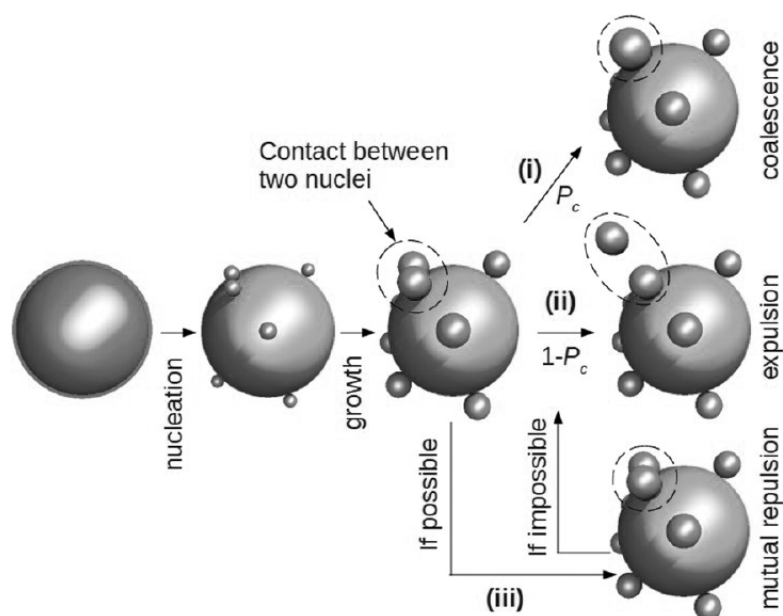


Figure 4-9, mechanism for the formation of colloidal clusters, based upon a heterogeneous nucleation route. Showing (i) coalescence, (ii) nuclei expulsion and (iii) nuclei mutual repulsion.²

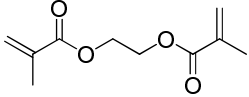
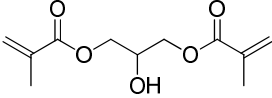
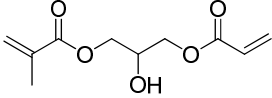
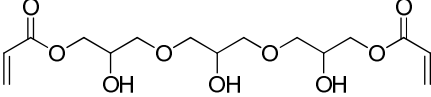
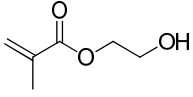
This reaction mechanism shows that if the growing polymer is of like chemistry and interacts then coalescence will occur on the particle surface forming fewer lobes. However the presence of crosslinker builds the molecular weight faster, so these small lobes may not interpenetrate leading to multiple lobes on the particle surface.

For the reactions under monomer starved conditions the situation is a little simpler as initially there is no monomer to swell the particles, and upon addition it will polymerise instantly, meaning that the precipitation mechanism is dominant. It was shown that the monomer conversion does not go to 100 % during the course of the reaction, so due to the low radical flux the monomer concentration will increase in the reaction vessel. This means that the monomer swelling mechanism becomes dominant toward the end of the reaction. As shown by monomer conversion graphs in Figure 4-2 the reaction rate is slow and does not lead to completion during the course of the reaction, meaning that monomer will be present during the reaction to swell the particles.

4.6 Implications of Varying the Crosslinker Polarity and Reactivity

Since the presence of EGDMA in the second stage reaction was found to have a profound effect on the particle morphology, the monomers shown in Table 4-6 have been selected with the aim to control precipitation of the polymer chains from solution and to the surface of the seed particles. Additionally phase separation may occur between the seed particle polymer and the new polymer formed inside the particle due to monomer swelling, as the interaction between the monomer and seed particle polymer will be marginally different, than the new polymer formed and the seed particle polymer.

Table 4-6, list of the crosslinking monomers of increasing hydrophilicity.

Crosslinking Monomer	Chemical Structure
Ethylene glycol dimethacrylate EGDMA	
Glycerol dimethacrylate GDMA	
3-(Acryloyloxy)-2-hydroxypropyl methacrylate AHPMA	
Glycerol 1,3-diglycerolate diacrylate GDGDA	
2-Hydroxyethyl methacrylate HEMA	

Along with changing the solubility of the crosslinking monomers their reactivity with respect to free radical polymerisations will also change. EGDMA and GDMA are both dimethacrylate based, whereas GDGDA is a diacrylate and AHPMA is an acrylate, methacrylate crosslinker. This will have implications on the monomer incorporation during the reaction as it is known that acrylate groups are more reactive than methacrylate groups.³

4.6.1 Hansen Solubility Parameters

Hansen solubility parameters have been used to estimate the polar crosslinking monomers solubility in dodecane, and how well they interact with PMMA.⁴ Figure 4-10 shows a Teas plot for the polar crosslinking monomers, PMMA, MMA and dodecane. The solubility sphere for PMMA is estimated based upon how the monomers interact with the polymer, either being good solvents, poor solvents or non-solvents. From the graph it is clear that dodecane should not be miscible with any of the chemicals as it is far removed from the others. This is not true in all cases, as EGDMA and MMA are miscible with dodecane, which is required for a dispersion polymerisation reaction.

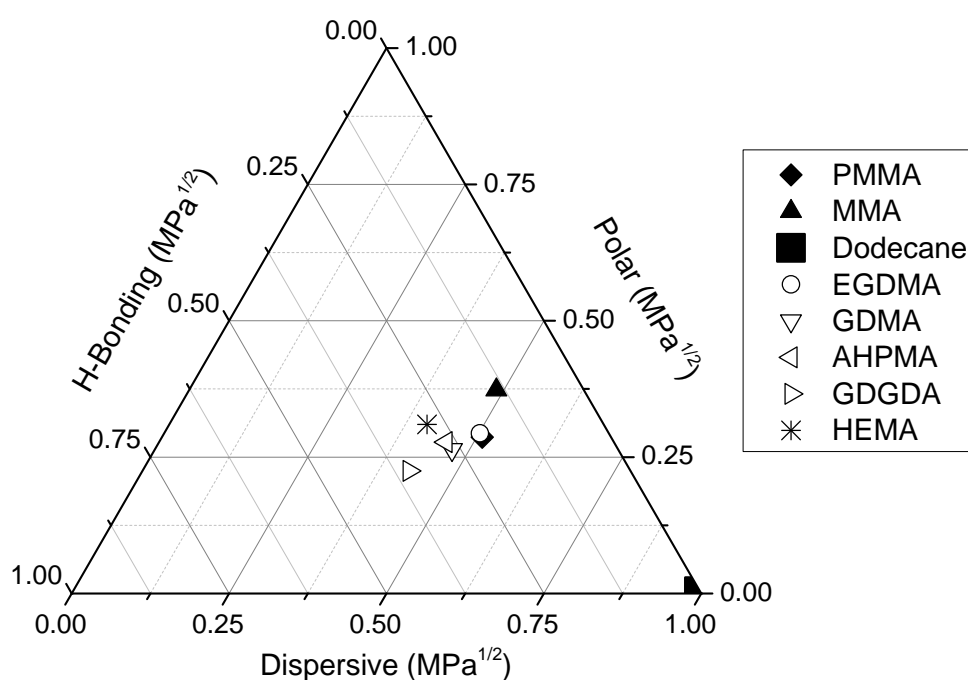


Figure 4-10, Teas plot for the crosslinking monomers along with PMMA, MMA and dodecane for comparison. The dashed circle is a representation of the solubility sphere for PMMA.

The Hansen solubility parameters for the monomers used have been calculated along with the radius of interaction with respect to dodecane in all cases. These are shown in Table 4-7.

Table 4-7, calculated solubility parameters for the monomers used and the relative energy difference against dodecane, in order of decreasing interaction.

Chemical	Solubility Parameter (MPa ^{1/2})				Radius of Interaction
	δ_T	δ_d	δ_p	δ_h	R_a
Dodecane	16.0	16.0	0.0	0.0	-
MMA	18.8	16.4	4.5	8.1	9.3
EGDMA	20.2	17.8	3.8	8.8	10.2
GDMA	22.9	18.2	4.0	13.3	14.5
AHPMA	23.1	18.1	4.3	13.8	15.0
HEMA	23.5	17.5	5.0	15.0	16.1
GDGDA	25.7	18.4	4.1	17.5	18.6

Given the obvious polarity increase for all the monomers down the series the calculated Hansen parameters for the polar monomers obeys the expected trend of increasing polar and hydrogen bonding contributions, thus becoming further removed from dodecane, increasing the radius of interaction.

Based upon the Hansen solubility parameters for these monomers it can be predicted that they should increase the precipitation of growing polymer chains upon incorporation, when polymerised in the continuous phase, and increased phase separation when polymerised in the swollen particles. This effect should be increased down the table due to the increasing immiscibility between the crosslinking monomer and the hydrocarbon solvent.

4.6.2 Implications of Monomer Reactivity

As the reactive groups on the monomers differ and their structure changes greatly, their incorporation into the growing copolymer will not be straight forward. For a homopolymerisation reaction the rate constants for chain propagation will be the same as the monomer does not change. However in a polymerisation with different monomers which are copolymerised together their incorporation will change. This could give rise to different polymer architectures as shown below in Figure 4-11.

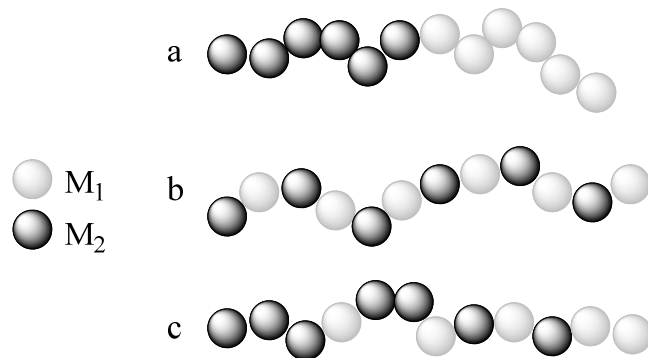


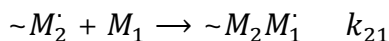
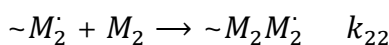
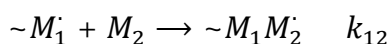
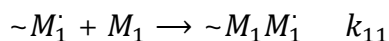
Figure 4-11, schematic representation of different polymer architectures which could be formed in a copolymerisation reaction, with a, where the reactivity of M_1 and M_2 are very different giving a block-copolymer, b, where $M_1 = M_2$ giving a statistical copolymer and c, where $M_1 > M_2$ giving a gradient copolymer.

The incorporation of monomers can be estimated by the reactivity ratios for the monomer pair, this is given by the Mayo-Lewis equation.⁵

$$\frac{dm_1}{dm_2} = \frac{M_1(r_1M_1 + M_2)}{M_2(r_2M_2 + M_1)} \quad 4-2$$

Where; m_1 and m_2 are the number of moles of monomer 1 and monomer 2 in the copolymer respectively, M_1 and M_2 are the number of moles of monomer 1 and monomer 2 in the total monomer mixture and r_1 and r_2 are the reactivity ratios.

The reactivity ratios are related to the rate constants for different chain propagation reactions shown below:



Where; $r_1 = k_{11}/k_{12}$, $r_2 = k_{22}/k_{21}$ and $\sim M \cdot$ represents a polymer chain ending in a radical from the monomer, M .

The reactivity ratios therefore show the probability of the addition of the next monomer unit to the growing radical, if the reactivity ratio is 1 there is an equal chance for either monomer 1 or monomer 2 to be incorporated.

The literature available on reactivity ratios is very small and limited almost exclusively to a list in the *Polymer Handbook*.⁶ As a consequence reactivity ratios for the various monomers used cannot be found. However reactivity ratios for monomers which are similar can be found and can be used as an estimate and are shown in Table 4-8. The equivalent monomers are 2-hydroxyethyl acrylate⁷ (HEA) and HEMA.⁸ These were chosen as they have the same reactive group toward radical polymerisation as the crosslinking monomers and the same “polar” nature.

Another way to display the reactivity of vinyl monomers is by the Alfey and Price Q and e numbers, where Q describes the relativity of the monomer, i.e. ability for stabilisation of the radical, and e constant takes into account monomer polarity and the effect on copolymerisation.⁹ The monomer reactivity can be calculated by the following equation.⁶

$$Q_2 = \left(\frac{Q_1}{r_1}\right) \exp[-e_1(e_1 - e_2)] \quad 4-3$$

However the Alfey Price system will not be considered as literature is unavailable for the monomers in question for this study.

It must be noted that the reactivity ratios were calculated for reactions with different solvent systems, the HEA copolymerisation was conducted in cyclohexane and the HEMA copolymerisation was conducted in chloroform. It has also been observed that changing the solvent can have an influence on the reactivity of the monomers depending upon their

structure. G. Saini *et al.*¹⁰ observed a change in the reactivity ratios for copolymerisations of acrylamide and methyl methacrylate in dioxane, ethanol and dioxane / ethanol mixtures.

Table 4-8, reactivity ratios for MMA – equivalent monomer.

Monomer	Equivalent Monomer	r_1^*	r_2
GDMA	HEMA	0.28	1.02
AHPMA	HEMA	0.28	1.02
	HEA	1.65	0.41
GDGDA	HEA	1.65	0.41
HEMA	HEMA	0.28	1.02

* r_1 reactivity ratio for MMA

The reactivity ratios for the monomers show that for the MMA / HEMA-like system, HEMA would preferentially add another HEMA monomer unit to the growing polymer chain over an MMA unit. This is reversed for the MMA / HEA-like system, where MMA would be preferentially added to the growing chain.

This will lead to the formation of gradient copolymers in both cases. However for a MMA / HEMA-like system the HEMA-like monomer would be incorporated faster than the MMA, indicating that this should lead to rapid precipitation due to the increasingly polar polymer being produced. For a MMA / HEA-like system the MMA monomer will be consumed preferentially, with the HEA-like monomer incorporated infrequently, but as the MMA is in vast excess it will not lead to a gradient copolymer. The crosslinker AHPMA shows an interesting case as it has acrylate and methacrylate groups and one group will incorporate faster than the other, meaning that initially it would behave as a monofunctional monomer and then later crosslink.

All following reactions were conducted under monomer starved conditions as they were shown to produce the cleanest dispersions. The monomer charge was pump fed into the reaction, which will have implications on monomer incorporation. The reactivity ratios are related to a batch style solution polymerisation where the total monomer charge is added at once, meaning that monomer incorporation may not follow as predicted.

4.7 Second Stage Polymerisation Reactions – Effect of Crosslinking Monomer Polarity and Reactivity

In this set of reactions the monomer feed contained 1 wt. % polar monomer with a 1 wt. % EGDMA crosslinked seed, and reactions were performed under monomer starved conditions.

Standard conditions for these reactions were as follows unless otherwise stated:

Reaction Component	Amount	Example
Initial solid content of seed dispersion	10 wt.%	10 g dispersion (1 g solid)
Monomers	4:1 monomer – solid particle	4.00 g
P(HAS- <i>g</i> -MMA) stabiliser	9.3 wt. % of total monomers	0.372 g
Radical initiator	0.5 wt. % of total monomers	0.020 g
Dodecanethiol	0.2 wt. % of monomers	0.008 g

These conditions allow for working in the stable region of 34 wt. % total solids content (TSC) outlined by Antl *et al.*¹ For specific examples of the second stage polymerisation reactions see the experimental section *Chapter 8*.

A series of seeded dispersion polymerisation reactions were undertaken with the inclusion of the polar crosslinking monomers at 1 wt. % of monomers, along with a no crosslinker comparison.

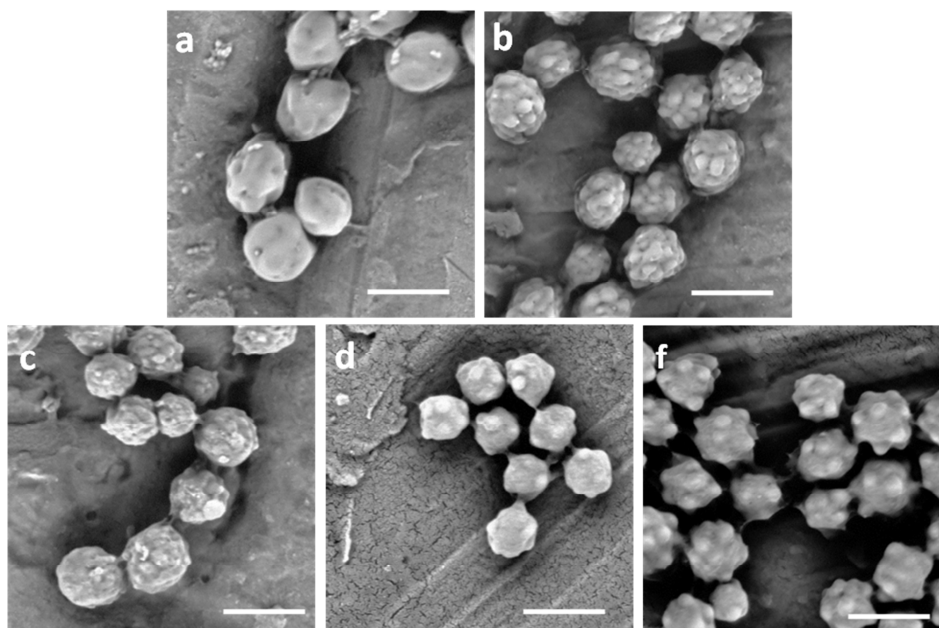


Figure 4-12, SEM images for reactions containing 1 wt. % polar monomer in the second stage reaction with; a, no crosslinker comparison, b, EGDMA, c, GDMA, d, AHPMA and e, GDGDA. Scale bars are 1 μm. Total solids content of the seed dispersion was 10 wt. %, monomer / particle ratio was 4:1, DDT concentration was 1 wt. % of monomers and initiator concentration was 0.5 wt. % of monomers.

The SEM images above in Figure 4-12 show that increasing the polarity of the crosslinking monomer in the second stage reaction gives rise to ‘cluster-like’ particles. With the addition of a monomer feed without crosslinker the particles appear smooth, but have lost their spherical shape.

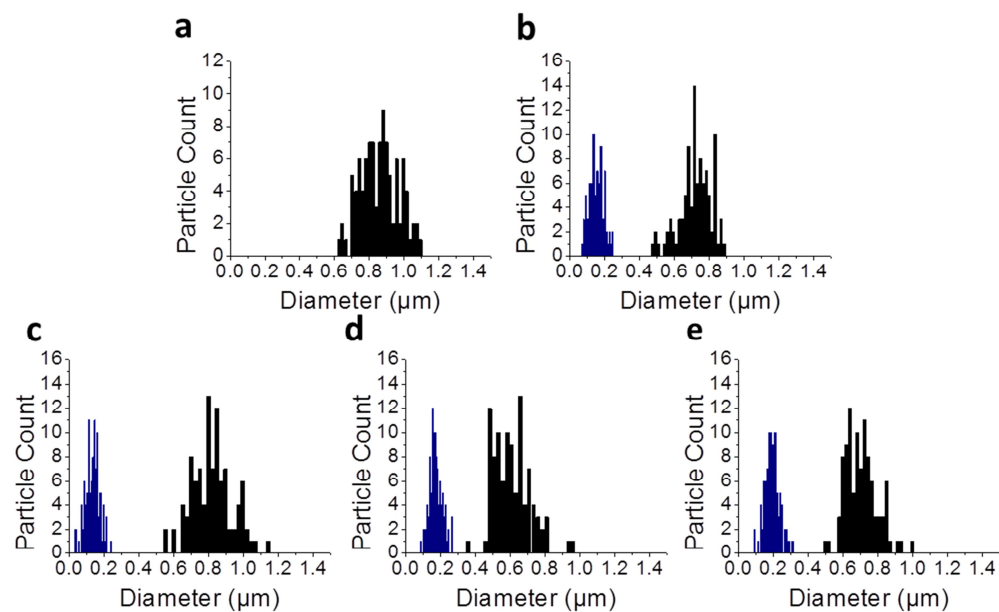


Figure 4-13, Size distribution graphs for dispersions containing 1 wt. % polar monomer in the second stage reaction with; a, no crosslinker for comparison, b, EGDMA, c, GDMA, d, AHPMA and e, GDGDA. Nodules on the particle surface are shown in blue, sizing based on counting 100 particles per population.

The size distribution plots above show that all the particles grew to the same approximate size, but there is a clear shift in the size of the nodules on the particle surface, increasing in size with increasing polarity of the crosslinking monomer. This is shown in the particle size data in Table 4-9.

Table 4-9, particle size data for dispersions shown in Figure 4-12, with the seed dispersion shown in italics.

Sample [†]	Small Nodule Diameter		Full Particle Diameter	
	Size (nm)	Coefficient of Variation	Size (nm)	Coefficient of Variation
<i>SRB-325-1% EGDMA</i>	-	-	<i>600</i>	<i>13 %</i>
SRB-351-no xl	-	-	870	12 %
SRB-349- 1% EGDMA	160	25 %	730	12 %
SRB-350-1% GDMA	140	30 %	830	14 %
SRB-334-1% AHPMA	180	20 %	620	18 %
SRB-335-1% GDGDA	200	21 %	720	13 %

[†] based on counting 100 particles per population

The data shows that the polydispersity of the full particles does not notably change across the series except for the case of AHPMA. This is a surprising result as given the fact that the surface morphology has changed so dramatically it would be thought that the average polydispersity of the samples would be increased. However in comparison the nodules on the surface of the seed particle appear to be very polydisperse, owing to the precipitation method of formation.

This series of experiments was repeated with 2 wt. % of the polar crosslinking monomer in the monomer feed, and can be found in the *Appendices* (Chapter 9.7). This series of experiments mirrors the results of the 1 wt. % series, with increasing polarity of the added crosslinker forming more cluster-like particles.

4.8 Effect of Changing Other Reaction Conditions

The effect of chain transfer concentration, seed particle concentration and replacement of the crosslinking monomer with a monofunctional monomer were considered with a view to obtaining greater insight into the mechanism.

4.8.1 Varying Chain Transfer Agent Concentration

The proposed dominant mechanism for the second stage polymerisation is one of precipitation to seed particle surface in the presence of crosslinker. If the precipitation could be slowed by capping the molecular weight of growing chains with chain transfer agent, then smooth spherical particles should be obtained opposed to the cluster-like particles seen. To prove this a control series of experiment with increasing chain transfer agent concentration were carried out. Figure 4-14 shows the resultant dispersions for reactions with increased chain transfer agent concentration with 1 wt. % GDMA included in the polymer feed.

When the chain transfer agent concentration is increased in the presence of crosslinking monomers linear polymers may not be formed, and hyperbranched polymers may form. Hyperbranched polymers will form when the ratio between the chain transfer agent and crosslinker is high. A hyperbranched polymer can be thought of as a small polymer gel network, and such polymers have been produced by one-pot processes containing crosslinker and balancing levels of a chain transfer agent.¹¹ This will affect the precipitation of polymer segments to the seed particle surface.

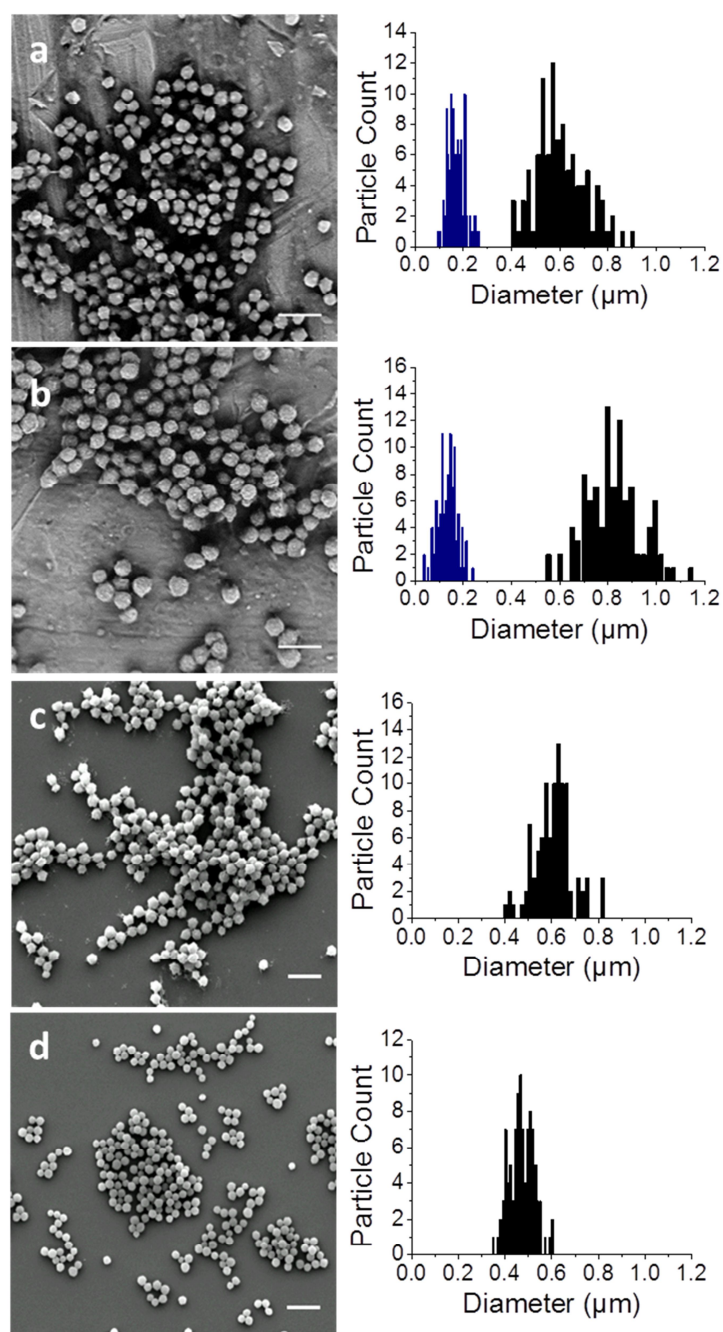


Figure 4-14, SEM images and size distribution plots for dispersions with varying chain transfer agent concentration; a, 0 wt. %, b, 1 wt. %, c, 2 wt. % and d, 4 wt. % of monomers. Nodules on the particle surface are shown in blue, scales bars are 2 μ m. Total solids content of the seed dispersion was 10 wt. %, monomer / particle ratio was 4:1 and initiator concentration was 0.5 wt. % of monomers.

The resultant dispersion obeys the expected trend with the particles becoming spherical and uniform with increasing concentration of DDT. At the point of 4 wt. % of monomers,

the particles have become spherical, despite the inclusion of a polar crosslinking monomer. At 1 wt. % small nodules are still observed as in the case without any chain transfer agent added to the reaction. The particle size data, shown in Table 4-10 shows that the particle size and polydispersity decreases with increased DDT concentration.

Table 4-10, particle size data for dispersions shown in Figure 4-14, with initial seed dispersion shown in italics.

Sample [†]	Small Nodule Diameter		Full Particle Diameter	
	Size (nm)	Coefficient of Variation	Size (nm)	Coefficient of Variation
<i>SRB-325-1% EGDMA</i>	-	-	<i>600</i>	<i>13 %</i>
SRB-328-1% GDMA, 0% DDT	170	20 %	610	17 %
SRB-350-1% GDMA, 1 % DDT	140	29 %	830	14 %
SRB-384-1% GDMA, 2 % DDT	-	-	620	13 %
SRB-385-1% GDMA, 4 % DDT	-	-	480	11 %

[†] based on counting 100 particles per population

There are some anomalous results such as the lack of particle growth in the experiment without DDT in the reactions, SRB-328-1% GDMA, 0% DDT. This could be due to secondary nucleation, where some of the particles precipitated to the seed particle surface and others grew to full sized particles. SRB-385-1% GDMA, 4 % DDT shows a decrease in particle size from the starting seed particle, this could be due to growth of a secondary population, or simply that the chain transfer agent concentration is now high enough to keep the growing polymer in solution so little or no precipitation will occur.

4.8.2 Varying Initial Seed Particle Total Solids Content

Assuming the mechanism of cluster-like particle formation is based upon precipitation to a seed particle surface, the amount of surface available to precipitate would influence the resultant particle morphology. It follows that if the seed particle solids content was decreased cluster-like formation would be promoted, whereas if the solids content of the seed dispersion was increased it would suppress cluster-like particle formation, as the surface area for precipitation will be changed.

Figure 4-15 shows SEM images of the resultant particles when the total solids content of the seed dispersion was changed and 1 wt. % of monomers GDMA was added to the monomer feed and the monomer feed was kept at a 4:1 monomer / particle ratio.

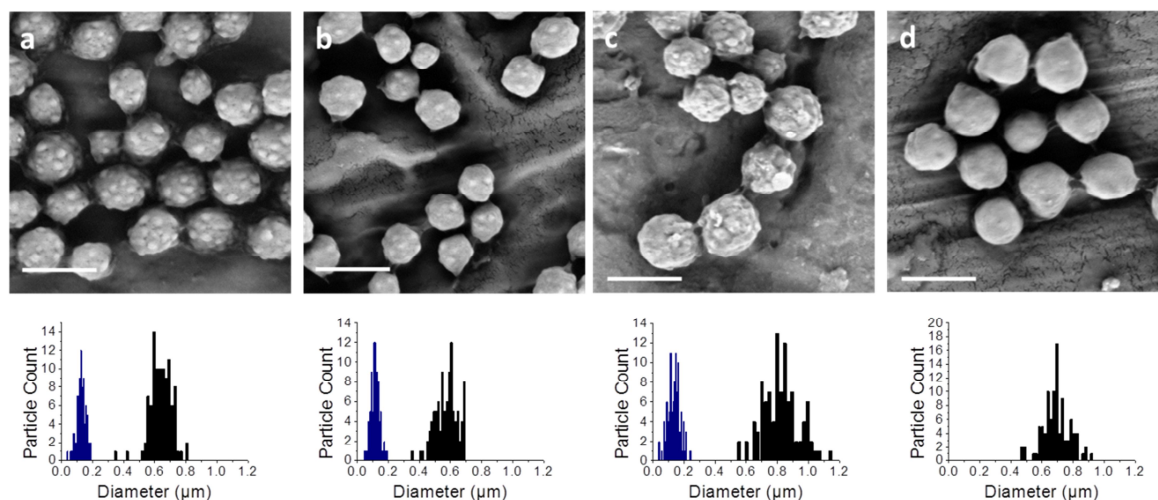


Figure 4-15, SEM images and size distribution plots for dispersions with varying total solids content in the seed dispersion where; a, 1 % solid (SRB-348-1% GDMA), b, 5 % solid (SRB-346-1% GDMA), c, 10 % solid (SRB-350-1% GDMA) and d, 20 % solid (SRB-347-1% GDMA). Nodules on the particle surface are shown in blue, scales bars are 1 μ m. Monomer / particle ratio was 4:1, DDT concentration was 1 wt. % of monomers and initiator concentration was 0.5 wt. % of monomers.

All reactions before this were run with the seed particle dispersion at 10 wt. % solid content, which shows small nodule formation on the surface of the particles. When the solids content was doubled to 20 wt. % solids, dramatically increasing the the surface available to precipitate onto, the resultant particles were smooth and spherical.

When the solids content of the seed was halved to 5 wt. % solids nodule growth appears to be promoted with more nodules per particle observed. This trend was exacerbated when the seed particle dispersion is diluted to 1 wt. % solid where multiple nodules are present on each particle.

Again the size of the nodules appears to be set by the monomer / particle ratio of 4:1 as the nodules grew to a similar size according to the data in Table 4-11 below. Again all the resultant particles are also close to monodisperse in size after the reaction

Table 4-11, particle size data for dispersions shown in Figure 4-15, with initial seed dispersion shown in italics.

Sample [†]	Estimated Surface Area (m ²)	Small Nodule Diameter		Full Particle Diameter	
		Size (nm)	Coefficient of Variation	Size (nm)	Coefficient of Variation
<i>SRB-325-1% EGDMA</i>	-	-	-	<i>600</i>	<i>13 %</i>
1% TSC	8.5x10 ⁸	130	23 %	650	11 %
5% TSC	4.2x10 ⁹	120	25 %	580	12 %
10% TSC	8.5x10 ⁹	140	30 %	830	14 %
20% TSC	1.7x10 ¹⁰	-	-	700	13 %

[†] based on counting 100 particles per population

The results above are expected as the nodule size is governed by the monomer / particle ratio which is set to 4:1 as is the effect of increasing the seed dispersion solids suppressing nodule formation. The results help to reinforce the model presented showing that precipitation to the seed particle surface is a dominant factor.

4.8.3 Effect of Replacing Polar Crosslinking Monomer with Polar Monofunctional Monomer

It is known that non-spherical particles will form if the molecular weight of the polymer formed has a large molecular weight. But the proposed mechanism deals with the solubility of growing polymer chains, of which molecular weight plays a role. A control experiment of introducing a monofunctional polar monomer was devised. Use of a monofunctional monomer will rule out large molecular weight increases due to crosslinking of polymer chains showing that solubility is important along with molecular weight increase. This would mean that the precipitation is solubility driven in this case. Figure 4-16 shows the resultant particles from a second stage polymerisation reaction with 1 and 2 mol. % of GDMA in the feed, with a comparison to HEMA at the same number of moles in the monomer feed.

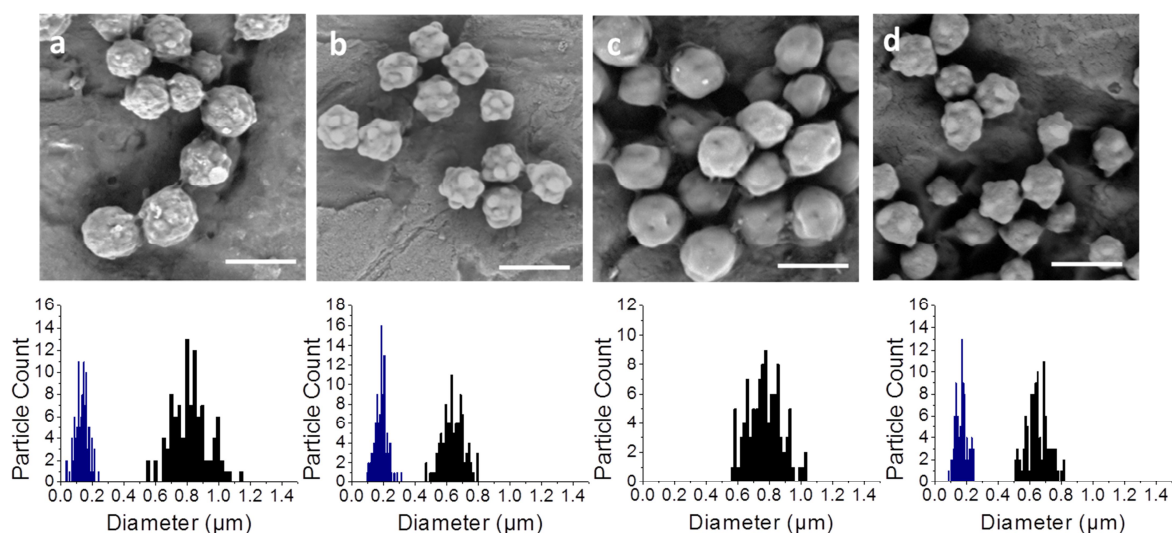


Figure 4-16, SEM images and size distribution plots for dispersions with; a, 1 wt. % GDMA b, 2 wt. % GDMA and c and d, with equivalent moles of HEMA in the second stage polymerisation. Nodules on the particle surface are shown in blue, scales bars are 1μm. Total solids content of the seed dispersion was 10 wt. %, monomer / particle ratio was 4:1, DDT concentration was 1 wt. % of monomers and initiator concentration was 0.5 wt. % of monomers.

From the SEM images in Figure 4-16 it is clear that HEMA has a lesser effect than GDMA in nodule formation, and does not form nodules at an equivalent 1 wt. % monomer inclusion. However the 2 wt. % example does show nodule growth, which means that triggering the precipitation of polymer chains, is not just governed by molecular weight.

The particle size data shown in Table 4-12 shows that the nodule size for all the samples are statistically the same, the nodule size must be set at a monomer / particle ratio of 4:1. This is also true for the full particles.

Table 4-12, particle size data for dispersions shown in Figure 4-16, with the seed dispersion shown in italics.

Sample [†]	Small Nodule Diameter		Full Particle Diameter	
	Size (nm)	Coefficient of Variation	Size (nm)	Coefficient of Variation
<i>SRB-325-1% EGDMA</i>	-	-	<i>600</i>	<i>13 %</i>
SRB-350-1% GDMA	140	30 %	830	14 %
SRB-340- 2% GDMA	180	24 %	700	13 %
SRB-352-1% HEMA	-	-	780	14 %
SRB-345-2% HEMA	170	21 %	600	11 %

[†] based on counting 100 particles per population

4.9 Rationalisation of Findings with Polar Monomer Inclusion

When the crosslinking monomer is changed it is important to remember that not only the solubility has changed but also the reactivity. The polarity increase will increase the precipitation of polymer chains upon incorporation, however prediction of monomer incorporation from like monomer reactivity ratios show that gradient polymers should be formed.

4.9.1 Varying Crosslinking Monomer

When the crosslinker was changed to a polar and reactive monomer, GDGDA, the cluster-like particle morphology was enhanced and the more hydrophobic monomer, EGDMA, shows ‘tuberculated’ (non-spherical) particles as described by Elesser *et al.*¹² The GDMA and AHPMA monomers appear to give similar results in terms of resultant particle morphologies. The polarity increase between these two is the loss of a methyl group from one methacrylate group, which may not be as significant as the Hansen values predict. Also this acrylate group will react faster than the methacrylate group leading the AHPMA monomer to act like that of GDMA.

4.9.2 Changing Chain Transfer Agent Concentration

Elsesser *et al.*¹² showed that the molecular weight of the growing polymer chains in a seeded dispersion polymerisation is paramount to achieving a smooth particle surface. In their work they decreased the chain transfer agent and initiator concentrations, which effectively increased the molecular weight of the polymers produced in the reaction, and obtained 'tuberculated' particles. when the chain transfer agent and initiator concentrations were increased the resultant particles remained smooth. This is shown in Figure 4-17 below in the figure from their publication.

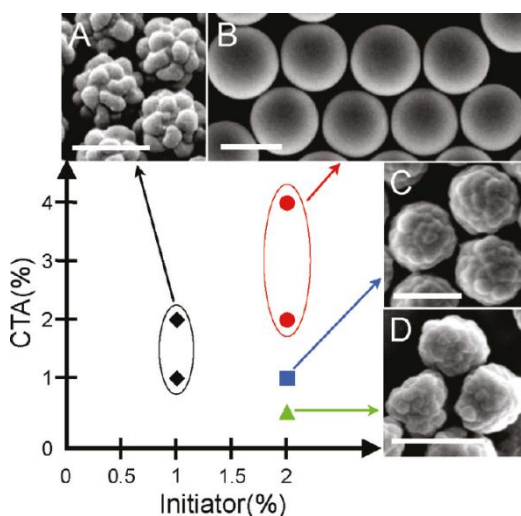


Figure 4-17, showing the effects of varying the chain transfer and initiator concentration from Elsesser *et al.*¹² Scale bars are 2 μm .

The addition of chain transfer agent terminates the growing of polymer chains and the initiation of a new chain, thus limiting the molecular weight of the polymers formed. The addition of a small amount of chain transfer agent is known to give smoother particles upon polymerisation, this is due to the lower polymer molecular weight.¹³ The addition of larger quantities has been shown to increase the polydispersity of particles produced by an ethanolic non-aqueous dispersion polymerisation of styrene.¹⁴ The argument was that chain transfer removed radicals from inside the particles to initiate more chain growth in the continuous phase, thus causing more particles to precipitate continuously leading to increased polydispersity. However this was for the production of particles and not a seeded dispersion polymerisation reaction. The effect is expected to be the opposite in this case with regards to polydispersity, as precipitation occurs in the continuous phase and the

small particles formed will aggregate to the seed particles and not grow to their own full size population.

In this experiment a decrease in particle size was observed as the DDT concentration was increased. This decrease in size could be attributed to the fact that the addition of chain transfer agent will cut the molecular weight of growing chains increasing solubility of the second stage polymer. This occurs as chain transfer to the chain transfer agent (dodecanethiol) is faster than chain transfer to monomer.³ The fact that smaller polymer chains will be produced will affect the crosslinking of the particles, potentially leading to the precipitation of hyperbranched units, or stopping precipitation of the second stage monomer.

4.9.3 Implications of Precipitation to Seed Particle Surface

As the second stage reaction progresses with the inclusion of hydrophilic monomer, nodules are formed, with the nodules being regions of increased polarity. This may be another reason for the enhanced nodule formation, as the polar crosslinking monomer units are added to the reaction vessel and precipitate, they will interact with the polar regions as this is the most favourable interaction. This means that during the reaction the precipitating polymer effectively builds in a certain regions which will act as a locus for growth.

4.10 Sequential Second Stage Polymerisation Reactions

The particle dispersions discussed previously only show small nodules or a rough particle surface. In order to produce true cluster-like particles, particles with spherical nodules protruding from a spherical central seed, sequential polymerisation reactions were undertaken to see the effect of having a clustered template seed particle.

The sequential polymerisation reactions were undertaken by performing a second stage reaction, this is then cleaned and used again for a successive reaction. It was thought that the surface area of the seed particles will now be dramatically increased from a smooth spherical particle of equal size. This surface area increase means that in the subsequent second stage polymerisation reactions the growing polymer will precipitate to the nodule

on the particle. The second stage reactions contained EGDMA and GDMA to study the effect of the monomer polarity on the successive reactions.

4.10.1 Effect of EGDMA on Sequential Second Stage Polymerisation Reactions

A sequential second stage polymerisation reaction was done with 1 wt. % EGDMA in the monomer feed to induce nodule formation. SEM images of the resultant particles are shown in Figure 4-18, which shown that the first reaction gave irregular, rough shaped particles but they do not appear to be cluster-like in morphology. However the second reaction gave particles which show clear nodules on the surface approximately 200 nm in size. Again the size is close to what has been found before for second stage polymerisation reactions that yield cluster-like particles. Also the polydispersity of the reactions is low, in both cases in near monodisperse samples.

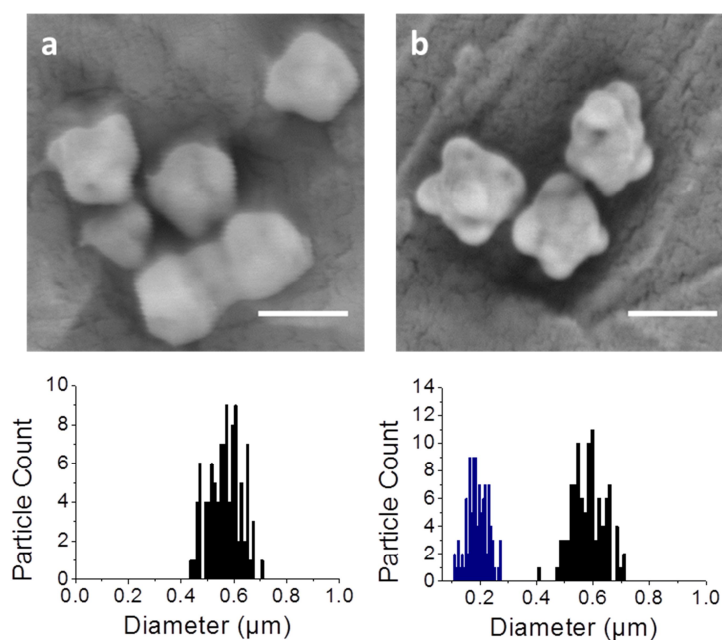


Figure 4-18, SEM images of resultant particles from sequential shell-growth steps with the inclusion of 1 wt. % EGDMA and size distribution plots, where; a, is the first and, b, the second consecutive polymerisation reaction. Small nodules on the surface are shown in blue, scale bars are 500 nm. Total solids content of the seed dispersion was 10 wt. %, monomer / particle ratio was 4:1, DDT concentration was 1 wt. % of monomers and initiator concentration was 0.5 wt. % of monomers.

Table 4-13, particle size data for dispersions shown in Figure 4-18, with the seed dispersion shown in italics.

Sample[†]	Small Nodule Diameter		Full Particle Diameter	
	Size (nm)	Coefficient of Variation	Size (nm)	Coefficient of Variation
<i>SRB-223-1% EGDMA</i>	-	-	530	14 %
SRB-225-1 % EGDMA-1 st	-	-	570	11 %
SRB-209-1 % EGDMA-2 nd	200	19 %	590	10 %

[†] based on counting 100 particles per population

The dispersion SRB-209-1 % EGDMA-2nd shows regular cluster-like particles which have greater cluster-like appearance than in the previous experiments. It appears that the irregular shaped seed particles had an effect on the precipitation of polymers to its surface giving particles of greater cluster-like character. If such a dramatic effect is shown for sequential second stage polymerisation reactions for 1 wt. % of a crosslinking monomer which is soluble in the continuous phase, the effects must be greatly enhanced with a polar crosslinking monomer.

4.10.2 Effect of GDMA on Sequential Second Stage Polymerisation Reactions

In this series 1 wt. % of GDMA was added to the monomer feed for multiple sequential second stage polymerisation reactions. As with the EGDMA example above any nodules formed were expected to act as loci for growth due to their large surface area. Also in this example if all the polymer formed goes to producing the nodules they will be rich with the polar monomer, with respect to the surface of the EGDMA crosslinked seed particle. Figure 4-19 below shows the resultant dispersions from the multiple seeded dispersion polymerisation reactions.

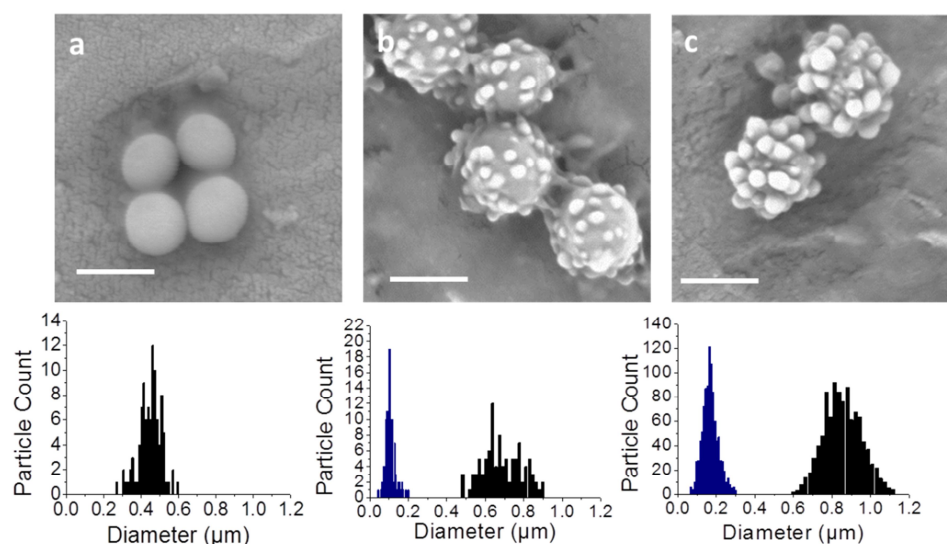


Figure 4-19, SEM images and size distribution plots for resultant dispersions after sequential second stage polymerisation reactions with 1 wt. % GDMA in the feed, where; a, is the first, b, the second and c, the third consecutive polymerisation reaction. Nodules on the particle surface are shown in blue, scales bars are 500 nm. Total solids content of the seed dispersion was 10 wt. %, monomer / particle ratio was 4:1, DDT concentration was 1 wt. % of monomers and initiator concentration was 0.5 wt. % of monomers.

From the SEM images true cluster-like particles have been formed. With multiple spherical nodules protruding from the particle surface, the sample also shows no signs of secondary nucleation so all the polymer must be precipitating to the surface of the seed particles.

From the images and the size distribution plots it is clear that the nodules have increased in size during each successive reaction upon the particles. However the first reaction looks to have not changed the particles as they remain smooth and spherical. This result is unexpected as in all other cases nodules were formed under these conditions. When comparing the size of particles to the seed in Table 4-14 the first reaction did not change the particle size. The other successive reactions regularly increased the particle size by roughly 200 nm, close to the size of the nodules on the surface.

Table 4-14, particle size data for dispersions shown in Figure 4-19, with the seed dispersion shown in italics.

Sample	Small Nodule Diameter		Full Particle Diameter	
	Size (nm)	Coefficient of Variation	Size (nm)	Coefficient of Variation
<i>SRB-207-1% EGDMA</i> *	-	-	<i>460</i>	<i>16 %</i>
SRB-208-1 % GDMA-1 ^{st,†}	-	-	460	12 %
SRB-209-1 % GDMA-2 ^{nd,†}	110	26 %	680	15 %
SRB-210-1 % GDMA-3 ^{rd,*}	170	24 %	870	11 %

* based on counting 1000 particles per population, † based on counting 100 particles per population

4.10.3 Effect of EGDMA followed by GDMA Sequential Second Stage

Polymerisation Reactions

To see if the extent of nodular character can be tuned a reaction series was devised where the first shell incorporated 1 wt. % EGDMA and the two successive reactions incorporated 1 wt. % GDMA. It is thought that the resultant particles after the three reactions should be somewhere in between that of the resultant EGDMA and GDMA particles. Figure 4-20 shows SEM images and size distribution plots for the resultant particles.

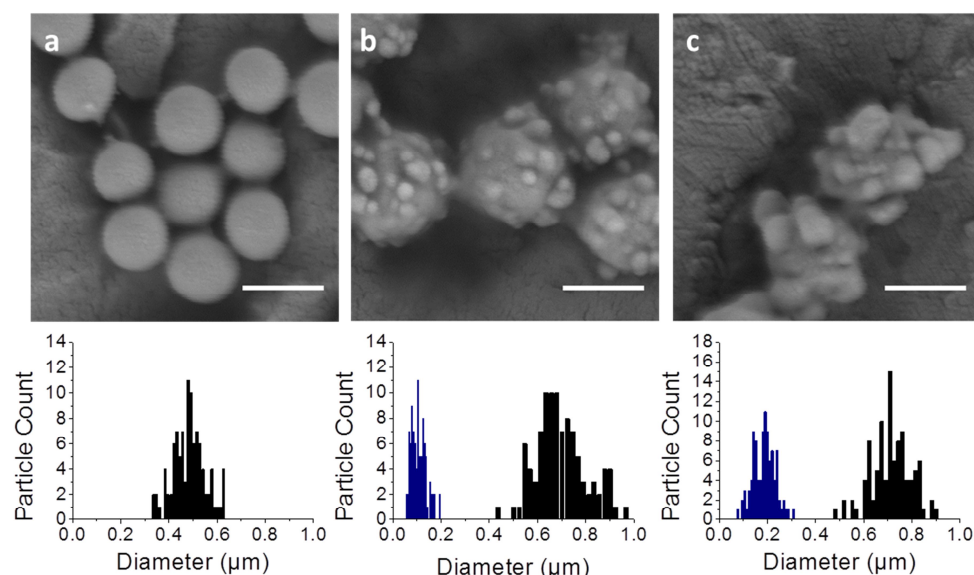


Figure 4-20, SEM images and size distribution plots for resultant dispersions after sequential second stage polymerisation reactions with 1 wt. % EGDMA in the first polymerisation and then 1 wt % GDMA in the others. Where; a, is the first, b, the second and c, the third consecutive polymerisation reaction. Nodules on the particle surface are shown in blue, scales bars are 500 nm. Total solids content of the seed dispersion was 10 wt. %, monomer / particle ratio was 4:1, DDT concentration was 1 wt. % of monomers and initiator concentration was 0.5 wt. % of monomers.

The SEM images show that the first reaction with EGDMA in the feed resulted in spherical particles much like the first reaction with GDMA in Figure 4-19. Looking at the particle size data in Table 4-15 there is a small increase in size, this could be due to the production of a secondary population of particles owing to secondary nucleation and growth. Between the first and second reaction there is an increase in particle size by again approximately 200 nm and small nodule formation. Between the second and third reaction again only a small size increase was noted but there was a larger increase in the nodule size.

However the resultant particles do show characteristics of particles produced with sequential polymerisations with GDMA in each monomer feed, i.e. multiple larger nodules from the surface of the seed particle. The inclusion of the 1 wt. % EGDMA into the first reaction appears to have no effect on the resultant particles for the following two reactions.

Table 4-15, particle size data for dispersions shown in Figure 4-20, with the seed dispersion shown in italics.

Sample	Small Nodule Diameter		Full Particle Diameter	
	Size (nm)	Coefficient of Variation	Size (nm)	Coefficient of Variation
<i>SRB-207-1% EGDMA</i> *	-	-	460	16 %
SRB-215-1 % EGDMA-1 st †	-	-	490	14 %
SRB-216-1 % GDMA-2 nd †	110	28 %	710	15 %
SRB-217-1 % GDMA-3 rd †	190	24 %	720	12 %

* based on counting 1000 particles per population, † based on counting 100 particles per population

4.11 Conclusions

A series of 1 wt. % EGDMA crosslinked PMMA nanoparticles of uniform size and spherical shape were produced by nonaqueous dispersion polymerisation for study into the effect of a second stage seeded dispersion polymerisation with MMA.

Originally it was thought that the MMA would penetrate PMMA seed particles and the second stage reaction would proceed by a swelling and growth mechanism. This could then be used to produce shape anisotropic particles by inverting the dynamic swelling method, used to produce dumbbell-like, rod-like and triangular particles. However initial experiments showed that the reaction mechanism does not proceed solely by swelling and growth, precipitation of polymer chain from solution must also be considered.

A new reaction mechanism was proposed based upon both precipitation of polymer chains from solution and swelling and growth due to the partitioning of monomer between particles and continuous phase. This partitioning of the monomer is explained by Hansen solubility theory which shows a stronger interaction of MMA with PMMA particles to that of dodecane (Table 4-5). The implications of this new mechanism are that cluster-like particle could be produced if the precipitation of the growing chains could be triggered to occur very quickly by changing the solubility of growing polymer. This will then be

enhanced by phase separation within the particle toward the end of the reaction due to the polymerisation occurring within the particles.

Steps toward proving the mechanism were taken by changing multiple parameters i.e. concentration of seed particles, chain transfer agent concentration and use of a monofunctional monomer opposed to a difunctional crosslinking monomer.

A range of polar monomers were tested with increasing immiscibility with the hydrocarbon solvent. Monomer choice was based upon the Hansen solubility parameters of the monomer relative to that of dodecane, which could be used to predict particle interactions.

Sequential seeded dispersion polymerisation reactions were undertaken giving cluster-like particles with high numbers of spherical nodules protruding from the seed particle surface. This was true for both polar and non-polar crosslinkers used, but the polar crosslinkers showed the greatest degree of nodules per particle.

4.12 References

- ¹ L. Antl, J. W. Goodwin, R. D. Hill, R. H. Ottewill, S. M. Owens, S. Papworth and J. A. Waters, *Colloids and Surfaces*, 1986, **17**, 67
- ² A. Thill, A. Désert, S. Fouilloux, J.-C. Taveau, O. Lambert, M. Lansalot, E. Bourgeat-Lami, O. Spalla, L. Belloni, S. Ravaine and E. Duguet, *Langmuir*, 2012, **28**, 11575
- ³ M. K. Mishra and Y. Yagci, '*Handbook of Radical Vinyl Polymerization*', Marcel Dekker, 1998
- ⁴ C. M. Hansen and T. S. Poulsen, '*Hansen Solubility Parameters*', CRC Press, 2nd Ed., 2007
- ⁵ F. R. Mayo and F. M. Lewis, *J. Am. Chem. Soc.*, 1944, **66**, 1594
- ⁶ J. Brandup, E. H. Immergut, E. A. Grulke, A. Abe and D. R. Bloch, '*Polymer Handbook*', John Wiley & Sons, 4th edn. 1998, Chapter 2, 181
- ⁷ L. I. Xinxin, Y. I. N. Xiaomin, W. U. Pingping, H. A. N. Zhewen and Z. H. U. Qingren, *Chinese Journal of Polymer Science*, 1998, **16**, 25
- ⁸ I. K. Varma and S. Patnaik, *Euro. Polym. J.*, 1976, **12**, 259
- ⁹ T. Alfrey and C. C. Price, *J. Polym. Sci.*, 1946, **2**, 101
- ¹⁰ G. Saini, A. Leoni and S. Franco, *Die Makromolekulare Chemie*, 1971, **144**, 235

¹¹ N. O'Brien, A. Mckee, D. C. Sherrington, A. T. Slark and A. Titterton, *Polymer*, 2000, **41**, 6027

¹² M. T. Elsesser, A. D. Hollingsworth, K. V. Edmond and D. J. Pine, *Langmuir*, 2011, **27**, 917

¹³ R. J. R. Cairns, R. H. Ottewill, D. W. J. Osmond and I. Wagstaff, *J. Colloid Interf. Sci.*, 1976, **54**, 45

¹⁴ H. Ahmad and K. Tauer, *Colloid and Polym. Sci.*, 2003, **281**, 686

5 Second Stage Polymerisation Reactions of 2-Hydroxyethyl methacrylate and *N*-Hydroxyethyl acrylamide with Poly(methyl methacrylate) Seed Particles

5.1 Introduction

In *Chapter 4*, the effect of crosslinker (≤ 2 wt. %) in the second stage polymerisation of methyl methacrylate (MMA) on a poly(methyl methacrylate) (PMMA) crosslinked seed particles, was considered. Increasing the polarity of the crosslinking monomer was found to increase the cluster-like particle morphology. This was also found to be true for the incorporation of a polar monofunctional monomer, 2-hydroxyethyl methacrylate (HEMA) of equal concentration. This chapter considers the second stage polymerisation reaction with monofunctional polar monomers of increased concentration. Here the predictions made in *Chapter 3* are tested with the second stage reaction monomer being either 2-hydroxyethyl methacrylate (HEMA) or *N*-hydroxyethyl acrylamide (HEAm). The two monomers show a solubility mismatch with the PMMA seed particles, shown by the Hansen solubility parameters Table 5-1.

Table 5-1, Hansen solubility parameters for PMMA, MMA, HEMA and HEAm.

Chemical	Solubility Parameter ($\text{MPa}^{1/2}$)			
	δ_T	δ_d	δ_p	δ_h
PMMA	22.7	18.6	10.5	7.5
MMA	18.81	16.39	4.54	8.05
HEMA	23.54	17.47	4.96	14.99
HEAm	25.70	18.00	9.40	15.80

5.2 Standard Reaction Conditions

Standard conditions for these reactions were as follows unless otherwise stated:

Reaction Component	Amount	Example
Initial solid content of seed dispersion	10 wt. %	10 g dispersion (1 g solid)
Monomers	4:1 monomer – solid particle	4.00 g
P(HAS- <i>g</i> -MMA) stabiliser	9.3 wt. % of total monomers	0.372 g
Radical initiator	0.5 wt. % of total monomers	0.020 g
Dodecanethiol	0.2 wt. % of monomers	0.008 g

These conditions allow for working in the stable region of 34 wt. % total solids content (TSC) outlined by Antl *et al.*¹ For specific examples of the second stage polymerisation reactions see the experimental section *Chapter 8*.

5.3 Second Stage Polymerisation Containing HEMA-MMA

In an effort to produce cleaner dispersions second stage polymerisations with methyl methacrylate (MMA) and increasing polar content were undertaken.

Reactions increasing the HEMA ratio in the second stage were undertaken using crosslinked seed particles, crosslinked with ethylene glycol dimethacrylate (EGDMA) or glycerol dimethacrylate (GDMA). It is thought that the GDMA inclusion would increase the interaction between the second stage monomer and the seed particle, allowing for swelling and phase separation to occur.

5.3.1 Use of EGDMA Crosslinked Seed Particles

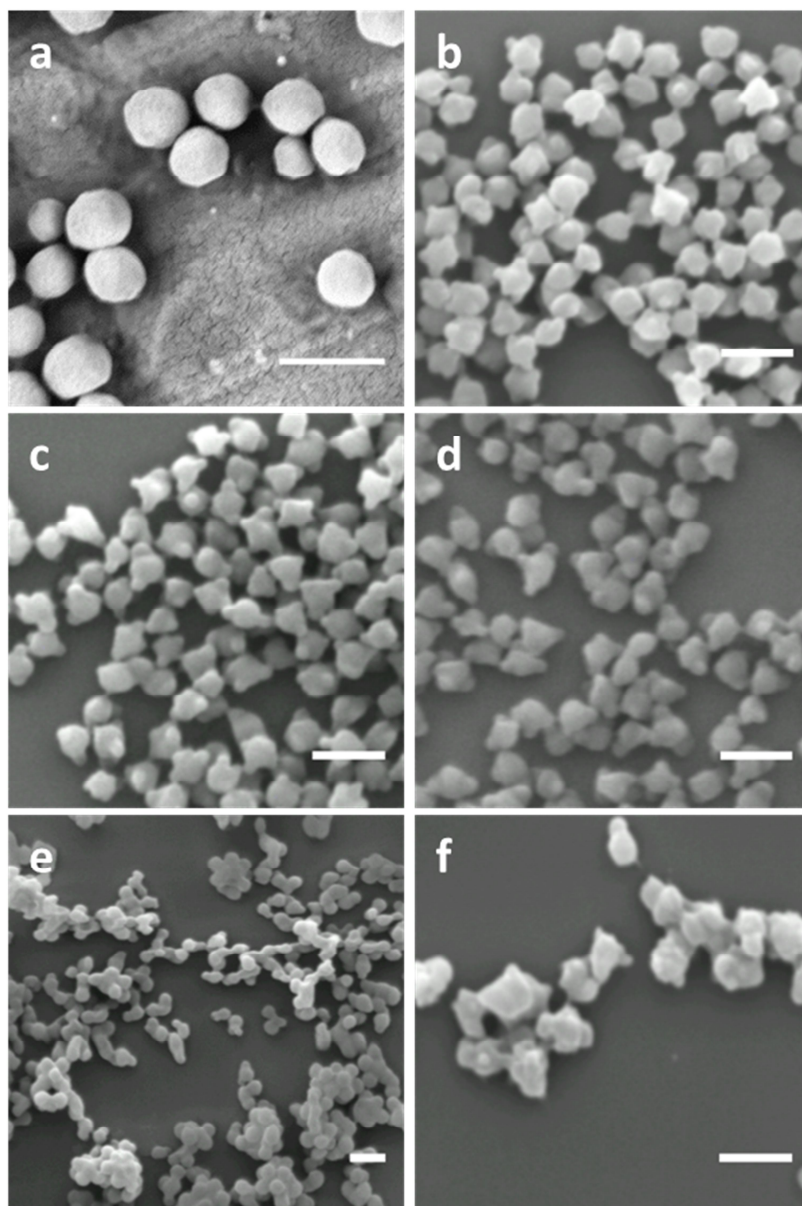


Figure 5-1, SEM images of reactions with increasing HEMA concentration in the monomer feed with an EGDMA crosslinked seed particle where; a, seed dispersion, b, 5 wt. % HEMA, c, 10 wt. % HEMA, d, 20 wt. % HEMA, e, 40 wt. % HEMA and f, 60 wt. % HEMA. Scale bars are 1 μm .

Particle morphology was found to change with increasing HEMA concentration which can be split into different regimes:

- At 5 and 10 wt. % HEMA there is an increase in nodules on the particle surface.
- At 20 wt. % HEMA these nodules decrease in number but appear to grow in size.

- At 40 wt. % HEMA the particles start to aggregate together and show 3 or less nodules per particle appear evident.
- At 60 wt. % HEMA particle aggregation becomes an issue, and the particles appear to have some large and some smaller nodules on the surface.

This trend can be seen in the size distribution plots (Figure 5-2) and particle size data in Table 5-2.

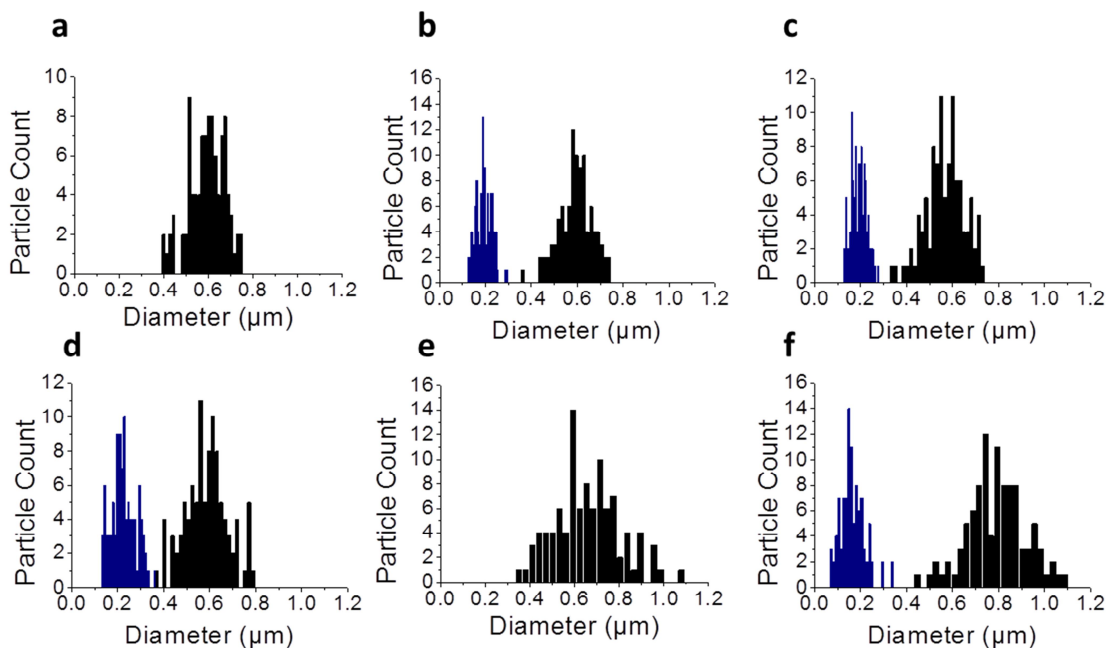


Figure 5-2, size distribution plots for reactions with increasing HEMA concentration in the monomer feed with EGDMA crosslinked seed particles where; a, seed dispersion, b, 5 wt. % HEMA, c, 10 wt. % HEMA, d, 20 wt. % HEMA, e, 40 wt. % HEMA and f, 60 wt. % HEMA. Nodules on the particle surface are shown in blue.

It is clear that the HEMA content in the reaction is driving phase separation of the particle and the growing polymer during the reaction, even at low concentrations. The particle size data in Table 5-2 shows that the particle size increases to statistically the same value except for the 60 % HEMA reaction, which has become uncontrolled and large particles or aggregates, were formed. The nodules that formed on the surface also grew to the same size.

Table 5-2, particle size data and aspect ratio for particles with increasing HEMA concentration in the monomer feed and EGDMA crosslinked seed particles, initial seed dispersion shown in italics.

Sample	HEMA Content	Particle Diameter* (nm)	Coefficient of Variation	Nodule Diameter* (nm)	Coefficient of Variation	Aspect Ratio†	Standard Deviation	Particle Shape
<i>SRB-325-1% EGDMA</i>	-	<i>500</i>	<i>11 %</i>	-	-	<i>1.1</i>	<i>0.11</i>	<i>Spherical</i>
SRB-353-5% HEMA	5 wt. %	600	12 %	200	18 %	-	-	Cluster, Small multiple Nodules
SRB-354-10 % HEMA	10 wt. %	570	15 %	190	17 %	-	-	Cluster, Small multiple Nodules
SRB-356-20% HEMA	20 wt. %	600	16 %	230	23 %	-	-	Cluster, Larger fewer Nodules
SRB-357-40% HEMA	40 wt. %	670	21%	-	-	1.7	0.41	Doublet/ Triplet Mixture
SRB-358-60% HEMA	60 wt. %	800	17 %	170	31 %	1.5	0.42	Cluster, losing control of reaction

* Based on counting 100 particles, † based on counting 50 particles

5.3.2 Use of GDMA Crosslinked Seed Particles

The use of a slightly more hydrophilic seed particle was to induce some interaction between the second stage monomer and the seed particles; the replacement of the EGDMA crosslinking monomer for GDMA in the seed dispersion was studied. The same series was repeated before with increasing HEMA content in the second stage polymerisation monomer feed, and resultant SEM images can be found in Figure 5-3.

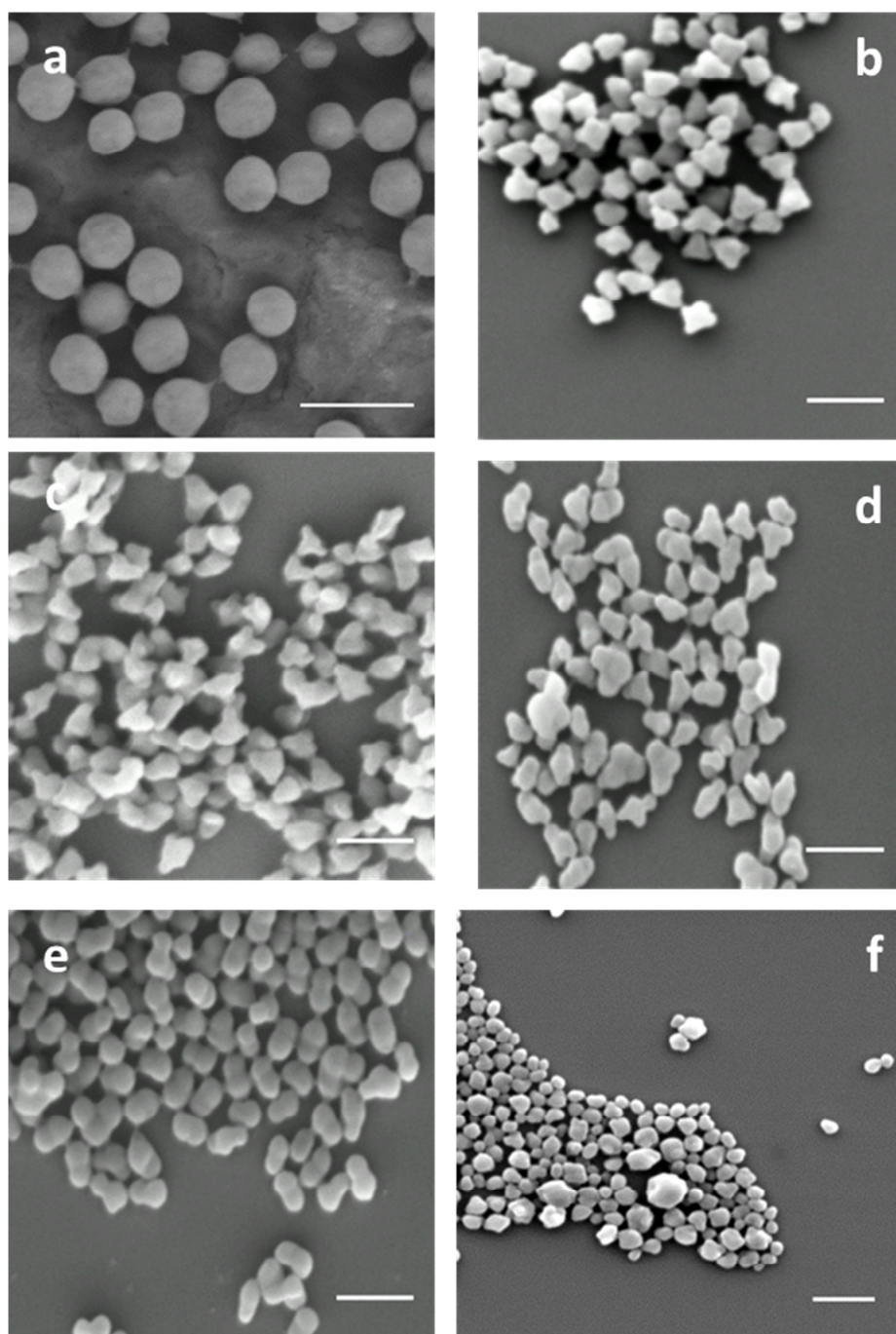


Figure 5-3, SEM images of reactions with increasing HEMA concentration in the monomer feed with GDMA crosslinked seed particles where; a, seed dispersion, b, 5 wt. % HEMA, c, 10 wt. % HEMA, d, 20 wt. % HEMA, e, 40 wt. % HEMA and f, 60 wt. % HEMA. Scale bars are 1 μm .

The images show a similar trend of low HEMA content giving clustered particles, which can again be split into different regimes:

- At 5 and 10 wt. % HEMA there is an increase in nodules on the particle surface.
- At 20 wt. % HEMA these nodules decrease in number but appear to grow in size.
- At 40 wt. % HEMA the particles only form one nodule of equal size, giving dumbbell-like particles or doublets.
- At 60 wt. % HEMA particle aggregation becomes an issue, but the particles appear to have some large and some smaller nodules on the surface.

Particle size distribution graphs, Figure 5-4, and the particle size data, Table 5-3 are shown below.

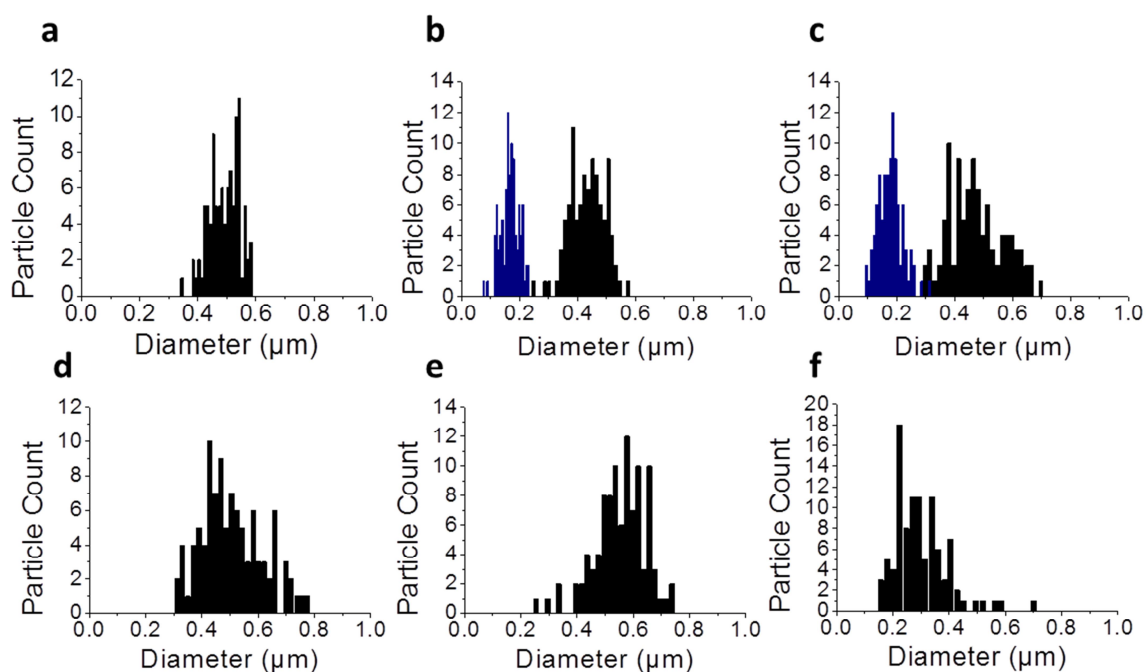


Figure 5-4, size distribution plots for reactions with increasing HEMA concentration in the monomer feed with GDMA crosslinked seed particles where; a, seed dispersion, b, 5 wt. % HEMA, c, 10 wt. % HEMA, d, 20 wt. % HEMA, e, 40 wt. % HEMA and f, 60 wt. % HEMA. Nodules on the particle surface are shown in blue.

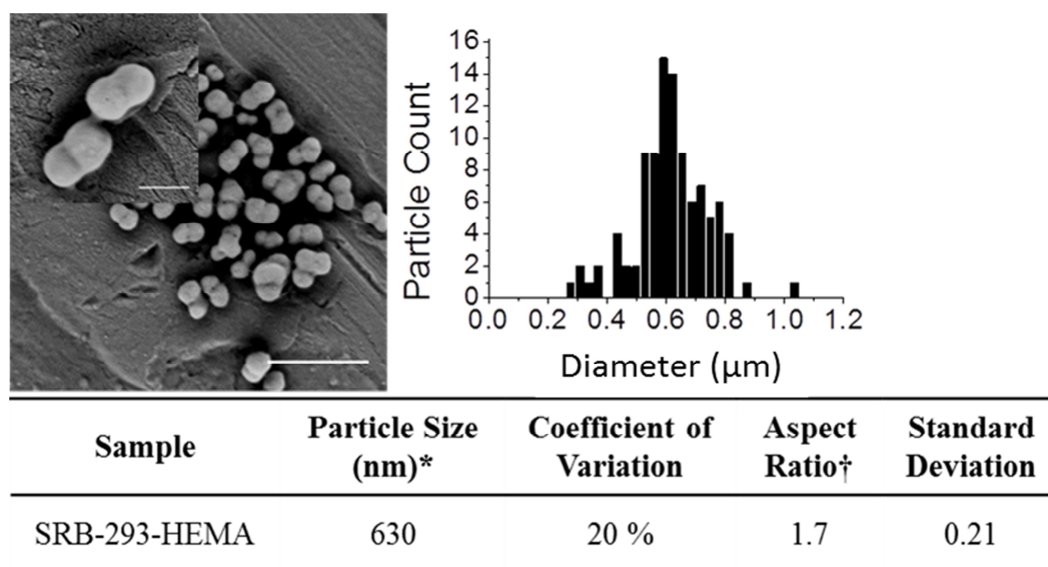
Table 5-3, particle size data and aspect ratio for particles with increasing HEMA concentration in the monomer feed and GDMA crosslinked seed particles, initial seed dispersion shown in italics.

Sample	HEMA Content	Particle Diameter* (nm)	Coefficient of Variation	Nodule Diameter* (nm)	Coefficient of Variation	Aspect Ratio†	Standard Deviation	Particle Shape
<i>SRB-288-1% GDMA</i>	-	<i>500</i>	<i>11 %</i>	-	-	<i>1.1</i>	<i>0.11</i>	<i>Spherical</i>
SRB-380-5% HEMA	5 wt. %	440	14 %	170	19 %	1.2	0.21	Cluster, Small multiple Nodules
SRB-359-10 % HEMA	10 wt. %	480	20 %	108	22 %	1.3	1.31	Cluster, Small multiple Nodules
SRB-360-20% HEMA	20 wt. %	520	21 %	-	-	1.8	0.42	Doublet/ Triplet Mixture
SRB-364-40% HEMA	40 wt. %	560	17 %	-	-	1.7	0.30	Doublets
SRB-407-60% HEMA	60 wt. %	310	31 %	-	-	1.6	0.53	Cluster, losing control of reaction

* Based on counting 100 particles, † based on counting 50 particles

The size distribution plots show that the polydispersity of the samples increased with increasing HEMA concentration, this could be due to small secondary particles forming which are rich in HEMA so precipitate fast. This would explain the size decrease between the seed dispersion and SRB-407-60% HEMA.

Despite the reaction conditions not favouring a clean polymerisation at 60 wt. % HEMA and above, one sample was isolated where the monomer feed was pure HEMA. The sample is very polydisperse and still shows the same morphology as the SRB-364-40% HEMA sample of doublet particles. SEM images and particle size data can be seen in Figure 5-5 below, the reaction was run using the same seed dispersion SRB-288-1% GDMA.



* Based on counting 100 particles, † based on counting 50 particles

Figure 5-5, SEM images and particle size data for SRB-293-HEMA, scale bars are 2 μm and 500 nm for inserts.

The data obtained for this sample shows that the aspect ratio is equal to that of SRB-364-40% HEMA but the size is slightly larger. Also there are a greater number of trimers in this sample, showing aggregation is occurring in the reaction, this is also evident in the polydispersity of the sample.

5.4 Second Stage Polymerisation Containing HEAm-MMA

For this series the HEMA was replaced by the more polar HEAm monomer. Due to the increased polarity and solubility mismatch of HEAm over HEMA different structures are expected. For this series GDMA crosslinked seed particles were used.

In this series of experiments the second monomer, *N*-hydroxyethyl acrylamide (HEAm) was tested with increased concentration in the monomer feed. The second stage reaction s with a 1 wt. % GDMA crosslinked seed dispersion showed cleaner reactions over the EGDMA crosslinked seed dispersion and good control over the polymerisation reactions. Below Figure 5-6 shows the SEM images of the resultant particles with increasing HEAm content.

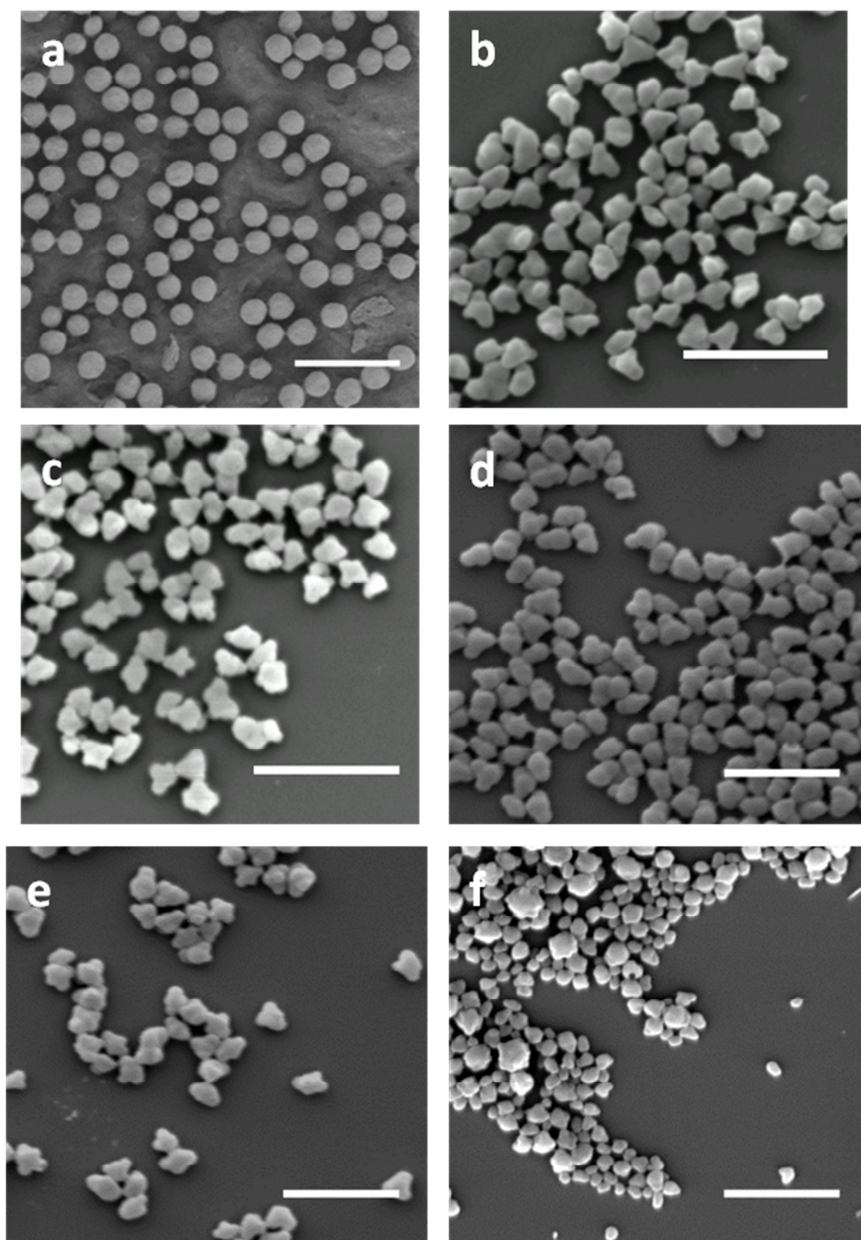


Figure 5-6, SEM images of reactions with increasing HEAm concentration in the monomer feed with GDMA crosslinked seed particles where; a, seed dispersion, b, 5 wt. % HEAm, c, 10 wt. % HEAm, d, 20 wt. % HEAm, e, 40 wt. % HEAm and f, 60 wt. % HEAm. Scale bars are 2 μm .

As with both cases previously with increasing HEMA content the resultant particle morphology goes through some transition points.

- At 5 and 10 wt. % HEAm there is an increase in nodules on the particle surface.
- At 20 wt. % HEAm these nodules decrease in number but appear to grow in size.

- At 40 wt. % HEAm the particles start to aggregate together and show that 3 or less nodules per particle appear evident.
- At 60 wt. % HEAm particle aggregation becomes an issue, and the particles appear to have some large and some smaller nodules on the surface.

Note that a point where doublet particles were formed was not found, looking at the trend with the increasing HEMA content, a point similar to doublet formation is SRB-394-20% HEAm, where only one or two nodules are formed.

The size distribution plots, Figure 5-7 and particles size data, Table 5-4, for these reactions can be found below.

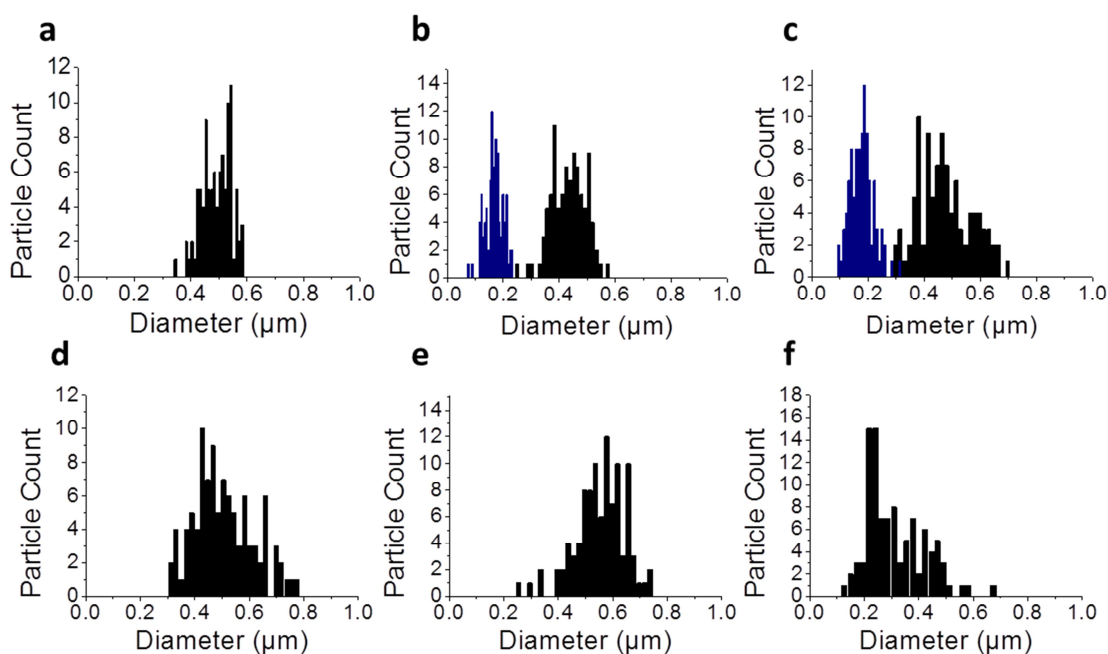


Figure 5-7, size distribution plots for reactions with increasing HEMA concentration in the monomer feed with GDMA crosslinked seed particles where; a, seed dispersion, b, 5 wt. % HEMA, c, 10 wt. % HEMA, d, 20 wt. % HEMA, e, 40 wt. % HEMA and f, 60 wt. % HEMA. Nodules on the particle surface are shown in blue.

Table 5-4, particle size data for particles with increasing HEAm concentration in the monomer feed and GDMA crosslinked seed particles, initial seed dispersion shown in italics.

Sample	HEAm Content	Particle Diameter* (nm)	Coefficient of Variation	Nodule Diameter* (nm)	Coefficient of Variation	Particle Shape
<i>SRB-288-1% GDMA</i>	-	<i>500</i>	<i>11 %</i>	-	-	<i>Spherical</i>
SRB-381-5% HEAm	5 wt. %	520	13 %	180	17 %	Cluster, Small multiple Nodules
SRB-383-10 % HEAm	10 wt. %	470	15 %	180	19 %	Cluster, Larger fewer Nodules
SRB-394-20% HEAm	20 wt. %	580	14 %	230	23 %	Doublet/ Triplet Mixture
SRB-395-40% HEAm	40 wt. %	590	10 %	200	19 %	Doublet/ Triplet/ Tetramer Mixture
SRB-411-60% HEAm	60 wt. %	330	33 %	-	-	Cluster, losing control of reaction

* Based on counting 100 particles, † based on counting 50 particles

The size distribution graphs and particle size data shows a small polydispersity increase with increasing HEAm content, with the exception of SRB-411-60 % HEAm which shows a very high polydispersity and a size decrease on the seed dispersion. This will be due to precipitation of the polymer which has not aggregated to the surface of the seed particles, forming a small second population of particles.

5.5 Rationalisation of Results

When increasing the polar monomer concentration in all three cases the particle morphology went through a transition from a multi-lobed cluster-like particle to particles with few larger lobes or nodules protruding from the particle surface. As discussed in *Chapter 4*, a small amount of polar monomer will trigger the precipitation of growing polymer chains and aid phase separation within the particle upon incorporation. At higher concentrations this is still valid but the monomer / resultant polymer miscibility with PMMA is of greater importance than before. If the monomer and resultant polymer are very matched to PMMA little phase separation will be observed between the seed particle and the second stage polymer. If this is the opposite case then phase separation will occur rapidly, forming multiple lobes of higher polarity.

It was also shown in *Chapter 4*, which the monomer in the second stage polymerisation reaction will partition between the particles and solvent, owing to a higher interaction potential between the particles than the solvent. However as before, the case for precipitation and heterogeneous nucleation cannot be ruled out, owing to the large concentration of polar monomer in the reactions. Upon polymerisation the polar polymer will act as a locus for growth for further monomer in solution.

To understand the miscibility of the second stage reaction with a large volume of polar monomer the Hansen solubility parameters for the polymer formed in the second stage polymerisation can be estimated, focusing on the P(MMA₆₀-co-HEMA₄₀) and P(MMA₆₀-co-HEAm₄₀) examples. The Hansen solubility parameters of the copolymers can be estimated from the values of the constituent monomers and the mole fraction of the monomers in the polymers. Table 5-5 shows the Hansen solubility parameters of statistical copolymers of P(MMA_x-co-HEMA_{100-x}) and P(MMA_x-co-HEAm_{100-x}) with radius of

interaction calculations against PMMA. The calculations were performed assuming 100 % conversion and formation of a statistical copolymer.

Table 5-5, Hansen solubility parameters of statistical copolymers of P(MMA_X-*co*-HEMA_{100-X}) and P(MMA_X-*co*-HEAm_{100-X}) with radius of interaction against PMMA.

Chemical	Solubility Parameter (MPa ^{1/2})				Radius of Interaction
	δ_T	δ_d	δ_p	δ_h	R_a
PMMA	22.7	18.6	10.5	7.5	-
MMA	18.81	16.39	4.54	8.05	7.49
HEMA	23.54	17.47	4.96	14.99	9.60
HEAm	25.70	18.00	9.40	15.80	8.47
P(MMA ₉₅ - <i>co</i> -HEMA ₅)	19.02	16.44	4.56	8.40	7.44
P(MMA ₉₀ - <i>co</i> -HEMA ₁₀)	19.22	16.50	4.58	8.74	7.41
P(MMA ₈₀ - <i>co</i> -HEMA ₂₀)	19.65	16.60	4.62	9.44	7.41
P(MMA ₆₀ - <i>co</i> -HEMA ₄₀)	20.55	16.82	4.71	10.82	7.61
P(MMA ₄₀ - <i>co</i> -HEMA ₆₀)	21.50	17.03	4.79	12.21	8.07
P(MMA ₉₅ - <i>co</i> -HEAm ₅)	19.11	16.47	4.78	8.44	7.24
P(MMA ₉₀ - <i>co</i> -HEAm ₁₀)	19.42	16.55	5.02	8.83	7.02
P(MMA ₈₀ - <i>co</i> -HEAm ₂₀)	20.04	16.71	5.51	9.60	6.65
P(MMA ₆₀ - <i>co</i> -HEAm ₄₀)	21.37	17.03	6.48	11.15	6.31
P(MMA ₄₀ - <i>co</i> -HEAm ₆₀)	22.76	17.36	7.45	12.70	6.55

This shows that again the statistical copolymers will interact with the PMMA colloidal particles to a greater extent than the pure monomer. This increased interaction will be due to the mixture the fact that the mixture of the two monomers is a better solvent for the polymer than the two components. This blending of solvents to give a better solvent is at the heart of Hansen solubility theory. Two non-solvents which are far removed from the polymer in Hansen space can be blended together to produce a good solvent due to the additive nature of mixing the components of the solvents. This idea of solvent blending explains the increasing interaction down the HEAm series in Table 5-5. As the polar HEAm monomer is effectively diluted by the addition of MMA the mixture becomes a better solvent for the system. This is shown by the decreasing R_a value for the HEAm data

set. This idea is shown for HEMA and MMA mixtures below in Figure 5-8, note that a closest point to PMMA is a solvent blend, hence the decrease in the R_a for the mixtures.

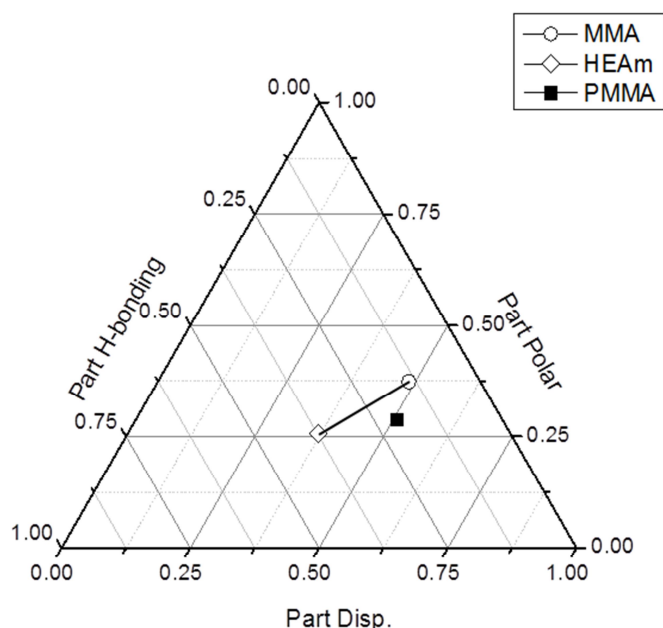


Figure 5-8, Ternary plot showing the Hansen parameters for MMA, HEAm and PMMA, the line indicates the predicted Hansen parameters for all mixtures of MMA and HEAm.

For the HEMA data set this is not the case, the R_a value increases upon mixing HEMA with MMA. This is due to the fact that the polar component of HEMA is very close to that of MMA, unlike HEAm. This means upon mixing the two the blend can never reach a value close to that for the polar component of PMMA. This slight difference gives the overall trend of increasing the R_a , but also explains the slight dip at low HEMA content to the blend.

5.5.1 Reaction Mechanism

It can be inferred that MMA will swell the particles over a short time scale (*Chapter 4*), this will still be true for this system with large quantities of polar monomer in the monomer feed. However the dynamic light scattering (DLS) experiments conducted for particle swelling cannot be carried out due to the insolubility of the polar monomers in dodecane.

Thill *et al.*² proposed a mechanism of formation for colloidal clusters based upon heterogeneous nucleation, by extension this model can also be used to explain the phase transition occurring with increasing polar monomer content.

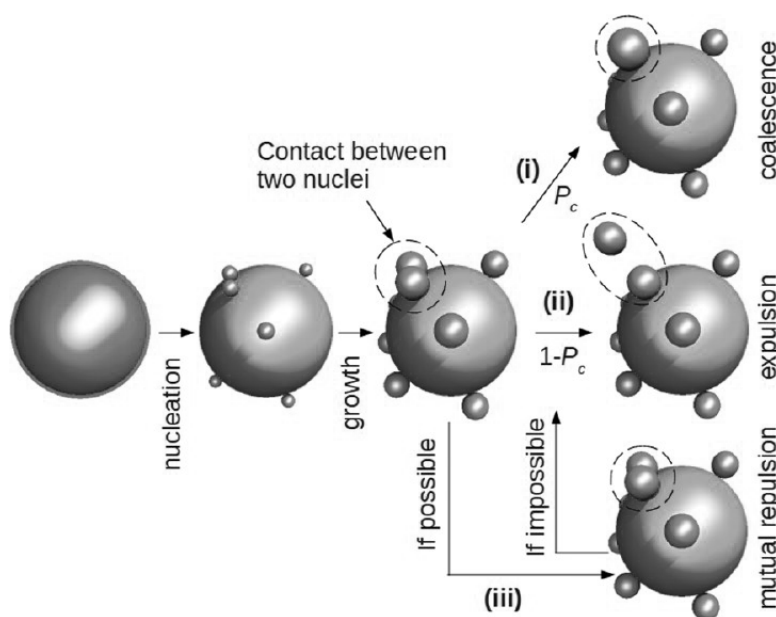


Figure 5-9, mechanism for the formation of colloidal clusters, based upon a heterogeneous nucleation route. Showing (i) coalescence, (ii) nuclei expulsion and (iii) nuclei mutual repulsion.

As the monomer swells the seed PMMA particles and polymerises giving rise to phase separate lobes on the surface, these will coalesce forming fewer larger lobes as the polar monomer content is increased. The increase in polar monomer will aid phase separation and will also further aid the coalescence of the lobes as they will interact more favourably which is shown by the Hansen solubility parameters above, Table 5-5. However the increased polar monomer concentration will give rise to precipitation and heterogeneous nucleation due to the increased polarity of the particle surface from the precipitated polar chains.

This precipitation of polar chains can then allow for the coalescence of the formed nuclei, Figure 5-9, i, give larger lobes. This will then be aided by phase separation of the second stage polymer with the more hydrophobic PMMA chains, allowing the formation of a single large nodule.

5.5.2 Reactions Failing at High Polar Monomer Concentration

The second stage reactions with 60 wt. % of the monomer feed consisting of polar monomer gave rise to very polydisperse samples, and was said to lose control. This could be due to the large volume of polar monomer being added to the reaction mixture in one drop, during the feed. This drop in both cases for HEMA and HEAm is not miscible with the dodecane/ hexane solvent, so will reside in droplets. These droplets could then be stabilised by the adsorption of the polymeric surfactant in solution. This would decrease the concentration of surfactant available to stabilise the growing colloid particle in dispersion and lead to the destabilisation of the reaction.

However it is well known that solid particles can stabilise liquid-liquid interfaces as a Pickering emulsion.³ In this case particles adsorb to the interface and will decorate the surface of the droplet, leading to polymerisation within the drop.⁴ Solid particles are bound to the surface far more strongly than surfactant molecules so they may not become free again during the course of the reaction.⁵ Below are light microscope images of the resultant emulsions formed from HEMA and HEAm mixed with the P(HSA-g-MMA) stabiliser and seed particles at reaction concentrations. This is shown in Figure 5-10 and shows HEMA and HEAm droplets in dodecane solvent, stabilised by the P(HSA-g-MMA) stabiliser and PMMA seed particles.

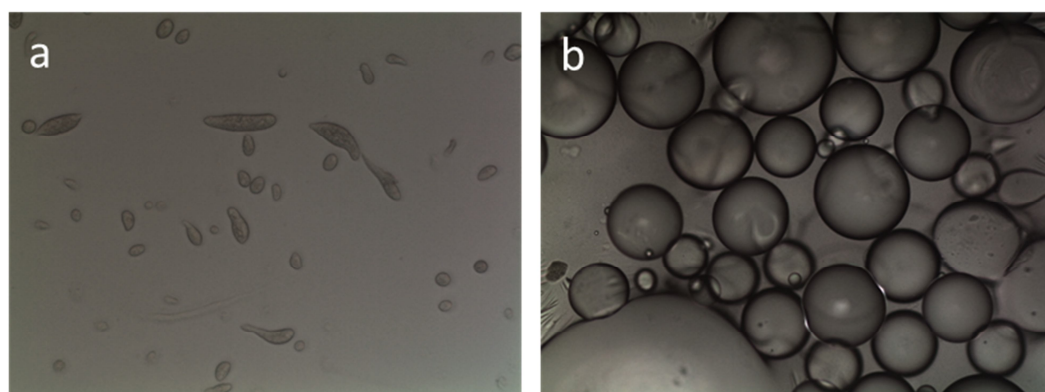


Figure 5-10, droplets formed when; a, HEMA and b, HEAm, is mixed in dodecane in the presence of particles and the P(HSA-g-MMA) stabiliser, under reaction concentrations. 4:1 monomer / particle ratio, 9.3 % P(HSA-g-MMA) stabiliser, diluted in dodecane to be imaged.

If multiple droplets are present in the reaction mixture they could effectively remove particles from the dispersion by locking them onto the liquid-liquid interface. This will

have drastic effects on the reaction and will lead to coagulum formation. It is for this reason that the reactions with pure polar monomer are very unreliable and unclean. As well as this effect if a propagating chain entered a monomer droplet, it would polymerise in a pseudo-suspension polymerisation type reaction. The SEM image below from the SRB-411-60% HEAm reaction shows such occurrence.

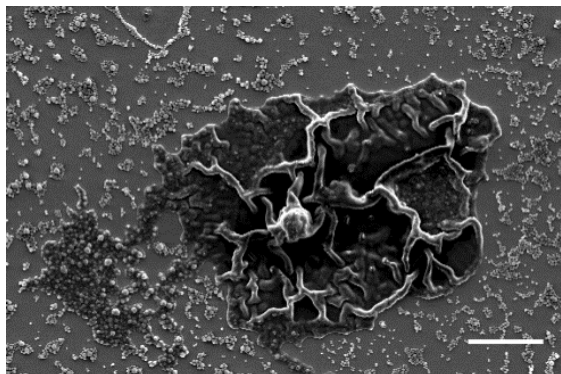


Figure 5-11, SEM image of pseudo-suspension polymerisation of HEAm occurring in SRB-411-60% HEAm. Scale bar is 10 μm .

5.6 Focusing on Dumbbell-like Particles

The reaction SRB-364-40% HEMA produced dumbbell-like particles, this morphology is of greater interest than the HEAm cluster-like particles produced. Due to their shape they may possess interesting properties such as:

- The ability to pack more efficiently with reduced void volumes compared to spheres.
- Potential to have a higher electrophoretic mobility, due to a reduction in friction.
- Greater scattering potential for the same electrophoretic mobility.

These aspects are of great interest for electrophoretic display technology, as they the potential to improve the final device performance by increasing screen refresh rate, or contrast ratio between black and white pixels.

For these reasons these doublet particles were further scrutinised to understand their formation.

5.6.1 Monomer Conversion Profile

It has been shown before (*Chapter 4*) that the monomer conversion rate did not reach 100 % when using 0.5 wt. % radical initiator. The monomer conversion rate will have implications on the size of any particle growth; the monomer conversion profile is shown below and it was found that the monomer conversion is 85 % by the end of the reaction.

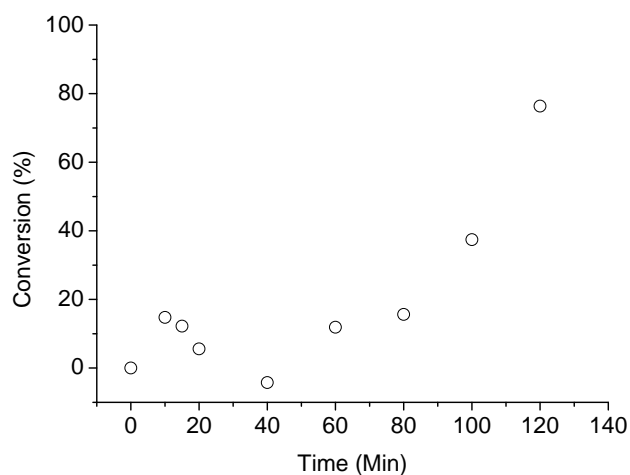


Figure 5-12, monomer conversion profile for SRB-413-40% HEMA.

5.6.2 Implications on Particle Size

If we assume that the doublet particles are two touching spheres with minimal interpenetration, and that one sphere grows on the edge of a seed particle. Then the size of that sphere can be approximated by simply treating it as a sphere.

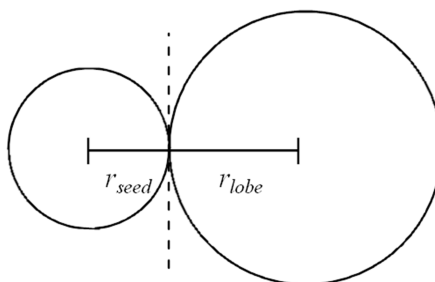


Figure 5-13, schematic view of treating dumbbell-like particles as two touching spheres.

The volume of a sphere is given by:

$$V = \frac{4}{3}\pi r^3 \quad 5-1$$

As in the reaction the monomer/ particle is fixed to 4:1, then the lobe should have a volume 4 times greater than the seed particle. Taking into account the 85 % monomer conversion this turns out to be 3.4 the volume of the seed. Therefore the radius of the two spheres will be given by:

$$\begin{aligned} r_{seed} &= \sqrt[3]{3/4\pi} & r_{lobe} &= \sqrt[3]{(3/4\pi \cdot 3.4)} \\ r_{seed} &= 1.3 & r_{lobe} &= 2.0 \end{aligned} \quad 5-2$$

This means that the lobe should be slightly bigger than the seed particle and can be measured on samples which form the doublet particles, by measuring the diameters of the lobes and expressed as a ratio. Where the smallest/largest = r_{seed} / r_{lobe} . This can be measured in two ways along the length of the whole particle, or across the width of the particle as shown in Figure 5-14 below.

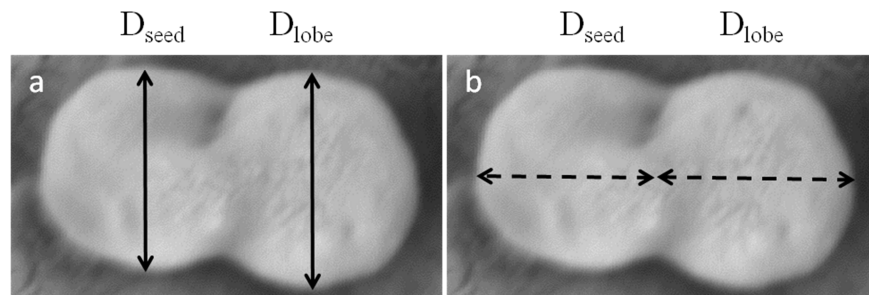


Figure 5-14, showing the measurement of the lobe ratio which can be done by, a, measuring across the whole particle width and b, along the length of the whole particle.

Table 5-6, showing measured and expected lobe ratio, r_{seed}/r_{lobe} .

Sample	Particle Width		Particle Length		Expected
	Measured*	Std. Dev.	Measured*	Std. Dev.	
SRB-364-40% HEMA	0.80	0.12	0.81	0.16	0.66
SRB-410- 40% HEMA 1 % naphthalene	0.83	0.09	0.78	0.14	0.66
SRB-293-HEMA	0.80	0.13	0.75	0.15	0.66

*based on counting 100 particles.

These results show that one lobe is larger than the other, and to a greater extent than expected. However this does show that during the reaction all the monomer must go into producing a new lobe for the measurements to be of the expected size.

This idea can be reinforced by comparing the size of the lobes of the dumbbell-like particles to the size of the initial seed dispersion. If the second stage polymerisation reaction proceeds by heterogeneous nucleation followed by coalescence of phase separated lobes, then the size of one lobe in the dumbbell-like particles should be equivalent to the starting seed dispersion.

Table 5-7, showing the difference between experimentally measured lobes in dumbbell-like particles compared to the seed particles.

Sample	Lobe Diameter (nm)		Seed Diameter (nm)	% Difference	
	Lobe 1	Lobe 2		Lobe 1	Lobe 2
SRB-364-40% HEMA	253	278	500	43	44
SRB-410- 40% HEMA 1 % naphthalene	224	285	460	51	38
SRB-293-HEMA	319	383	500	36	23

Table 5-7 shows the effective difference in the lobe size of the particles compared to that of the seed dispersion. The results show that the lobe size decreases from that of the seed particles by between 25 – 50 % depending upon sample. This result of the effective shrinking of the seed dispersion is an unexpected result. It is thought that upon phase separation the swollen gel-like particles deform and ‘flow’ with the phase separating

second stage polymer. This deformation will be in line with polymer rearrangement due to the phase separation.

Such a deformation should be viable due to the weakly crosslinked nature of the seed dispersion. This was shown in the thermal characteristics of the 1 wt. % crosslinked seed particles in *Chapter 2*, Figure 2.21, which showed that despite being crosslinked and unable to dissolve in good solvent they still maintained a glass transition, T_g , of 113.6 °C. This is down to the low degree of crosslinking, giving long polymer chains between crosslinked units which exhibit the glass transition behaviour. This idea is known and is related to the increasing of the T_g point in the sample.⁶ The glass transition temperature of the copolymers can be estimated by the Fox equation⁷:

$$\frac{1}{T_{g\ 12}} = \frac{\omega_1}{T_{g\ 1}} + \frac{\omega_2}{T_{g\ 2}} \quad 5-3$$

Where; $T_{g\ 1}$, $T_{g\ 2}$ and $T_{g\ 12}$ are the T_g values for polymer 1, polymer 2 and the statistical copolymer of 1 and 2 respectively, ω_1 and ω_2 are the weight fraction of polymer 1 and polymer 2 in the statistical copolymer.

Table 5-8, glass transition temperatures of homopolymers and polymer blends estimated from the Fox equation.

Polymer	T_g (°C)
PMMA ⁸	104
PHEMA ⁹	85
P(MMA ₉₅ -co-HEMA ₅)	103
P(MMA ₉₀ -co-HEMA ₁₀)	102
P(MMA ₈₀ -co-HEMA ₂₀)	100
P(MMA ₆₀ -co-HEMA ₄₀)	95
P(MMA ₄₀ -co-HEMA ₆₀)	92

Although the T_g of all the polymers is above the reaction temperature (85 °C) the value of the glass transition temperature is molecular weight dependant.⁶ In most cases increasing the molecular weight of the polymer will increase its associated T_g . So during the reaction as the polymers grow they will have a lower T_g than represented in Table 5-8. As the

reaction proceeds any polymer formed will also be plasticised by any of the unreacted monomer in the reaction vessel.

This means that it is likely that both the seed particles and the second stage polymer formed will be in a gel-like interpenetrated state.

5.7 Anisotropy of Samples

Certain samples produced by increasing the polar monomer concentration are anisotropic. A particle is said to be anisotropic if it has directionality in some aspect of its character, such as shape, magnetic or chemical. The particles with 40 wt. % polar monomer in the monomer feed can be classed as chemically anisotropic in case of HEAm and shape and chemically anisotropic in the case of HEMA.

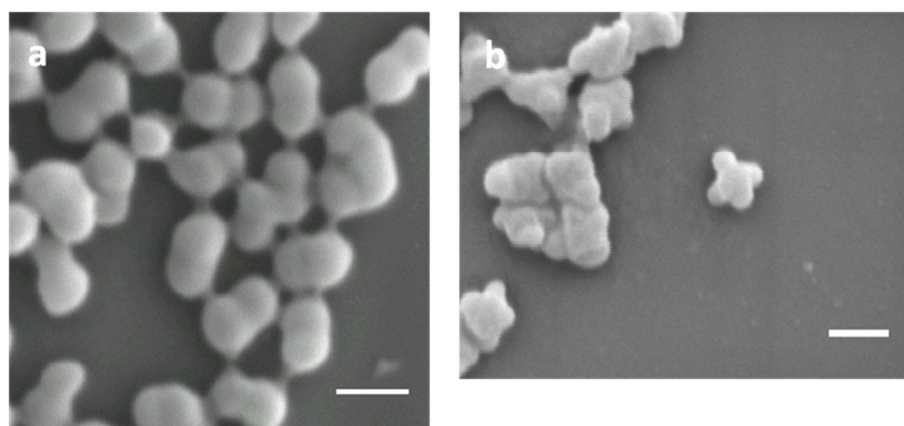


Figure 5-15, SEM images of a, SRB-364-40% HEMA and b, SRB-395-40% HEAm. Scale bars are 500 nm.

Assuming the polymerisation reaction only occurs to form the nodules and the whole particle is not coated then the nodules will be chemically distinct from the core, seed particle. Another term for chemically anisotropic particles is Janus particles. Janus particles are particles which differ from one side to the other, this can be in chemistry, colour, charge or magnetic properties, the name comes from the roman two headed god Janus.

However due to the size range and chemical environment of the colloidal particles no easy technique exists to prove that they have Janus character. Simple methods such as complexing metal ions to the surface of the particles or selectively tagging with fluorescent dyes are not applicable. The size regime is too small for the use of light methods to image the particles and prove that tagging has only occurred selectively on the particle and due to the contentious phase solvent metal ions cannot be easily incorporated.

Two methods have been adopted to attempt to prove the Janus nature of the particles focusing on the more interesting case of the doublets formed by 40 wt. % HEMA in the reaction:

- The use of fluorescent markers in the seed particles and in the second stage polymerisation to look for Förster resonance energy transfer (FRET) between the two chromophores.
- The coupling of chlorosilane reagents to the free hydroxyl groups present in the HEMA monomer, followed by imaging and chemical mapping.

5.7.1 Proof of Janus Character - Fluorescence Spectroscopy

The structure of polymer particles can be characterised by fluorescence quenching techniques,^{10,11} by the incorporation of fluorescent dyes into the polymerisation reaction. This quenching is known as FRET. FRET works by the transfer of energy from the electronic excited state of the donor to the acceptor by non-radiative dipole coupling. FRET is most efficient when the donor and acceptor are in very close proximity and there is good spectral overlap between the emission spectrum of the donor to the absorption spectrum of the acceptor.¹²

If the core seed particles contain a dye which can act as an energy acceptor and the shell contains another dye which can act as an energy donor, then fluorescence quenching can be measured. This quenching effect is a very short range interaction and can be used to show if the structure of the particles has a well-mixed interface, giving an ideal core-shell structure or some deviation from the ideal. This is shown schematically below in Figure 5-16.

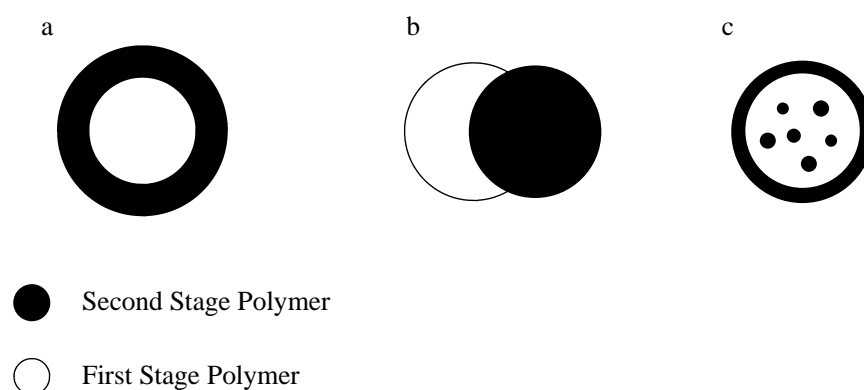


Figure 5-16, schematic view of particles resulting from a second stage polymerisation where; a, is an ideal core-shell particle, b and c, shows deviations from ideal.

The electronic properties of the dye particles are very important so the two overlap to allow energy transfer. This intermolecular energy transfer has been known to occur between anthracene and naphthalene.¹³ Use of vinyl functionalised derivatives can be used to allow incorporation into the polymer, and the chemical structure of the two is shown below.

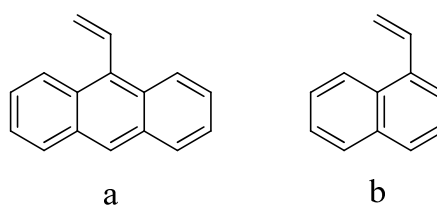


Figure 5-17, chemical structure of a, vinyl anthracene and b, vinyl naphthalene.

A particle dispersion was produced incorporating 1 wt. % vinyl anthracene and crosslinked with 1 wt % GDMA. This was then used as seed dispersion for a second stage polymerisation reaction incorporating 40 wt. % HEMA in the monomer feed and 1 wt. % vinyl naphthalene to produce doublet particles. SEM images and size distribution data are shown in Figure 5-18 and particle size and aspect ratio measurements are shown in Table 5-9.

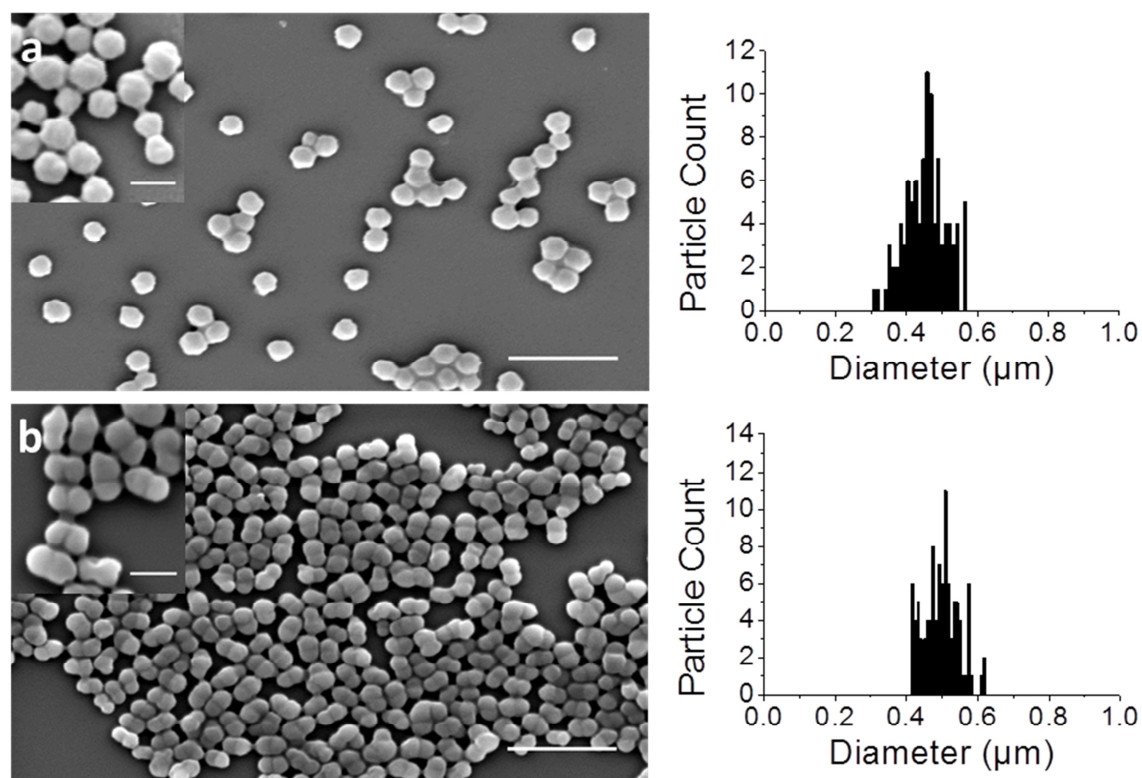


Figure 5-18, SEM images and particle size data for, a, seed dispersion containing 1 wt. % vinyl anthracene and b, second stage polymerisation containing 40 wt. % HEMA and 1 wt. % vinyl naphthalene. Scale bars are 2 μm and 500 nm for inserts.

Table 5-9, particle size data for fluorescent particles produced.

Sample	Particle Diameter (nm)*	Coefficient of Variation	Aspect Ratio†	Coefficient of Variation
SRB-406-1 % anthracene	460	13 %	1.2	0.181
SRB-410- 40% HEMA, 1 % naphthalene	500	10 %	1.7	0.24

* Based on counting 100 particles, † based on counting 50 particles

5.7.2 Proof of Janus Character - Selective Surface Functionalisation

The doublet particles produced in SRB-364-40 % HEMA will have free hydroxyl groups, from the HEMA monomer, which are open for reactions. If the particles are truly Janus in nature and if a coupling reaction can be undertaken and well controlled it should only

functionalise one half of the particle. This sample could then be taken and imaged in a transmission electron microscope and the added electron density should give a contrast difference from one side of the particle to the other.

One well known coupling reaction is the reaction of chlorosilane molecules with hydroxyl groups and is used routinely in the formation of self-assembled mono-layers in organic transistor fabrication and in the formation of polymer brushes from surfaces by controlled radical polymerisation. A typical reaction goes by the following:

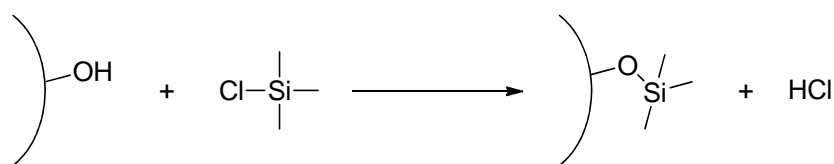


Figure 5-19, reaction of chlorosilane to a surface with free hydroxyl groups.

However in order to maintain solubility in the dodecane solvent and to give high electron density a simple chlorosilane may not be sufficient. For this preliminary work 1H,1H,2H,2H-Perfluorodecyltrichlorosilane, was used as the coupling silane reagent and the chemical structure is shown below.

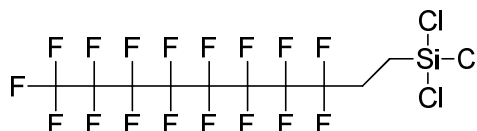


Figure 5-20, chemical structure of 1H,1H,2H,2H-Perfluorodecyltrichlorosilane.

Initially as a proof of concept, the perfluorosilane was added to a dispersion of SRB-364-40 % HEMA particles (10 μl silane to 0.5 ml dispersion at 5 wt. % TSC) and allowed to mix for an hour at 30 $^{\circ}\text{C}$. The resultant dispersion was then imaged by SEM, images before and after along with size distribution plots can be found in Figure 5-21 and particle size data can be found in Table 5-10.

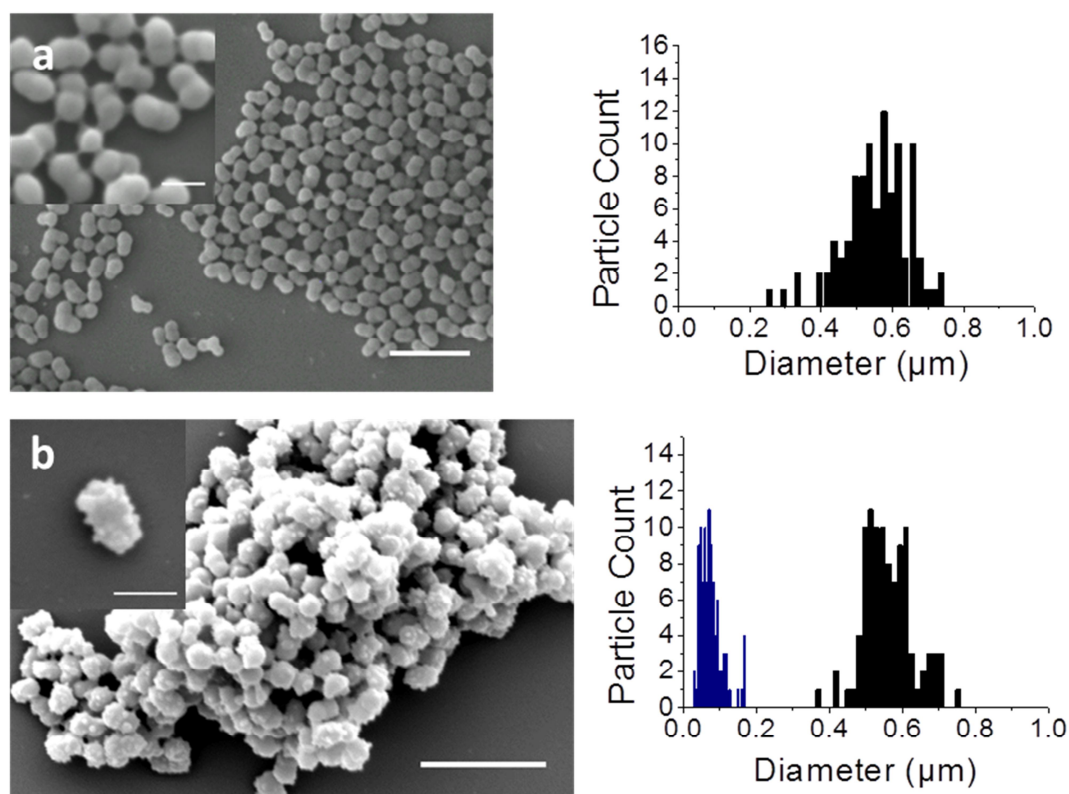


Figure 5-21, SEM images and particle size data for, a, seed dispersion containing 40 wt. % HEMA and b, surface treatment with perfluoro silane. Scale bars are 2 μm and 500 nm for inserts, nodules on the particle surface are shown in blue in size distribution graph.

Table 5-10, particle size data for particles before and after surface treatment with perfluoro silane.

Sample	Particle Diameter* (nm)	Coefficient of Variation	Nodule Diameter* (nm)	Coefficient of Variation	Aspect Ratio [†]	Std. Dev.
SRB-364-40 % HEMA	560	17 %	-	-	1.7	0.30
SRB-405-Silane treated	570	12 %	80	40 %	1.6	0.24

*based on counting 100 particles, [†] based on counting 50 particles

From the SEM images it is clear that the addition of the perfluorosilane reagent has aggregated the sample and that the silane has reacted all over the particle forming small nodules. This is evidence of the silane crosslinking with other units building small islands

on the particle surface. The aggregation occurring may be due to the fluorine containing carbon chains interacting with each other over the dodecane solvent.

The chlorosilane coupling all over the particle can be explained by the fact that the seed particle contains carboxylic acid units and the stabiliser contains epoxide groups, both of which the chlorosilane will react with. These groups are present to allow the covalent coupling of the stabiliser to the particle surface, by an acid-epoxide reaction. However the second stage polymerisation was found not to work after the stabiliser is covalently attached to the particle surface. The failure of the second stage after chemical attachment of the stabiliser is thought to be due to the fact that the P(HAS-*g*-MMA) once attached cannot migrate away from the particle surface allowing for swelling of the particle. Instead the polar monomer fed into the reaction will form droplets in the reaction mixture leading to unclean reactions and coagulum formation.

5.8 Conclusions

Particle dispersions have successfully been produced which exhibit anisotropic properties in terms of shape and are expected to be also chemically anisotropic. These particles were produced by a second stage seeded dispersion polymerisation reaction using spherical seed template particles. It was found that the monomer-particle interaction was critical for producing particles other than cluster-like particles. Tuning this interaction was achieved by the incorporation of GDMA as a crosslinker for the second stage reaction. It was also found that this aided the formation of cleaner dispersions.

The reaction mechanism is extended from that set out by Thill *et al.*² of heterogeneous nucleation followed coalescence of any lobes formed on the particle surface. This will be enhanced by phase separation due to the large quantity of mismatched polar monomer in the second stage reaction. These phase separated lobes will coalesce to a greater extent with increased polar monomer due to increased interactions between the lobes. It was also shown that it is likely that the seed particles will be in a gel-like state during the reaction which then deform during phase separation giving two lobes of smaller size than the original seed particles.

The doublet particles are expected to be chemically anisotropic and hence Janus particles. Steps toward proving this have been taken by two methods; studying fluorescence quenching due to FRET by dyes included in the first and second stage polymerisation reactions, and by selective surface functionalisation. Both the methods outlined show merit to prove the Janus character of the dispersions, but due to time constraints the systems have not been optimised to give the final definitive result.

The formation of shape anisotropic particles, SRB-364-40 % HEMA, is the first reporting of such particles produced in non-polar solvents.

5.9 References

- ¹ L. Antl, J. W. Goodwin, R. D. Hill, R. H. Ottewill, S. M. Owens, S. Papworth and J. A. Waters, *Colloids and Surfaces*, 1986, **17**, 67
- ² A. Thill, A. Désert, S. Fouilloux, J.-C. Taveau, O. Lambert, M. Lansalot, E. Bourgeat-Lami, O. Spalla, L. Belloni, S. Ravaine and E. Duguet, *Langmuir*, 2012, **28**, 11575
- ³ S. U. Pickering, *J. Chem. Soc., Trans.*, 1907, **91**, 2001
- ⁴ R. F. A. Teixeira, H. S. McKenzie, A. A. Boyd, and S. A. F. Bon, *Macromolecules*, 2011, **44**, 7415
- ⁵ B. P. Binks, *Curr. Opin. Colloid In.*, 2002, **7**, 21
- ⁶ M. Chanda and S. K. Roy, '*Plastics Technology Handbook*', 2006, CRC Press, 4th ed. Chp.1
- ⁷ J. W. Nicholson, '*The Chemistry of Polymers*', RSC Publishing 3rd Ed., 2007, Chapter 3, 48
- ⁸ W. Knappe and H. J. Ott, *Colloid Polym. Sci.*, 1977, **255**, 837
- ⁹ Y. Zheng, K. Yao, ; D. Chandler, S. Sangmin and C. Tang, *Polymer Preprints, Am. Chem. Soc.*, 2010, **51**, 448
- ¹⁰ M. A. Winnik, '*Photophysical and Photochemical Tools in Polymer Science*', D. Reidel, Holland, 1986.
- ¹¹ M. A. Winnik, H. Xu and R. Satguru, *Makromole. Chem., Macromol. Symp.*, 1993, **70**, 107
- ¹² P. Atkins and J. de Paula. '*Atkins' Physical Chemistry*', Oxford University Press, 8th Ed. 2006, Chapter 23

¹³ O. Schnepp and M. Levy, *J. Am. Chem. Soc.*, 1962, **84**, 172

6 Surface Charging and Zeta Potential

6.1 Introduction

This chapter considers preliminary work on particles produced in this project for use in an electrophoretic display device.

As discussed in *Chapter 1*, in order for the particles to have any net charge, charging surfactants are added, one which is known to give positive charge to poly(methyl methacrylate), (PMMA), particles in non-polar media and the other which is known to give a negative charge to particles in non-polar media as shown in Figure 6-1.

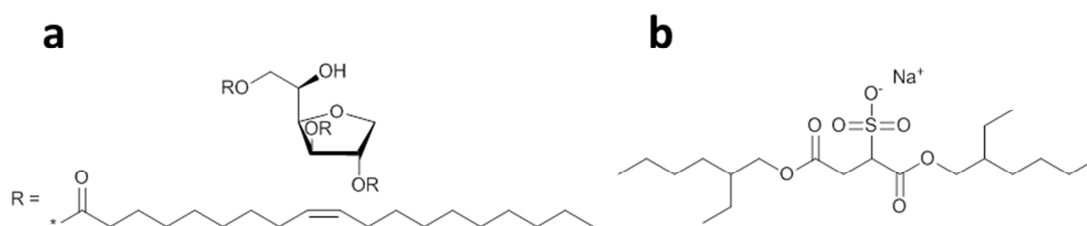


Figure 6-1, chemical structures of charging surfactants, a, the positive charging agent sorbitan trioleate, Span 85¹ and b, the negative charging agent dioctyl sodium sulfosuccinate, AOT.²

6.2 Zeta Potential and Particle Size Measurement Theory by Light Scattering

6.2.1 Particle Size Measurements

All measurements were conducted using a Malvern ZetaSizer, which is an example of a particle sizer which works by dynamic light scattering (DLS). DLS works by measuring the diffusion coefficients of particles due to Brownian motion. Brownian motion is the random movement of particles due to collision with solvent molecules. The diffusion coefficient can be used to calculate the particle size using the Einstein-Stokes equation which relates the diffusion coefficient, D , to the particle radius, r :

$$D = \frac{k_B T}{6\pi\eta r} \quad 6-1$$

Where; k_B is Boltzmann's constant, T is the absolute temperature in Kelvin and η is the sample viscosity.

Larger particles are less affected by solvent collisions so will diffuse slower and smaller particles will move faster. This means the movement of particles is affected by the sample temperature and viscosity. For this reason the temperature must be very carefully controlled and the sample viscosity known. The other important consideration is the refractive index of the medium, which again must be known. Equation 6-1 is only valid for a perfect sphere and a monodisperse sample, however real samples are not monodisperse and perfectly uniform.

In order to measure the diffusion coefficient of a sample in the DLS experiment, laser light is scattered off the particles and an autocorrelation function is applied, giving the diffusion coefficient. The autocorrelation works on the principle that if the sample was stationary then imaged after a very short time, τ , the scattering intensity would be the same as $\tau = 0$, giving a correlation of 1. But the translational and rotational motion of the particles in the sample causes the scattering of the incident laser light. This causes interference with the photons of light from neighbouring particles and the loss of correlation. The faster the particle moves the greater the difference between $t = 0$ and $t = \tau$. This is shown diagrammatically in Figure 6-2.

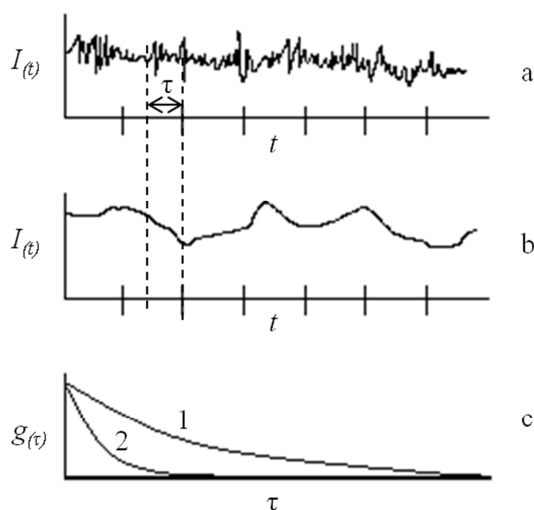


Figure 6-2, intensity of scattered light as a function of time for, a, small particles and b, large particles, c shows the autocorrelation function for larger particles, 1 and small particles, 2.³

In order to give a distribution of sizes from the raw intensity signal the CONTIN algorithm is used, which deconvolutes the signal giving the distribution of sizes.⁴

6.2.2 Zeta Potential Measurements

Zeta potential measurements are measured by a similar method in that the diffusion coefficient is determined for a sample but in an applied electric field, this is called laser Doppler electrophoresis (LDE). Particles travel to the electrodes in the cell and their diffusion coefficient is measured. This translational movement is added to Brownian motion of the particles so the light is scattered as before but also shifted in frequency due to the net movement of particles.

In order to measure the diffusion coefficient the Doppler shift needs to be measured, in order to do this a reference beam is passed through the sample to the detector and compared to the scattered light, the frequency shift then gives the Doppler shift and hence the particle velocity.

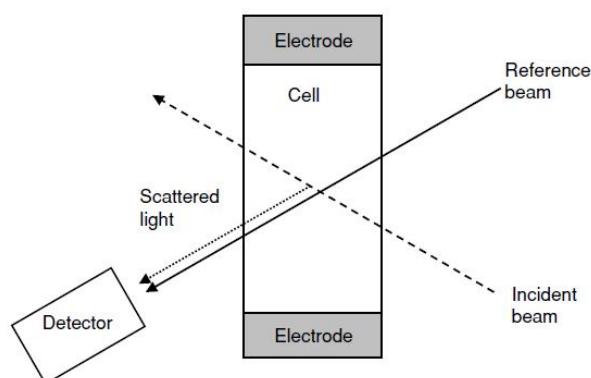


Figure 6-3, schematic view of principal features of a LDE experiment. ⁵

LDE is a very good technique for measuring samples which are highly charged, however for samples of low charge, samples of high ionic strength or samples in non-polar solvents LDE lacks sensitivity to measure the slow moving particles. In order to measure such samples phase analysis light scattering (PALS) was developed, the PALS experiment allows the measurement of samples with zeta potentials up to 1000 times lower than LDE. In a PALS experiment the reference beam is phase modulated to the phase of the incident beam, the phase shift between the two is then compared with the shift of when no electric field is applied. A phase plot is shown below for an aqueous sample and a non aqueous sample.

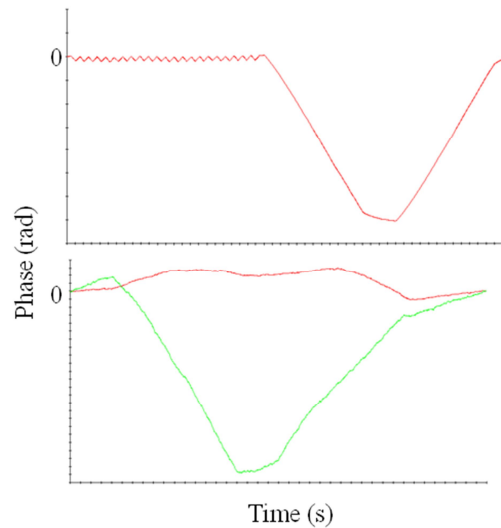


Figure 6-4, phase plot for; a negatively charge aqueous polystyrene latex, top, and a non aqueous PMMA sample with (green) and without (red) charging surfactant (3 wt. % AOT), bottom.

The phase plots between an aqueous sample and non aqueous sample are very different, note in the aqueous sample a long period before the particles are detected compared to the non aqueous sample. The PMMA sample with charging surfactant (in green) is an example of a sample with “good phase” where as the sample without charging surfactant shows “poor phase” and therefore the result could not be trusted.

To convert the electrophoretic mobility to a zeta potential the Henry equation is used:

$$U_e = \frac{2\varepsilon\zeta f(ka)}{3\eta} \quad 6-2$$

Where; U_e , is the electrophoretic mobility, ε , is the dielectric constant, ζ , is the zeta potential, η , is the sample viscosity and $f(ka)$, is known as Henry’s function and relates to the thickness of the electric double layer or the Debye length.⁶

This can be treated by two approximations; the Huckel approximation, that treats all the charges as point charges, or the Smoluchowski approximation, which treats the particles as a flat sheet. In non aqueous systems the Huckel approximation is valid as the particles have a large electric double layer, due to the lack of charge screening from the solvent, so a large Debye length making $f(ka) \gg 0$.

The Malvern ZetaSizer uses an adapted technique called M3-PALS which is a combination of both LDE and PALS.⁷

6.3 Zeta Potential of Spherical Seed Particles

The zeta potential was measured for SRB-131-1 % EGDMA and SRB-288-1 % GDMA to ascertain if there is any appreciable different in the samples due to the polar crosslinking monomer. Figure 6-5 shows SEM images of the particles and Table 6-1 gives the zeta values measured for the two dispersions with the addition of AOT and Span 85.

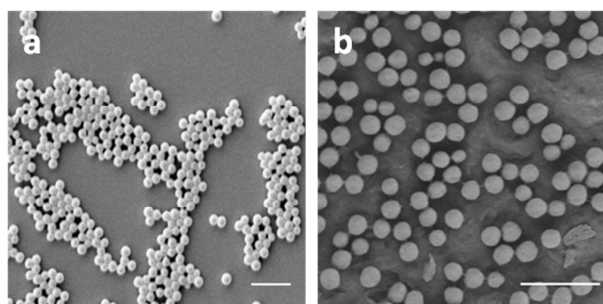


Figure 6-5, SEM images of dispersions, a, SRB-131-1% EGDMA and b, SRB-288-1% GDMA. Scale bars are 2 μm .

Table 6-1, zeta potential data for crosslinked spherical seed particles, run at 20 V.

Sample	Zeta Potential (mV)	
	AOT	Span 85
SRB-131-1% EGDMA	- 96.8	+ 31.8
SRB-288-1% GDMA	- 51.4	+ 44.8

The zeta potential measurements show that both particles are highly charged by the addition of the charging surfactant, but the EGDMA crosslinked sample appears to be more easily negative charged and the GDMA crosslinked sample appears to be more easily charged positively. Experiments were not run with the absence of charging surfactant as the measurement gave a poor phase signal.

6.3.1 Switching Videos for Spherical Seed Particles

The switching videos are a qualitative measurement of particle performance in a display cell. The cells are reused multiple times and as a consequence a measurement of the electrophoretic mobility cannot reliably be obtained by this method. This is because the cells cannot be guaranteed to be perfectly clean and electrode damage cannot be ruled out. Switching videos for SRB-131-1% EGDMA and SRB-288-1% GDMA are shown in Figure 6-6 and Figure 6-7 respectively.

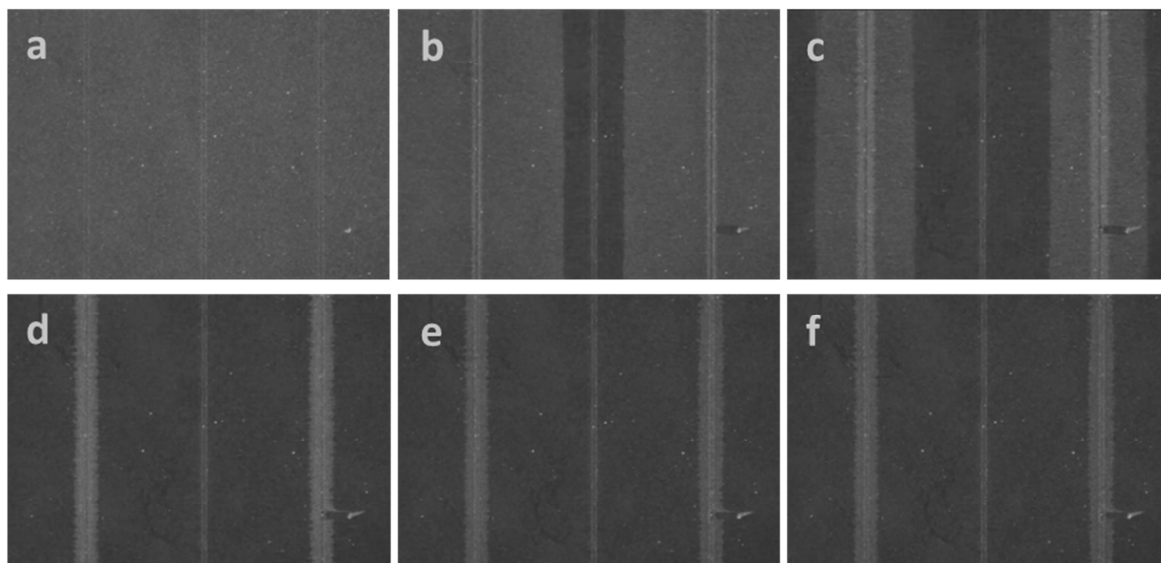


Figure 6-6, still images of particle switching taken at 1 s intervals for SRB-131-1% EGDMA where; a, is at $t = 0$ s, b, is at $t = 1$ s, c, is at $t = 2$ s... Formulation is 3 wt. % particles 3 wt. % AOT charging surfactant and is driven at a 120 V.

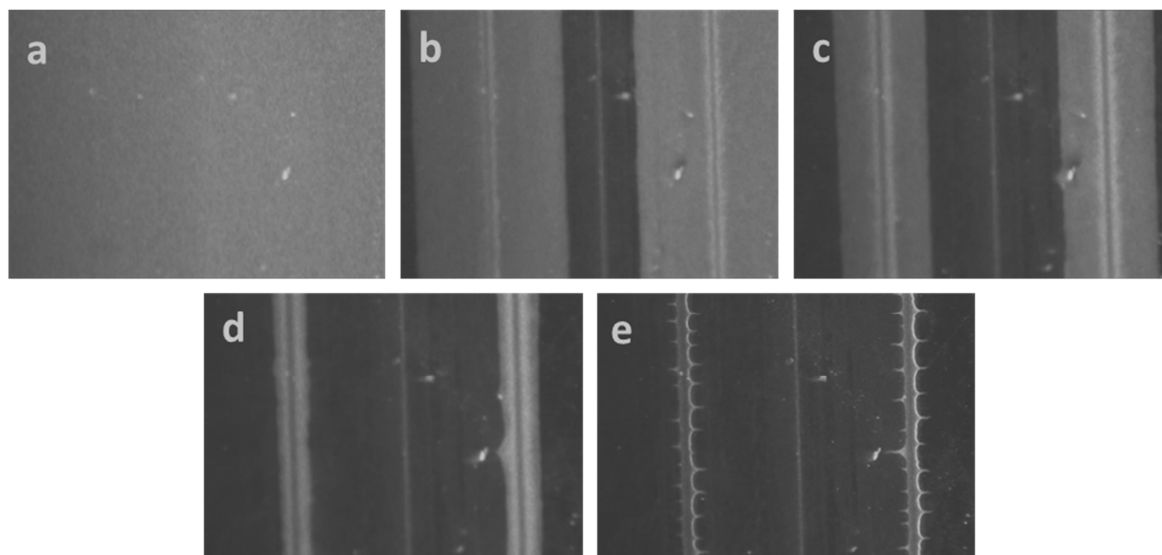


Figure 6-7, still images of particle switching taken at 2 s intervals for SRB-288-1% GDMA where; a, is at $t = 0$ s, b, is at $t = 2$ s, c, is at $t = 4$ s... Formulation is 3 wt. % particles 3 wt. % Span 85 charging surfactant and is driven at a 120 V.

Both samples show clean switching from the electrodes with little adsorption to the cell walls. The main differences between the two samples are that SRB-288-1% GDMA switches slower than SRB-131-1% EGDMA, and SRB-288-1% GDMA shows some build-up of electrohydrodynamic instability at the electrodes. This is shown by the particle build up at the electrode walls rippling, due to the electrical charges on the particles and shown in the still image as ‘spiky’ electrode walls.

6.4 Zeta Potential of Particles with Increasing HEMA Content

The zeta potential of particle dispersions of increasing HEMA content in the second stage polymerisation was measured in this section. SRB-293-HEMA, contains pure HEMA in the second stage reaction so any polymer which has grown from the particle surface must be P(HEMA). The other examples, SRB-344-1 % HEMA and SRB-364-40 % HEMA, contain a copolymer lobe. SEM images of the dispersions are shown in Figure 6-8 and the zeta potential results in Table 6-2 for dispersions with added AOT and Span 85.

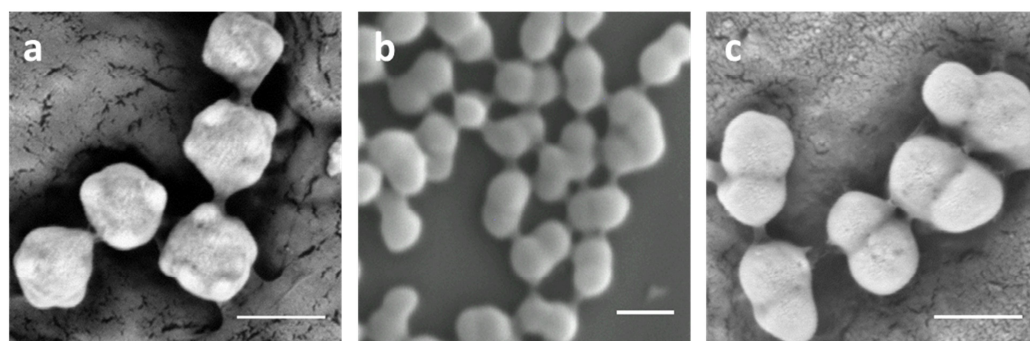


Figure 6-8, SEM images of, a, SRB-344-1 % HEMA, b, SRB-364-40 % HEMA and c, SRB-293-HEMA particles, scale bars are 500 nm.

Table 6-2, zeta potential data for particles of increasing HEMA content, run at 20 V.

Sample	Zeta Potential (mV)	
	AOT	Span 85
<i>SRB-288-1 % GDMA</i>	- 51.4	+ 44.8
SRB-344-1 % HEMA	- 82.1	- 136
SRB-364-40 % HEMA	- 45.5	- 28.0
SRB-293-HEMA	- 70.8	+ 11.9

The zeta potential measurements show good charging with the AOT but Span 85 does not charge the particles to a great extent. Compared to the seed particle dispersion the doublet particles are more highly negatively charged.

However due to the shape of the particles the data cannot be trusted to a great extent. This is because the method by which the zeta potential was measured equates everything to an equivalent spherical particle. As these particles appear as two spheres fused together, the rotational movement of the particles is not isotropic which may lead to unusual scattering events.

6.4.1 Switching Videos for Dumbbell-like Particles

The switching videos show that the particles were charged and moved slower than the spherical precursors SRB-288-1 % GDMA. The particles also appeared to adsorb to the glass cell to a greater extent than the other samples tested in this way.

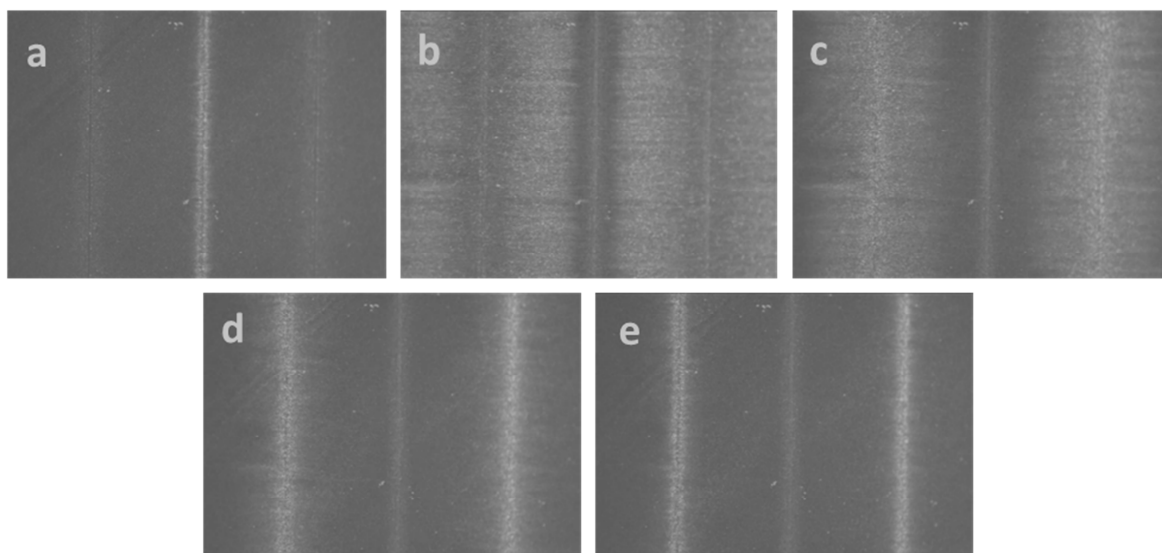


Figure 6-9, still images of particle switching taken at 2 s intervals for SRB-293-HEMA where; a, is at $t = 0$ s, b, is at $t = 2$ s, c, is at $t = 4$ s... Formulation is 3 wt. % particles 3 wt. % Span 85 charging surfactant and is driven at a 120 V.

The sample shows clean switching from the electrodes with adsorption to the cell walls becoming evident in the second pass. This sticking to the glass walls of the electrode could be due to the increased particle interactions with glass due to the hydroxyl groups now present on the particles.

6.5 Zeta Potential of Particles with Increasing HEAm Content

Zeta potential measurements were carried out on dispersions containing 1 wt. % and 40 wt. % HEAm monomer in the second stage polymerisation. SEM images of the particles can be found in Figure 6-10 and the zeta potential data found in Table 6-3.

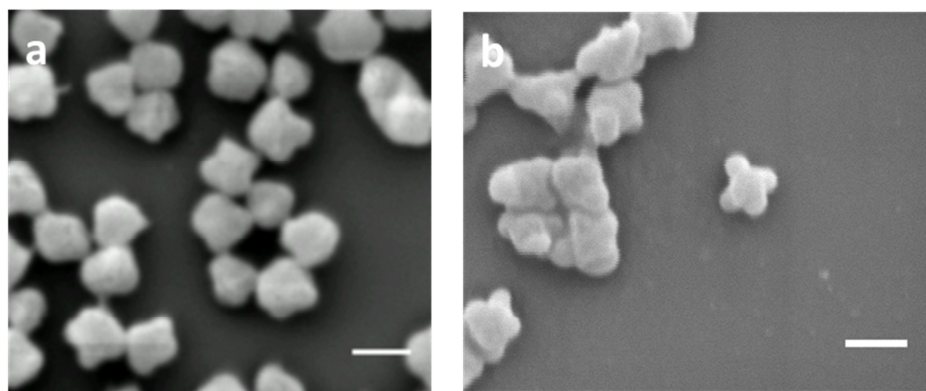


Figure 6-10, SEM images of resultant particles after second stage polymerisation with; a, 1 wt. % HEAm in the monomer feed and b, 40 wt. % HEAm in the monomer feed. Scale bars are 500 nm.

Table 6-3, zeta potential data for particles of increasing HEAm content, run at 20 V.

Sample	Zeta Potential (mV)	
	AOT	Span 85
<i>SRB-288-1 % GDMA</i>	- 51.4	+ 44.8
SRB-382-1 % HEAm	- 90.5	+ 36.1
SRB-395-40 % HEAm	- 48.2	+ 10.7

The zeta potential data shows that both the surfactants charge the particles in the expected way. In all cases the AOT negative charging surfactant gave a large negative charge to the particles. Whereas the Span 85 surfactant only gave a weak positive charge to the 40 % HEAm particles, this result could be due to the increasing non-spherical character of SRB-395-40 % HEAm over SRB-382-1 % HEAm.

No switching videos were obtained for the HEAm series due to time constraints.

6.6 Conclusions

Zeta potential measurements for multiple dispersions were undertaken and it was found that AOT and Span 85 acted in the manner which they were expected for spherical particles, negative zeta potential for AOT and positive for Span 85. The in-plane switching

videos show that the particles produced are able to switch between electrodes without adsorbing too strongly to the electrode or cell walls.

For the non-spherical particles tested the results are unreliable in some cases giving a positive zeta potential and other a negative zeta potential for similar particles and the same surfactant. This may be due to their inherent shape leading to misleading data from the machine and the potential for non-uniform particle charging across the particle. This may be due to the chemical anisotropy of the samples or simply from their shape.

As the charge on the particles is due to the interaction with surfactant reverse micelles if one area on the particle is charged greater than the other, this highly charged patch will align with the electric field, and move to the opposite electrode. However the other charges on the particle surface will also want to align which will cause rotation in the sample. With a sphere is this fine as it is shape isotropic, so all light scattering events will be equal. However for cluster-like and dumbbell-like particles light scattering events will not be even due to the anisotropy of the sample. This may become more complex when one area of the particle is chemically different, as the chemical difference may allow for differences in charge across the particle that may not happen in a particle made of one chemical. This idea of non-uniform charging across a particle is shown in Figure 6-11 below.

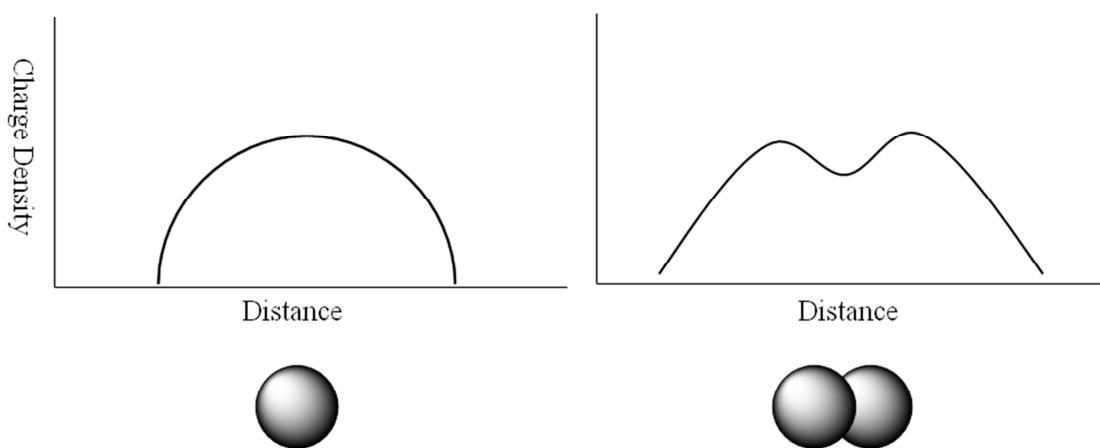


Figure 6-11, schematic view of non-uniform charging.

6.7 References

¹ Merck Chemicals, *Unpublished work*

² G. S. Roberts, R. Sanchez, R. Kemp, T. Wood and P. Bartlett, *Langmuir*, 2008, **24**, 6530

³ R. J. Hunter, '*Foundation of Colloid Science*', Oxford University Press, 2nd Ed., 2001

⁴ R. Finsy, *Adv. Colloid Interface Sci.*, 1994, **52**, 79

⁵ T. Cosgrove, '*Colloid Science - Principles, Methods and Applications*' Wiley, 2nd Ed., 2010

⁶ D. C. Henry, *Proc. R. Soc. London, Ser. A.*, 1931, **133**, 106

⁷ Malvern technical note, MRK654-01, '*Zeta Potential An Introduction in 30 Minutes*'

7 Summary and Further Work

7.1 Introduction

This chapter contains an overall summary of the work done for this project, along with future work which could be used to expand this project further.

7.2 Summary of Work

This thesis outlines a procedure for the first production of shape anisotropic particles in a low dielectric constant medium and preliminary assessment of the particles for electrophoretic display (EPD) applications. These non spherical particles produced can be split into two categories; cluster-like and dumbbell-like particles or doublets. These particles were produced by an inversion of the dynamic swelling method (DSM) based on dumbbell-like particle formation in polar media.¹

The formation of these anisotropic particles required the production of spherical template particles by non aqueous dispersion polymerisation. Optimisation of uncrosslinked particle formation was guided by previous work outlined by Antl *et al.*² and led to the production of highly uniform poly(methyl methacrylate) (PMMA) particles. It was found that the solvent system played an important role in the polymerisation reaction and use of solvent mixtures allowed for greater control of the polymerisation reaction. The DSM utilises crosslinked particles, however formation of uniform crosslinked particles by a batch style non aqueous dispersion polymerisation was problematic due to the mechanism of formation. Optimisation and the use of a pump feed method to produce crosslinked nanoparticles yielded uniform particles with a narrow size distribution (< 13 %), eligible for further study.

In order to produce shape anisotropic particles monomers were selected that interacted favourably with the PMMA seed particles, and less favourably with the dodecane solvent. In order to screen potential monomers the use of Hansen solubility parameters was employed to predict the monomer-particle and monomer-solvent interactions. This led to the selection of two monomers, 2-hydroxyethyl methacrylate (HEMA) and *N*-hydroxyethyl acrylamide (HEAm), these monomers were predicted to lie on and just outside the radius

of interaction for PMMA respectively. Methyl methacrylate (MMA) was selected as a control monomer as it is very close to PMMA in the radius of interaction.

From this monomer choice the ability of the monomer to produce anisotropic particles was modelled based on a system outlined by Waters,³ in which the total interfacial energy of the system is summed revealing the resultant particle morphology based on the mixing of two polymers. This modelling work proposed that intermediate morphologies between that of a core-shell morphology and a separated morphology should arise for the two polar monomers HEMA and HEAm. Although the modelling could not be done for MMA (due to solubility in dodecane) it was assumed that due to the high affinity the monomer has for the polymer that a core-shell morphology would be produced.

The MMA system was first investigated to understand the system for a monomer with favourable interactions with the seed particles. This work showed again that batch style second stage polymerisations do not produce stable dispersions and that the cleanest reactions occur when the monomers are pump fed into the reaction mixture under monomer starved conditions. This was shown to be due to the monomer swelling the seed particles and removing the steric stabiliser from the particle surface, leading to aggregation. when the reaction conditions for the second stage polymerisation were changed by introduction of low levels (1 or 2 wt. % of total monomers) crosslinking monomer then cluster-like morphologies were observed. This was exacerbated by increasing the polarity of the crosslinking monomer, resulting in an increase in the nodule number on the seed particle surface. This phenomenon was exploited further by undergoing sequential polymerisation reactions to grow the nodules leading to highly clustered PMMA cluster-like particles.

Building on the work from the production of PMMA cluster-like particles second stage polymerisations with the polar monomers were undertaken. However the reactions were very unclean giving large amounts of coagulum, this was worse for HEAm than for HEMA. This was determined to be caused by monomer forming droplets in the dodecane, which were stabilised by the P(HSA-*g*-MMA) stabiliser and the seed PMMA particles, and worse for HEAm than HEMA as HEMA interacts more favourably with dodecane than HEAm. To remove this problem the polar monomers were added with MMA, as they are miscible. From studying the resultant particles with increasing polar monomer content it was found that initially cluster-like particles were produced, but with increasing content the number of nodules decreased but their size increased. This occurred until the reaction

produced a single nodule, in the case of HEMA at 40 wt. % in the monomer feed (SRB-364-40% HEMA) giving dumbbell-like particles. For HEAm the point at which one nodule was formed was not found but it was believed to be around 20 wt. % HEAm in the monomer feed. Doublet particle formation was then studied in more detail and it is thought that they are produced by precipitation of monomer to the seed particle surface, and phase separation from polymerisation occurring within the particles. However deconvolution of the two mechanisms could not be achieved but it is thought that precipitation dominates early on in the reaction, giving over to monomer swelling and phase separation later on in the reaction.

As the dumbbell-like particles produced in this work have been produced with a different monomer to that of the seed particle, they are thought to be Janus in nature. Steps toward proving this were taken by two different routes. The first route was to quantify the mixing of the two polymers, PHEMA and PMMA from the seed particle and second stage polymerisation by including reactive fluorescent dyes into each stage. 9-vinylanthracene and 1-vinylnaphthalene were introduced into the seed particles and second stage polymer respectively. Measuring the Förster resonance energy transfer (FRET) of the samples can yield information on particle morphology.⁴ The second route was by the selective reaction of a chlorosilane tag onto the particle surface by the free hydroxyl group from the HEMA monomer. The tag molecule was highly fluorinated to allow detection by EDAX, allowing for element mapping. Unfortunately due to time constraints initial steps were taken for both these routes but neither were completed.

Finally samples were assessed for their EPD applicability, by the measurement of their zeta potential using a Malvern Zetasizer and by producing test switching cells at Merck. It was found that seed particles can be charged uniformly and to levels above what is deemed stable for electrostatic stabilisation in aqueous systems. In test cells the seed particles switched from electrode to electrode smoothly and with little adsorption to the cell walls or electrodes. For the anisotropic particles the charging was problematic owing to the particle morphology deviating from a sphere giving error to the zeta potential measurements. There was also no clear trend for the particle charging for increasing HEMA and HEAm content. This may be due to inaccuracies in the measurement due to particle morphology or non-uniform particle charging from the potential Janus nature of the particles. A sample of dumbbell-like particles were tested in a switching cell and were found to be prone to electrohydrodynamic instabilities, and adsorption to the cell and electrodes. This was

rationalised to be due to increasing polar monomer content leading to increasing interactions with the glass cell walls.

7.3 Further Work

Potential future work for this project include:

- Proving the Janus character of dumbbell-like particles
 - Proof of Janus character of dumbbell-like particles, by chlorosilane coupling.

A large amount of formulation time and testing is still required to selectively react the chlorosilane moiety to the seed particle surface. Obstacles to overcome on this are to chemically attach the P(HSA-g-MMA) stabiliser to the particles surface after the second stage polymerisation to remove methacrylic acid units in the particles and epoxide units in the stabiliser. Then to find the ideal concentration needed to react onto the particle surface without causing aggregation.

- Proof of Janus character of dumbbell-like particles, by FRET.

UV-Vis and fluorescence spectroscopy must be undertaken on the seed particles with dye incorporated to find the concentration needed to get the required signal as a baseline. This must be then undertaken for the dumbbell-like particles to look for a FRET signal.

- Further assessment of particles produced for EPD applications.
 - Further zeta potential testing.

This will include the production of more particles of dumbbell-like morphology and measuring the zeta potential of multiple batches. Building of a library of data in this fashion will allow for greater interpretation of results obtained.

- More in-plane test cell measurements.

This will allow for greater understanding of the particle switching to unequivocally state if particle morphology does play an important role in the electrophoretic mobility.

- Investigating colloidal crystal formation and packing.

It has been shown that ellipsoidal particles can pack with decreased void volume compared to that of spheres,⁵ and assumed this would give a benefit to the contrast ratio of any devices produced. However the link between particle shape and contrast ratio has not been established to the knowledge of the author.

- Production of ‘torpedo-like’ triplet particles by surface initiated controlled radical polymerisation.

The selective surface functionalization with a chlorosilane reagent as explained above could be used to attach an initiator for atom transfer radical polymerisation (ATRP) by reaction of a chlorosilane with a ATRP initiator such as allyl 2-bromo-2-methylpropionate. This initiator should then be bound to one half of the particle. This can then be used to build a third lobe onto the particle surface by a third stage controlled dispersion polymerisation reaction. Much like the methods outlined by Armes *et al.* for aqueous dispersion polymerisation.^{6,7} Controlling this methodology will allow for the production of linear triplet particles or ‘torpedo-like’ particles, with the new third stage lobe size easily controllable by varying monomer concentration.

- Production of dumbbell-particles with HEAm.

It is assumed that the point at which doublet formation may occur is 20 wt. % HEAm in the monomer feed for the second stage reaction. Mapping this out will round off this area of work and will reinforce the proposed reaction mechanism.

- Assessment of particles as novel Pickering stabilisers.

It was noted that the polar second stage monomer can form droplets in the reaction mixture which will be stabilised by the seed particles. Such particles can be used to stabilise oil-water interfaces.⁸ However due to the believed Janus character of the dumbbell-like particles formed, they will have hydrophobic and hydrophilic lobes giving increased stability to any emulsion formed. This could be coupled with increased particle packing at the oil-water interface due to the elliptical quality of the particles.

- Synthesis of thermoresponsive Pickering stabilisers.

These could be produced by adapting the second stage polymerisation to the use of a thermoresponsive monomer. If the second stage polymerisation reaction were to be done

using enough *N*-isopropylacrylamide (NIPAm) to give dumbbell-like particles then a thermoresponsive lobe will be formed. This would allow the triggering of emulsion destabilisation, which may be useful in many industrial applications.

- Further investigation into the shape-dependence of particles on the suppression of the coffee-ring effect.

A recent letter to Nature detailed how the use of ellipsoidal particles can suppress the coffee-ring effect in the drying of droplets.⁹ This has implications in many industries from inkjet printing to agricultural spraying. Inkjet printing studies of formulations of particles of differing morphology produced by the methods outlined in this thesis could be tested.

7.4 References

- ¹ J-W. Kim, R. J. Larsen and D. A. Weitz, *Adv. Mater.*, 2007, **19**, 2005
- ² L. Antl, J. W. Goodwin, R. D. Hill, R. H. Ottewill, S. M. Owens, S. Papworth and J. A. Waters, *Colloids and Surfaces*, 1986, **17**, 67
- ³ J. A. Waters, *Colloid Surface A*, 1994, **84**, 167
- ⁴ M. A. Winnik, H. Xu and R. Satguru, *Makromole. Chem., Macromol. Symp.*, 1993, **70**, 107
- ⁵ Y. Lu, Y. Yin, Z-Y. Li and Y. Xia, *Langmuir*, 2002, **18**, 7722
- ⁶ Y. Li and S. P. Armes, *Angrew. Chem. Int. Ed.*, 2010, **49**, 4042
- ⁷ A. Blanazs, J. Madsen, G. Battaglia, A. J. Ryan and S. P. Armes, *J. Am. Chem. Soc.*, 2011, **133**, 16581
- ⁸ S. U. Pickering, *J. Chem. Soc., Trans.*, 1907, **91**, 2001
- ⁹ P. J. Yunker, T. Still, M. A. Lohr and A. G. Yodh, *Nature*, 2011, **476**, 308

8 Experimental

8.1 List of Materials

Methyl methacrylate (MMA) 99 %, methacrylic acid (MAA) 99%, ethylene glycol dimethacrylate (EGDMA) 98 %, 1,4 butanediol dimethacrylate (BDDMA) 95 %, 1,6 hexanediol dimethacrylate (HDDMA) $\geq 90\%$, glycerol dimethacrylate (GDMA) mixture of isomers 85 %, 3-(acryloyloxy)-2-hydroxypropyl methacrylate (AHPMA), glycerol 1,3-diglycerolate diacrylate (GDGDA) technical grade, 2-hydroxyethyl methacrylate (HEMA) 99+ %, *N*-hydroxyethyl acrylamide (HEAm), *N,N'*-dimethylethanolamine 97 %, 9-vinylanthracene 97 %, 1-vinylnaphthalene 95 %, 2-butanone (MEK) $\geq 99.7\%$, isopropyl alcohol (IPA) $\geq 99.7\%$, sorbitan trioleate (Span 85), dioctyl sodium sulfosuccinate (AOT) 98 %, dodecanethiol $\geq 98\%$, tetrahydrofuran (THF) HPLC grade, butyl acetate HPLC grade, dodecane $\geq 99\%$, and hexane HPLC grade, were all bought from Aldrich.

2,2'-Azobis(2-methylbutyronitrile (Vazo-67) radical initiator was from DuPont and the PHSA-g-MMA stabiliser was supplied by Merck Chemicals as a solution at 30 wt. % in ethyl acetate / butyl acetate 1:1 (w/w) mixture for this project.

All chemicals were used as received.

8.2 Characterisation Techniques

8.2.1 Nuclear Magnetic Resonance (NMR)

All ^1H experiments were run on a Bruker Ultrashield 400 MHz spectrometer. With the chemical shifts, δ , quoted in parts per million (ppm) down-field from tetramethylsilane. Splitting patterns are abbreviated as follows: singlet (s), doublet (d), triplet (t), quartet (q), multiplet (m), or a combination of these.

8.2.2 Total Solids Content (TSC) and Monomer Conversion

TSC was measured by weight loss upon drying until no change in weight was observed. This was typically done on 0.5 g of dispersion by placing the sample into a pre-tared aluminium pan. Once the sample was added it was covered with a pierced foil lid and put

into a vacuum oven close to the boiling point of the solvent. To remove random error each value quoted is an average of three tests.

8.2.3 Gel Permeation Chromatography (GPC)

Gel permeation chromatography was carried out in THF using a Viscotek GPCmax VE2001 solvent / sample module with 2 x PL gel 10 μ m Mixed-B and PL gel 500A columns, a Viscotek VE3580 RI detector and a VE 3240 UV/Vis multichannel detector. The flow rate was 1 mL/min and the system was calibrated with low polydispersity poly(methyl methacrylate) standards in the range of 200 to 180 \times 10⁴ g/mol from Polymer Laboratories. The analysed samples contained n-dodecane as a flow marker.

Gel permeation chromatography was carried out in Aqueous conditions using two columns, TSK gel 5000 and TSK gel 6000. The solvent system was 0.1 M citric acid solution containing 1% azide as anticoagulant. The flow rate was 1 mL/min, and the detector was an ERCn7515A DR detector.

Gel permeation chromatography carried out in dimethylacetamide (DMA) using two PL 2x Mixed-B and a 500 Å column. The solvent system was DMA with 1 % lithium nitrate and 1 % azide anticoagulant. The flow rate was 1 mL/min, and the detector was an ERCn7515A DR detector.

The average molecular weight of a polymer is typically expressed as the number average molecular weight, M_n , or the weight average molecular weight, M_w . Which are expressed in equations 8-1 and 8-2 below:¹

$$M_n = \frac{\sum M_i N_i}{\sum N_i} \quad 8-1$$

$$M_w = \frac{\sum M_i^2 N_i}{\sum M_i N_i} \quad 8-2$$

Where, N_i is the number of molecules of i of molecular weight M_i .

The polydispersity index of a polymer indicates the degree of the distribution of polymer chains and is given by the following equation:

$$PDI = M_w / M_n \quad 8-3$$

8.2.4 Particle Size and Zeta Potential Measurements

Carried out using a ZetaSize nano series from Malvern Instruments, samples were added to a 10 mm quartz glass cuvette for analysis and run at 25 °C. The machine is fitted with a back scattering detector at 173° from an incident laser source (He-Ne laser with wavelength 632.8 nm).²

All solutions tested were formulated to be 3 wt. % dispersion and 3 wt. % surfactant in dodecane; this was then allowed to mix for at least 30 min before measurement. For in-plane switching videos one drop of this dispersion was added to the switching cell. For zeta potential measurement three drops of the dispersion was added to 1.2 g of dodecane and allowed to mix for 30 min. prior to measurement.

In all DLS experiments the CONTIN algorithm was used to deconvolute the scattered light signal to give the size distribution.

8.2.5 In-plane Switching Videos

In-plane switching videos were produced at Merck Chemicals with their specialist equipment. The in-plane switching cells consist of a glass slide treated with indium tin oxide, ITO, to give transparent conductive channels each 5 µm in diameter and equally spaced 50 µm apart, as shown in Figure 8-1. This ITO treated glass is then sandwiched together with a plain piece of microscope glass and clamped together. One drop of the dispersion was added to the side of the cell and capillary interactions drove the fluid to coat the glass. The sample was then imaged using an optical microscope with a x5 objective lens.

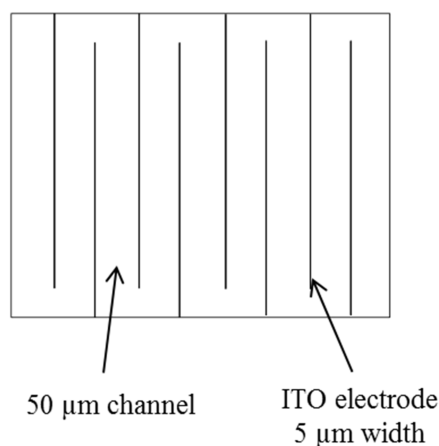


Figure 8-1, schematic view of in-plane switching cell, produced at Merck Chemicals.

All the zeta potential values quoted are for samples with “good phase signal” and therefore should be reliable results; however questions about the reliability of the measurement remain, due to the non-spherical nature of the particles.

8.2.6 Scanning Electron Microscopy (SEM) Imaging of Samples

SEM imaging was run on multiple machines; LVEM5 from DeLong Instruments, Phillips FEGXL30 SEM and a Cambridge S360 SEM. Particle size was obtained by using ImageJ sizing software.

Samples were diluted in hexane and drop cast directly onto the SEM sample stub in the case of use of the LVEM5. In the case of the other microscopes silicon wafer was mounted onto the SEM stub with carbon tape and the diluted dispersion was drop cast onto the wafer.

All samples were sputter coated with gold prior to imaging.

8.2.7 Thermal Gravimetric Analysis (TGA)

TGA measurements were run on a TA Instruments, TGA Q5000. Typically 10 – 15 mg of solid dried sample was added to a platinum-HT pan and heated to the required temperature at 10 °C per min., under a nitrogen atmosphere.

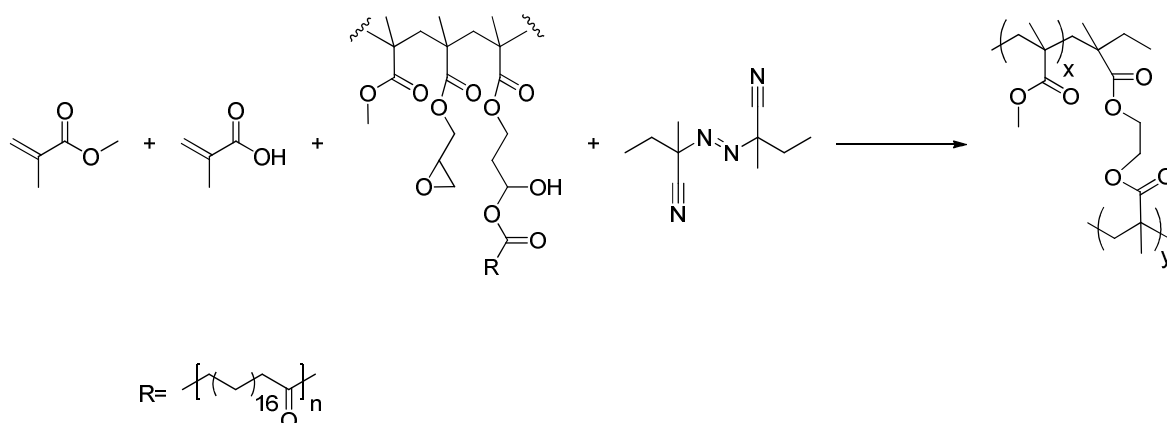
8.2.8 Differential Scanning Calorimetry (DSC)

DSC measurements were recorded using a Perkin Elmer Jade DSC instrument under nitrogen atmosphere, 5–10 mg of the sample was sealed in an aluminium pan with a crimping tool. The sample was heated from 30 °C to 150 °C at a heating rate of 10 °C/min, held for 2 minutes at 150 °C and then cooled to 30 °C at a rate of 10 °C/min. This cycle was repeated once.

8.3 Synthetic Procedures

8.3.1 Formation of Uncrosslinked Spherical Particles

All reactions to produce uncrosslinked particles followed this method unless otherwise stated, and is exemplified by SRB-077-0% xl.



Scheme 1.

MMA (10.63 g, 0.106 mol), MAA (0.21 g, 0.002 mol), PHSA-g-MMA stabiliser (1.75 g), Vazo-67 (0.21 g, 0.001 mol), dodecanethiol (0.43 g, 0.002 mol), dodecane (5.14 g, 0.003 mol) and hexane (10.28 g, 0.119 mol) were added to a round bottom flask fitted with a condenser. This mixture was degassed by nitrogen bubbling for approximately 30 min. while stirred. Once degassed the reaction mixture was heated rapidly to 85 °C by immersing into an oil bath at temperature. The reaction was allowed to proceed for 2 hours upon which the resultant particle dispersion was cleaned by passing through tightly packed glass wool and then centrifuged into fresh hexane three times then finally into a solvent mixture of hexane / dodecane in a 1:1 ratio (w/w).

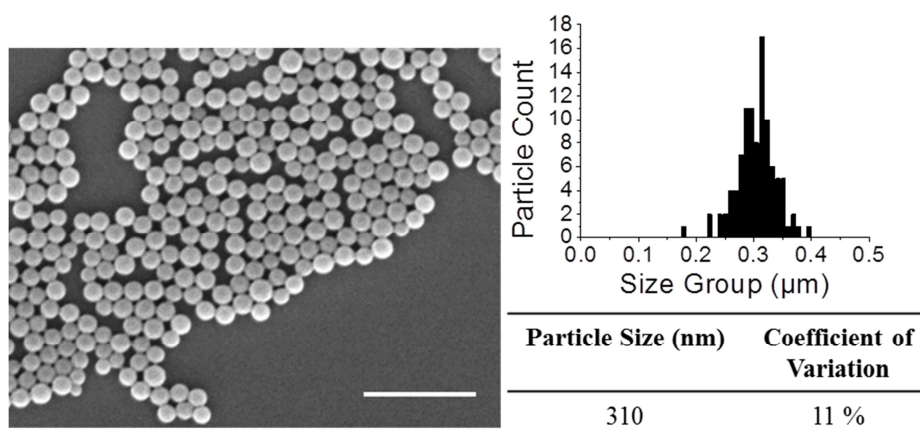
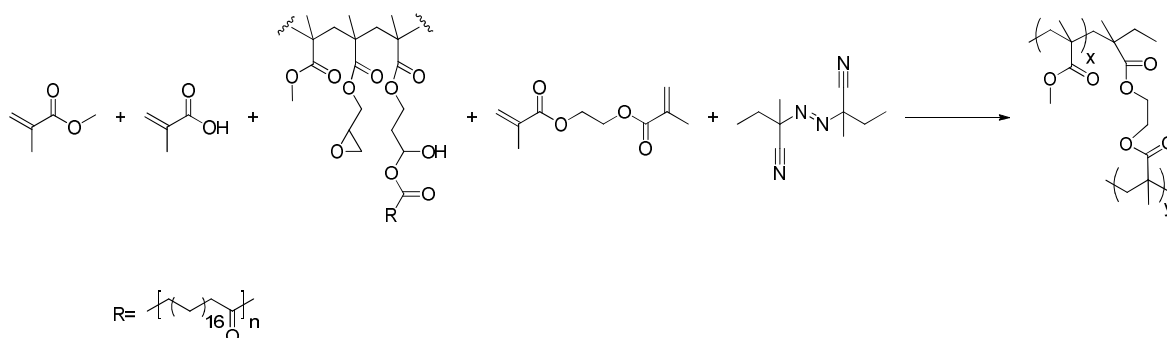


Figure 8-2, SEM image, particle size distribution and particle size data for SRB-077-0% xl. Scale bar is 2 μm, based on counting 100 particles.

8.3.2 Formation of Crosslinked Spherical Particles

All reactions to produce crosslinked particles followed this method unless otherwise stated, and is exemplified by SRB-131-1% EGDMA.



Scheme 2.

Vazo-67 (0.21 g, 0.001 mol), dodecanethiol (0.43 g, 0.002 mol), MMA (10.63 g, 0.106 mol), MAA (0.21 g, 0.002 mol), PHSA-g-MMA stabiliser (1.75 g), dodecane (5.14 g, 0.003 mol) and hexane (10.28 g, 0.119 mol) were added to a round bottom flask fitted with a condenser. This mixture was degassed by nitrogen bubbling for approximately 30 min. while stirred. Once degassed the reaction mixture was heated rapidly to 85 °C by immersing into an oil bath at temperature. The reaction mixture was heated for 1 min. before the monomer feed was added, EGDMA (0.21 g, 0.001 mol), dodecane (0.5 g, 0.003 mol) and hexane (1.0 g, 0.012 mol) by peristaltic pump (Watson-Marlow 205) so that the charge was added over a 20 minute period. The reaction was allowed to proceed for 2 hours upon which the resultant particle dispersion was cleaned by passing through

tightly packed glass wool and then centrifuged into fresh hexane three times then finally into a solvent mixture of hexane / dodecane in a 1:1 ratio (w/w).

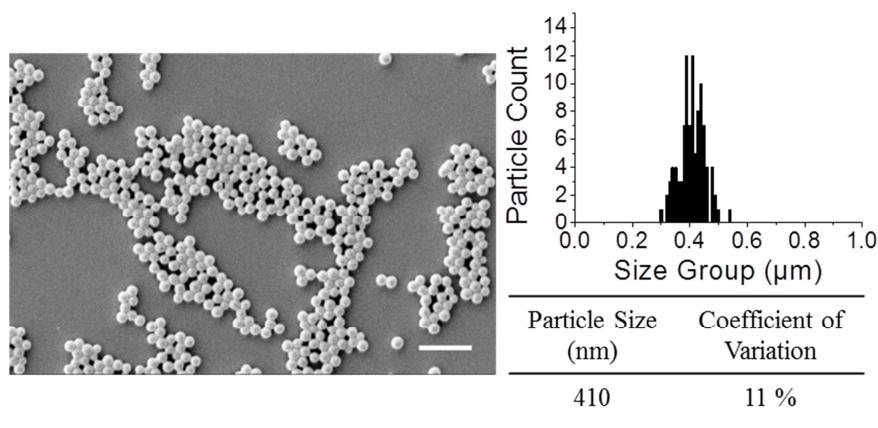
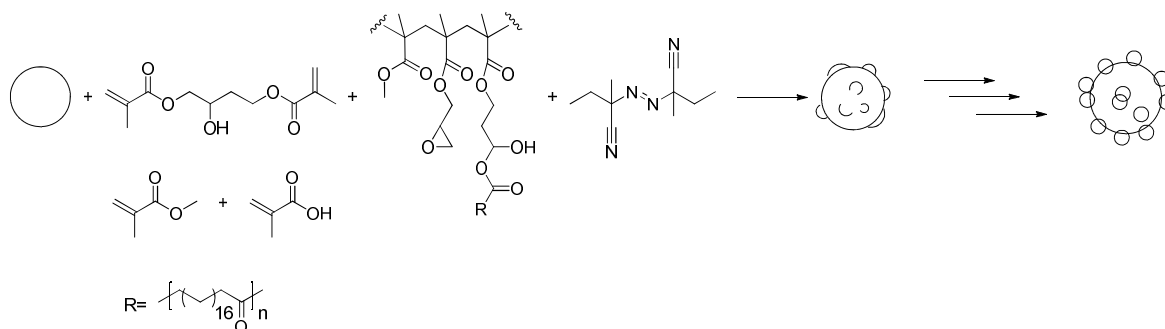


Figure 8-3, SEM image, particle size distribution and particle size data for SRB-131-1% EGDMA. Scale bar is 2 μm, based on counting 100 particles.

8.3.3 Seeded Non Aqueous Dispersion Polymerisation: Toward Different Particle Morphologies

8.3.3.1 Formation of Cluster-like Particles

All reactions to produce cluster-like particles followed this method unless otherwise stated, and is exemplified by SRB-210-1% GDMA.



Scheme 3.

A seed particle dispersion (5.0 g) was taken and the solids content adjusted to 10 wt. % by centrifugation and dispersed into a solvent mixture of hexane\ dodecane (1:1, w/w), this was added to a round bottom flask along with the Vazo-67 (0.01g, 0.0001 mol) and dodecanethiol (0.02 g 0.0001 mol). This was then heated rapidly to 85 °C and left to stir for 2 min. to allow for solvent reflux. After which the monomer feed, GDMA (0.02 g,

0.0001 mol), MMA (1.89 g, 0.189 mol), MAA (0.04 g, 0.0005 mol), PHSA-g-MMA stabiliser (0.6 g), dodecane (0.075 g, 0.0004 mol) and hexane (0.075 g, 0.0009 mol), was added by peristaltic pump (Watson-Marlow 205) over the course of 20 min. to the reaction flask. The reaction was allowed to proceed for 2 hours upon which the resultant particle dispersion was cleaned by passing through tightly packed glass wool and then centrifuged into fresh hexane three times then finally into a solvent mixture of hexane / dodecane in a 1:1 ratio (w/w).

In the case of multiple growth steps the second stage polymerisation step was repeated until the desired particle morphology was obtained.

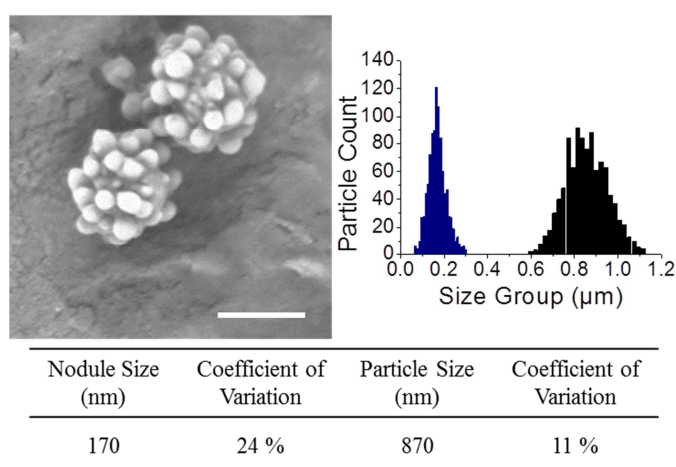
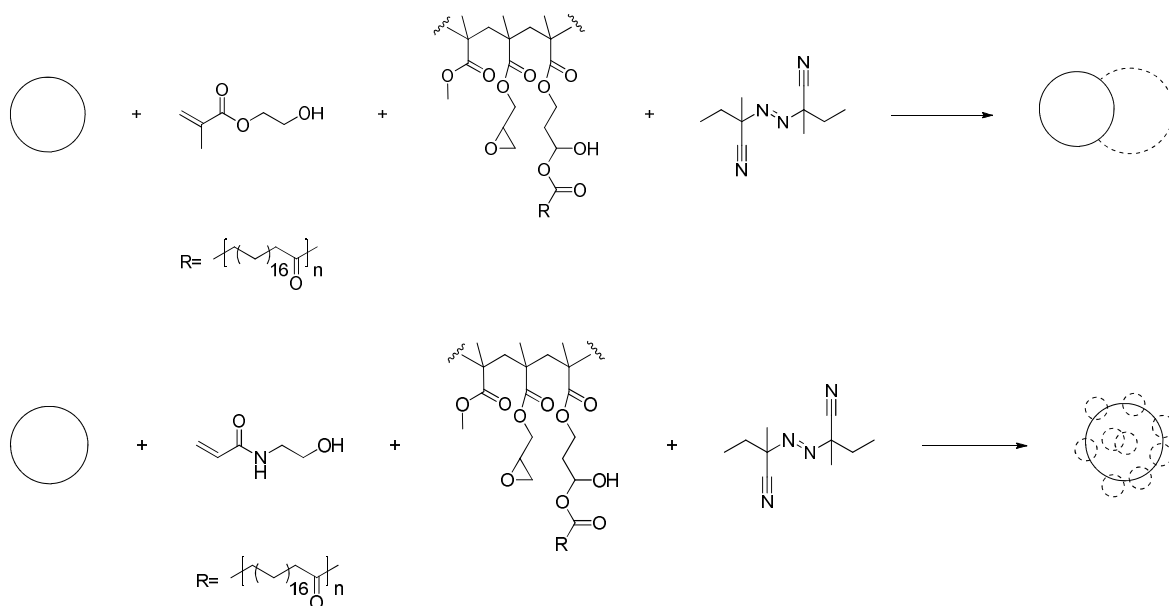


Figure 8-4, SEM image, particle size distribution and particle size data for SRB-210-1% GDMA after three subsequent second stage polymerisation reactions. Scale bar is 2 μm , based on counting 1000 particles, blue shows nodule distribution.

8.3.3.2 Formation of Shape and Chemical Anisotropic Particles at 40 wt. % Polar Monomer

All reactions to produce doublet-like particles followed this method unless otherwise stated, and is exemplified by SRB-364-40% HEMA. All reactions to produce chemically anisotropic clusters-like particles followed this method unless otherwise stated, and is exemplified by SRB-395-40% HEAm.



Scheme 4.

A seed particle dispersion (5.0 g) was taken and the solids content adjusted to 10 wt. % by centrifugation and dispersed into a solvent mixture of hexane \ dodecane (1:1, w/w), this was added to a round bottom flask along with the Vazo-67 (0.01g, 0.0001 mol) and dodecanethiol (0.02 g 0.0001 mol). This was then heated rapidly to 85 °C and left to stir for 2 min. to allow for solvent reflux. After which the monomer, HEMA (0.78 g, 0.006 mol), or HEAm (0.78 g, 0.007 mol) MMA (1.89 g, 0.189 mol), MAA (0.04 g, 0.0005 mol), PHSA-g-MMA stabiliser (0.6 g), dodecane (0.075 g, 0.0004 mol) and hexane (0.075 g, 0.0009 mol), feed was added by peristaltic pump (Watson-Marlow 205) over the course of 20 min. to the reaction flask. The reaction was allowed to proceed for 2 hours upon which the resultant particle dispersion was cleaned by passing through tightly packed glass wool and then centrifuged into fresh hexane three times then finally into a solvent mixture of hexane / dodecane in a 1:1 ratio (w/w).

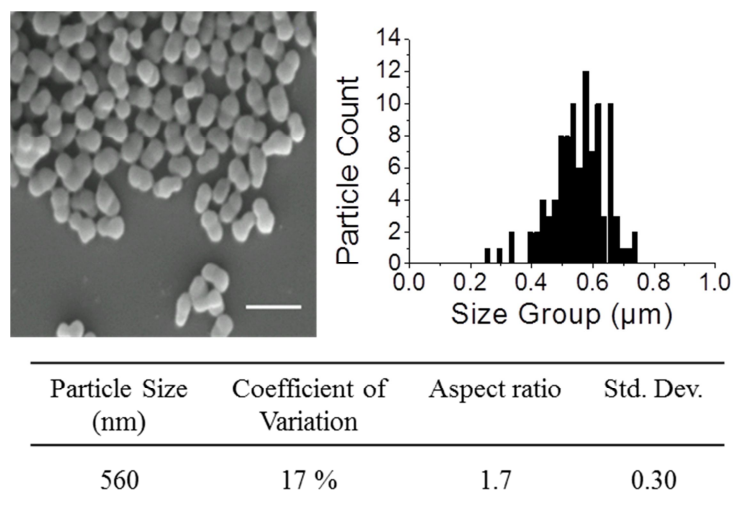


Figure 8-5, SEM image, particle size distribution and particle size data for SRB-364-40% HEMA. Scale bar is 1 μm , based on counting 100 particles.

8.3.4 “Locking on” of Physisorbed Polymeric Stabiliser

Exemplified by SRB-389-1% GDMA-locked on.

Seed dispersion (20 g) was taken and adjusted to 30 wt. % total solid content; this was then added to a 50 ml 2 neck round bottom flask. The particle dispersion was added to a hot oil bath at 120 °C, upon refluxing 0.2 % of the dispersion mass of *N,N'*-dimethylethanolamine (0.04 g, 0.0006 mol) was added to the flask by injection. This was kept at temperature for 2 hours to allow the reaction of the acid within the particle with the epoxide groups on the stabiliser. The particle dispersion was then allowed to cool and cleaned by passing through tightly packed glass wool and then centrifuged into fresh hexane three times then finally into a solvent mixture of hexane / dodecane in a 1:1 ratio (w/w).

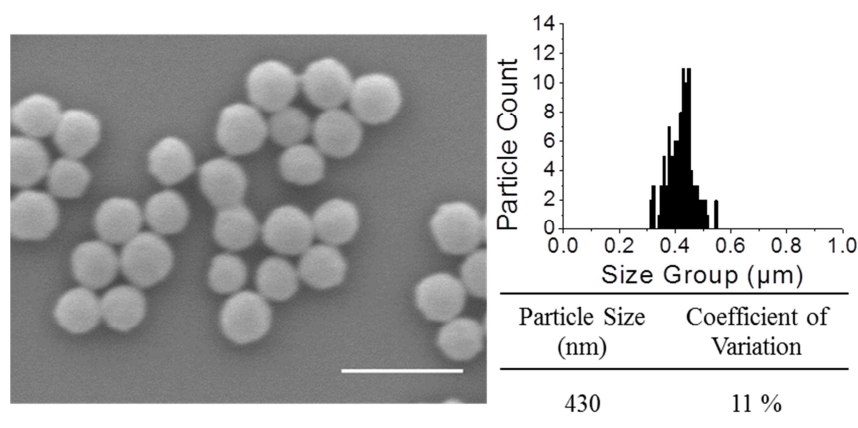
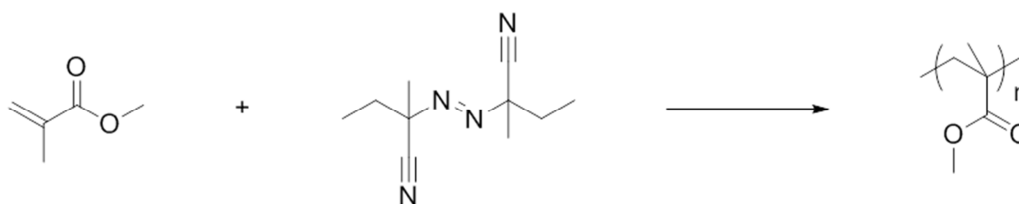


Figure 8-6, SEM image, particle size distribution and particle size data for SRB-389-1% EGDMA – locked on. Scale bar is 1 μm, based on counting 100 particles.

8.3.5 Synthesis of Polymers for Modelling Studies by Solution Polymerisation

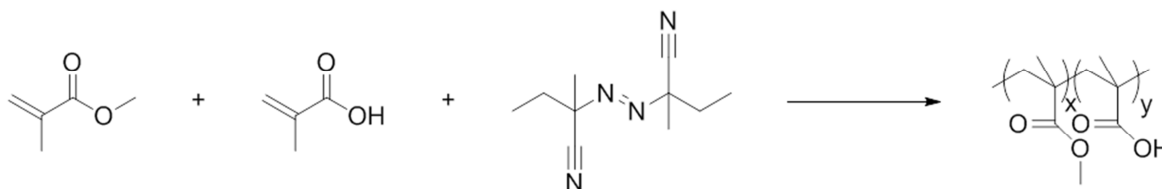
8.3.5.1 Synthesis of Poly(methyl methacrylate) (PMMA)



Scheme 5.

Vazo-67 (0.4 g, 0.002 mol) was weighed into a 250 ml round bottom flask fitted with a condenser; to this methyl methacrylate (20.0 g, 0.2 mol) and the butyl acetate (50.0 g, 0.43 mol) solvent were added. The reaction flask was then heated to 85 °C and allowed to polymerise for 3 hours. The resultant polymer was purified by precipitation into cold hexane.

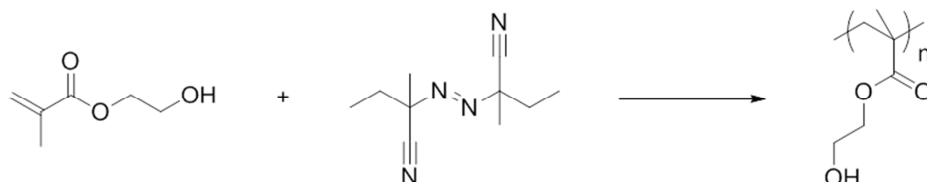
8.3.5.2 Synthesis of Poly(methyl methacrylate-co-methacrylic acid) (P(MMA-co-MAA))



Scheme 6.

Vazo-67 (0.4 g, 0.002 mol) was weighed into a 250 ml round bottom flask fitted with a condenser; to this methyl methacrylate (20.0 g, 0.2 mol) and methacrylic acid (0.4 g, 0.005 mol) and the butyl acetate solvent (50.0 g, 0.43 mol) were added. The reaction flask was then heated to 85 °C and allowed to polymerise for 3 hours. The resultant polymer was purified by precipitation into cold hexane.

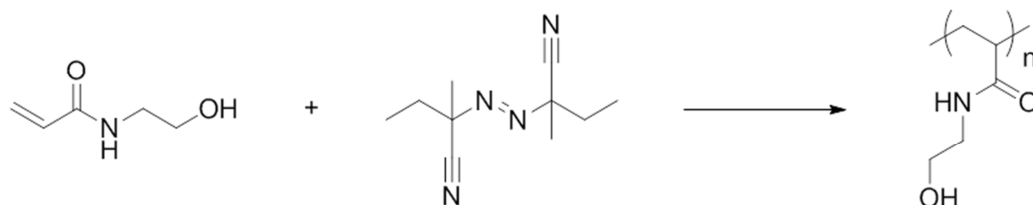
8.3.5.3 Synthesis of Poly(2-hydroxyethyl methacrylate) (PHEMA)



Scheme 7.

Vazo-67 (0.2g, 0.001 mol) was weighed into a 250 ml round bottom flask fitted with a condenser; to this 2-hydroxyethyl methacrylate (20.0 g, 0.154 mol) and a solvent mixture of 70:30 v/v 2-butanone (MEK) (38.5 g, 0.641) and isopropyl alcohol (IPA) (16.5 g, 0.275 mol) were added. The reaction flask was then heated to 85 °C and allowed to polymerise for 3 hours. The resultant polymer was purified by precipitation into cold hexane.

8.3.5.4 Synthesis of Poly(*N*-hydroxyethyl acrylamide) (PHEAm)

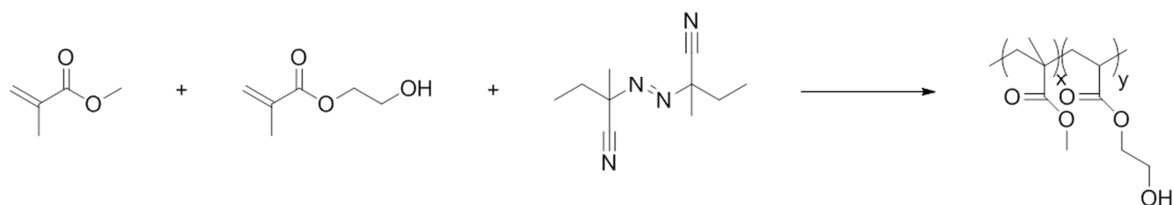


Scheme 8.

Vazo-67 (0.2 g, 0.001 mol) was weighed into a 250 ml round bottom flask fitted with a condenser; to this *N*-hydroxyethyl acrylamide (20.0 g, 0.174 mol) and a solvent mixture of 70:30 v/v 2-butanone (MEK) (38.5 g, 0.641) and isopropyl alcohol (IPA) (16.5 g, 0.275 mol) were added. The reaction flask was then heated to 85 °C and allowed to polymerise for 3 hours. The resultant polymer was purified by precipitation into cold hexane.

8.3.5.5 Synthesis of Poly(methyl methacrylate-co-2-hydroxyethyl methacrylate) *P*(MMA-co-HEMA) of Differing Composition

Example given is solution polymerisation of MMA: HEMA in a 9:1 ratio.



Scheme 9.

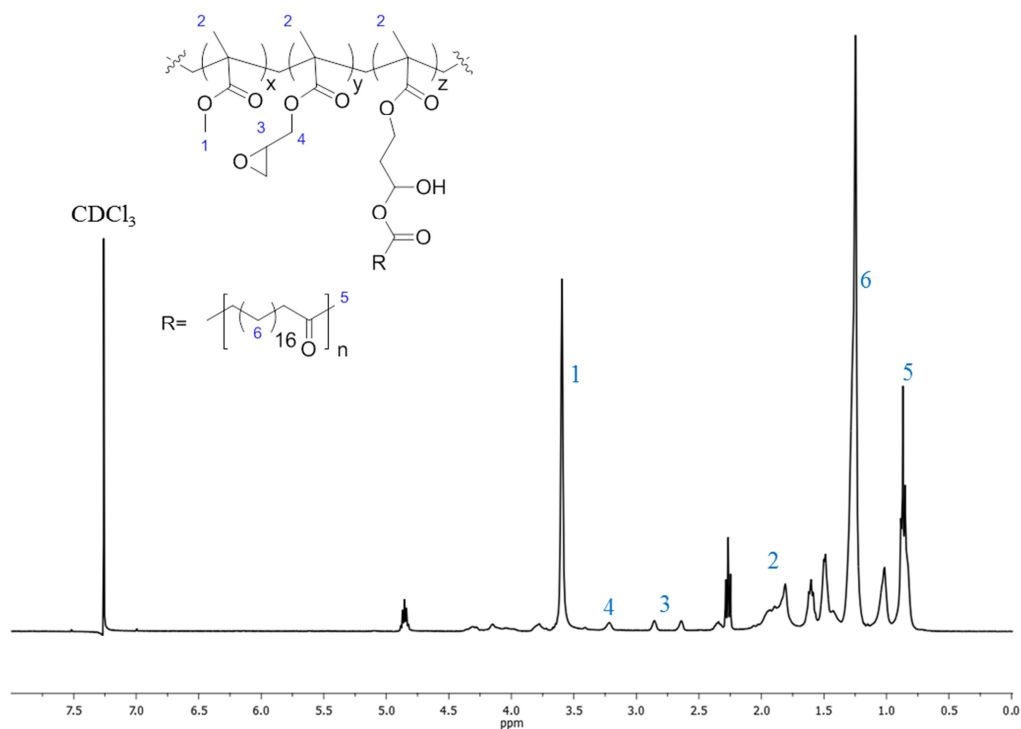
Vazo-67 (0.1 g, 0.0005 mol), methyl methacrylate (9.0 g, 0.09 mol) and 2-hydroxyethyl methacrylate (1.0 g, 0.008 mol) in 9:1 ratio and the solvent mixture (MEK / IPA 70:30), MEK (33.81 g, 0.563 mol), IPA (14.15 g, 0.235 mol), were weighed into a 100 ml round bottom flask and heated to 85 °C. The mixture was allowed to polymerise for 3 hours, to give statistical copolymers.

Table 8-1, chemicals used in the synthesis of P(MMA-*co*-HEMA) at various ratios.

Chemical	90:10		80:20		60:40		50:50	
	Amount (g)	Moles						
Vazo-67	0.1	0.0005	0.1	0.0005	0.1	0.0005	0.1	0.0005
MEK	33.81	0.563	33.81	0.563	33.81	0.563	33.81	0.563
IPA	14.15	0.235	14.15	0.235	14.15	0.235	14.15	0.235
MMA	9.0	0.090	8.0	0.080	6.0	0.060	5.0	0.050
HEMA	1.0	0.008	2.0	0.015	4.0	0.031	5.0	0.038

8.4 Characterisation of P(HSA-*g*-MMA) Polymeric Stabiliser

The stabiliser for this project was supplied by Merck Chemicals and was a graft copolymer of poly(hydroxystearic acid) and poly(methyl methacrylate-*co*-glycidyl methacrylate) which acts as a comb-like polymeric stabiliser. The poly(hydroxystearic acid) acts as the comb-like region of the polymer extending to the hydrocarbon solvent while as the poly(methyl methacrylate-*co*-glycidyl methacrylate) main chain physisorbs to the PMMA particles surface which precipitate from the solvent.³ The glycidyl methacrylate was present to allow for covalent attachment of the stabiliser to the particle surface by an acid / epoxide reaction with the methacrylic acid in the particle.

8.4.2 ^1H NMR SpectraFigure 8-9, ^1H NMR spectra of the P(HSA-g-PMMA) stabiliser run in CDCl_3 .

^1H -NMR (400 MHz, CDCl_3): $\delta = 3.57$ (s, 3H), $\delta = 3.19$ (s, 2H), $\delta = 2.83$ (s, 1H), $\delta = 2.63$ (s, 1H), $\delta = 1.92$ - 1.78 (m, 3H), $\delta = 1.22$ (s, 32H), $\delta = 0.843$ (s, 3H).

8.4.3 Thermal Characteristics

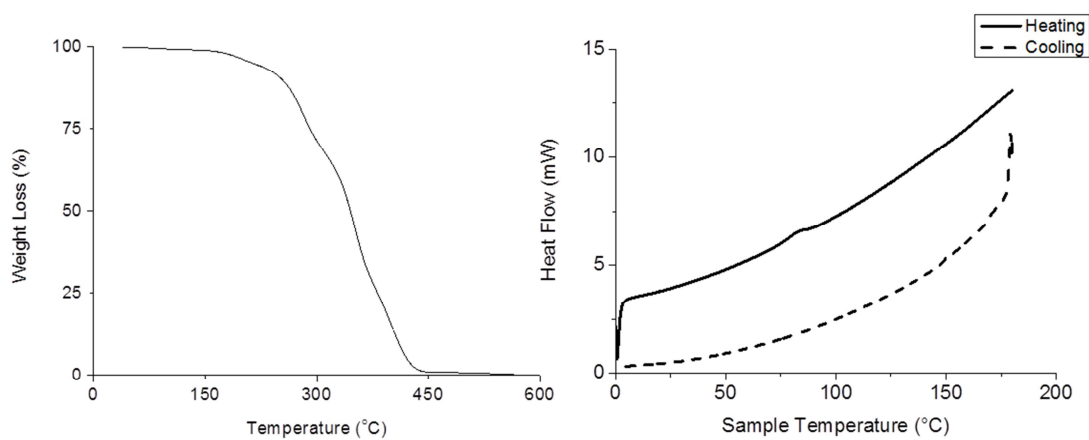


Figure 8-10, TGA (left) and DSC (right) traces for P(HSA-g-PMMA) stabiliser.

The DSC data shows a slight peak at 80 °C; this could be the glass transition temperature, T_g , of the PMMA back bone in the polymer. As this has a low molecular weight compared to the molecular weight of the poly(hydroxyesteric acid) it is hidden in the spectrum. The T_g of PMMA is known to be approximately 100 °C but is dependent upon the molecular weight and environment of the sample. The PMMA may have a low molecular weight and is surrounded by liquid poly(hydroxyesteric acid) chains which allows for increase heat transfer in the sample lowering the molecular weight.

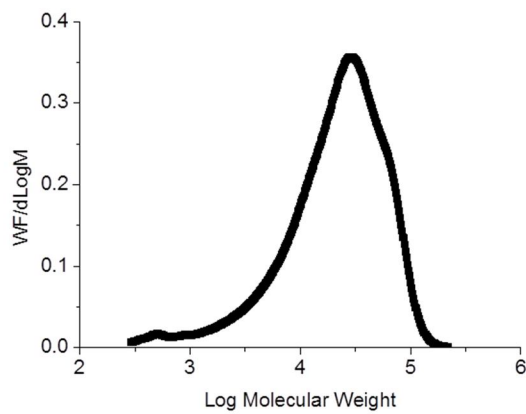
8.5 References

- ¹ P. J. Flory, *Principles of Polymer Chemistry*, Cornell University Press, 1971
- ² Malvern Instruments, *Technical Pamphlet – Zeta Sizer Nano*, 2010
- ³ K. E. J. Barrett, *Dispersion Polymerisation in Organic Media*, Wiley, 1975

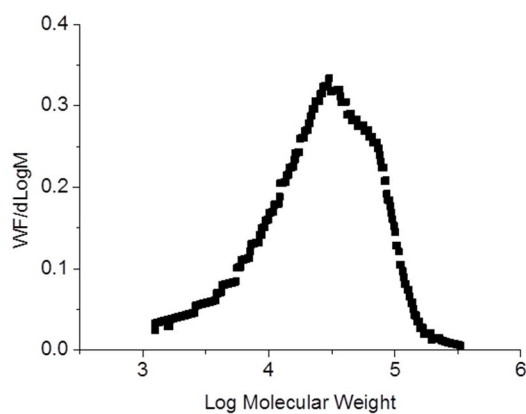
9 Appendices

9.1 GPC Traces for Modelling Polymer Substrates

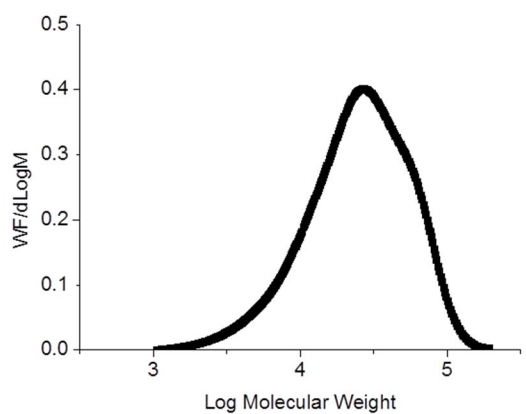
9.1.1 PMMA-28 *KDa*



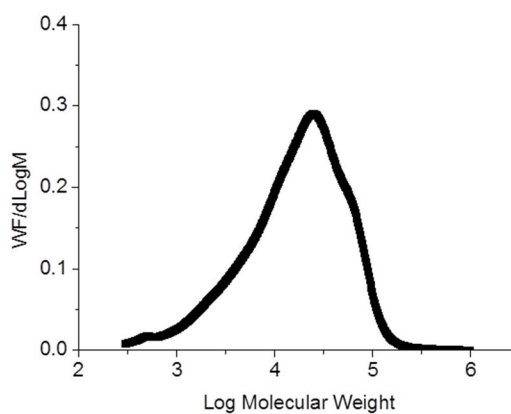
9.1.2 PMMA-35 *KDa*



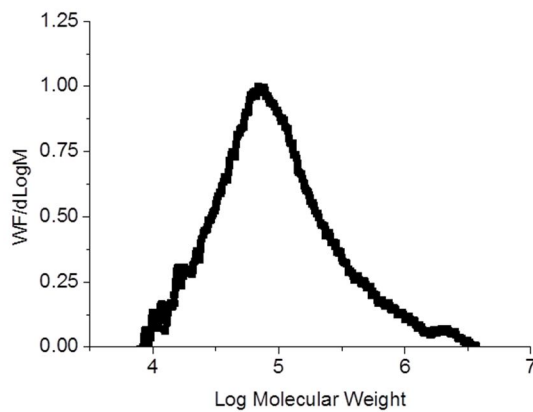
9.1.3 P(MMA₉₈-MAA₂)



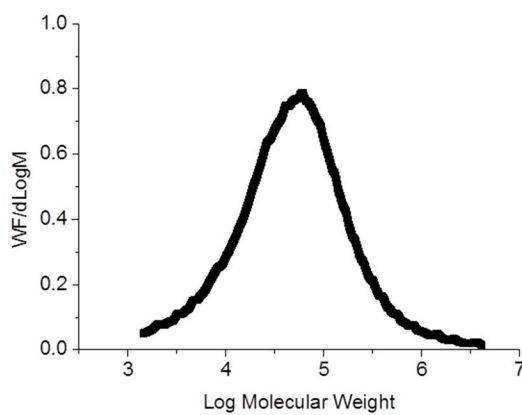
9.1.4 P(MMA₉₈-MAA₂)-stabiliser



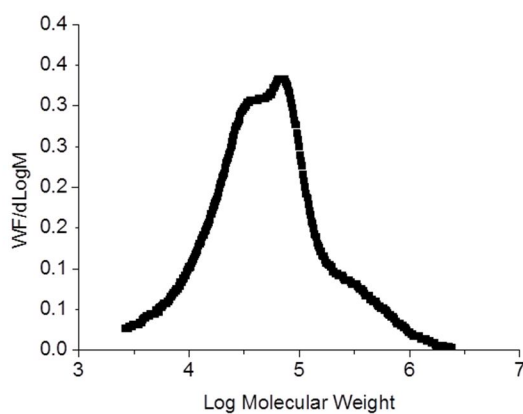
9.1.5 PHEMA



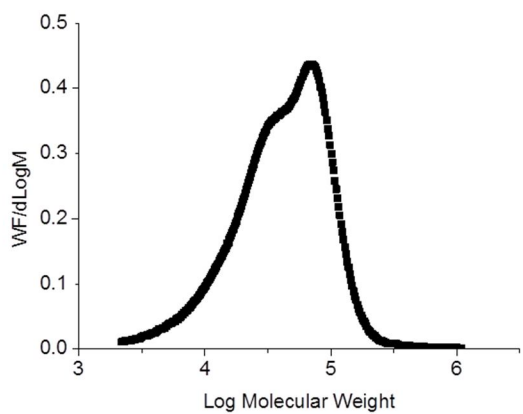
9.1.6 PHEAm



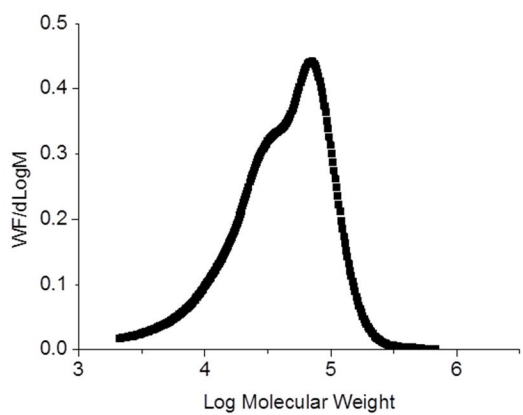
9.1.7 P(MMA₉₀-co-HEMA₁₀)

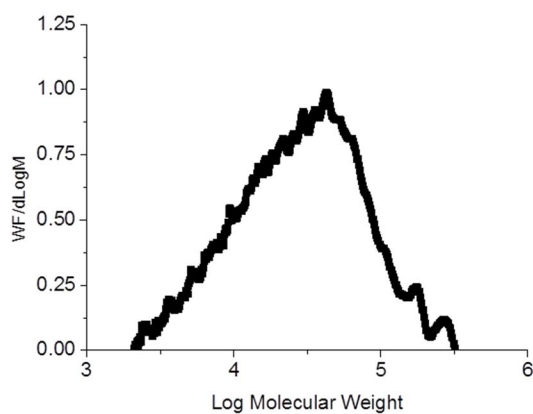
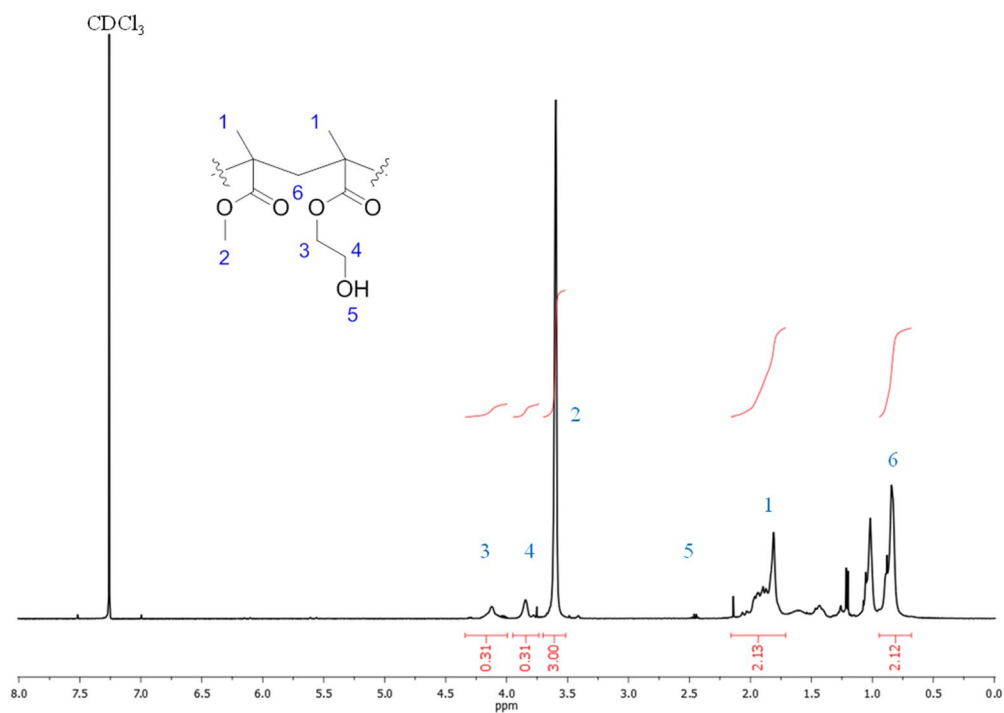


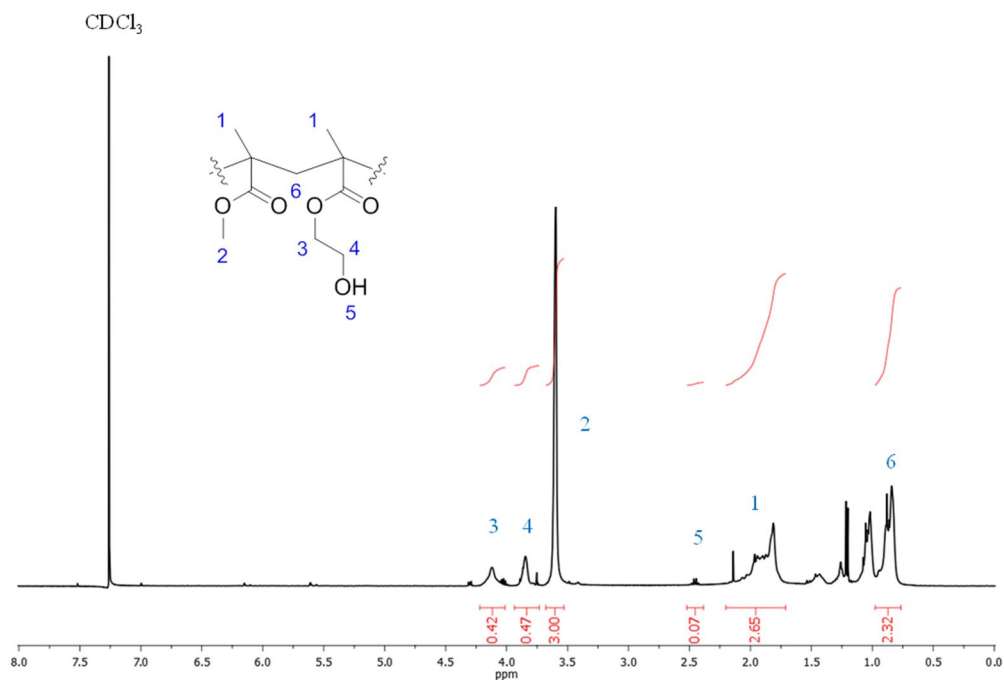
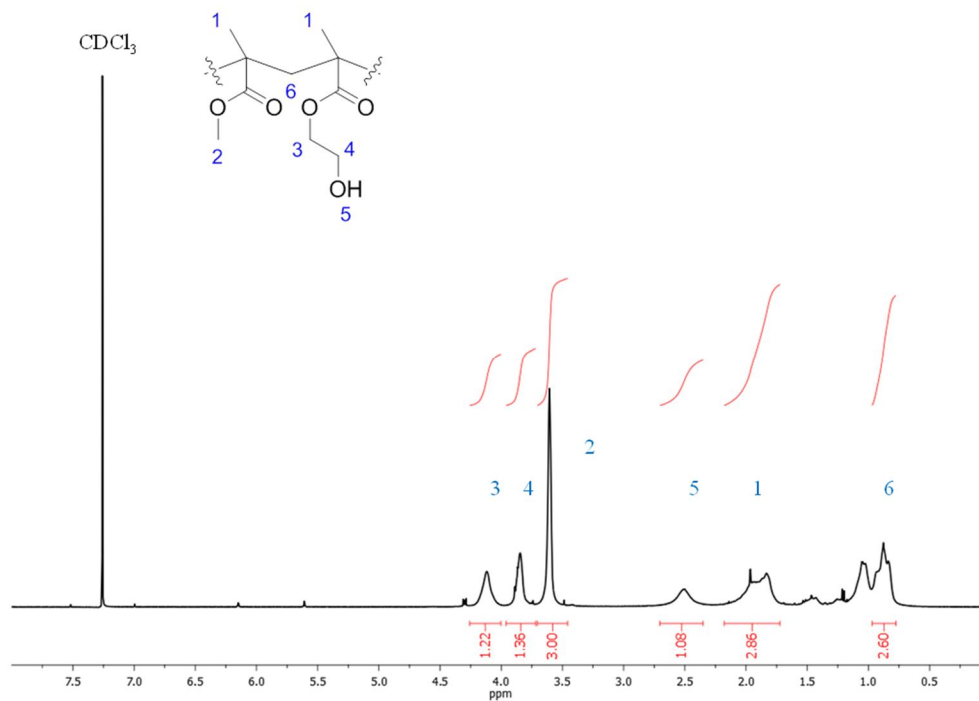
9.1.8 P(MMA₈₀-co-HEMA₂₀)

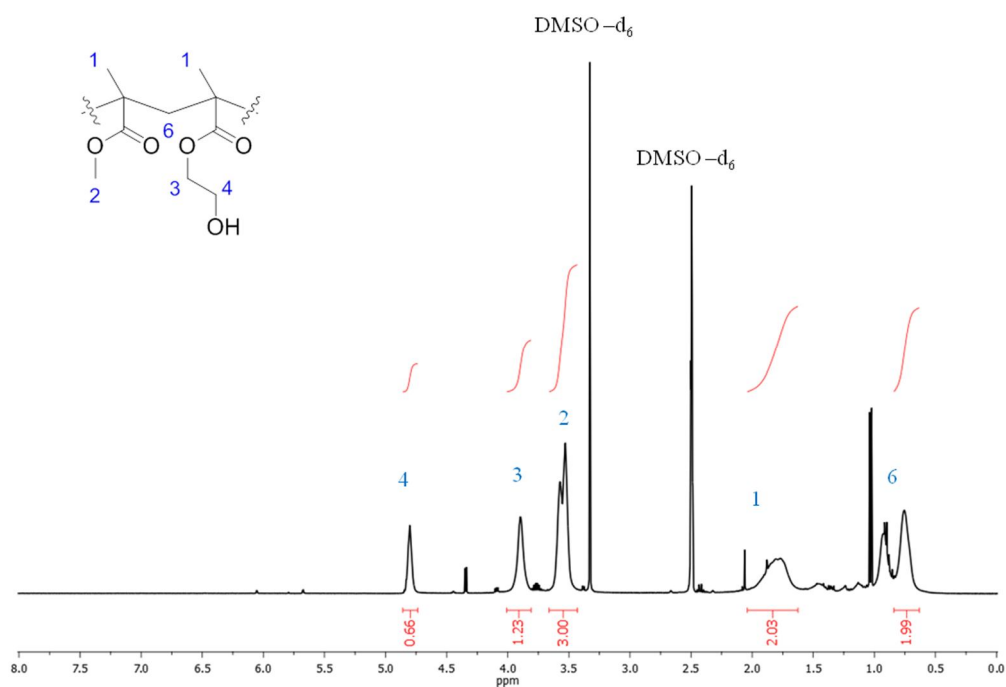


9.1.9 P(MMA₆₀-co-HEMA₄₀)



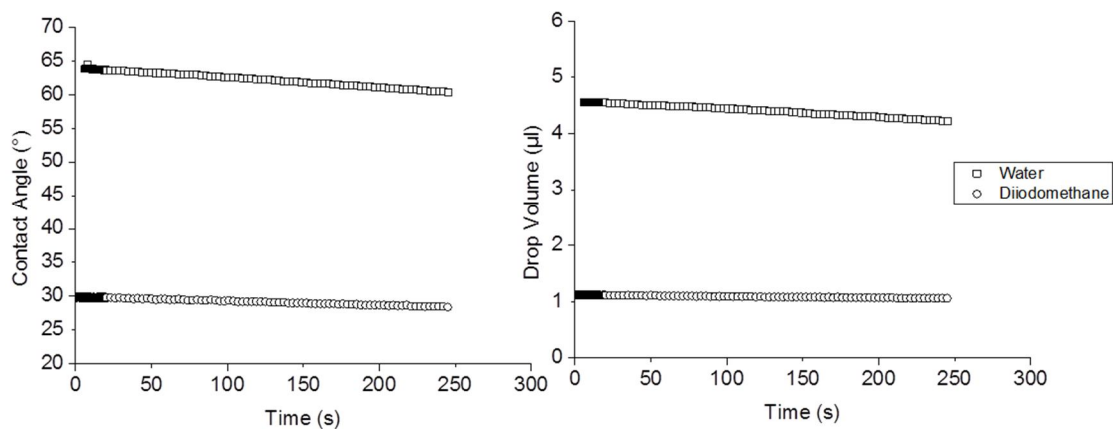
9.1.10 P(MMA₅₀-co-HEMA₅₀)9.2 ¹H NMR of Statistical Copolymers of P(MMA_x-co-HEMA_y)9.2.1 P(MMA₉₀-co-HEMA₁₀)

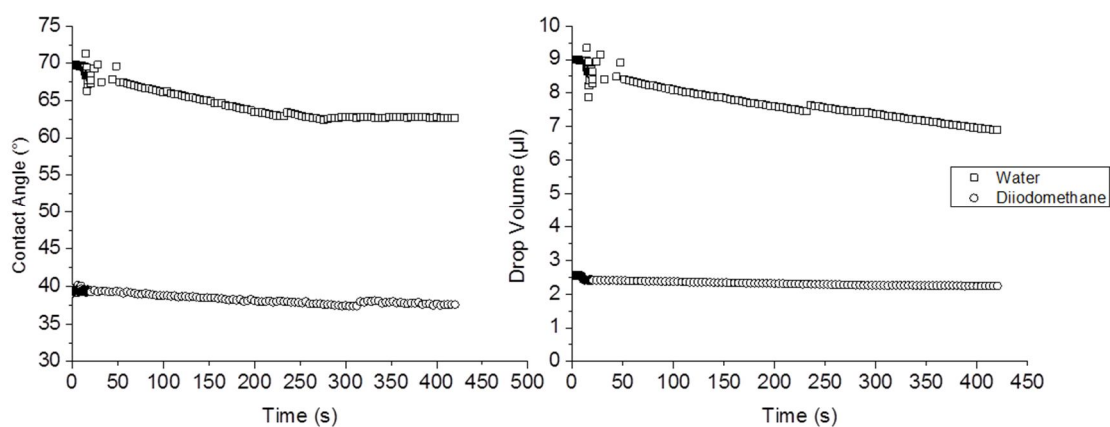
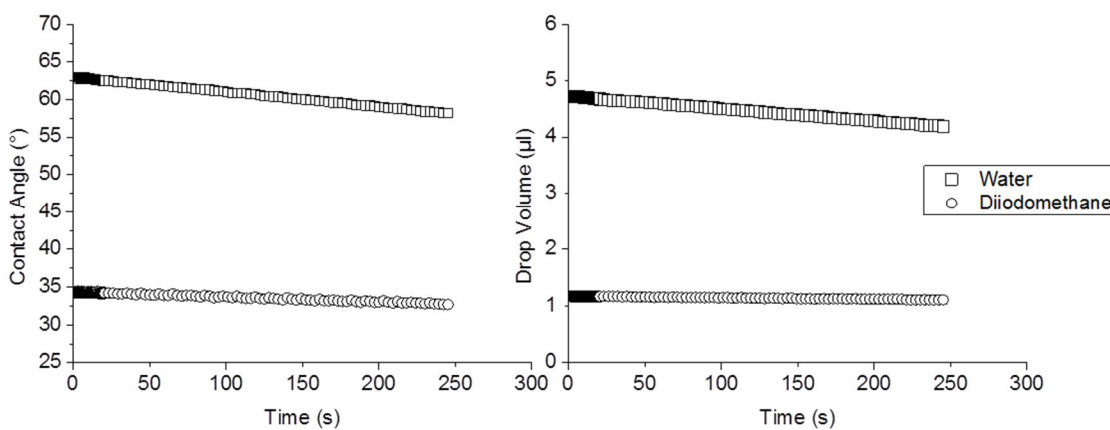
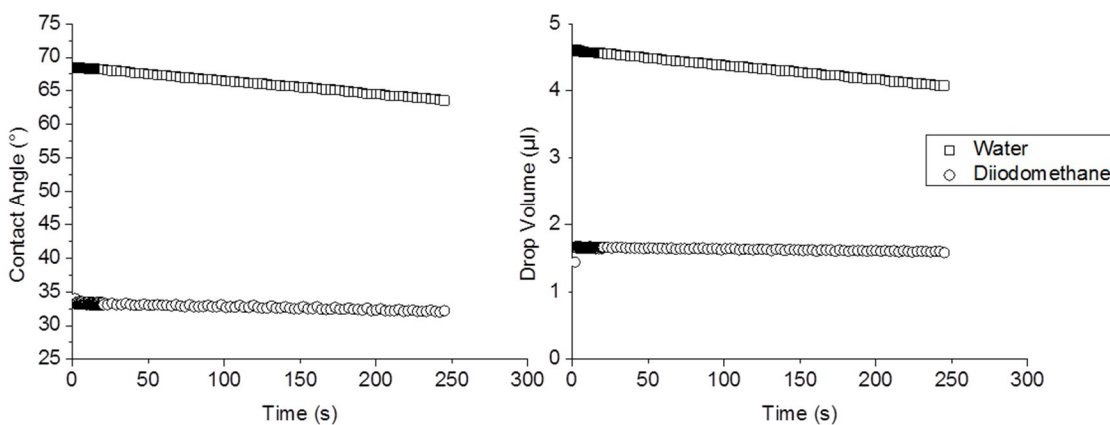
9.2.2 P(MMA_{80-co}-HEMA₂₀)9.2.3 P(MMA_{60-co}-HEMA₄₀)

9.2.4 P(MMA₅₀-*co*-HEMA₅₀)

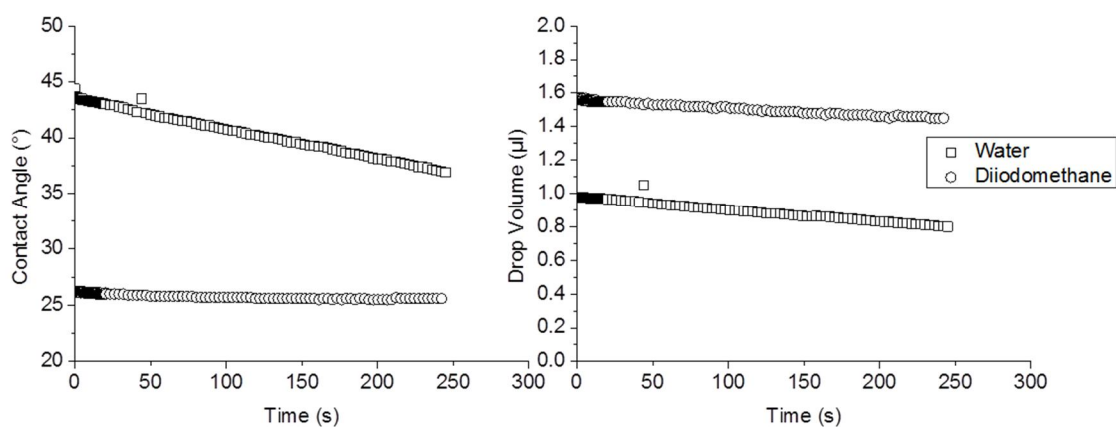
9.3 Contact Angle vs. Time for Surface Energy Calculations

9.3.1 PMMA-28 KDa

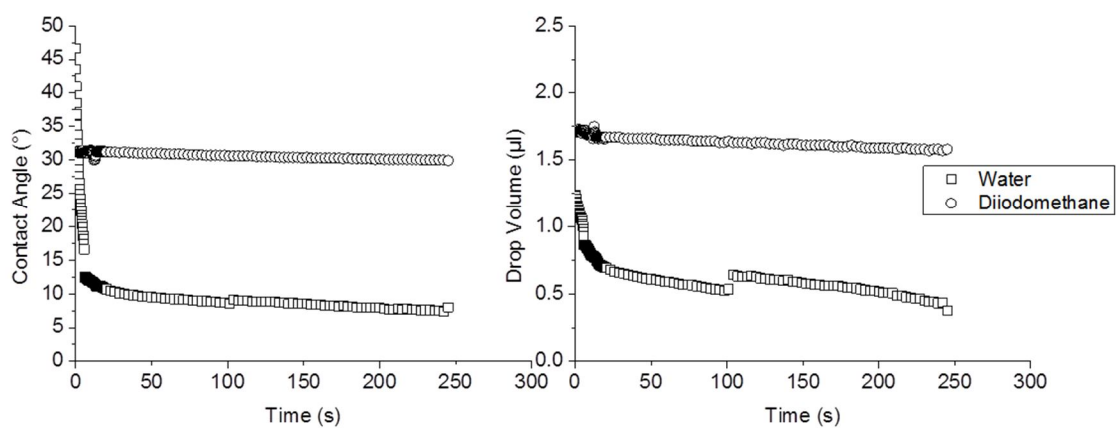
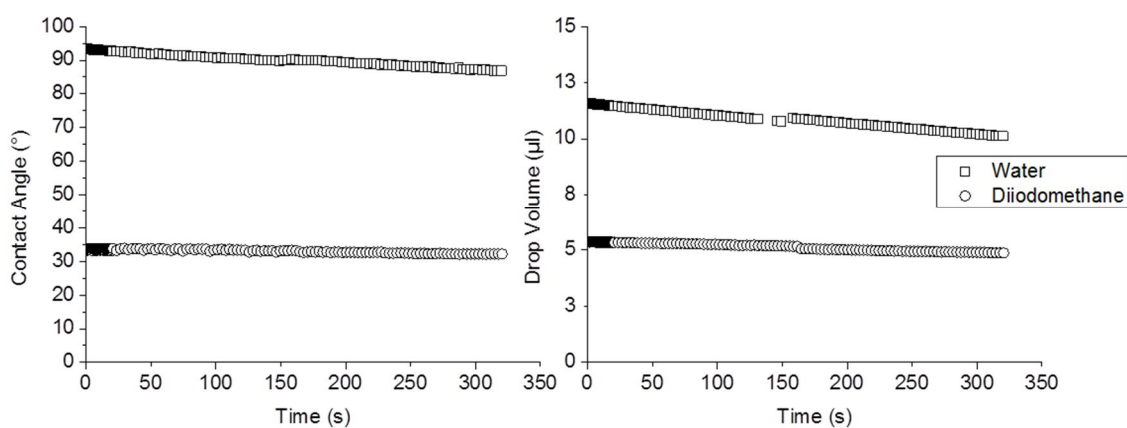


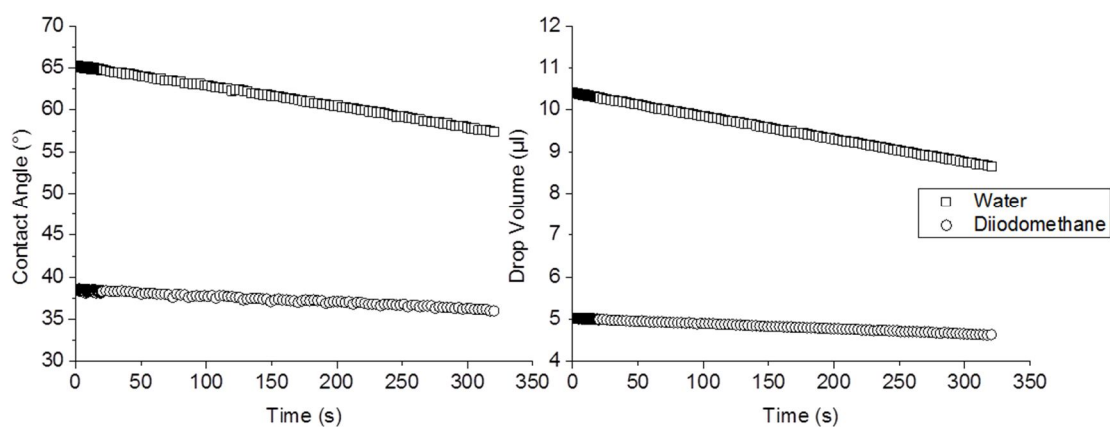
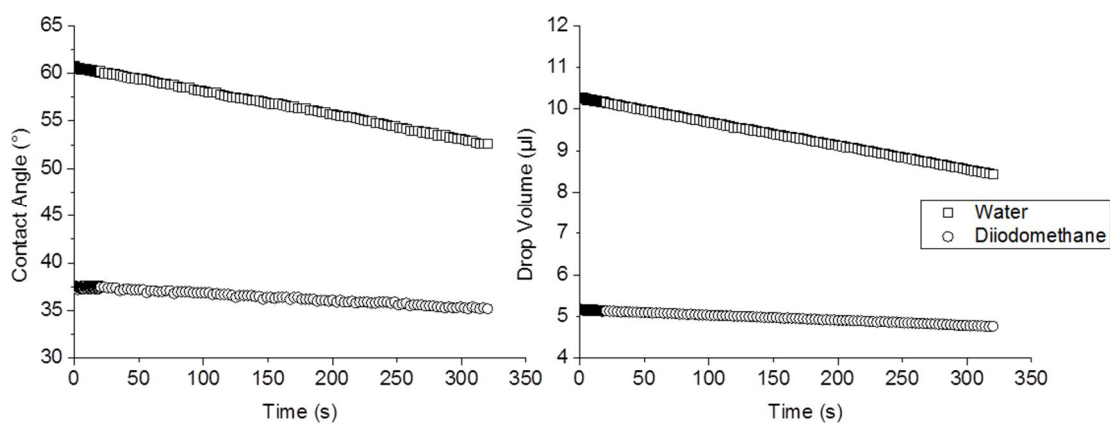
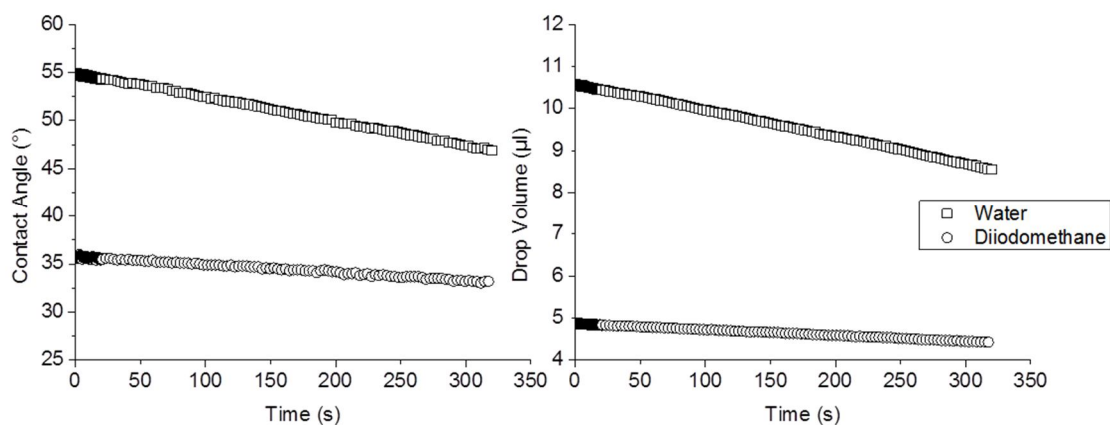
9.3.2 PMMA-35 KDa**9.3.3 P(MMA₉₈-MAA₂)****9.3.4 P(MMA₉₈-MAA₂)-stabiliser**

9.3.5 PHEMA



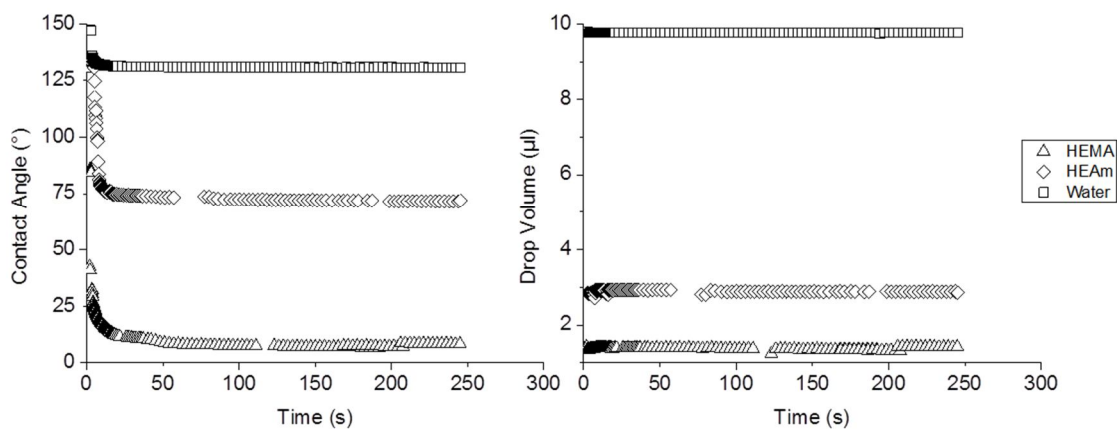
9.3.6 PHEAm

9.3.7 P(MMA₉₀-co-HEMA₁₀)

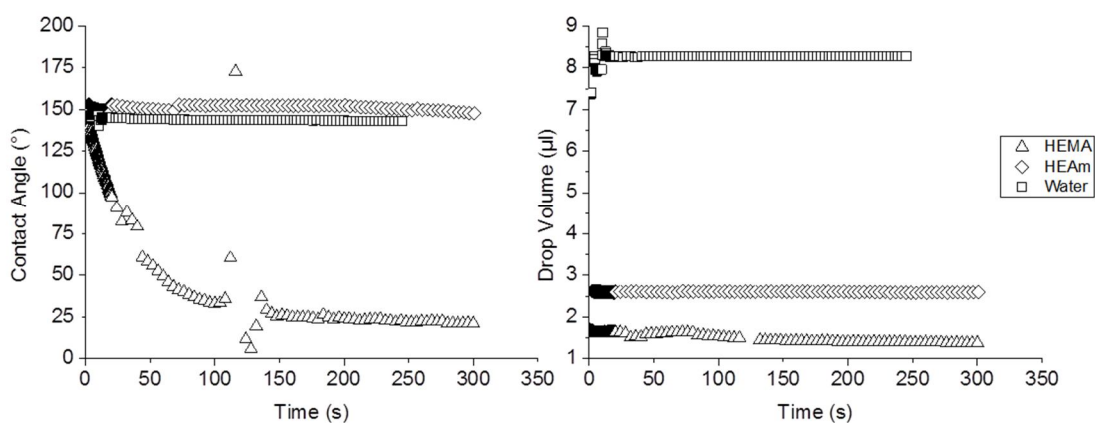
9.3.8 P(MMA₈₀-co-HEMA₂₀)**9.3.9 P(MMA₆₀-co-HEMA₄₀)****9.3.10 P(MMA₅₀-co-HEMA₅₀)**

9.4 Contact Angle vs. Time for Monomer on Substrates under Dodecane

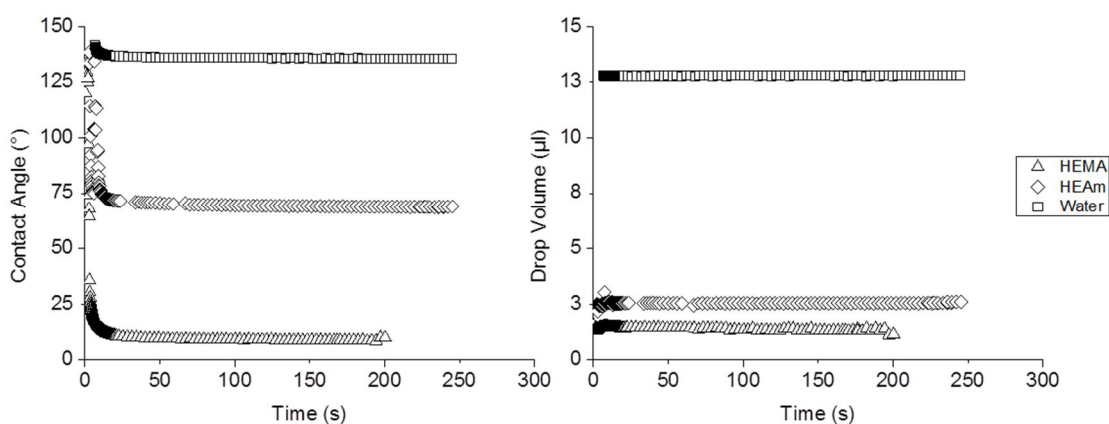
9.4.1 PMMA-28 KDa

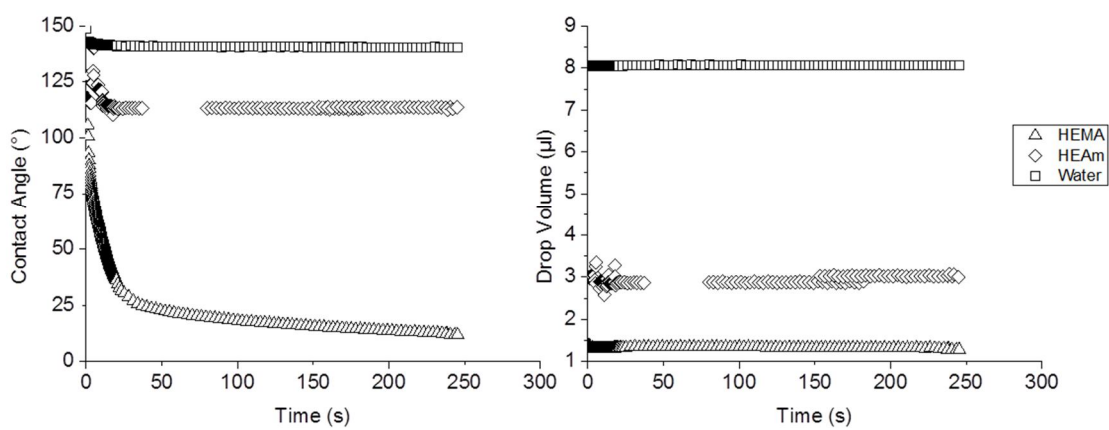


9.4.2 PMMA-35 KDa

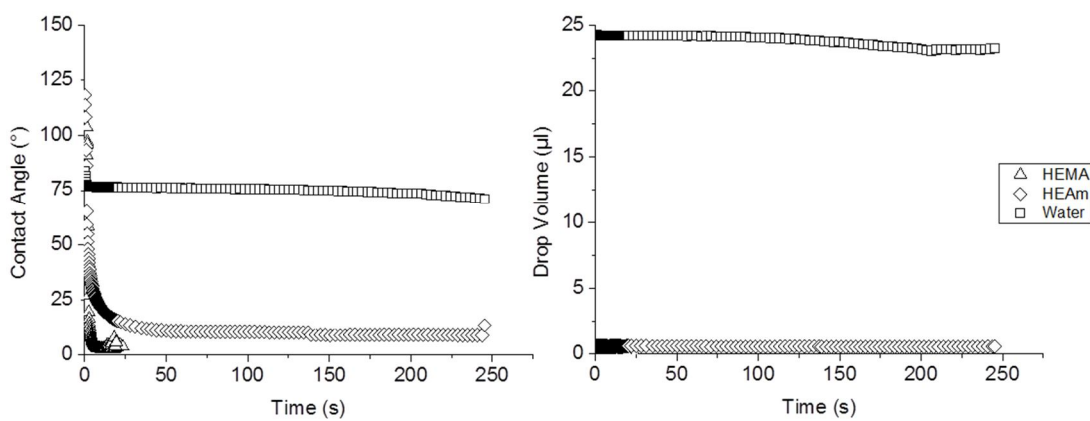


9.4.3 P(MMA₉₈-MAA₂)

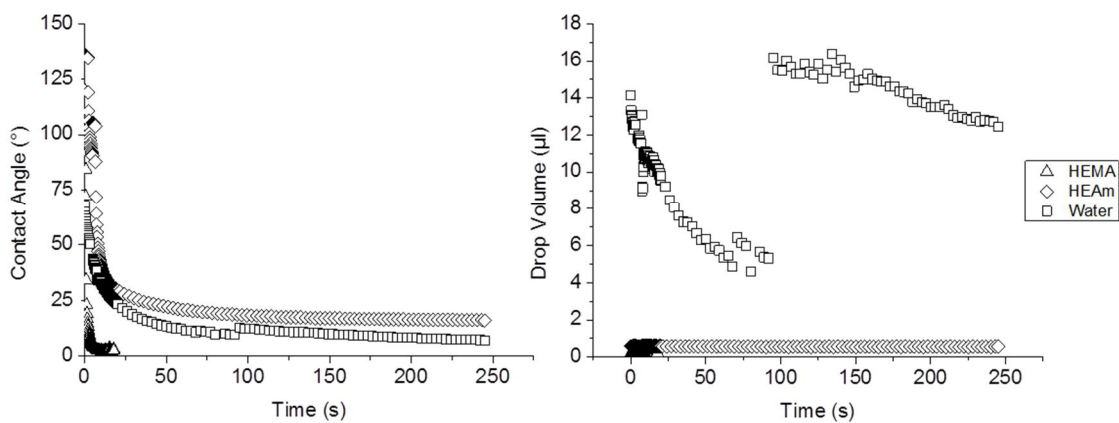


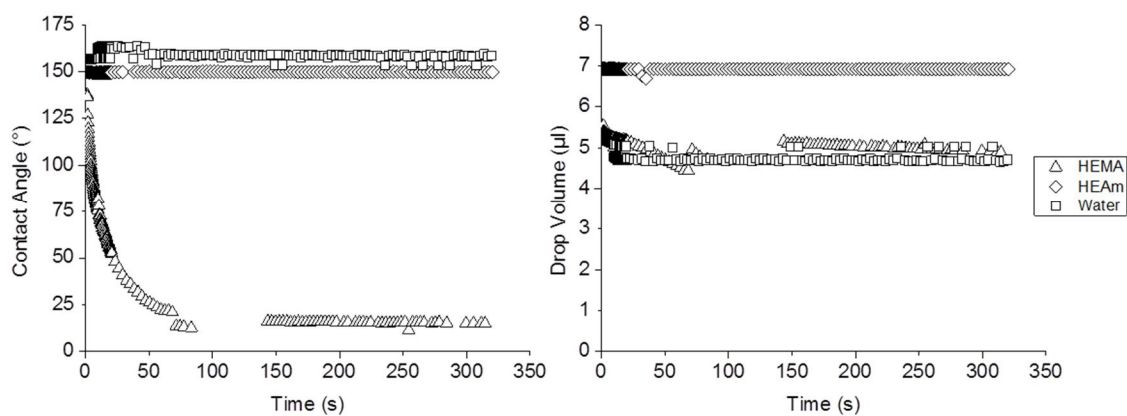
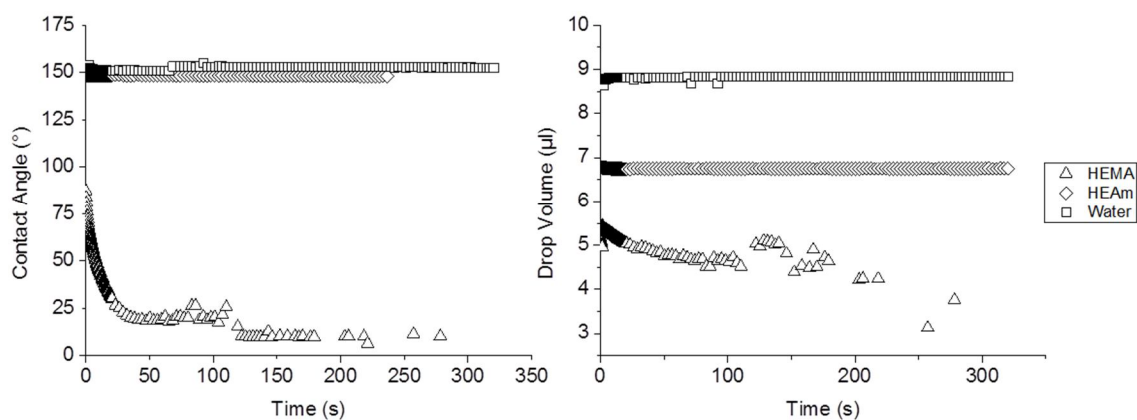
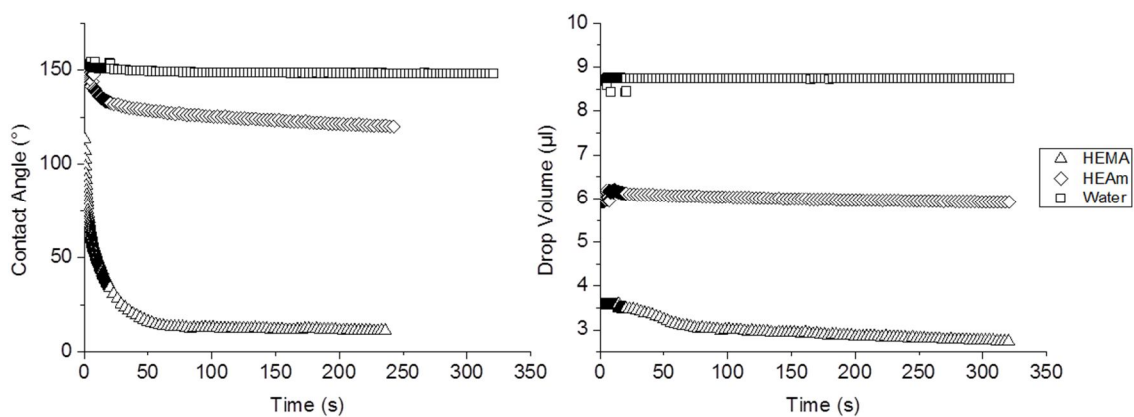
9.4.4 P(MMA₉₈-MAA₂)-stabiliser

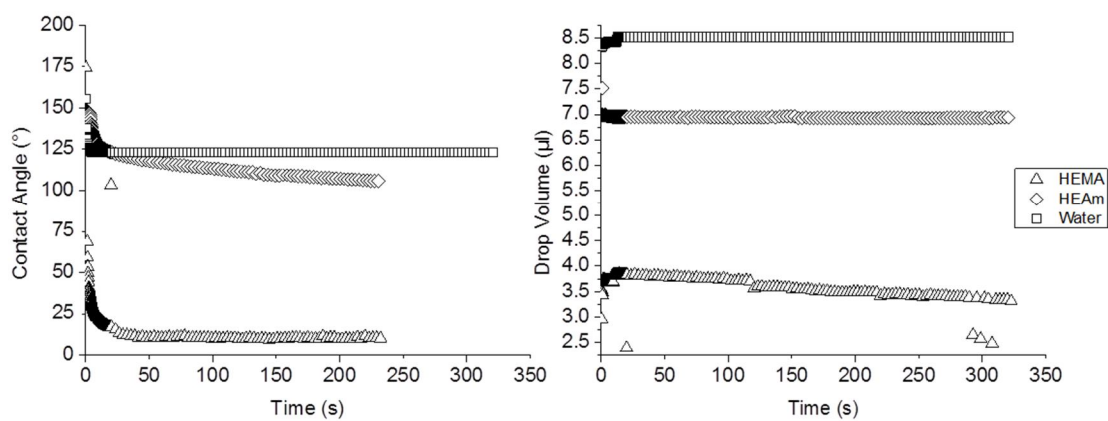
9.4.5 PHEMA



9.4.6 PHEAm

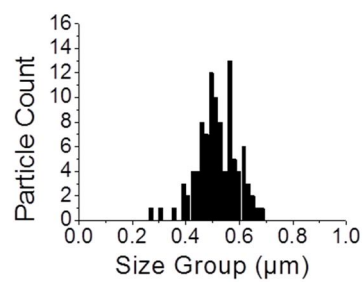
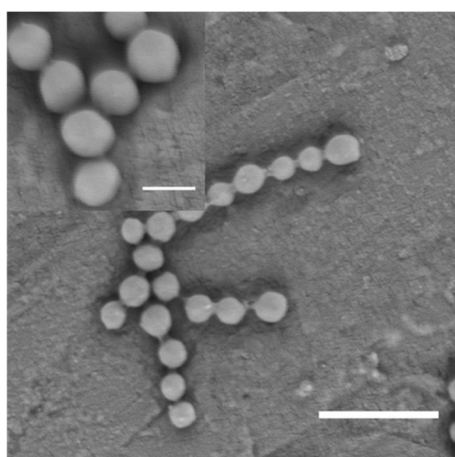


9.4.7 P(MMA₉₀-co-HEMA₁₀)9.4.8 P(MMA₈₀-co-HEMA₂₀)9.4.9 P(MMA₆₀-co-HEMA₄₀)

9.4.10 P(MMA₅₀-co-HEMA₅₀)

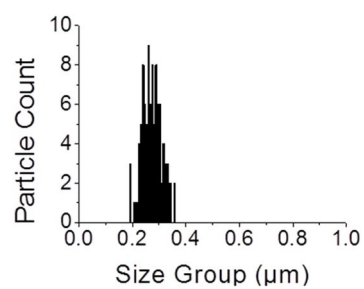
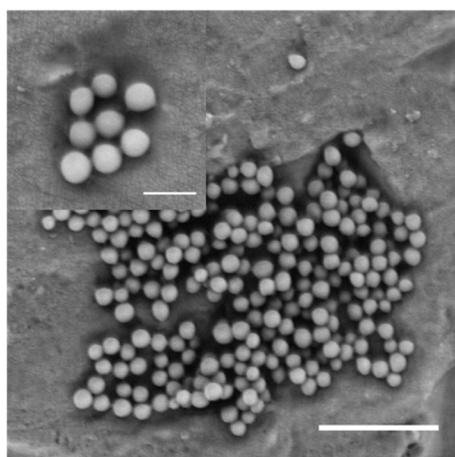
9.5 Seed Dispersions

9.5.1 Seed dispersion SRB-223-1% EGDMA and size data, based on counting 100 particles



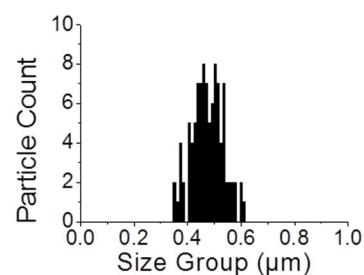
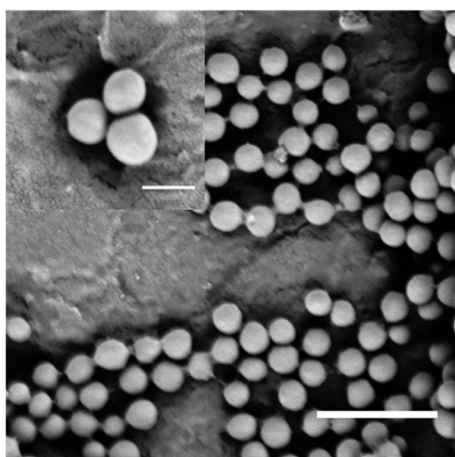
Particle Size (nm)	Coefficient of Variation
530	14%

9.5.2 Seed dispersion SRB-243-1% EGDMA and size data, based on counting 100 particles



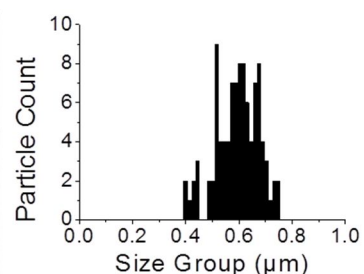
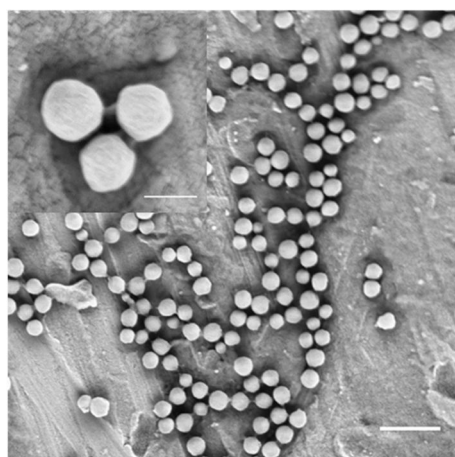
Particle Size (nm)	Coefficient of Variation
280	13 %

9.5.3 Seed dispersion SRB-253-1% EGDMA and size data, based on counting 100 particles



Particle Size (nm)	Coefficient of Variation
480	12 %

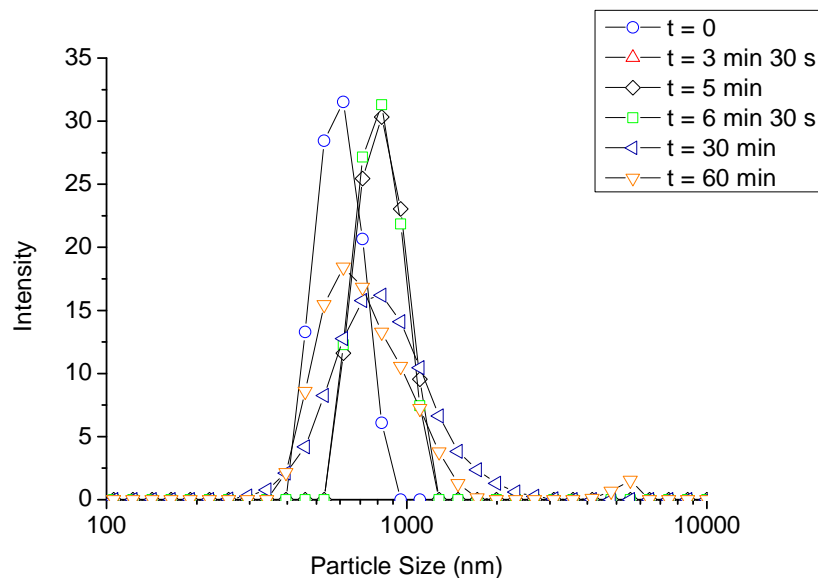
9.5.4 Seed dispersion SRB-325-1% EGDMA and size data, based on counting 100 particles



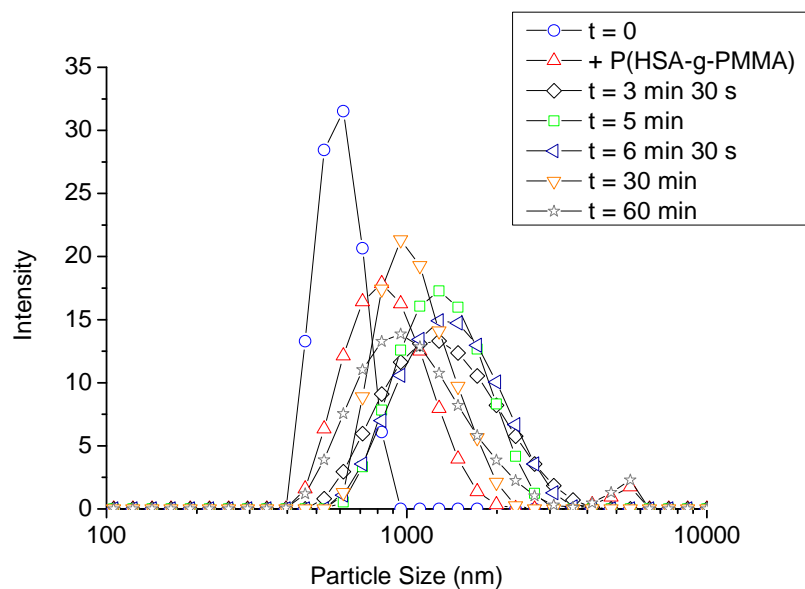
Particle Size (nm)	Coefficient of Variation
600	13 %

9.6 DLS Traces for Monomer Swelling

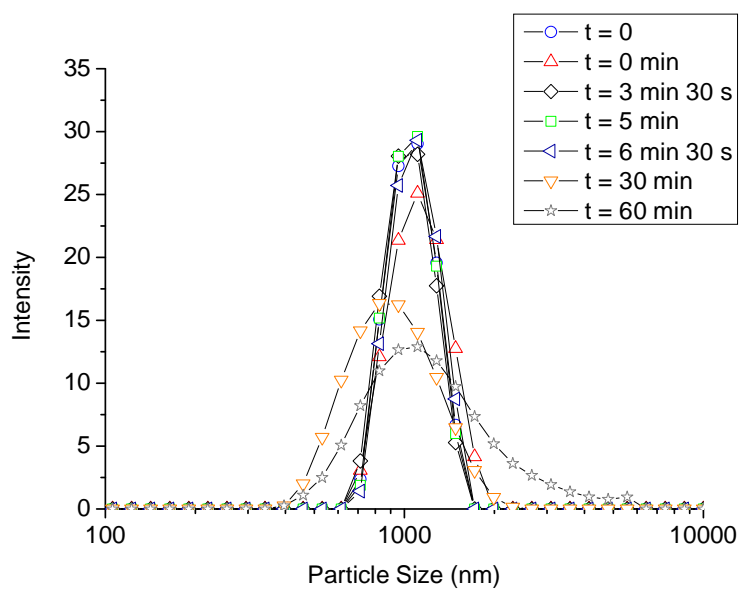
9.6.1 DLS traces for monomer swelling experiment with MMA at 4:1 monomer/particle ratio



9.6.2 DLS traces for monomer swelling experiment with MMA at 4:1 monomer/particle ratio, with added P(HSA-g-PMMA)



9.6.3 DLS traces for monomer swelling experiments, with ethyl acetate and butyl acetate (1:1, w/w) added to the dispersion



9.7 Effect of Increasing Hydrophilic Crosslinker Concentration

9.7.1 SEM images for reactions containing 2 wt. % polar monomer in the second stage reaction

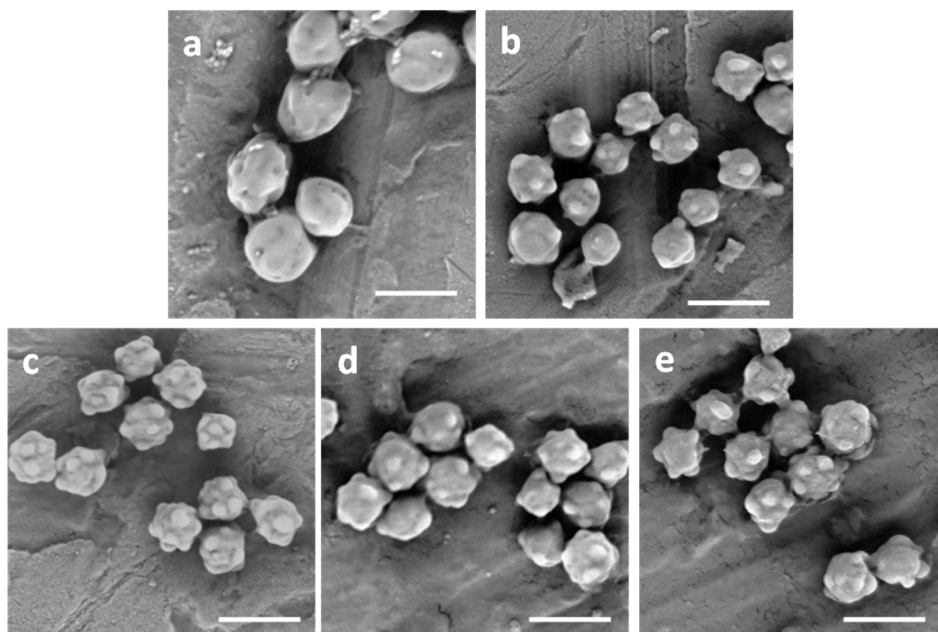


Figure 9-1, SEM images for reactions containing 2 wt. % polar monomer in the second stage reaction with; a, a no crosslinker comparison, b, EGDMA, c, GDMA, d, AHPMA and e, GDGDA. Scale bars are 1 μm . Total solids content of the seed dispersion was 10 wt. %, monomer/ particle ratio was 4:1, DDT concentration was 1 wt. % of monomers and initiator concentration was 0.5 wt. % of monomers.

9.7.2 Size distribution graphs for dispersions containing 2 wt. % polar monomer in the second stage reaction

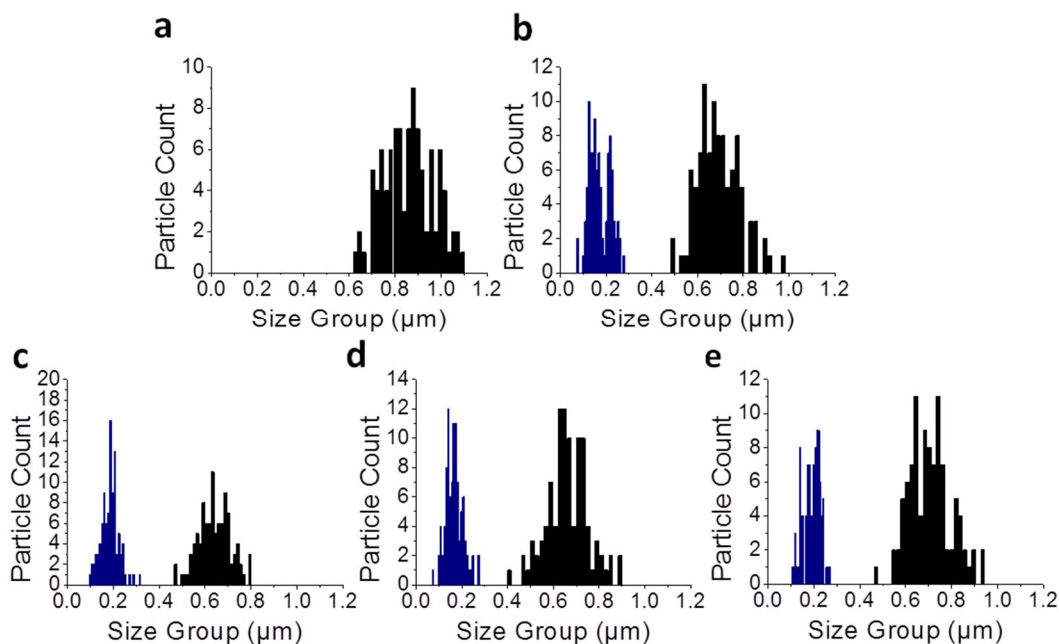


Figure 9-2, Size distribution graphs for dispersions containing 2 wt. % polar monomer in the second stage reaction with; a, no crosslinker for comparison, b, EGDMA, c, GDMA, d, AHPMA and e, GDGDA. Nodules on the particle surface are shown in blue, sizing based on counting 100 particles per population.

9.7.3 Particle size data for resultant dispersions containing 2 wt. % polar monomer in the monomer feed

Sample	Small Nodule Diameter		Full Particle Diameter	
	Size (nm)	Coefficient of Variation	Size (nm)	Coefficient of Variation
SRB-325-1% EGDMA	-	-	600	13 %
SRB-351-no xl	-	-	870	12 %
SRB-340- 2% EGDMA	180	24 %	700	13 %
SRB-320-2% GDMA	190	20 %	650	11 %
SRB-337-2% AHPMA	170	22 %	670	14 %
SRB-336-2% GDGDA	190	19 %	720	13 %